

**e-ISSN : 2320-0847**  
**p-ISSN : 2320-0936**



# **American Journal of Engineering Research (AJER)**

**Volume 4 Issue 6– June 2015**

**[www.ajer.org](http://www.ajer.org)**

**[ajer.research@gmail.com](mailto:ajer.research@gmail.com)**

## Editorial Board

### American Journal of Engineering Research (AJER)

**Dr. Moinuddin Sarker,**

Qualification :PhD, MCIC, FICER,  
MInstP, MRSC (P), VP of R & D  
Affiliation : Head of Science / Technology  
Team, Corporate Officer (CO)  
Natural State Research, Inc.  
37 Brown House Road (2nd Floor)  
Stamford, CT-06902, USA.

**Dr. June II A. Kiblasan**

Qualification : Phd  
Specialization: Management, applied  
sciences  
Country: PHILIPPINES

**Dr. Jonathan Okeke  
Chimakonam**

Qualification: PHD  
Affiliation: University of Calabar  
Specialization: Logic, Philosophy of  
Maths and African Science,  
Country: Nigeria

**Dr. Narendra Kumar Sharma**

Qualification: PHD  
Affiliation: Defence Institute of Physiology  
and Allied Science, DRDO  
Specialization: Proteomics, Molecular  
biology, hypoxia  
Country: India

**Dr. ABDUL KAREEM**

Qualification: MBBS, DMRD, FCIP, FAGE  
Affiliation: UNIVERSITI SAINS Malaysia  
Country: Malaysia

**Prof. Dr. Shafique Ahmed Arain**

Qualification: Postdoc fellow, Phd  
Affiliation: Shah Abdul Latif University  
Khairpur (Mirs),  
Specialization: Polymer science  
Country: Pakistan

**Dr. Sukhmander Singh**

Qualification: Phd  
Affiliation: Indian Institute Of  
Technology, Delhi  
Specialization : PLASMA PHYSICS  
Country: India

**Dr. Alcides Chaux**

Qualification: MD  
Affiliation: Norte University, Paraguay,  
South America  
Specialization: Genitourinary Tumors  
Country: Paraguay, South America

**Dr. Nwachukwu Eugene Nnamdi**

Qualification: Phd  
Affiliation: Michael Okpara University of  
Agriculture, Umudike, Nigeria  
Specialization: Animal Genetics and  
Breeding  
Country: Nigeria

**Dr. Md. Nazrul Islam Mondal**

Qualification: Phd  
Affiliation: Rajshahi University,  
Bangladesh  
Specialization: Health and Epidemiology  
Country: Bangladesh

<b>S.No.</b>	<b>Manuscript Title</b>	<b>Page No.</b>
<b>01.</b>	Assessment and analysis of indices of urban sustainable development in small cities (case study of Soran) Bahram Irandegani    Maryam karimian Bostani    Gholam Reza Miri	01-07
<b>02.</b>	Microcontroller based new single-phase transformer less inverter for grid-tied photovoltaic system with constant common mode voltage Nadia Afrin    Monirul Islam    Anarul Islam	08-17
<b>03.</b>	Measurement and Analysis of Magnetic Barkhausen Noise on the Surface of Grain Oriented Electrical Steels at Power Frequency Nkwachukwu Chukwuchekwa    Onojo J. Ondoma    Joy U. Chukwuchekwa	18-30
<b>04.</b>	Research on the Application of Fluid-Structure Interaction in Soil Rock Mixture Slope Wang Yongcun    Wang Wei	31-35
<b>05.</b>	Multipath Rayleigh and Rician Fading Channel Simulation Using MATLAB Md. Golam Sadeque    Shadhon Chandra Mohonta    Md. Firoj Ali	36-42
<b>06.</b>	Soyabean Fibre – A Substitute to Silk Fibre Sanjida Sultana    AzmaryAkteer Mukthy	43-45
<b>07.</b>	A Study on Overlay Design of Repeatedly Deteriorating Flexible Pavement Mahendrakar Kiran Kumar    D.Gouse Peera    Konge Praveen Kumar	46-51
<b>08.</b>	MISSING HEART?... ("RAMANUJAM HEART") M.Arulmani    V.R.Hema Latha	52-63
<b>09.</b>	On the Transmission Line Pulse Measurement Technique X. Rodriguez    M. Eduardo    M. Harington	64-67
<b>10.</b>	Unsteady MHD flow and heat transfer of nanofluid over a permeable shrinking sheet with thermal radiation and chemical reaction Srinivas Maripala    Kishan.N	68-79
<b>11.</b>	Modelling Compressor's Initial Operating Conditions Effect on Turbine Performance in the Tropical Rainforest Adumene Sidum    Le-ol Anthony Kpegele    Amadi Rex Kemkom Chima	80-88
<b>12.</b>	Design and Construction of a Prototype Gas Fired Kiln Using Nsu Clay Refractory Bricks Oduagwu Ferdinand Azubuike    Koreyo Victor Dorawa    Azubuike Thaddeus Chukwuemeka	89-101
<b>13.</b>	Human Body Motion Detective Home Security System with Automatic Lamp and User Programmable Text Alert GSM Mobile Phone Number, Unique PIN to Allow Universal Users Using PIR Sensor Oyebola B. O.	102-111
<b>14.</b>	Adaptation of compromise programming approach for multi-criteria material selection A. D. Adeyeye    G. O. Odu    O. E. Charles-Owaba	112-122

## CONTENTS

<b>15.</b>	Blood Donation Management System K M Akkas Ali   Israt Jahan   Md. Ariful Islam   Md. Shafa-at Parvez	123-136
<b>16.</b>	Groundwater Resources Assessment For Joypurhat District Using Mathematical Modelling Technique Md. Iquebal Hossain   Md. Tarikul Islam   Prof. Iqbal Matin	137-143
<b>17.</b>	Implementation of RSA Encryption Algorithm on FPGA Amit Thobbi   ShriniwasDhage   Pritesh Jadhav   Akshay Chandrachood	144-151
<b>18.</b>	Improving Atm Security Check Using DNA Biometrics Igwe, Agu Felix   Eneh, I.I	152-159
<b>19.</b>	Biomedical Waste Treatment: A Case Study of some Selected Hospitals in Bayelsa State, South-South, Nigeria Zekieni R. Yelebe   Revelation J. Samuel    Blessing Z. Yelebe	160-164
<b>20.</b>	Development of Roofing Sheet Material Using Groundnut Shell Particles and Epoxy Resin as Composite Material Jacob Olaitan AKINDAPO    Umar Alhaji BINNI    Olawale Monsur SANUSI	165-173
<b>21.</b>	Problem Prevention Method for Product Designs Based on Predictive Technical Evaluation: A Study of Bolt-loosening Mechanisms in Automobiles Ryota Nomura    Kimihiro Hori    Kakuro Amasaka	174-178
<b>22.</b>	Impact of rejection of non-industrial wastewater treated origin: savex case in batambo district of second Bangui Koyassambia Marcel Landry    Prof Li Jiang Feng    Dr Zaguy Raoul G    Poungo Nicole Elizabeth    Nzoussi Hilaire Kevin    Bangala Yamokito Sandrine	179-187
<b>23.</b>	Effect of variation of pick density on the properties of jute fabric samples woven in S4A loom and a comparative study with the standard fabric (IS 12650: 2003 2nd revision) Prof. Swapan Kumar Ghosh    Mr. Rajib Bhattacharyya    Mr. Chinmoy De	188-195
<b>24.</b>	Analyzing the impact of rural housing credits on indices of physical development and housing patterns (Case study: villages in the central part of the city of Kashmar) Javad Bazrafshan    Ali Vaez Tabasi	196-202
<b>25.</b>	Study on Hydrographic properties in the coastal waters along South East Coast of India James Balgan Anand D    Mary Jelastin Kala S	203-214
<b>26.</b>	Alternative Room Cooling System Md. Fazle Rabbi    Mrittunjoy Sarker    Mohammad Mashud	215-218
<b>27.</b>	Induce Drag Reduction of an Airplane Wing Md. Fazle Rabbi    Rajesh Nandi    Mohammad Mash	219-223

## Assessment and analysis of indices of urban sustainable development in small cities (case study of Soran)

<sup>1</sup>, Bahram Irandegani, <sup>2</sup>, Maryam karimian Bostani , <sup>3</sup>, Gholam Reza Miri

<sup>1</sup>, MSc student in Department of Geography and Urban Planning, College of human science, Zahehan Branch, Islamic Azad University, Zahedan, Iran

<sup>2</sup>, Assistant professor in Department of Geography and Urban Planning, College of human science, Zahehan Branch, Islamic Azad University, Zahedan, Iran

<sup>3</sup>, Assistant professor in Department of Geography and Urban Planning, College of human science, Zahehan Branch, Islamic Azad University, Zahedan, Iran

**ABSTRACT:** *density and villagers migrate to the cities attention and emphasis was planning to strengthen and grow small towns. The study by researchers in different countries shows that small towns are one of the most successful examples of settlement in the area of sustainable development. Soran and the social and physical areas of urban sustainability indicators in urban areas is presented. The research method of this study is survey method and the data has been obtained from the questionnaire. The results of findings show that in terms of urban sustainability indices, the city of Soran has not a desirable situation in relation to the medium of urban system but it is in the same state in terms of more social, economic and physical indices in relation to urban system of country which it is noticeable clearly.*

**KEY WORDS:** *development, sustainable urban development, small towns, Soran*

### I. INTRODUCTION

The city is the main base of human civilization and it is the technological and mind crystallization of human. The study of urban growth reflects that the growth of urban population is growing rapidly (Saifadini, 1999: 75). In the past, the changes in urban growth were slow and the possibilities, variety of tools, and technology and also the interests were limited and the system of common and popular culture didn't served well and their product was a city with a harmonious and sustainable appearance. Rapid population growth and its focus in cities all over the world will effect on the majority of human's prospect of living in cities. The crises of this rapid growth are poverty, environmental degradation, lack of urban services, the fall of existing infrastructure, lack of access to land and shelter. Urban planning of twentieth century ended when this plan is not only positive but it has supplied an unseemly figure of city against urban environment and it has threatened social integration and biological structures by using of the culture of technology and it will have no result except the instability and imbalance in natural, social, economic and physical infrastructure (Ziari, 2001: 371).

In the early of 21<sup>th</sup> century, the urban population of the world was 50 percent population of the world and it will be foreseen that it will be more than 61 percent of the population of the world until 2025. Nearly 12 percent of the population will be living in cities of over 10 million people and the cities with 25 to 30 million people will be possible and foreseeable. So all over the world, on the one hand we will observe some imbalances between economic development and population growth and on the other hand we are to conserve natural resources and living conditions that are closely related to policies and practices in urban areas. Throughout human history, the present age has seen the greatest environmental benefit because the demand and function and the development of cities and urbanization. Cities, especially the large and medium cities are conjuncture and the focus of most impact and influence on nature. Sustainable development is the thought-provoking discussion of recent developments that will be questioned this unhealthy relation in some ways (Fanni, 2003: 48). The theory of urban sustainable development will propound some issues such as regional and urban pollution prevention, reducing the production local, regional and national capacity, support the renewable processes of materials, and not to support the harmful development and finally it want to close the gap between the poor and the rich. The ways to achieve the goals of the theory are urban, rural and regional and national planning that is known equal to the law of more control of application and more controlling on cities and villages progress (Papelli yazdi, 2003: 340) and this theory also propounded the urban development and introduction of the

principle of sustainable development, paying more attention to issues of sustainability. The existing problems, especially in big cities are the sign of non-fulfillment of their stability characteristics. In this situation, the urban geography will have new dimensions and realms and by studying the important issues of the third world countries and the problems of large cities growth, the population density and also rural migration to cities caused that the planners emphasize on boosting the growth of small towns (Rezvani and et al, 2007: 45). The development of small town is a suitable method for spatial development and economic growth and social stability and it can act as an alternative to the growth of large cities. But it seems that such a development will be obtained and formed if such cities have not the problems of big cities in small scales and provide a suitable atmosphere for present and next generation. But at the local level, a problem that more than any other issue must be considered is attention to equality and justice on the basis of socio-economic and physical dimensions and indices from the view of urban sustainable development. Up to now, the development planning has considered the large and medium cities and less attention has paid to small cities. So, except of the attraction of crowds and functions diversity, the small cities face the same problems of large cities. These problems are seen in various aspects of economic, social, environmental and physical. So, according to the increase of the number of small cities and their progress, it will be reasonable to predict a comprehensive and multidimensional development planning and suitable for those cities, a plan and program that will consider all environmental, physical, economic, social and urban dimensions of the city. Today's small cities are the basis of future large cities and by adoption of new functions and physical progressing will be changed to larger cities with larger problems and different limitations if there is no suitable and proper planning and programs. So the planning for the sustainable development of small towns has entered as a new approach in the field of urban studies but an important question that will be propounded is that the sustainable development of these settlements will be achieved by which factors (Naderi, 2008: 3). The city of Soran is located in a plain with same name in the city of Sib and Soran with a population of 12158 is a sample of a small city. The city of Soran located along the plain and with its 12158 population is a sample of a small city and according to statistical analysis it can be said that the population of the city has increased dramatically in recent decades so, due to population growth and its related problems such as physical urban growth horizontally because of social tensions, lack of services, difficulties in transportation within the city, the increase in per capita residential, agricultural land degradation, low per capita green space in the city as well as social security in present time and future, it is difficult to be able to continue its development suitably and ideally and play a role in the urban system of the province so for not facing the difficulties of lack of programs in future a comprehensive and multilateral program should be speculated for it. So, finally it is tried to study and examine the economic, social and physical indices as much as possible.

### The hypothesis of the research

In terms of statistical indices of sustainable development, the city of Soran has a good performance.

### The history of the research

Sluiter & de Jong (2007) in a research, studied «Factors affecting urban development». The results suggest that in addition to the human factors, a combination of physical and biological factors is important in extraction patterns of urban development. Luederitz et al In their study on the guiding principles for sustainable development of urban neighborhoods of Germany, concluded that there are various factors in the city that can be effective in improving of that region and it often prevails in most cases of the city and the can be empowerment of managers and leaders of the city's administrative, technical and technological infrastructure and landscape design for city.

Table (1): Background research on the topic under study

Research Title	researchist
Analysis of the role of small towns in the socio - economic development surrounding villages	M. Housain abadi, 2010
The role of small towns in sustainable development	B. Naderi, 2008
Small town and its position in third world, New York	UNCHC,2009
small Towns and urban planning in developing country, Urban studies	Nile Hinrey,2007

Reference: research findings

### Basics theoretical

#### Town

Mainly defined small-town on the population size is emphasized the reasons for the limited information on other characteristics of these cities (Fani, 2003,14) To towns, cities which are less than 10 thousand to 50 thousand populations and have some roles such as urban retail, marketing, and transport center of the local administration (Shakvei,1998, 414). The Islamic Republic of Iran Cities Setiran and land use planning initiatives between 5 thousand to 25 thousand people were considered as small towns. The National Physical Plan into compliance with the standards provided by the United Nations, the city of 50 thousand people is seen as a small town. (Izadi Kharama, 2001, 138).

**Small towns and reasons affecting their ductility**

Reasons different at form accessibility towns small involved is with attention to location geographic and other factors environmental, city small, to title focus area the influence own known by and with charge catch other the role of service and social and cultural, with development agriculture and creation centers market at the species areas set to name city small the people the if (Shirazi, 1999, 27).

**Small towns and their socio-demographic characteristics**

Role city small to title a location central at an area more dependence space the between the location and villages prepared the won. Prove connection economic with city, preparations a series movements population the provided and at towns small section wide of population to activity of agriculture occupation have and of the as in same enjoying of some utility of life at city, of quality environment rural and small the interest brand. (Babie, 2002, 27).

**Small towns and service characteristics and economic**

Study of urban geography mainly focuses on large cities but also smaller paths influence of geography on urban issues (Yamashita, 2004: 473). Provide services support agriculture and services other to villagers under area influence one of tasks the basic towns at a system series hierarchical and accommodation proportional the bee. rural to reason close to city small can at form location services the basic at the cities to easily of the facilities use do . One of the roles of the small towns that economic performance through various markets, capital flows, consumption and the order of the income is realized. cities small share large of occupation at section agriculture industries manual and workshop small scale and services category low that rate growth rather lower at total occupation the city is on responsibility have. (Razaei, 1999: 19). To general of perspective economy areas rural cities to title centers market business role axial at strengthening durable sector agriculture expand its creation base the diversity activity of economic area and process increase regional income have farms of by marketing export their the first tools business income of economy external to within a area rural to count the come (Shakvei, 1998: 295). Creation centers market with reliance on form a series more proper of centers development, one of elements development rural is and towns small at form the series more role important have and the gap can between towns and megalopolises the full do and centers marketing the at level local distribution to (Izadi Kharama, 2001: 198). At a sum classification final the power said that strengthening role town's small, opportunity and background of new for employment, capital mark, mobilization services and facilities welfare and social area to existence the won. These action development process the center to areas margin a brought is (Dashtei Brinje, 2000: 31).

**The small cities and sustainable development**

Large and small cities and villages have their own response toward these dimensions so; there will not be the same prescription and draft for sustainable development of all of urban communities. To the proportion of urban population and industrial employment, the cities have some impacts on urban environment and its surrounding. In contrast, the small towns have their own issues in accordance with their own performance. The small cities with their environment have features and barriers and constraints for achieving sustainable development.

The pro and the fans of small cities and perhaps they can be known as the opponent of large cities, believed that the agricultural and industrial development are not separated and emphasizes on economy of centers of small cities. Emphasizing on human issues, this group believe that the citizens will lost their private relationships in large cities (Zebardast, 2004: 24).

Feeling and sentiments will be weakened in large cities and human will reach to a level of self alienating and a result of it, he will reach to the level of social vacuum. This group has studied the problem from the view of biologic- environmental and believed that the small cities harms environment less and the air and sound pollution are less in small cities. They have an aesthetic look on the size of cities and believe that the most beautiful and most historical cities in 20<sup>th</sup> century were small cities (Dashti barzanja, 2000: 36).

**Identifying of the studying region**

The city of Soran and Sib is located in south-east of Iran at latitude of 27/2' N and at the longitude of 62' S with the population of 52 thousand people and its density of population is 10 people in 10 square kilometer. 75% of the population engaged in farming combined with livestock and it also has 364 residential small villages and 220 villages and 8724 families. The extent and area of this city is 9324 square kilometer. This city leads from North to the city of Khash, from east to the city of Saravan, from south to the city of Bam and from west it leads to the city of Zaboli (Mehrestan). Based on statistics of 2011, the population of the city of Soran is about 12158 people (detailed plan of the city of Soran, 2009).



Figure (1): Map of the study area, Reference: research findings

## II. DISCUSSION AND CONCLUSION

### The analysis of hypothesis in direction of chosen indices of institutional- physical

For analyzing of hypothesis in direction of chosen indices of institutional- physical, the variables and indices of the following table is used.

Table (2): indices of institutional-physical of variables between the city of Soran and urban areas of the country.

index	The city of Soran	Urban regions of country
residential Per capita	45/68	25/19
Commercial Per capita	1/37	0/98
Educational per capita	4/5	1/02
High educational per capita	0/54	1/3
Religious per capita	0/09	0/17
Cultural per capita	0/09	0/17
Tourist per capita	0/06	0/12
Health care per capita	3/7	0/88
Sport per capita	1/25	0/12
Green space per capita	1/95	3/88
Transport per capita	1/94	21/4

Reference: the author's studies (the unit of indices is square meter)

According to the amount of possibility related to the Wilcoxon test, one sample is equal to 0/534 which is more than 0.05 so with certainty of 90% the statistic assumption or the hypothesis of H<sub>0</sub> that «the city of Soran has not proper function in respect to urban medium system according to the institutional-physical indices of sustainable development» cannot be rejected. Therefore a significant correlation in the institutional-physical indices of the region is not observed.

So as the result, the hypothesis of the research in direction of the institutional-physical indices isn't confirmed.

In the following of this research, the analysis of the first hypothesis in respect to the chosen institutional-physical indices of the sign test will be studied. According to Table (2), the probability of a sample sign test is equal to 1/000 that is larger than 0.05. So with certainty of 90 % the statistic assumption or the hypothesis of H<sub>0</sub> that «the city of Soran has not proper function in respect to urban medium system according to the institutional-physical indices of sustainable development» cannot be rejected. Therefore a significant correlation in the institutional-physical indices of the region is not observed. So as the result, the hypothesis of the research in direction of the institutional-physical indices isn't confirmed.

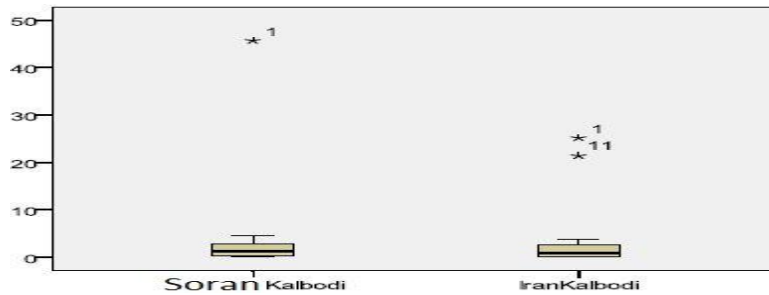


Figure (2): the comparison of chosen constitutional-physical of the city of Soran and urban regions of the country, Reference: research findings

**The analysis of the hypothesis in direction of economic chosen indices**

The variables and the indices of table (3) have been used to analyze the hypothesis in direction of economic chosen indices.

Table (3): The comparison of economic chosen indices of the city of Soran and urban regions of the country

Index	The city of Soran	Urban regions of the country
Percent of the economically active population	38/6	38/77
Percent of the economically inactive population	61/4	61/23
The percent difference in men's and women's activity	39/8	38/95
Unemployment rate	9/6	11/82
Employment percent of population aged 10-14	0/7	0/8
Relationship ratio	1/5	0/43
Percent of families who owns land and buildings	64/8	62/2
Percent of renter families	21/4	9/2

Reference: research findings

According to table (3), the amount of possibility related to the Wilcoxon test, one sample is equal to 0/233 which is more than 0.05 so with certainty of 95 % the hypothesis of H0 that «the city of Soran has not proper function in respect to urban medium system according economic indices of sustainable development» cannot be rejected. So as the result, a significant difference in chosen economic indices isn't confirmed.

Table (4): direction of economic chosen indices

The comparison of economic chosen indices of urban regions of country and Soran	
-1.192	The amount of Z
.233	Significance level

Reference: research findings

In the following of this research, the hypothesis will be analyzed in direction of economic chosen indices of one sample test. The amount of one sample is equal to 0/727 which is more than 0.05 so with certainty of 95% the hypothesis of H0 that «the city of Soran has not proper function in respect to urban medium system according economic indices of sustainable development» cannot be rejected. So as the result, a significant difference in chosen economic indices of the two regions isn't observed.

So the hypothesis of the research in direction of economic chosen indices won't be confirmed.

Table (5): the analysis of hypothesis in direction of economic chosen indices within one sample test

The comparison of economic chosen indices of urban regions of country and Soran	
.722	Exact sig

Reference: the research findings

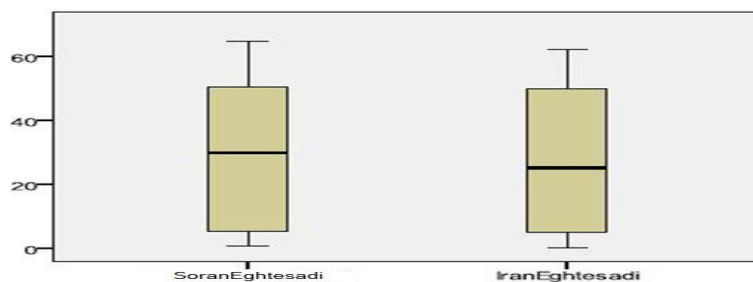


Figure (3): The comparison of economic chosen indices of urban regions of country and Soran Reference: research findings

**The analysis of hypothesis in direction of social chosen indices**

The variables and indices of the following table (6) are used for analysis of hypothesis in direction of social chosen indices.

Table (6): the chosen indices of social sustainability of the city of Soran and urban regions of country

Index	The city of Soran	Urban regions of country
The population growth rate at 2006-2011	2/33	1/61
The population proportion of men to women	1/03	1/04
The percent of male literate population	87/25	88/93
The percent of female literate population	37/43	85/55
The percent of families with no illiterate member	79/6	73/1
The difference of literate male and female percentage	2/39	6/64
Families' growth rate at 2006-2011	3/82	4/5
families' growth rate with 5 people and more	25/08	32/21
The percent of population aged 0-14	33/13	23/7
The percent of population aged 65 and more	4/4	4/77
The medium of families' dimensions	5/4	3/89

The reference: research findings

According to table (6) the amount of possibility related to the Wilcoxon test, one sample is equal to 0/594 which is more than 0.05 so with certainty of 95 % the statistic assumption or the hypothesis of H0 that there is no significance difference is not rejected so no significance difference in social chosen indices of the region is observed. So as a result of it, the first hypothesis of the research in direction of social chosen indices will not be confirmed.

Table (7): the analysis of hypothesis in direction social chosen indices within the Wilcoxon test

The comparison of social chosen indices of urban regions of country and the city of Soran	
-.533	The amount of Z
.594	Significance level

Reference: research findings

In the following of this research, the hypothesis will be analyzed in direction of social chosen indices of one sample test. According to table 7 the amount of possibility related to the Wilcoxon test, one sample is equal to 0/549 which is more than 0.05 so with certainty of 95 % the statistic assumption or the hypothesis of H0 that there is no significance difference is not rejected so no significance difference in social chosen indices of the two regions is observed. So as a result of it, the first hypothesis of the research in direction of social chosen indices will not be confirmed.

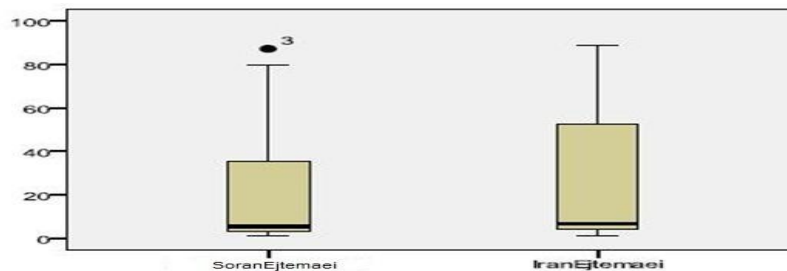


Figure (4): The comparison of social chosen indices of urban regions of country and the city of Soran, the Reference: research findings

**III. CONCLUSION**

The results of findings show that in terms of urban sustainability indices, the city of Soran has not a desirable situation in relation to the medium of urban system but it is in the same state in terms of more social, economic and physical indices in relation to urban system of country which it is noticeable clearly. The city of Soran has a high per capita of residential housing but the quality of housing is average and in terms of access to safe drinking water and plumbing, electricity and telephone are at a high level. The city of Soran has desirable health facilities but it has some defects in terms of positioning and citizens' access to pharmacies, medical institutions and doctors because a large portion of these facilities are located in the central part of the city and will cause a kind of population density in the center of city and will have a negative impact on intramural transportation. Inefficient management and lack of attention to the region's talent have caused that the city of Soran be dependent on service jobs and important activity is not done in the industrial sector in the city and this factor will cause that the unemployment rate go up. The city's workforce is also reluctant to invest in agricultural occupations and prefer to invest on service jobs which affect the rate of employment.

**Suggestions**

1. Increasing and accelerating of investment in public sector for constructing and launching of major infrastructure projects such as airports, universities, hospitals and connecting roads.
2. Support agricultural production in order to reduce rural and urban migration.
3. Develop technical and training centers.
4. Increasing the proportion of literates and providing of special facilities for training women.
5. Strengthening of municipalities to attain relative self-sufficiency, particularly in the provision of land for construction projects.

**REFERENCES**

- [1]. Babaei, A. (2002), Role Towns Small at Distribution Space Population (Case Study: Sistan and Baluchistan Province), M.A Thesis in Geography, University Sistan Baluchistan.
- [2]. Dashtei Brinj. C. (2000), Role Towns Small at Development Area (Case study: Tekab) M.A Thesis Shahid Beheshti University in Tehran.
- [3]. Fani. Z. (2003), Small towns in regional development approach, first edition, IMO publication.
- [4]. Hinrey, N. (2007), small Towns and urban planning in developing country, urban studies, vol33, N946.
- [5]. Hossainabadi. M. (2010), Analysis of the role of socio-economic development of small towns in the surrounding villages (Case Study: Ghiro kazin), Urban and Regional Studies and Research, No. 13, Vol 4, pp. 115 to 126
- [6]. Izadi Kharam. H. (2001), Role Currency Towns to City at Development Rural (Case Study: Fars Province), Thesis of PhD Geography and Program Planning Rural, Tarbiat Modarres University, Tehran.
- [7]. Lodrites and Wang. (2013). *A theory of good city from*. Cambridge: mit press
- [8]. Nadri. B. (2008), the role of small towns in sustainable development (case study: Ghaemieh \_ Fars), M.A thesis, Geography and Urban Planning, Shahid Beheshti University, Tehran.
- [9]. Papelli yazdi, M.H. (2003), Theory and around the city. Tehran: Publication SAMT. p 340.
- [10]. Razaei. M. (1999), Role Towns Small at Development Area A Sample Case Elam Province, M.A Thesis Isfahan University.
- [11]. Rezvani and et al, (2007), the role of the small towns in rural development using network analysis Roniz villages, Journal of Geographical Research, No. 61.
- [12]. Saifadini, F. (1999), The process of urbanization, the problem of big cities, Geographical Journal of Research, No. 1, P 75.
- [13]. Shakvei, H. (2008), New perspectives in urban geography, twelfth edition, Samt publisher, Tehran.
- [14]. Shirazi. M. (1999), Role Functional Towns Small at Development Rural (Case study: Hamidieh Province Khuzestan), M.A Thesis Shahid Beheshti University, Tehran.
- [15]. Slater and Dg, T. (2007). An evaluation of the sustainability of inner city residential projects. Housing, Theory and Society, 28(2), 144.
- [16]. UNCHC, (2009), small town and its position in third world, New York.
- [17]. Yamshita, M. (2004), Dec live and Approaches to Revitalization in Small Cities, the Case of Saga, Japan, Dela 21, P461-473.
- [18]. Ziari, K. (2001), Principles and methods of regional planning. Yazd, Yazd University Published, P 371.

## Microcontroller based new single-phase transformer less inverter for grid-tied photovoltaic system with constant common mode voltage

Nadia Afrin<sup>1</sup>, Monirul Islam<sup>2</sup>, Anarul Islam<sup>3</sup>

<sup>1</sup>Dept. of EEE, Pabna University of Science and Technology (PUST), Bangladesh.

<sup>2</sup>Dept. of EE, University of Malaya (UM), Malaysia.

<sup>3</sup>Dept. of CSE, Khulna University (KU), Bangladesh

**ABSTRACT**-Recently, transformerless inverters are becoming more attractive for grid-tied photovoltaic (PV) system because of high efficiency and low cost. Unfortunately, leakage current may flow through the whole grid-tied PV system due to fluctuating common mode (CM) voltage that depends on the topology structure and control strategy. Therefore, to meet the safety regulations, leakage current of transformerless PV inverter has to be addressed carefully. In this paper, a new microcontroller based transformerless topology with low leakage current is proposed for grid-tied PV system. A 16-bit dSPIC microcontroller is implemented to control the proposed topology. The proposed circuit structure and detail operation principle are presented in this paper. One additional switch with conventional full-bridge inverter and a diode clamping branch ensure the disconnection of PV module from the grid at the freewheeling mode and clamp the short-circuited output voltage to the half of DC input voltage. Therefore, the CM leakage current is minimized considerably. Meanwhile, MOSFET switches have been used in the proposed inverter to improve the efficiency at light-load condition. Finally, a prototype has been developed to verify the theoretical analysis and the experimental results show that the performance of the proposed inverter is as expected. It is found that the maximum efficiency and European efficiency of the proposed inverter is 98% and 97.52%, respectively.

**Keywords**-Common mode voltage; Converter; Grid connected; Leakage current; Photovoltaic; Transformer less.

### I. Introduction

Transformerless grid-tied inverter has many advantages such as high efficiency, low cost, smaller size, and weight. However, there is a galvanic connection between the power grid and the PV module due to the omission of transformer. As a result, a resonant circuit can be formed and a high frequency voltage fluctuation between the solar array and the ground that depends on the topology structure and control strategy, can electrify this resonant circuit. Thus a leakage current  $i_{\text{Leakage}}$  may induce due to the fluctuating CM voltage across the parasitic capacitor, flowing through the loop involving the inverter bridge, output filter, parasitic capacitors ( $C_{\text{pv1}}$  and  $C_{\text{pv2}}$ ), and the power grid [1-3]. Consequently, the grid current harmonics and total system losses are increased. A person, who touch the PV array and connected to the ground, may be conducted by the capacitive current. In the meantime, conducted and radiated interference will be brought in by the ground current [1, 4]. The instantaneous CM voltage and leakage current in the conventional full-bridge inverter shown in Figure 1 is defined as follows [5]:

$$V_{CM} = \frac{1}{2}(V_{AN} + V_{BN}) \quad (1)$$

$$i_{CM} = c_{PV} \frac{dV_{CM}}{dt} \quad (2)$$

where  $V_{AN}$  and  $V_{BN}$  are the voltages from mid-point A and B of the bridge leg to the reference terminal N. From the above analysis, it is clear that the CM voltage must be kept constant during the whole operation period to reduce the leakage current and many solutions have been proposed as follows [5-20]:

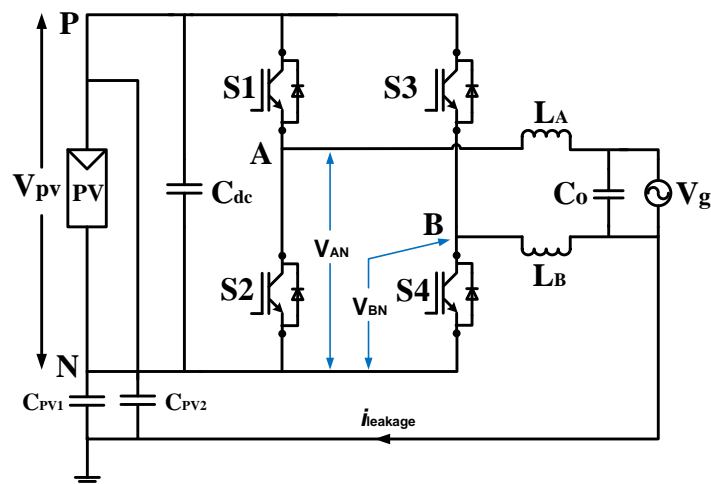
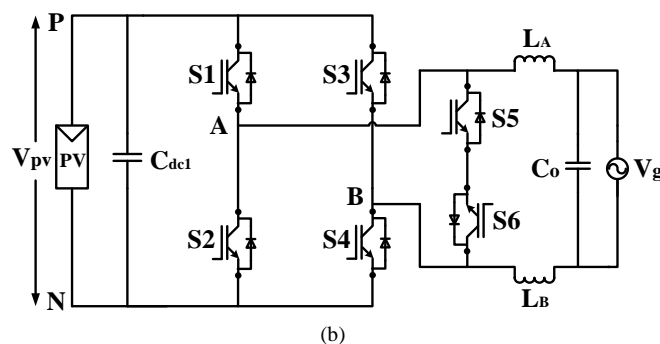
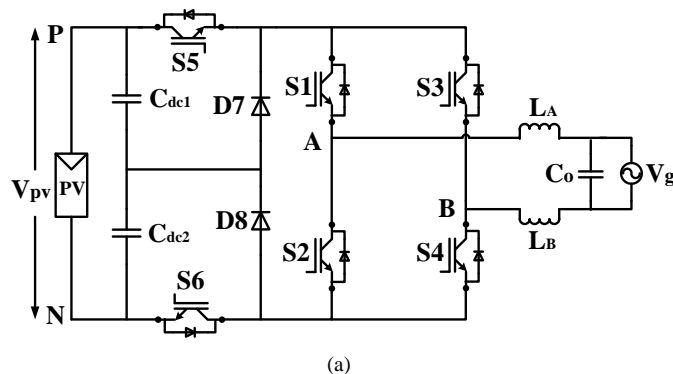


Figure 1: leakage current and parasitic capacitance in transformerless grid connected PV system

**(1) Bipolar sinusoidal pulse width modulated (SPWM) full-bridge inverter:** Bipolar SPWM modulation can be used to address the problem of leakage current in the conventional full-bridge inverter. This inverter can keep the CM voltage constant during the whole grid period. The main drawback of this inverter is the two-level output voltage. Consequently, the current ripples across the filter inductors are increased, results large inductor size, high losses and low efficiency. As well, it is difficult to maintain a good synchronization among the gate pulses of the power switches [2].

**(2) Unipolar sinusoidal pulse width modulated full-bridge inverter:** Unipolar SPWM is the most popular modulation implemented in full-bridge topology, because it shows a lot of benefits in comparison to bipolar SPWM such as lower current ripple at high frequency, better efficiency, lower electromagnetic interferences emission, etc. However, when unipolar SPWM is employed to the conventional full-bridge inverter; in active mode, the CM voltage  $V_{CM}$  is equal to  $0.5V_{pv}$  but in the freewheeling mode  $V_{CM}$  is equal to  $V_{pv}$  or 0 depending on the bridge-leg mid-points (point A and B in Fig. 1) coupled to the positive or negative terminal of the DC input. Therefore, the CM voltage of conventional full-bridge inverter fluctuates with high frequency which leads to high leakage current [2, 21, 22].



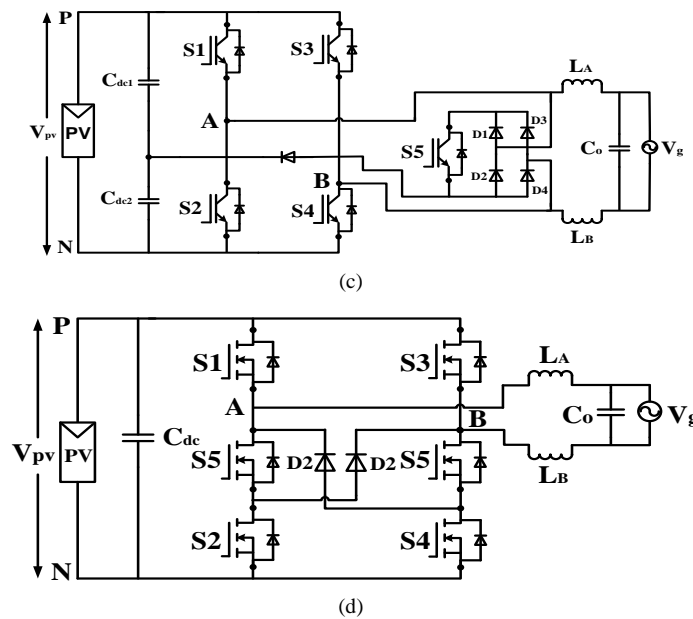


Figure 2: Some existing transformerless topologies for grid-tied PV inverter (a) H6 topology proposed in [5] (b) HERIC topology proposed in [16] (c) HB-ZVR topology proposed in [14] (d) H6 type topology proposed in [13].

In order to solve the problem of leakage current, the PV module should be separated from the grid during the freewheeling period and a lot of depth researches have been conducted from different countries. Most of the topology proposed in the literature is based on the structure of the freewheeling path, where a new freewheeling path has been created [5-18].

In this paper, a new structure of transformerless inverter for grid-tied PV system is proposed by adding an extra switch and a diode clamping branch with the conventional full-bridge inverter. The proposed inverter ensures the decoupling of PV module from the grid during the freewheeling period and the clamping of freewheeling voltage to the half of DC input voltage. As a result, the CM mode voltage is kept constant during the whole operation period and the induced leakage current is minimized to zero. In addition, unipolar SPWM can be employed to the proposed topology with three-level output voltage. The efficiency of the proposed inverter, H6 inverter and HERIC inverter are calculated and compared. Finally, a 1kW prototype is built and tested. The experimental results verify the theoretical analysis.

## II. H5 TOPOLOGY

### 2.1 Circuit configuration and operation principle

An explicit inverter topology proposed in [17] is called H5 topology which is shown in Figure 3. It is made up by adding an extra switch S5 with the full-bridge inverter. Unipolar SPWM has been applied to control this topology with three-level output voltage. This topology can meet the condition of eliminating CM leakage current. In the positive half cycle of grid current, switch S5 and S4 are commutated with switching frequency. During the zero voltage vectors, S5 and S4 are turned-off and freewheeling current flows through S1 and the anti-parallel diode of S3. In the negative half cycle, S5 and S2 are commutated with switching frequency and the freewheeling current flows through S3 and the anti-parallel diode of S1. A fluctuation of CM voltage can be observed with this topology because the freewheeling voltages are not clamped at the mid-point of DC input voltage. As a result, leakage current may not be fully eliminated with this topology.

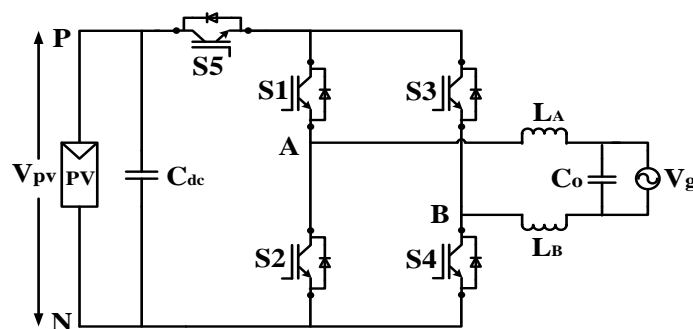


Figure 3: Power circuit of H5 topology

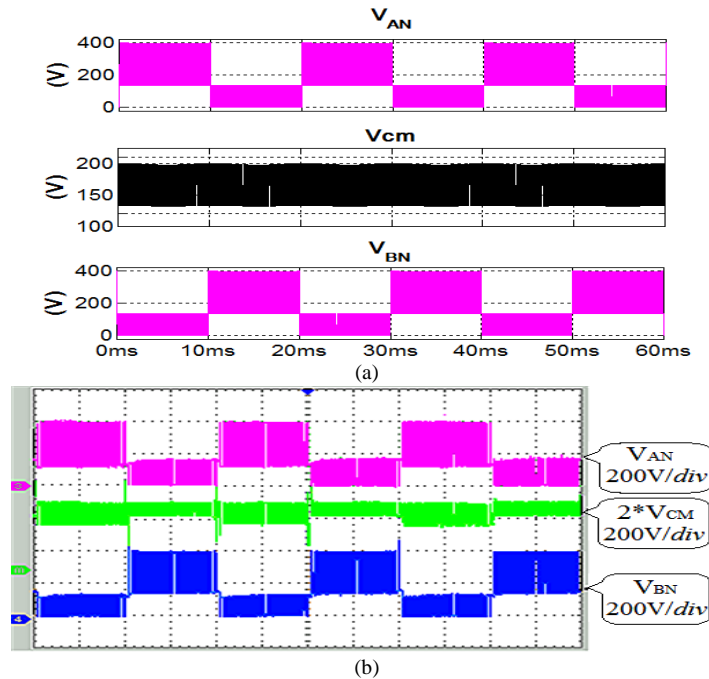


Figure 4: Waveform of  $V_{AN}$ ,  $V_{BN}$ , and  $V_{CM}$  of H5 topology: (a) simulation result (b) experimental result  
2.2 CM voltage and leakage current of H5 topology

The CM voltage and the leakage current for H5 topology can be calculated using equation (3) and (4) as follows:

$$V_{CM} = \frac{V_{AN} + V_{BN}}{2} \tag{3}$$

$$i_{CM} = c_{PV} \frac{dV_{CM}}{dt} \tag{4}$$

Figure 4 shows the simulated and experimental waveform of CM voltage and leakage current of H5 topology. It can be seen that a fluctuation of CM voltage is presented. Since there is no clamping circuit to clamp the freewheeling voltage; as a result, a fluctuation of CM voltage and non-negligible leakage current is observed with this topology. Therefore, it is important to clamp the freewheeling path voltage to the mid-point of DC bus to keep CM voltage constant.

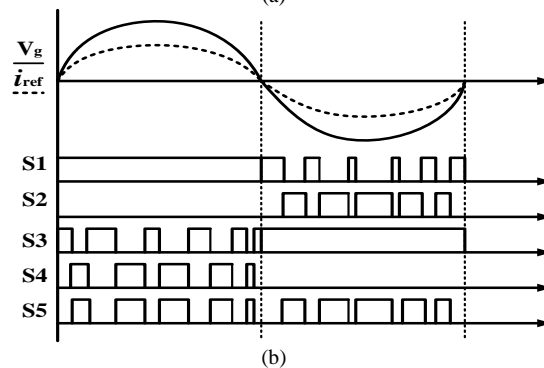
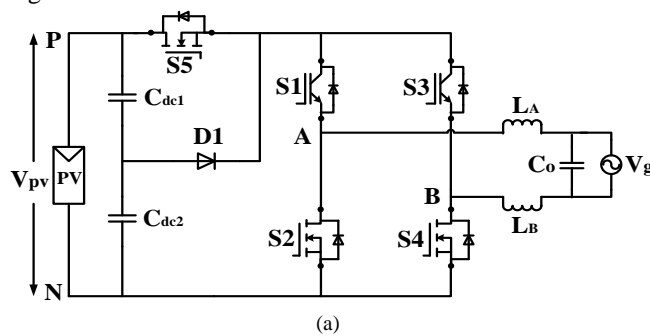


Figure 5: Proposed transformerless grid-tied PV inverter: (a) proposed circuit configuration (b) switching signals with unity power factor.

### III. PROPOSED TOPOLOGY

#### 1.1. Circuit Structure

In order to clamp the freewheeling path voltage to the mid-point of DC bus, a unidirectional clamping branch made up by a diode and a capacitor divider is added to the conventional H5 topology and the high-frequency IGBT switches from each phase leg are replaced by MOSFET switches which is shown in Figure 5(a). As a result, the PV module is decoupled during freewheeling period and also the CM voltage is clamped to half of DC input voltage.  $L_A$ ,  $L_B$ , and  $C_o$  constructs the LC type filter coupled to the grid. This topology can achieve three-level output voltage with unipolar SPWM.

#### 1.2. Operation principle analysis

Grid tied photovoltaic system generally operates at unity power factor. Figure 5(b) shows the waveform of the switching pattern for the proposed topology. The operation principle of the proposed topology is very similar to the H5 topology, which is shown in Figure 6. Consequently, four operational modes are proposed that produce the output voltage states of  $+V_{PV}$ , 0, and  $-V_{PV}$ .

Mode 1 is the active mode in the positive half cycle of grid current. When S1, S4 and S5 are turned-on, the voltage  $V_{AN} = V_{PV}$  and  $V_{BN} = 0$ , thus  $V_{AB} = V_{PV}$  and the CM voltage become:

$$V_{CM} = \frac{1}{2}(V_{AN} + V_{BN}) = \frac{1}{2}(V_{PV} + 0) = \frac{V_{PV}}{2} \quad (5)$$

Mode 2 is the freewheeling mode in the positive half cycle of grid current as shown in Fig. 6(b). The freewheeling current flows through S1 and body-diode of S3. In this mode, the CM voltage is clamped to the half of DC input voltage through diode D1, thus  $V_{AN} = V_{BN} = V_{PV}/2$  and  $V_{AB} = 0$ . The CM voltage could be as follows:

$$V_{CM} = \frac{1}{2}(V_{AN} + V_{BN}) = \frac{1}{2}\left(\frac{V_{PV}}{2} + \frac{V_{PV}}{2}\right) = \frac{V_{PV}}{2} \quad (6)$$

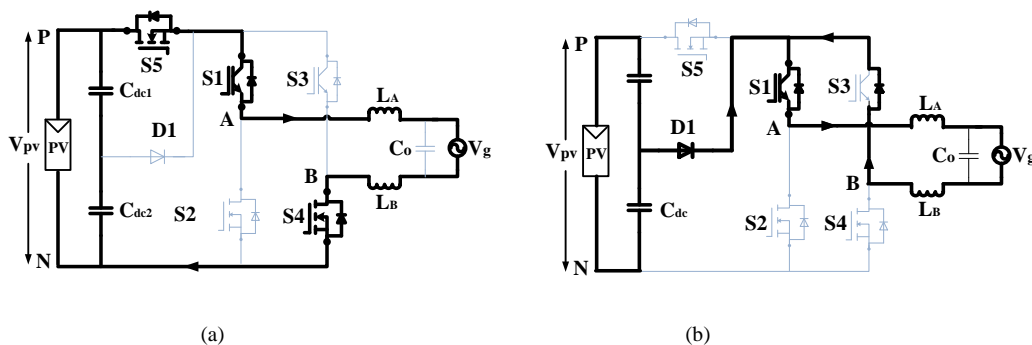
Mode 3 is the active mode in the negative half cycle of grid current. Like as mode 1, when S2, S3 and S5 are turned-on, the voltage  $V_{AN} = 0$  and  $V_{BN} = V_{PV}$ , thus  $V_{AB} = -V_{PV}$  and the CM voltage is,

$$V_{CM} = \frac{1}{2}(V_{AN} + V_{BN}) = \frac{1}{2}(0 + V_{PV}) = \frac{V_{PV}}{2} \quad (7)$$

Mode 4 is the freewheeling mode in the negative half cycle of grid current. When S5 and S2 are turned-off, the freewheeling current flows through S3 and body diode of S1 and the freewheeling path voltage is clamped to the mid-point of DC bus through D1. In this mode,  $V_{AN} = V_{BN} = V_{PV}/2$ , thus  $V_{AB} = 0$  and the CM voltage become,

$$V_{CM} = \frac{1}{2}(V_{AN} + V_{BN}) = \frac{1}{2}\left(\frac{V_{PV}}{2} + \frac{V_{PV}}{2}\right) = \frac{V_{PV}}{2} \quad (8)$$

As analysis above, the CM voltage remains constant during the four commutation modes of the proposed inverter and equals to  $V_{PV}/2$ . As a result, the inverter hardly generates any CM leakage current. However, if the freewheeling path voltage ( $V_{AN} \approx V_{BN}$ ) is less than  $V_{PV}/2$ , the diode D1 is forward biased and the freewheeling current flows from DC link to the freewheeling path. In contrast, if the freewheeling path voltage ( $V_{AN} \approx V_{BN}$ ) is greater than  $V_{PV}/2$ , the diode D1 is reverse biased. As a result, the CM voltage is not clamped at the mid-point of DC bus.



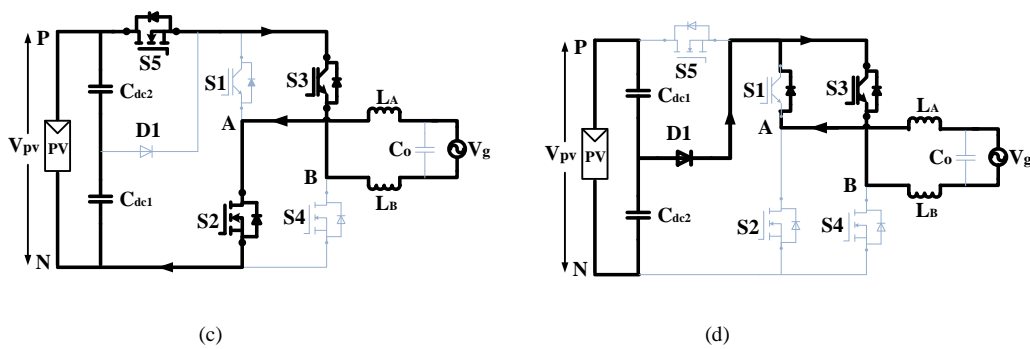


Figure 6: Operation principle of the proposed topology: (a) active mode and (b) freewheeling mode in the positive half cycle of grid current (c) active mode and (d) freewheeling mode in the negative half cycle of grid current

#### IV. SIMULATION AND EXPERIMENTAL RESULTS

In order to verify the theoretical analysis, a 1kWp PV array is simulated by MATLAB/Simulink software, having the frame of panels connected to the ground with the parasitic capacitance of 75nF. As well, a 1kW proposed inverter prototype is built and tested in our laboratory. The detail components and parameters are given in Table 1.

Table 1: Specification of the prototype

Inverter Parameter	Value
Input Voltage	400VDC
Grid Voltage / Frequency	230V / 50Hz
Rated Power	1000 W
AC output current	4.2A
Switching Frequency	20kHz
DC bus capacitor	470µF
Filter capacitor	2.2µF
Filter Inductor LA, LB	1mH
PV parasitic capacitor Cpv1, Cpv2	75nF
MOSFET switches	IPW60R041C6
IGBT switches	STGW30NC120HD

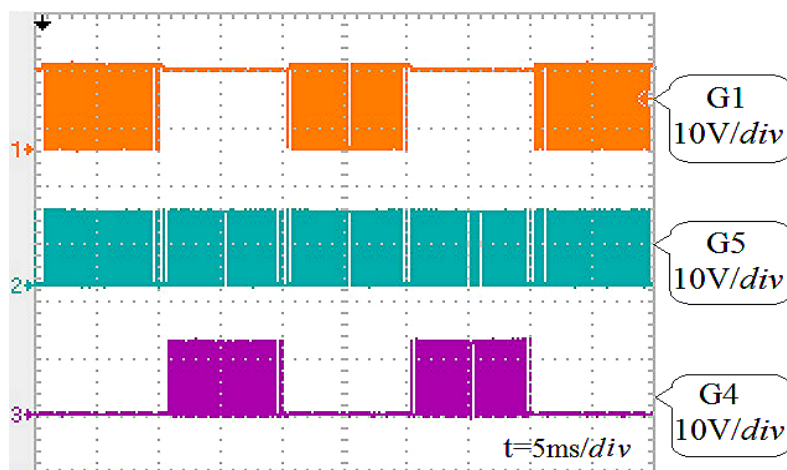


Figure 7: Gating signal of switches S1, S4, and S5

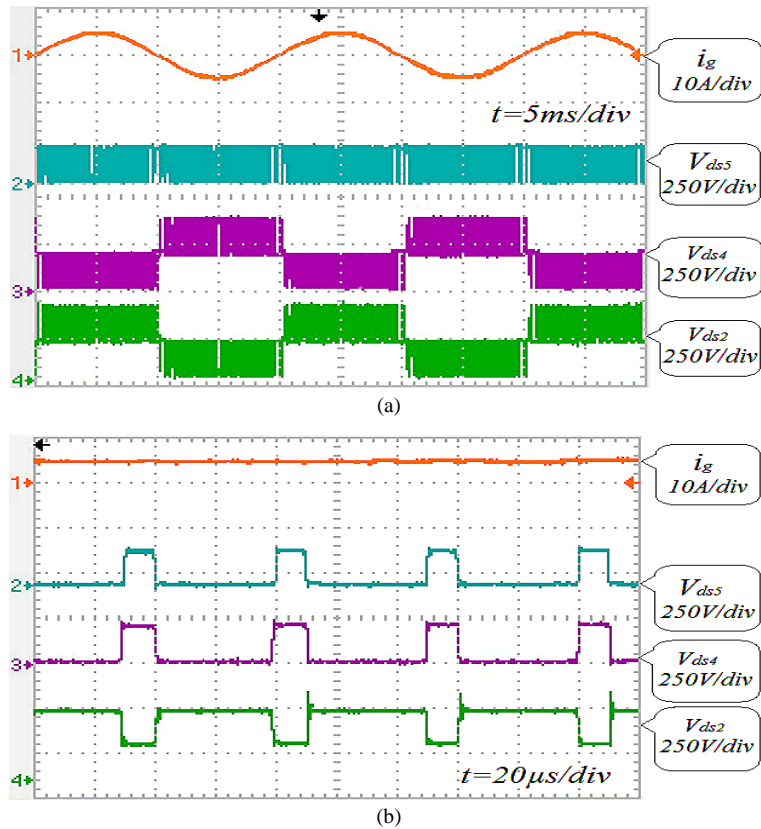


Figure 8: Drain-source voltage of the switches S2, S4, and S5 at (a) Grid cycle (b) PWM cycle

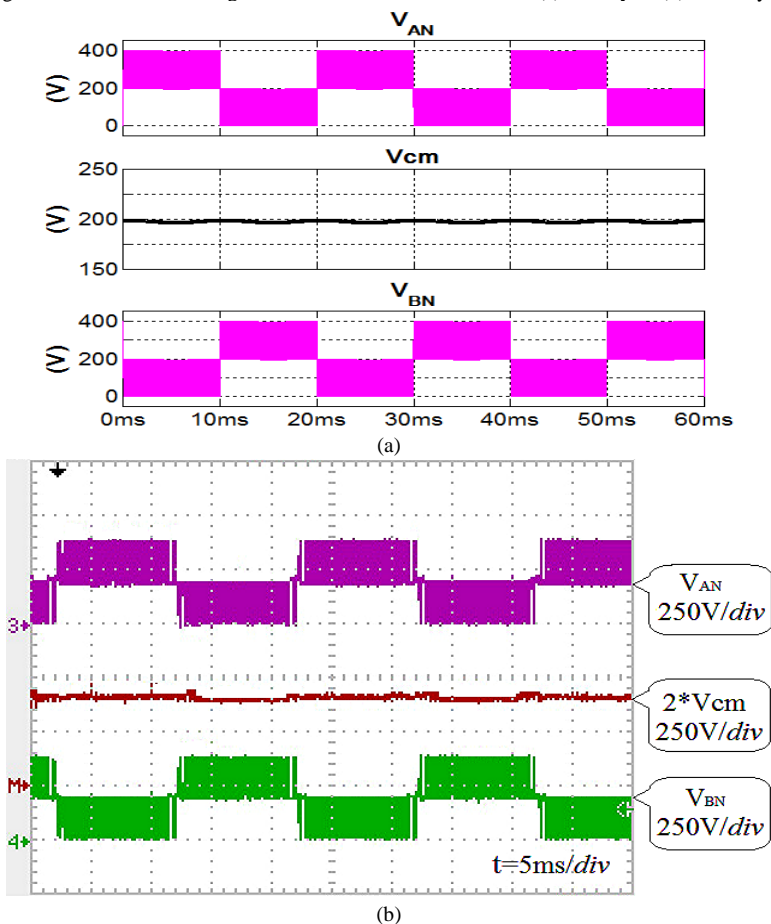


Figure 9: Waveform of volatge  $V_{AN}$ ,  $V_{BN}$  and  $V_{CM}$ : (a) simulation result (b) experimental result

The experimental gate signals are shown in Figure 7 for the grid cycle. It is clear that the gate signals are in agreement with the theoretical analysis made in section 3 and also the gate drive voltages are kept constant at the desired level. The voltage across drain to source of the MOSFET switches is shown in Figure 8. It can be seen that under symmetric transient condition, the switching voltage across the switches is clamped to the half of input voltage. As a result, the switching losses are reduced considerably.

Figure 9 shows the simulated and experimental waveform of voltage  $V_{AN}$ ,  $V_{BN}$ , and  $V_{CM}$ . As seen in Figure 9(a), the CM mode voltage is kept constant at 200V which is the half of the DC input voltage. The experimental waveforms are similar to the simulation results which are shown in Figure 9(b). As a result, the generated leakage current is very low as shown in Figure 10. The peak value and RMS value of CM leakage current is measured less than 20mA and 8mA, respectively. These peak and RMS values are lower in magnitude corresponding to the German standard VDE0126-1-1.

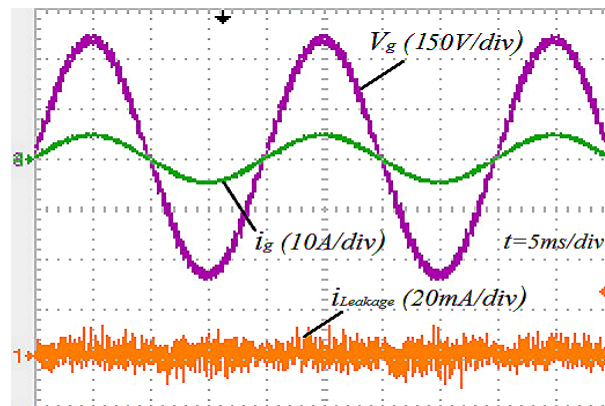


Figure 10: waveform of grid voltage, grid current and leakage current

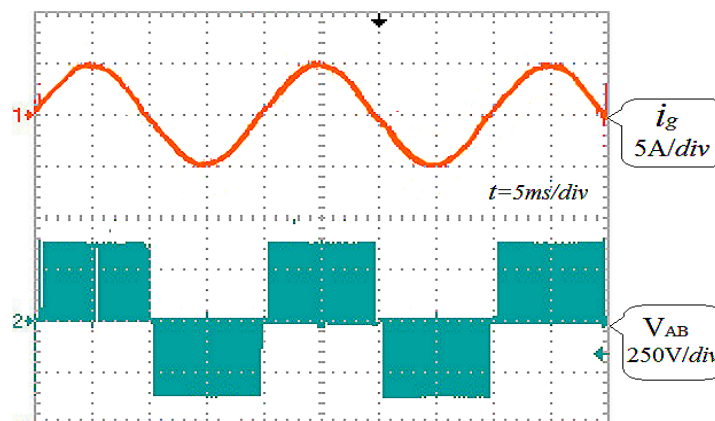


Figure 11: Differential mode characteristics of the proposed topology

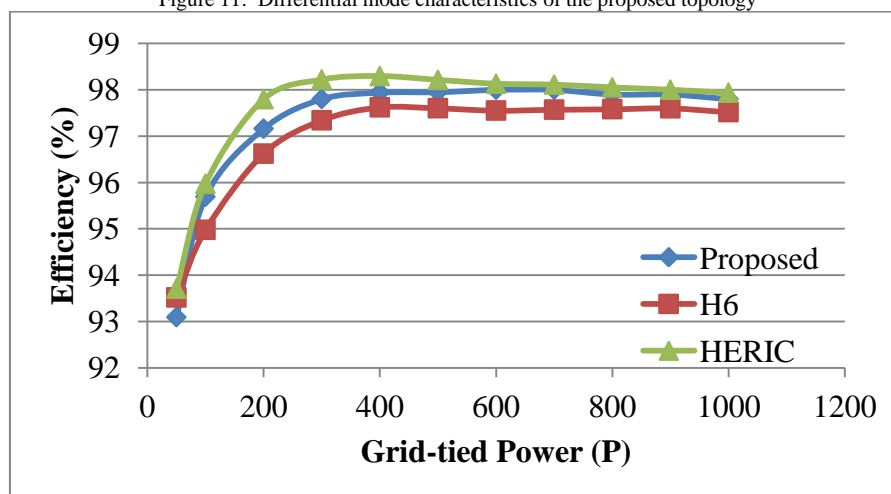


Figure 12: Efficiency comparison between the proposed topology, HERIC topology and H6 topology

The experimental waveform of grid current and grid voltage with full load condition are presented in Figure 10. It is varified from Figure 10 that the proposed inverter is operated with unity power factor. As well, the output voltage and current has low harmonic distortion which can meet the requirements of IEEE Std 1547.1™-2005. The experimental waveform of differential output voltage is shown in Figure 11. It can be seen that the proposed inverter has three-level output voltage as  $+V_{PV}$ , 0, and  $-V_{PV}$ . It designates that the proposed topology is modulated with unipolar SPWM having excellent differential mode characteristics. The efficiency comparison curve of the proposed topology, HERIC topology and H6 topology are illustrated in Figure 14. Note that the presented efficiency diagram covers the total device losses and the output filter losses but it does not include the losses for the control circuit. It is clear that the efficiency of the proposed topology is higher than the H6 topology and almost same to the HERIC topology. The European efficiency of the proposed topology, H6 topology and HERIC topology are 97.51, 97.15, and 97.83 respectively, which are calculated in equation (10).

$$\eta_{EU} = 0.03\eta_{5\%} + 0.06\eta_{10\%} + 0.13\eta_{20\%} + 0.10\eta_{30\%} + 0.48\eta_{50\%} + 0.2\eta_{100\%} \quad (10)$$

## V. CONCLUSION

In this paper, a new single phase transformerless inverter for grid connected PV system is presented. The proposed inverter has some advantages as: (1) the CM voltage of the proposed topology is clamped to the half of DC input voltage; as a result, leakage current is well suppressed, (2) it can achieve three-level output voltage by employing unipolar SPWM with good differential-mode characteristics, (3) no dead time is required at grid zero crossing instant which reduces the total harmonic distortion (4) the output current shows that the proposed inverter can convert the solar power into high quality ac power which constitutes an attractive feature. The maximum efficiency and European efficiency of the proposed inverter is measured 98% and 97.8%, which make it very attractive. Therefore, it can be concluded that the proposed inverter is very suitable for single-phase grid connected PV system.

## REFERENCE

- [1] Z. Li, S. Kai, F. Lanlan, W. Hongfei, and X. Yan, "A Family of Neutral Point Clamped Full-Bridge Topologies for Transformerless Photovoltaic Grid-Tied Inverters," *IEEE Transactions on Power Electronics*, vol. 28, pp. 730-739, 2013.
- [2] I. Patrao, E. Figueres, F. González-Espín, and G. Garcerá, "Transformerless topologies for grid-connected single-phase photovoltaic inverters," *Renewable and Sustainable Energy Reviews*, vol. 15, pp. 3423-3431, 9// 2011.
- [3] M. Islam, S. Mekhilef, and M. Hasan, "Single phase transformerless inverter topologies for grid-tied photovoltaic system: A review," *Renewable and Sustainable Energy Reviews*, vol. 45, pp. 69-86, 2015.
- [4] M. Islam and S. Mekhilef, "H6-type transformerless single-phase inverter for grid-tied photovoltaic system," *IET Power Electronics*, vol. 8, pp. 636-644, 2015.
- [5] R. Gonzalez, J. Lopez, P. Sanchis, and L. Marroyo, "Transformerless Inverter for Single-Phase Photovoltaic Systems," *IEEE Transactions on Power Electronics*, vol. 22, pp. 693-697, 2007.
- [6] H. Xiao, X. P. Liu, and K. Lan, "Zero-Voltage-Transition Full Bridge Topologies for Transformerless Photovoltaic Grid-Connected Inverter," *IEEE Transactions on Industrial Electronics*, vol. PP, pp. 1-1, 2014.
- [7] S. H. Lee, K. T. Kim, J. M. Kwon, and B. H. Kwon, "Single-phase transformerless bi-directional inverter with high efficiency and low leakage current," *IET Power Electronics*, vol. 7, pp. 451-458, 2014.
- [8] L. Zhang, K. Sun, Y. Xing, and M. Xu, "H6 Transformerless Full-Bridge PV Grid-tied Inverters," *IEEE Transactions on Power Electronics*, vol. PP, pp. 1-1, 2013.
- [9] W. Yong and L. Rui, "Novel High-Efficiency Three-Level Stacked-Neutral-Point-Clamped Grid-Tied Inverter," *IEEE Transactions on Industrial Electronics*, vol. 60, pp. 3766-3774, 2013.
- [10] G. Bin, J. Dominic, L. Jih-Sheng, C. Chien-Liang, T. LaBella, and C. Baifeng, "High Reliability and Efficiency Single-Phase Transformerless Inverter for Grid-Connected Photovoltaic Systems," *IEEE Transactions on Power Electronics*, vol. 28, pp. 2235-2245, 2013.
- [11] J. Baojian, W. Jianhua, and Z. Jianfeng, "High-Efficiency Single-Phase Transformerless PV H6 Inverter With Hybrid Modulation Method," *IEEE Transactions on Industrial Electronics*, vol. 60, pp. 2104-2115, 2013.
- [12] Y. Bo, L. Wuhua, G. Yunjie, C. Wenfeng, and H. Xiangning, "Improved Transformerless Inverter With Common-Mode Leakage Current Elimination for a Photovoltaic Grid-Connected Power System," *IEEE Transactions on Power Electronics*, vol. 27, pp. 752-762, 2012.
- [13] W. Yu, J.-S. Lai, H. Qian, and C. Hutchens, "High-efficiency MOSFET inverter with H6-type configuration for photovoltaic nonisolated AC-module applications," *IEEE Transactions on Power Electronics*, vol. 26, pp. 1253-1260, 2011.
- [14] T. Kerekes, R. Teodorescu, P. Rodriguez, G. Vazquez, and E. Aldabas, "A New High-Efficiency Single-Phase Transformerless PV Inverter Topology," *IEEE Transactions on Industrial Electronics*, vol. 58, pp. 184-191, 2011.
- [15] X. Huafeng, X. Shaojun, C. Yang, and H. Ruhai, "An Optimized Transformerless Photovoltaic Grid-Connected Inverter," *IEEE Transactions on Industrial Electronics*, vol. 58, pp. 1887-1895, 2011.
- [16] D. Schmidt, D. Siedle, and J. Ketterer, "Inverter for transforming a DC voltage into an AC current or an AC voltage," ed: EP Patent 1,369,985, 2009.
- [17] M. Victor, F. Greizer, S. Bremicker, and U. Hübler, "Method of converting a direct current voltage from a source of direct current voltage, more specifically from a photovoltaic source of direct current voltage, into a alternating current voltage," ed: United States Patents, 2008.

- [18] T. Salmi, M. Bouzguenda, A. Gastli, and A. Masmoudi, "A Novel Transformerless Inverter Topology Without Zero-Crossing Distortion," *International Journal of Renewable Energy Research (IJRER)*, vol. 2, pp. 140-146, 2012.
- [19] M. Islam, S. Mekhilef, and F. M. Albatsh, "An improved transformerless grid connected photovoltaic inverter with common mode leakage current elimination," in *7th IET International Conference on Power Electronics, Machines and Drives (PEMD 2014)*, 2014, pp. 1-6.
- [20] M. Islam and S. Mekhilef, "An improved transformerless grid connected photovoltaic inverter with reduced leakage current," *Energy Conversion and Management*, vol. 88, pp. 854-862, 2014.
- [21] X. Huafeng and X. Shaojun, "Leakage Current Analytical Model and Application in Single-Phase Transformerless Photovoltaic Grid-Connected Inverter," *IEEE Transactions on Electromagnetic Compatibility*, vol. 52, pp. 902-913, 2010.
- [22] M. Islam and S. Mekhilef, "High efficiency transformerless MOSFET inverter for grid-tied photovoltaic system," in *2014 Twenty-Ninth Annual IEEE Applied Power Electronics Conference and Exposition (APEC) 2014*, pp. 3356-3361.

## Measurement and Analysis of Magnetic Barkhausen Noise on the Surface of Grain Oriented Electrical Steels at Power Frequency.

Nkwachukwu Chukwuchekwa<sup>1</sup>, Onojo J. Ondoma<sup>1</sup> and Joy U. Chukwuchekwa<sup>2</sup>

<sup>1</sup>Electrical/Electronic Engineering Department, Federal University of Technology Owerri, Nigeria

<sup>2</sup>Department of Mathematics, Federal University of Technology Owerri Nigeria

**ABSTRACT:** Magnetic characteristics of Grain-Oriented Electrical Steel are generally measured at high flux densities (above 0.2 T) for applications in all electromagnetic devices. However, magnetic measurements at very low inductions are useful for characterisation of electrical steel used as cores of metering current transformers and low frequency magnetic shielding such as for protection from high field magnetic resonance imaging (MRI) medical scanners. In this work, Barkhausen noise, which is a non-destructive evaluation means of characterisation of electrical steels was accurately measured at very low flux densities for several samples of Conventional grain-oriented (CGO) and High Permeability grain-oriented (HGO) electrical steels. High flux density measurements were also carried out and compared. The results show that the Barkhausen signal amplitude sum and the root mean square values are higher for HGO than CGO steels at high flux densities. However, at lower flux densities the trend reverses. HGO steels are adjudged to have better magnetic properties than CGOs and so are more expensive but this work shows that CGO steels are better for very low flux density applications. This new understanding of low flux density performance of engineering magnetic materials will provide manufacturers with a more reliable and meaningful foundation for their designs.

**KEY WORDS:** Amplitude sum, Barkhausen noise, Electrical steel, RMS, Grain size

### I. INTRODUCTION

Electrical steel is comprised of grain oriented and non-grain oriented steels. Grain oriented electrical steel (GOES) is so called because it contains a grain structure with a distinct preferred orientation. The relative permeability and power loss are optimised when the material is magnetised along this direction of preferred orientation. For this reason GOES is usually used in the construction of medium to large transformer cores. GOES is comprised of the conventional grain oriented (CGO) and high permeability grain oriented (HGO) steels.

Non grain oriented (NGO) electrical steels contain a much finer grain structure and exhibit little or no preferred orientation. They are most commonly used in applications such as rotating electrical machines and small transformers used in domestic appliances that require isotropic magnetic properties in the plane of the sheet. In these applications, the magnetic flux is oriented at various angles with respect to the rolling direction of the sheet. As these materials are extensively used, they are responsible for a large portion of the energy loss in electrical power systems because of the non-linearity of the B-H characteristic. For this reason, the study and the control of the magnetic and microstructural parameters of these steels becomes a very important economic issue [1] and this accounts for the reason why these materials are investigated in this study.

Barkhausen Noise (BN) is a very important tool for non-destructive characterisation [2-4]. The BN mechanism can provide understanding of the microstructure of the material, without the use of laborious methods such as the Epstein frame typically used for characterisation of electrical steels. The Barkhausen effect arises from the discontinuous changes in magnetisation under the action of a continuously changing magnetic field when domain walls encounter pinning sites [5]. This noise phenomenon can be investigated statistically through the detection of the random voltage observed on a search coil placed on the surface or encircling the material during the magnetisation of the material. BN are related to the way domain walls interact with pinning sites, such as defects, precipitates and grain boundaries, as domains reorganise to align magnetic moments in the direction of the applied magnetic field. The number of Barkhausen emissions is determined by the number of pinning sites provided that the volume of the sites is sufficient to cause pinning. BN is therefore an important tool for evaluating the scale of interaction between pinning sites of varying sizes and magnetic domains [6].

Microstructural features such as grain size, number and distribution of pinning sites, grain boundaries and grain-grain misorientation are the main parameters that distinguish CGO from HGO steels in relation to their bulk magnetic properties. Magnetic characteristics of electrical steel are usually measured at the high flux densities suitable for applications in power transformers, motors, generators, alternators and a variety of other electromagnetic applications. Magnetic measurements at very low inductions are useful for magnetic characterisation of electrical steel used as cores of metering instrument transformers and low frequency magnetic shielding such as for protection from high field MRI (magnetic resonance imaging) medical scanners. Magnetisation levels in these applications are generally believed to be in the low flux density region so material selection based on high flux density grading is seriously flawed.

In this work, Barkhausen noise measurement was carried out on samples of CGO and HGO steels, 305 mm x 30 mm x 0.27 mm from two different producers named P1 and P2. 40 strips from P1 comprising 20 CGO and 20 HGO strips were tested. Another 40 strips from P2 comprising 20 CGO and 20 HGO strips were also tested. The average grain size for CGO is 4  $\mu\text{m}$  and that of HGO is 9  $\mu\text{m}$ . The samples were demagnetized by annealing in vacuum at 810 $^{\circ}$  for 1 hour.

Each strip was singly magnetised under sinusoidal flux density,  $B_{\text{peak}}$ , from 8.0 mT to 1.5 T at a magnetising frequency of 50 Hz. Each measurement of BN was made three times and then averaged. BN studies aimed at non-destructive testing applications are usually carried out under quasi-static or very low frequency magnetisation conditions but 50 Hz has been chosen in this work because it is believed that at this frequency the BN signal is possibly more related to dynamic processes and can give more information about the magnetisation processes which low frequency BN measurements cannot. Such information include eddy current anomalous loss influence on magnetisation.

## II. METHODOLOGY

A computer-controlled system capable of providing high accuracy and automatic measurements was developed for the measurement of BN of electrical steels at high and low flux densities. Figure 1 shows a schematic diagram of the system. It comprises a personal computer (PC) in which LabVIEW (Laboratory Virtual Instruments Engineering Workbench) version 8.5 from National Instruments (NI) was installed, a NI 4461 data acquisition (DAQ) card [7], an impedance matching transformer, Krohn-Hite model MT- 56R, to match the 600  $\Omega$  minimum load impedance of the DAQ card with the 5 to 20  $\Omega$  low impedance of the magnetising circuit, and a 4.7  $\Omega$  shunt resistor ( $R_{\text{sh}}$ ) from Tyco Electronics BDS2A1004R7K having less than 40 nH inductance corresponding to reactance of 12.6  $\mu\Omega$ , so adds virtually no error to amplitude and phase of the current measurement. The shunt resistor has 100 W power rating and low Temperature Coefficient of Resistance (TCR) (150ppm/ $^{\circ}\text{C}$ ). Low TCR was necessary to ensure that changes in its temperature will not affect the overall accuracy of the system. The shunt was attached to a thermo electric heat sink device, model TDEX3132/100, in conjunction with silicon based thermal grease. A double vertical yoke made of grain-oriented (GO) steel which is 290 mm long and 32 mm wide was used. A 500-turn secondary winding (search coil,  $N_2$ ), about 80 mm in length, was wound around a plastic former, 270 mm x 40 mm, housing the sample, while a 100-turn primary winding (magnetising coil), covering the entire length of the plastic former was wound over the secondary winding. A standard Epstein strip (305 mm x 30 mm) to be tested is placed between the yokes.

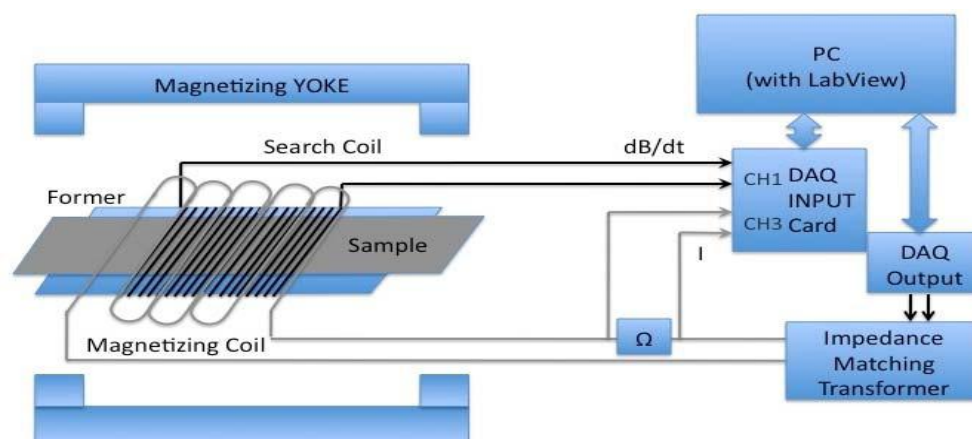


Fig 1: Block diagram of Barkhausen Noise measurement system.

The magnetising voltage was generated by the LabVIEW program through a voltage output from the DAQ card. The voltage drop across the shunt resistor,  $V_{\text{sh}}$ , and the secondary voltage,  $e$ , were acquired by the

card for calculation of magnetic field strength and flux density respectively. The sampled waveforms of  $e$  and  $V_{sh}$  had 3000 points per cycle which is large enough to avoid quantization errors. The instantaneous magnetic field strength,  $H(t)$  was calculated inside the LabVIEW program thus;

$$H(t) = \frac{N_1 i(t)}{l_m} \quad (1)$$

where  $i(t) = \frac{V_{sh}}{R_{sh}}$ ,  $N_1$  is the number of primary turns,  $l_m$  is the magnetic path length, which is the distance between the inner edges of the yoke which is 0.27 m in this system. The instantaneous flux density  $B(t)$  was obtained by means of digital integration of the  $e$  signal as:

$$B(t) = - \frac{l\rho}{N_2 m} \int e dt \quad (2)$$

where  $l$  is the sample length,  $m$  is the mass of the sample, and  $\rho$  is the density of the sample. A feedback control system implemented in LabVIEW was used to control the flux density and to make the induced secondary voltage waveforms sinusoidal to have repeatable and comparable measurements. The form factor (FF) of the induced secondary voltage was maintained at  $1.111 \pm 0.3\%$  which satisfies the recommendation in [8] to ensure that the time variation of the flux density was sinusoidal over the measurement range. Figure 2 shows the procedure for each measurement. Firstly, a table of peak flux density ( $B_{peak}$ ) values and the measurement criteria which are the 0.3% error of  $B_{peak}$  and the 0.3% error of the ideal FF of the induced secondary voltage was read. This is followed by applying the first magnetising waveform to the single sheet tester. If the criteria are met, the flux density and the magnetic field waveforms are averaged to minimise random errors and improve repeatability [9], otherwise the magnetising waveform is adjusted by the feedback algorithm. After averaging, the criteria are re-checked then the measurement data for this point is saved. A spread sheet file is generated if all the values of  $B_{peak}$  are measured and the sample is demagnetised by reducing the magnetic field gradually to zero.

The system is capable of low-field measurements because the 24 bit resolution of the NI data acquisition card makes it capable of sensing signals as small as  $10^{-6}$  V.

The secondary voltage was filtered to remove the dominant Faraday emf in order to obtain the BN signals. A digital band pass filter was used so that components in the range 25 kHz to 75 kHz were detected at a magnetizing frequency of 50 Hz. It was at this bandwidth that the Barkhausen emission which is maximum at the coercive points was detected. One search coil technique rather than a double coil arrangement was used to avoid losing some Barkhausen events in the subtraction process [10].

The major challenge in BN measurement is the reduction of background noise. The low noise NI4461 card with 24 bit resolution and a sampling rate of 204.8 KHz and 92 KHz bandwidth was chosen to take the measurements to minimize the influence of thermal noise. The card was placed in a PXI (Peripheral component interconnect eXtension for Instrumentation) platform instead of in a computer system hence it operates in a predictable environment which means the measurements are more reliable and repeatable. In order to reduce environmental noise, the yokes, sample and search coil carrier were placed in a noise shielding chamber. Figure 3 shows the measurement system in the noise shielding chamber and the DAQ in a PXI interface. The computer monitor was remote from the measuring system to avoid interference with the measurements. Coaxial cables were used for all connection leads.

The acquired data was analysed using a number of algorithms that included root mean square (RMS) and total sum of amplitudes (TSA). The data was saved to a file for further processing after analysis. RMS is the mean event amplitude over the range of flux in the BN cycle and is expressed as:

$$\text{rms}\psi = \sqrt{\frac{1}{N} \sum_{i=0}^{N-1} x_i^2} \quad (3)$$

where  $x$  represents each event amplitude and  $N$  stands for the number of events.

The measured sum of amplitudes (over  $n$  cycles) is given by:

$$\text{Amplitude sum} = \sum_{i=1}^{z=n} \left( \sum_{k=1}^m (|a_k|) \right)_i \quad (4)$$

where variable 'a', represents the amplitude of a measured data point, index 'k' shows its position within the measured data point array 'm'. Variable 'z' indicates that the measurement has been taken n times successively. Index 'i' displays how often the measurement has been carried out [11].

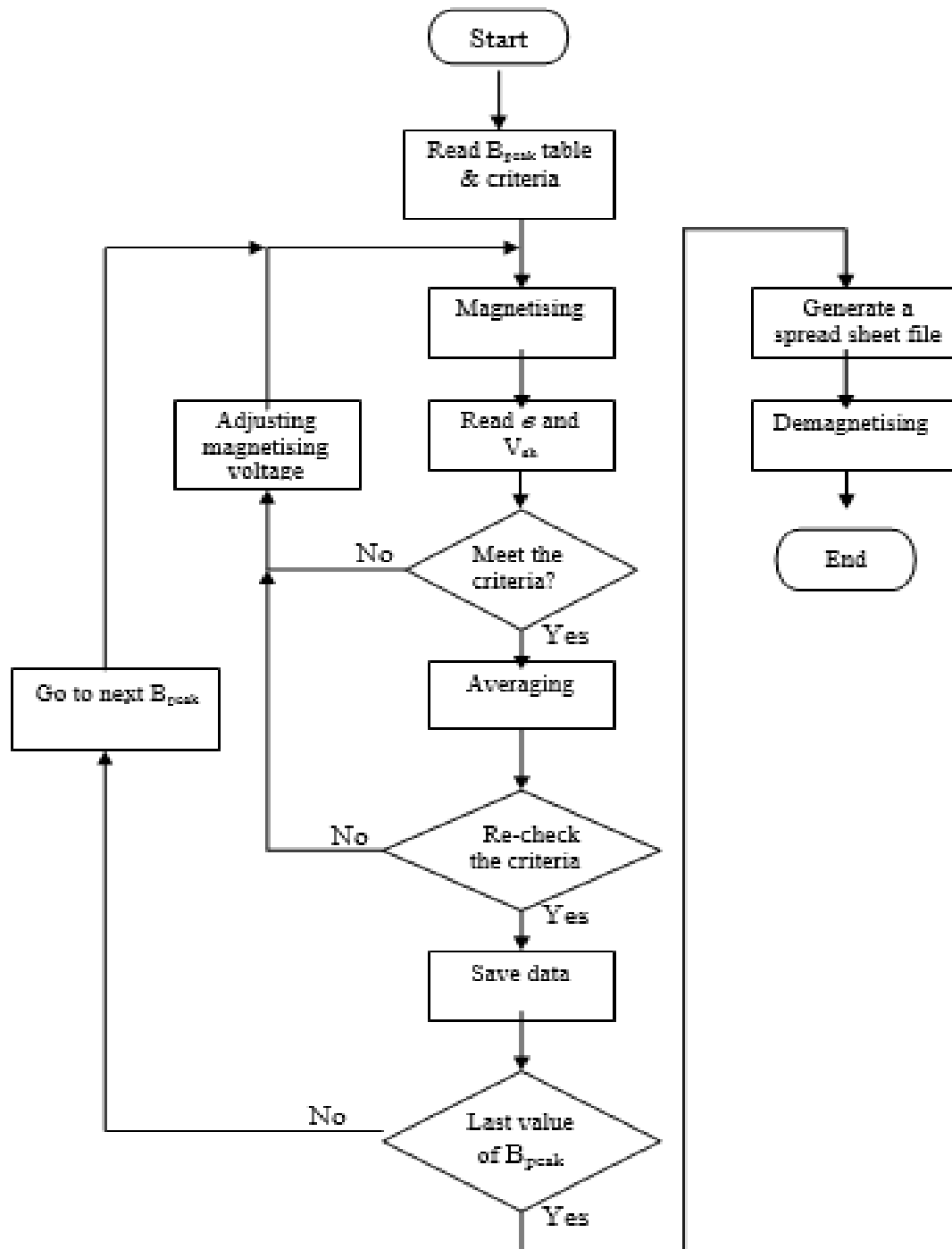


Fig. 2 Flowchart showing procedure of each measurement of the single strip tester

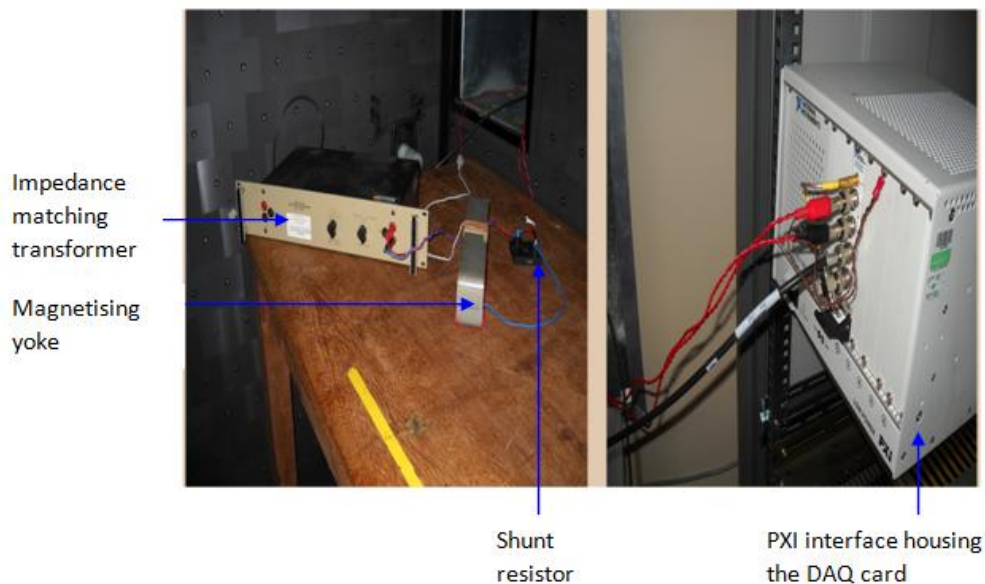


Fig. 3: Barkhausen Noise measurement system in the noise shielding chamber and the PXI platform housing the data acquisition card [12].

### III. RESULTS AND DISCUSSION

Figures 4 and 5 show typical BN spectra obtained from HGO and CGO steels at 1.2 T and 50 Hz. The sinusoidal curve is the flux density waveform at a 1000 times smaller scale. One cycle of magnetisation is shown. As expected, the BN is highest at points in time corresponding to when the material was experiencing maximum rate of change of magnetisation at the coercive fields [11, 13]. The coercive fields are the points where the flux density waveforms are zero in the figures. As can be observed from the figures, the BN amplitude is higher in HGO with the maximum peak occurring at 2mV while the maximum peak in CGO occurs at 1.4mV and this shows that the BN induced voltage in HGO is higher than that of CGO especially at high flux densities as subsequent results in this investigation show.

Figure 6 shows the RMS values of the BN spectra shown in figures 4 and 5 above as well as the background noise of the experimental set up at all the peak flux densities measured. Preliminary test determined the background noise level in the experimental set up. The same relationship was obtained when the background noise was plotted against the TSA. It can be observed from the figure that the background noise is more than 100 times less than the BN amplitude of the test samples. This was achieved by applying all the background noise reduction techniques outlined earlier. Background noise reduction is particularly challenging at very low inductions and measurements must be made in an environment free from electromagnetic interference.

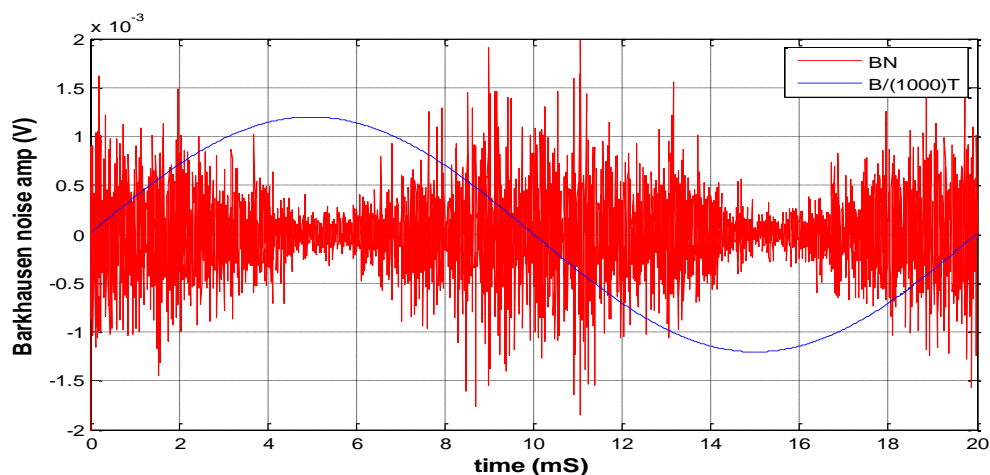


Fig.4: BN spectrum of HGO steel during one cycle of magnetisation at 1.2 T and 50 Hz showing variation of BN amplitude with time.

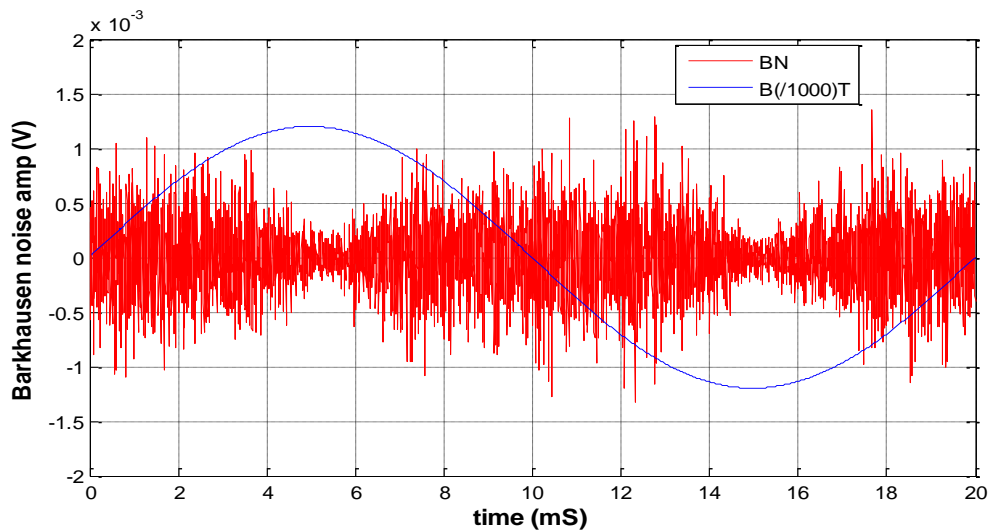


Fig. 5: BN spectrum of CGO steel during one cycle of magnetisation at 1.2 T and 50 Hz showing variation of BN amplitude with time.

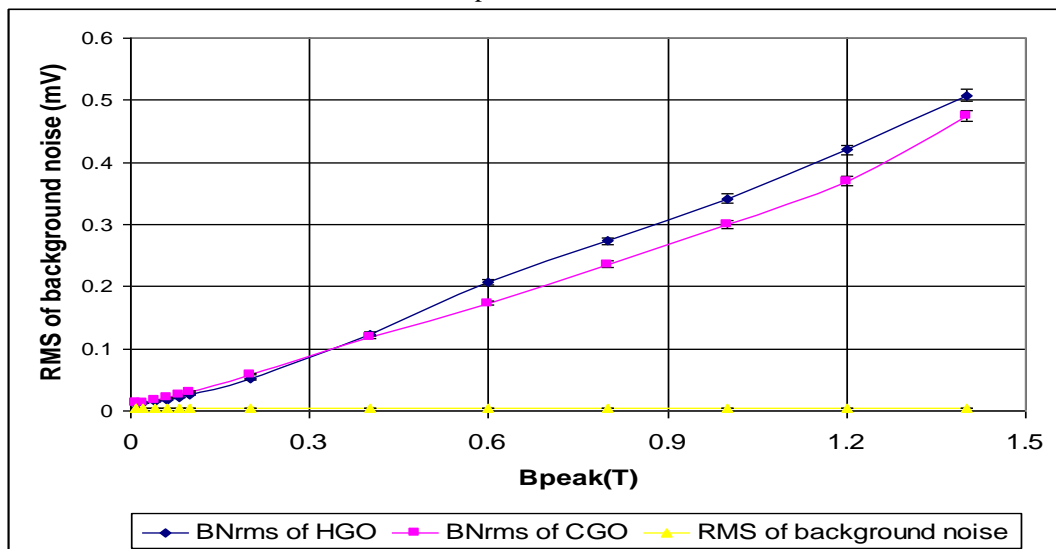
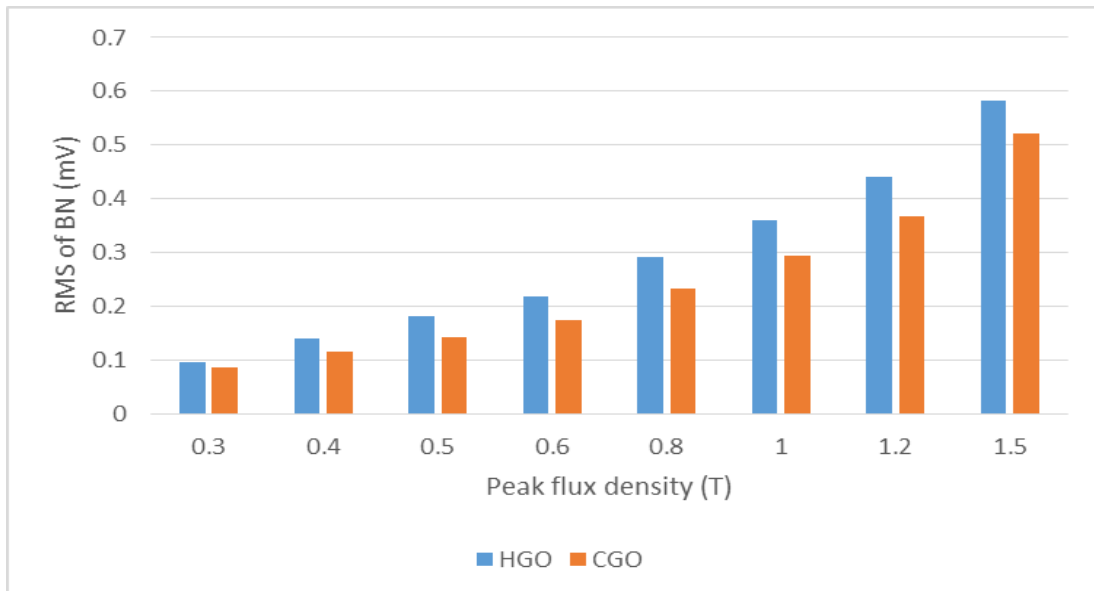


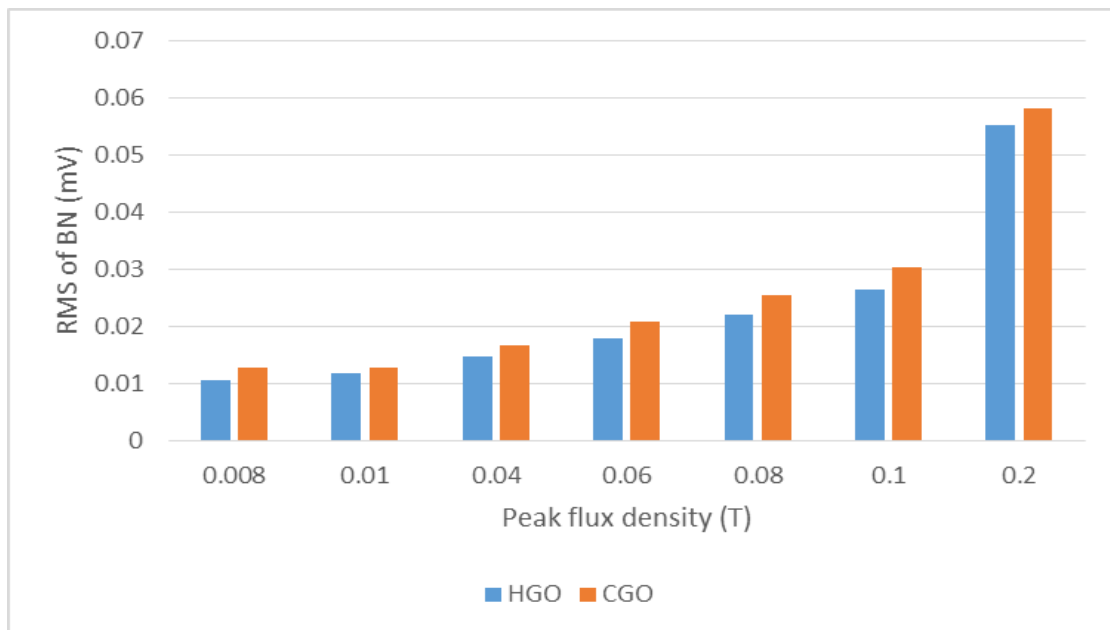
Fig. 6: Comparison of average rms BN of CGO and HGO strips at different flux densities at 50 Hz with background noise of Experimental set-up.

Figure 7 shows the variation of average RMS BN of 20 strips of CGO and 20 strips of HGO from P1 at both high and low flux densities. It can be observed that the average RMS BN is higher in HGO than in CGO above 0.2 T but at lower flux densities the trend changes. A similar characteristic was obtained when the same number of test samples from P2 was investigated at both magnetisation regimes. This is shown in figure 8. The variation of the percentage difference of the average rms BN of these test samples with peak flux density is shown in figure 9.

Figure 10 shows the same BN signals expressed in terms of the average TSA of BN peaks of the test samples from P1. As with the rms BN, the TSA of HGO is higher than that of CGO above 0.2 T and the trend changes at lower flux densities. TSA of samples from P2 show the same relationship as with P1 and is plotted in figure 11 with the variation in percentage difference at both high and low flux densities shown in figure 12.

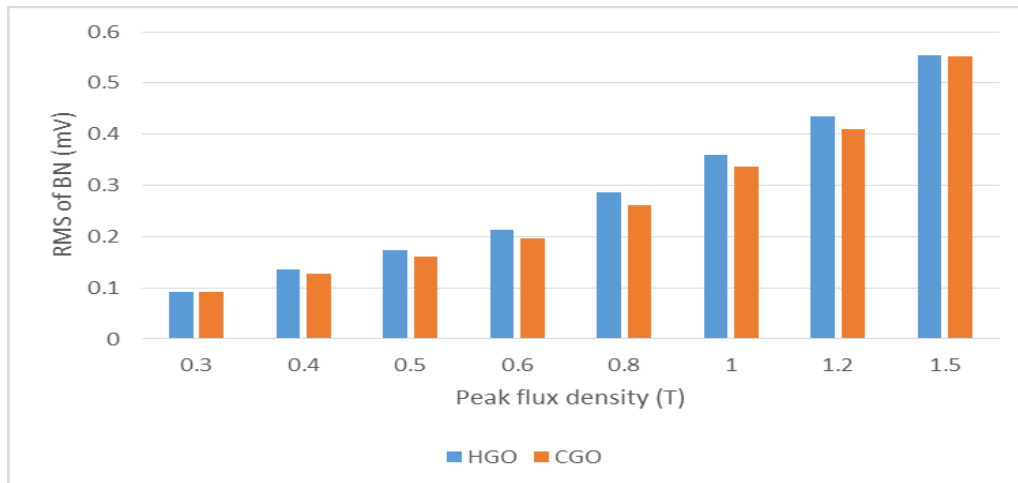


(a)

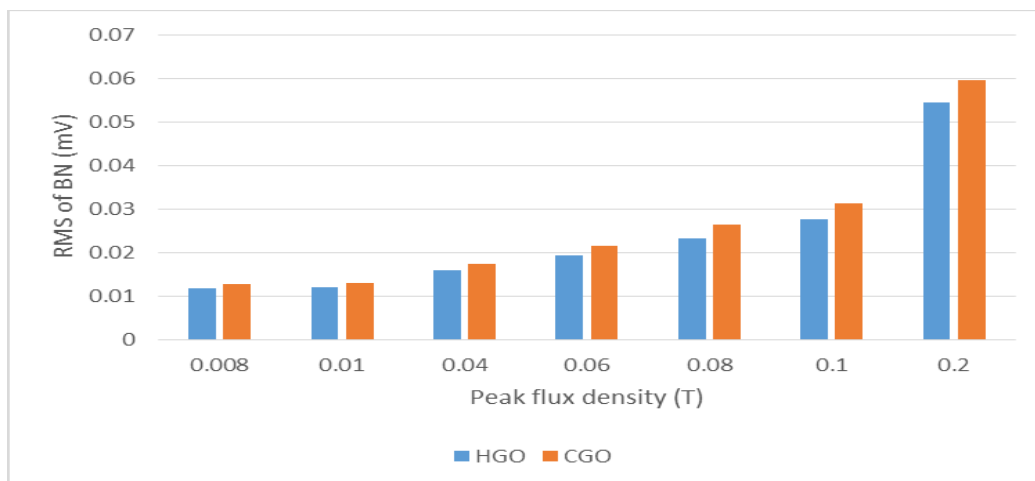


(b)

Fig. 7: (a) Variation of average rms BN of 20 strips each of CGO and HGO from P1 with peak flux density (b) the same comparison in the low field regime.



(a)



(b)

Fig. 8: (a) Variation of average BNrms of 20 strips each of CGO and HGO from P2 with peak flux density (b) the same comparison in the low field regime.

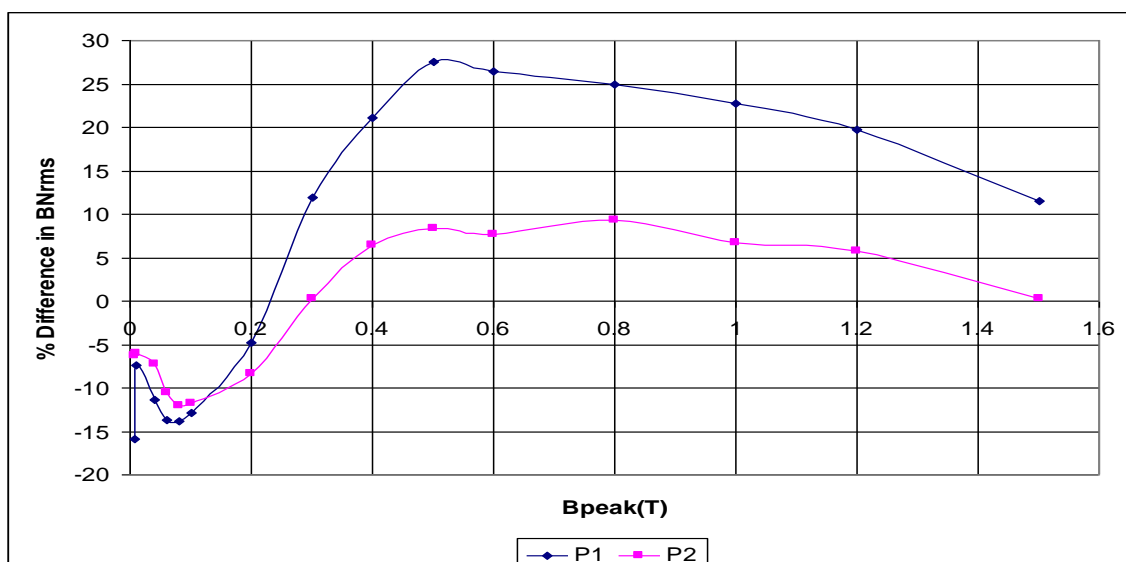
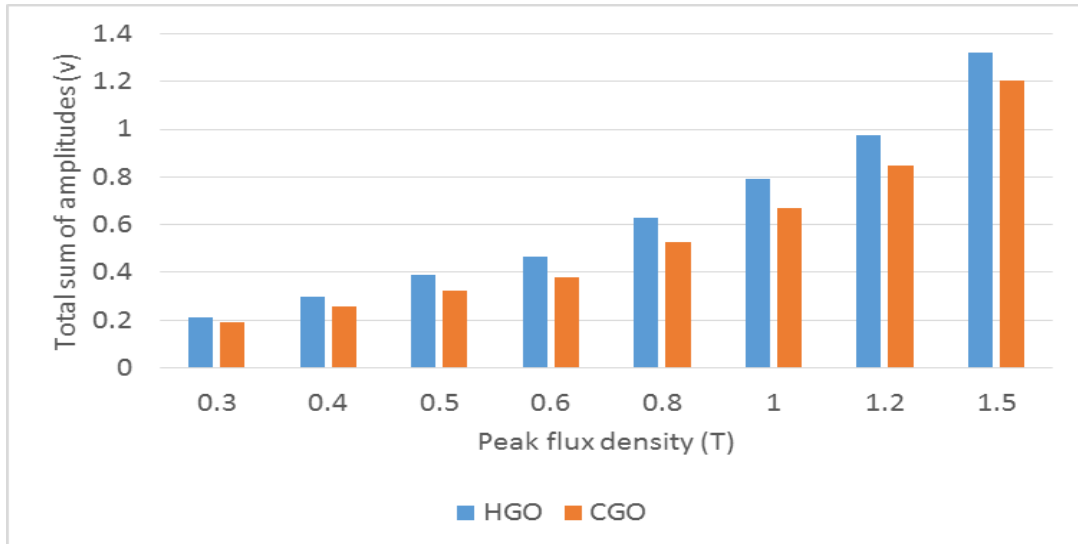
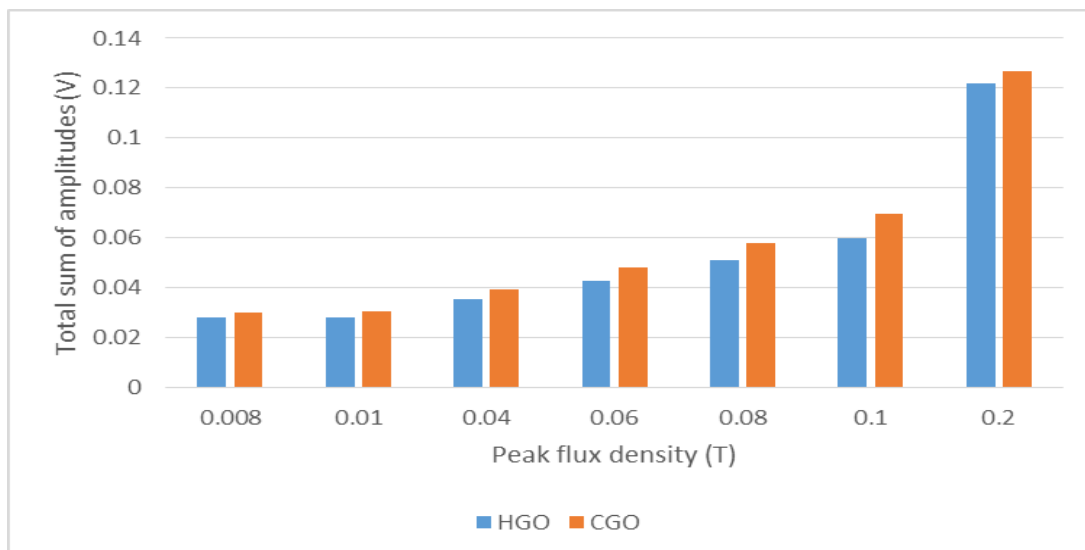


Fig. 9: Variation of percentage difference of average rms BN of HGO and CGO from P1 and P2 with peak flux density.

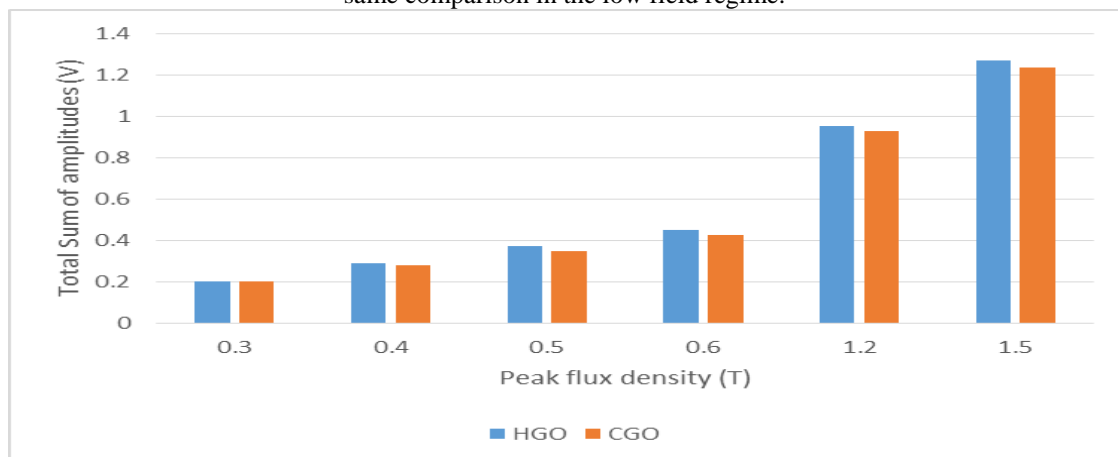


(a)



(b)

Fig. 10: (a) Variation of average TSA of 20 strips each of CGO and HGO from P1 with peak flux density (b) the same comparison in the low field regime.



(a)

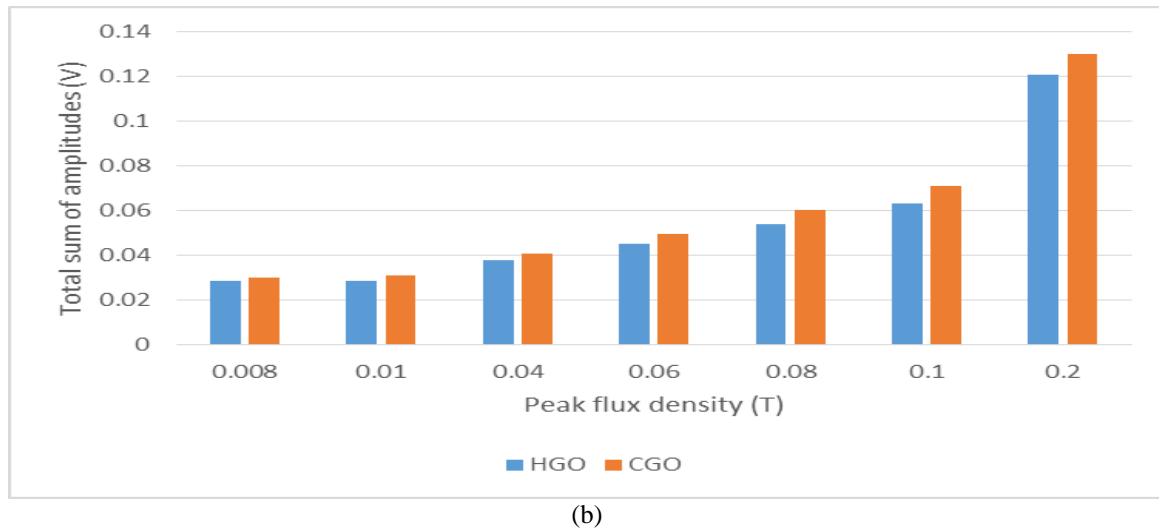


Fig. 11: (a) Variation of average TSA of 20 strips each of CGO and HGO from P2 with peak flux density (b) the same comparison in the low field regime.

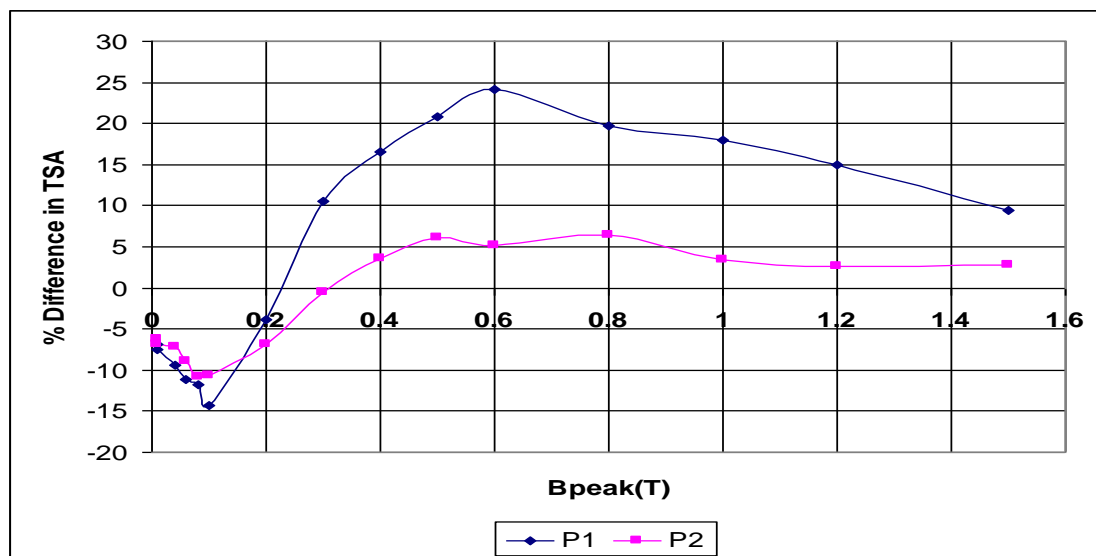


Fig. 12: Variation of percentage difference of average TSA of HGO and CGO from P2 with peak flux density.

As figures 9 and 12 show, it is interesting that below 0.2 T, the percentage difference in average rms BN of the test samples from P1 and P2, and that of the average TSA respectively are very similar but at high flux densities, they are far different. This is because domain wall activity is higher at high flux densities so the effects of the difference in microstructure of the samples which account for BN will be more pronounced than at low field regime.

The observed higher BN response in terms of average rms and average TSA of HGO over CGO at higher flux densities in this work is because the grain size of HGO is higher than that of CGO and also grain to grain misorientation in CGO is higher than that of HGO. The domain width in GOES increases with increasing grain size. Increased grain size means that domain walls will move further between pinning sites and thereby generate larger changes in magnetization which results in a larger BN signal amplitude. The theoretical analysis below confirms that BN is proportional to the mean free path of domain wall movement. For the purpose of analysis of the theoretical relationship between BN and the microstructures of electrical steels, an induced voltage (Barkhausen) pulse is approximated by a Gaussian pulse to facilitate mathematical treatment [14].

A Gaussian pulse at a time  $t$ , is expressed mathematically as:

$$v(t) = \frac{A}{\sigma \sqrt{2\pi}} \exp\left[-(t - t_0)^2 / 2\sigma^2\right] \quad (5)$$

Where  $A$  is a quantity which is a function of maximum applied field,  $H$ , rate of change of field with time,  $dH/dt$  and the magnetic flux change,  $\Delta\Phi$ , in the magnetization region,  $\sigma$  is the pulse duration and  $t_0$  is the time when the pulse is a maximum value. The total voltage induced in a search coil wound around a sample during experiment are obtained by summing the successive Gaussian pulses.

Assuming that  $\sigma$  and the time interval of Gaussian pulse,  $\tau$ , are constant;

$$v_{total}(t) = \sum_{k=1}^N v_k(t) = \frac{A}{\sigma \sqrt{2\pi}} \sum_{k=1}^N \exp\left[-\{t - t_0 - (k-1)\tau\}^2 / 2\sigma^2\right] \quad (6)$$

where  $v_k(t)$  the  $k$ 'th Gaussian pulse and  $N$  is the number of total Gaussian pulses in a magnetization period,  $T$ .

$$N = T / \tau \quad (7)$$

The amplitude value of the Gaussian pulse is

$$P_y = \frac{A}{\sigma \sqrt{2\pi}} \quad (8)$$

The sum of the amplitude values of the Gaussian pulses,  $P$ , in a whole period,  $T$ , is

$$P = \int_T P_y dt \quad (9)$$

The number of Gaussian pulses in  $T$  is  $N$ . The RMS value is the average of  $P_y$  over the range of the time for magnetization reversal. Thus,

$$\begin{aligned} RMS &= kP_y \tau \\ &= C_r \frac{\tau}{\sigma} \end{aligned} \quad (10)$$

where  $C_r = \frac{AK}{\sqrt{2\pi}}$  depends on the magnetizing conditions and  $K$  is a constant.  $\sigma$  and  $\tau$  are correlated with

microstructure of the material and depends on the mean free distance.

When a domain wall moves from one pinning site to another, a Gauss pulse is generated and the Barkhausen jump occurs with a time duration  $\sigma$ .

$$\sigma = D / S \quad (11)$$

Where  $D$  is the displacement of the domain wall (mean free distance) and  $S$  is the average speed of the domain wall movement.

The average speed of the domain motion is proportional to the external field, thus;

$$S = C_s H_n \quad (12)$$

where  $H_n$  is the minimum field strength of the external magnetic field required to unpin a domain wall from the pinning site and produce irreversible motion.  $C_s$  is a proportionality constant.

$$H_n = \frac{1}{2\mu_0 M_s \cos \Theta} \left(\frac{\partial E}{\partial x}\right)_{\max} \quad (13)$$

where  $\mu_0$  is the initial permeability,  $M_s$  is the saturation magnetization,  $E$  is the domain wall energy, and  $\Theta$  is the angle the external field axis makes with the direction of easy magnetization.

Assuming that the inclusion that pin a domain wall is spherical, its diameter is  $l$  and its arrangement is a regular and simple cubic lattice, the domain wall is pinned and stopped in the center of the inclusion and the total free energy of the domain wall is a minimum. The wall is in the most stable condition.

Considering the area of a single domain wall in the inclusion lattice, suppose that the displacement of the domain wall is  $d$  after it is unpinned from an inclusion, the area of the domain wall:

$Y = b^2 - \pi \left( \frac{l^2}{4} - d^2 \right)$  where  $b$  is the average grain diameter.

If  $q$  is the energy density of the domain wall, then the energy of the wall may be expressed as;

$$E_q = qY \quad (14)$$

when the domain wall moves a distance of  $d$ , the variation of the domain wall energy per volume is;

$$\Delta E_q = \frac{\partial q}{\partial d} + \frac{q}{Y} \frac{\partial Y}{\partial d}, \quad q \text{ is a constant so;}$$

$$\Delta E_q = \frac{q}{Y} \frac{\partial Y}{\partial d} = q \frac{\partial \ln Y}{\partial d} \quad (15)$$

Under the action of external field,  $H$ , when the domain wall is in the equilibrium state,  $\Delta E_H + \Delta E_q = 0$

when the external field is varied, the energy of the  $180^\circ$  domain wall will be:

$$-\Delta E_H = -\mu_0 M_s H \cos \left|_{\Theta=0}^{\Theta=180} \right. = \mu_0 M_s H \quad (16)$$

Substituting (15) into (13) and simplifying,

$$H_n = \frac{q}{2\mu_0 M_s H} \left( \frac{\partial}{\partial d} \ln Y \right) = \frac{\pi q l}{2\mu_0 M_s H b^2} \quad (17)$$

The volume swept by one domain wall,  $V_w$ , is approximated by a sphere:

$$V_w = \frac{4}{3} \pi \frac{l^3}{8} = \pi \frac{l^3}{6} \quad (18)$$

The ratio of the volume swept by a domain wall to the volume of a grain is expressed as;

$$\beta = \frac{\pi l^3}{6b^3} \quad (19)$$

Substituting (19) into (17),

$$H_n = \left( \frac{6}{\pi} \right)^{\frac{1}{3}} \frac{k_1 \delta}{\mu_0 M_s} \beta^{\frac{1}{3}} \frac{1}{b} \quad (20)$$

Where  $\delta = \frac{q}{2k_1}$  which is the thickness of the domain wall and  $k_1$  is the anisotropic coefficient of the material.

From (11) and (12),

$$\sigma = \frac{D}{C_s H_n} \quad (21)$$

Substituting (20) into (21);

$$\sigma = \left( \frac{\pi}{6} \right)^{\frac{1}{3}} \frac{\mu_0 M_s}{C_s k_1 \delta} \beta^{\frac{1}{3}} D^2 \quad (22)$$

When the magnetization period,  $T$ , of the external field is constant and the time of producing a Barkhausen pulse is also constant, the total number of Barkhausen jumps in the magnetization process,  $N$ , is equal to the total number of pinning sites that caused domain walls to be pinned in the sweeping volume of the domain wall.

The mean free distance of the domain wall is  $D$ , therefore,

$$N = \frac{1}{D^3} \quad (23)$$

From (7),

$$\tau = \frac{T}{N} = TD^3 \quad (24)$$

Substituting (22) and (24) into (10),

$$BN_{rms} = C_f D \quad (25)$$

$C_f$  depends on the magnetization conditions.

This results of above analysis, (9) and (25), show that  $BN_{rms}$  and amplitude sum is proportional to the mean free path of domain wall motion which is one of the bases of the interpretation of my experimental result.

Secondly, the grain-grain misorientation which is higher in CGO [15, 16] results in strong depression of the BN level which is caused by a decrease in the instantaneous rate of change of the magnetic flux during Barkhausen jumps, because of increased demagnetizing effects.

BN measurement has not been carried out at low flux densities (below 0.2 T) before. At low fields, domain wall motion has an intermittent, jerky character, with sparse Barkhausen jumps. The implication of this is that smaller grain samples (CGO) which have more grain boundaries acting as pinning sites and hence large fractional volume than HGO will have a greater number of these sparse Barkhausen jumps which will sum up to higher Barkhausen noise amplitude. This explains why at low flux density, the BN amplitude is higher in CGO material.

#### IV. CONCLUSION

BN have been measured at power frequency at high and low flux densities and show repeatability for the discussed parameters. The use of low noise components was essential to obtain the signal.

The results presented show strong correlation between structure and BN in different grades of grain-oriented steel as well as interesting high and low field differences. This new understanding of low flux density performance of engineering magnetic materials will provide manufacturers with a more reliable and meaningful foundation for their designs thus leading to improved metering CTs and greater confidence of users in the accuracy of large scale electrical power measurement.

#### REFERENCES

- [1] J. P. Hall, Evaluation of residual stresses in electrical steel, PhD thesis, Cardiff University, 2001.
- [2] A Moses, H. Patel, and P. I. Williams, AC Barkhausen noise in electrical steels: Influence of sensing technique on interpretation of measurements, *Journal of Electrical Engineering*, Vol. 57. No. 8/S, pp. 3-8, 2006.
- [3] C. C. H. Lo, J. P. Jakubovics, and C. B. Scrub, Non-destructive evaluation of spheroidized steel using magnetoacoustic and Barkhausen emission, *IEEE Transactions on Magnetics*. Vol. 33, No. 5, pp.4035-4037, 1997.
- [4] H. Kikuchi, K. Ara, Y. Kamada, and S Kobayashi, Effect of microstructure changes on Barkhausen noise properties and hysteresis loop in cold rolled low carbon steel, *IEEE Transactions on Magnetics*, Vol. 45, No.6 ,pp.2744-2747, 2009.
- [5] M. F. de Campos, M. A. Campos, F. J. G. Landgraf and L. R. Padovese, Anisotropy study of grain oriented steels with magnetic Barkhausen noise, *Journal of Physics, Conference Series* 303, 012020, 2011.
- [6] S. Turner, A. Moses, J. Hall and K. Jenkins, The effect of precipitate size on magnetic domain behaviour in grain-oriented electrical steels, *Journal of Applied Physics*, 107, 09A307-09A309-3, 2010.
- [7] National Instruments, Dynamic signal acquisition user manual, August 2002.
- [8] BS EN 10280:2001 + A1:2007, Magnetic Materials- Methods of measurement of the magnetic properties of electrical sheet and strip by means of a single sheet tester, British Standard, 2007.
- [9] S. Zurek, P. Marketos, P. I. Anderson, and A. J Moses, Influence of digital resolution of measuring equipment on the accuracy of power loss measured in Epstein frame, *Przegląd Elektrotechniczny (Electrical Reviews)*, Vol. R. 83, pp. 50-53, 2007.
- [10] ([www.omega.com/techref/pdf/strain-gage-technicaldata.pdf](http://www.omega.com/techref/pdf/strain-gage-technicaldata.pdf)). Strain gauge technical data manufacturer's manual. Accessed on 15<sup>th</sup> July 2011.
- [11] K. Hartmann, Relationships between Barkhausen noise, power loss and magnetostriction in grain-oriented silicon iron, PhD thesis, Cardiff University 2003.
- [12] N. Chukwuchekwa, Investigation of Magnetic Properties and Barkhausen Noise of Electrical Steel, PhD thesis, Cardiff University, 2012
- [13] H.V. Patel, S. Zurek, T. Meydan, D.C Jiles and L. LI, A new adaptive automated feedback system for Barkhausen signal measurement, *Sensors and Actuators A*, Vol. 129, pp.112-117, 2006.
- [14] H Sakamoto, etal, *IEEE Transactions on Magnetics*, Vol. 23 No.5, Sept. 1987
- [15] S. Taguchi, A. Sakakura and H. Takashima, US Patent 3287183, 1966.
- [16] M. F. Littmann, Structures and magnetic properties of grain oriented 3.2% silicon-iron, *Journal of Applied Physics*, Vol. 38, issue 3, pp. 1104-1108, 1967.

## Research on the Application of Fluid-Structure Interaction in Soil Rock Mixture Slope

Wang Yongcun<sup>1</sup>, Wang Wei<sup>1</sup>,

<sup>1</sup>(Chongqing Jiaotong University, Department of civil and architecture, Chongqing, 400074)

<sup>2</sup>(China Merchants Chongqing Communication Technology Research & Design Institute, Chongqing, 400074)

**ABSTRACT:** traditional seepage theory has defects, and the fluid-structure interaction research has developed. Through the analysis of the fluid-structure interaction problems in engineering, this paper expounds the characteristics of fluid-structure interaction, research methods and research status quo, mathematical model of the slope is put forward.

**Keywords** -Earth-rock mixture slope; Fluid-structure interaction; The research status; Mathematical model

### I. INTRODUCTION

In 1856, through many experiments Darcy's law was concluded by Darcy, which laid the foundation for the development of the theory of seepage and also provided the theoretical support for researching on rock slope stability under the effect of water. Some experts and scholars at home and abroad also improved the seepage theory, and studied instability mechanism earth-rock mixture slope from the angle of seepage. However, the traditional percolation theory has its limitations<sup>[1]</sup>. In traditional theory, porous skeleton is perfectly rigid, that is to say, in the process of pore fluid pressure change, deformation of solid skeleton will not produce (elastic or plastic), and the seepage problem can be treated as a coupling problem.

This simplification can get an approximate solution to the problem, but there are many shortage, and it is not conform to the actual production. As long as there is water, stress field and seepage field will occur mutual influence. Both are in a complex dynamic process, which is called Fluid-Structure Interaction (FSI). This paper focuses on the principle, characteristic and research status of Fluid-Structure Interaction, and mathematical model of the Fluid-Structure Interaction in the earth-rock mixture slope.

### II. THE FLUID-STRUCTURE INTERACTION IN ENGINEERING

The instability of the slope is a complex dynamic process, and the influence factors can be divided into internal factors and external factors. Internal factors mainly refers to the joint of side slope and lithology etc. and external factors mainly refers to a variety of external force acting on the slope. Among them, the effect of water is the key factor affecting the stability of slope. In general, water inside the slope is influenced by external factors, inducing the deformation and failure of slope. Its induced ways mainly include rainfall and melting snow causing the dynamic change of water, the dynamic change of water caused by river water level change and human engineering activities causing the softening effect of rock and soil strength and pore water pressure changing, etc. The relationship between the seepage field and stress field in landslide mainly embodies in two aspects: one is that the change of pore fluid pressure can cause the change of effective stress of porous skeleton, which leads to soil properties such as porosity, permeability coefficient change. On the other hand, the change of the properties such as porosity and permeability will influence the distribution of pore fluid flow and pressure. The interaction and mutual influence of seepage field and stress field finally makes the seepage field and stress field coupling to achieve a state of equilibrium, which respectively form the stability of the seepage field under the influence of the stable stress field and stable seepage field under the influence of the stress field. For earth-rock mixture slope, seepage field and stress field coupling is mainly reflected in two ways. For the rock mass, by applying tangential lift force and normal penetration on the fracture surface, seepage field affects the stress distribution of rock mass, and stress change permeability coefficient by changing the width of the crack, thus affecting the permeability and seepage field of rock mass. For soil, by applying distribution of seepage body force in the area of the seepage and seepage pressure in a certain surface, the seepage change stress distribution, and stress affect the permeability coefficient by changing the soil porosity and soil volume strain, which changes the seepage field.

### III. THE FEATURES, RESEARCH METHODS AND RESEARCH STATUS OF FLUID-STRUCTURE INTERACTION

In mesoscopic level, fluid and solid respectively have their own area. Because of the complexity of pore structure, size, geometry, the order and the extension direction have no certain rules to follow, so it has no any precise mathematical method that is used to describe complicated geometry of pore inner surface. Moreover, under the influence of fluid-structure interaction, pore channel is constantly changing. Therefore, it is difficult to accurately determine the boundary conditions. In order to overcome these difficulties, as well as classic seepage mechanics, we should study it from a macro point of view, that is to say, the macroscopic continuum method should be used. In this way, a significant feature of fluid-structure interaction is that fluid and solid should be considered to be an interacting unit, and it is difficult to be clearly separated.

Fluid-structure interaction research methods includes analytical method and numerical method.

The natural state of geological body make fluid-structure interaction problems difficult to obtain analytical solution. Definitely, based upon a large number of simplification and assumption, the analytical solution can be gotten. Especially for nonlinear problems, heterogeneous materials, the discontinuity problem and arbitrary geometry problems, the analytical method is difficult to calculate the real solution<sup>[2]</sup>. Therefore, fluid-structure interaction problem commonly uses numerical method.

Numerical methods includes finite element method and finite difference method. The basic idea of the finite element is to use the approximate solution to approach precise solution of differential equation, which is a regional discrete method. Its characteristic is that there is no limit to the shape of solution domain, and boundary conditions are easy to handle. And finite difference method is a classical method for numerical solution of partial differential equation. In solution domain, continuous domain will be divided into a finite discrete point set by finite difference grid or difference node, and then derivative terms of partial differential equations will be replaced by difference quotient, deducing the algebraic equations that contains discrete point and a finite number of unknowns. The solution of algebraic equation is a solution of partial differential equations. From mathematical perspective, approximate degree of finite difference method is higher than finite element method, but in practice, the finite element method is far better than finite difference method, because the finite element method is simple and flexible. The finite element method not only can adapt to the complex geometric shapes and various types of boundary conditions, but also can deal with all kinds of complex material nature problem. At the same time, the finite element method can also solve the problem of heterogeneous continuum.

A large number of scholars at home and abroad studied earth-rock mixture slope failure mechanism from the point of view of seepage. From the point of water Seepage in rock-soil mass, the deformation and damage of rock-soil mass because of the changes of pore-pressure and osmotic-pressure were summarized, and kinds of harmful effects because of the underwater were concluded by Hu yuanxin<sup>[3]</sup>. Based on an indoor physical simulation test and FLAC numerical simulation method, changing regulations of pore water stress and total stress of roadbed along reservoir or river are studied in the dynamic fluctuation of river or reservoir water level by Zhang Lijuan<sup>[4]</sup>.

Chen Ping think that the hydraulic and deformation characteristics of jointed rock are mainly determined by the distribution, density and dimension of its joints. A coupled seepage/stress analysis procedure is proposed based on hydraulics and deformation constitutive law of fractures in rock. Numerical analysis of a gravity dam/foundation is given as an example<sup>[5]</sup>. The mechanism of the action and reaction between the seepage and stress field in the single-zone embankment dam is analyzed according to the seepage characteristic of the single-zone embankment dam. The continuum mathematical model for coupled stress and seepage field in the single-zone embankment dam is presented, and the finite element numerical solution method of the mathematical model is discussed. Based on the principle of virtual displacements, the direct coupling formulae of FEM in the anisotropic saturated soils with the assumptions of homogeneous and continuous elastic-plastic porous media are derived by Yang Linde<sup>[6]</sup>. Taking into account the behavior that the permeability of deformable porous media varies with their porosity, the liquid-solid problem of liquid flowing through porous media under general plain stress condition is discussed. First the governing equations are published, then a decoupled method is proposed, and the fields of pore pressure, the stresses, strains and displacement of media are derived analytically by Xu Cenghe<sup>[7]</sup>. The analysis software CFX and ANSYS were adopted to analyze the two-way fluid-solid coupling of the debris flow blocking dam with small- and medium-scale landslide silting up by Zhu Yanpeng<sup>[8]</sup>. The fluid movement of debris flow and the stress-strain and displacement of the dam were obtained.

#### IV. A MATHEMATICAL MODEL OF THE FLUID-STRUCTURE INTERACTION

Mathematical model of Earth-rock mixture slope of the Fluid-Structure Interaction should meet the following several aspects<sup>[9]</sup>:

- (1) soil-rock-mixture is completely saturated isotropic body line elastomer;
- (2) The solid particle and pore water can be compressed;
- (3) The deformation of solid skeleton follows Terzaghi effective stress principle;
- (4) The seepage of pore water obeys the Darcy's law;
- (5) The displacement of rock and soil particle will happen in the process of seepage;
- (6) The porosity and permeability coefficient is dynamic change.

On the basis of satisfy the basic assumption, from two aspects: under the influence of seepage field on stress field and under the influence of stress field on the seepage field, partial differential equation is established.

##### 4.1 Stress field under the influence of seepage field

The influence of seepage field on stress field is summarized as water load, which is shown by penetration volume force and penetration pressure. So the effect of seepage field on stress field is through the change of stress field load (water load) to change the distribution of stress field<sup>[10]</sup>. Thus there is

$$p = r_w (H - z)$$

Among:  $z$  is potential head.

Infiltration volume force can also be calculated:

$$\begin{Bmatrix} f_x \\ f_y \\ f_z \end{Bmatrix} = \begin{Bmatrix} -\frac{\partial p}{\partial x} \\ -\frac{\partial p}{\partial y} \\ -\frac{\partial p}{\partial z} \end{Bmatrix} = \begin{Bmatrix} r \frac{\partial H}{\partial x} \\ r \frac{\partial H}{\partial y} \\ r \left( \frac{\partial H}{\partial z} - 1 \right) \end{Bmatrix}$$

So the constitutive relation can be gotten:

$$\sigma'_{ij} = D_{ijkl} \varepsilon_{kl} = \lambda \varepsilon_v \delta_{ij} + 2\mu \varepsilon_{ij} \quad (1)$$

Geometric relationships is

$$\varepsilon_{ij} = \frac{1}{2} (W_{j,i} + W_{i,j}) \quad (2)$$

Stress equilibrium equations is

$$\begin{cases} (\lambda + \mu) \frac{\partial \varepsilon_v}{\partial x} + \mu \nabla^2 W_x + \frac{\partial p}{\partial x} + \frac{\partial f_x}{\partial x} = 0 \\ (\lambda + \mu) \frac{\partial \varepsilon_v}{\partial y} + \mu \nabla^2 W_y + \frac{\partial p}{\partial y} + \frac{\partial f_y}{\partial y} = 0 \\ (\lambda + \mu) \frac{\partial \varepsilon_v}{\partial z} + \mu \nabla^2 W_z + \frac{\partial p}{\partial z} + \frac{\partial f_z}{\partial z} = 0 \end{cases} \quad (3)$$

From equations (1) (2) (3), stress field equation can be gotten under the influence of seepage field:

$$\begin{cases} \frac{G}{(1-2\nu)} \frac{\partial \varepsilon_v}{\partial x} + G \nabla^2 W_x + \frac{\partial p}{\partial x} + \frac{\partial f_x}{\partial x} = 0 \\ \frac{G}{(1-2\nu)} \frac{\partial \varepsilon_v}{\partial y} + G \nabla^2 W_y + \frac{\partial p}{\partial y} + \frac{\partial f_y}{\partial y} = 0 \\ \frac{G}{(1-2\nu)} \frac{\partial \varepsilon_v}{\partial z} + G \nabla^2 W_z + \frac{\partial p}{\partial z} + \frac{\partial f_z}{\partial z} + F'_z = 0 \end{cases}$$

Among :  $G$  is the elastic constants,  $\varepsilon_{ij}$  is strain tensor field,  $\nu$  is Poisson's ratio,  $\nabla^2$  is Lamé equation:  $\nabla^2 = \frac{\partial^2}{\partial x^2} + \frac{\partial^2}{\partial y^2} + \frac{\partial^2}{\partial z^2}$ ,  $\varepsilon_v$  is volume strain.

##### 4.2 Seepage field under the influence of stress field,

In general, the greater the porosity or void ratio of soil, the greater permeability coefficient. Soil coefficient of permeability and porosity or void ratio has the following relationship[18]:

$$K = K(n)$$

Setting the initial porosity for one unit is  $n_0$ . Under the effect of the stress field, volume strain is

$\varepsilon_v = \Delta V / V$  (compressive strain is negative).  $V$  is as the total volume of soil,  $\Delta V$  is the change of pore volume. Assuming that all the volume strain is caused by pore volume change, the porosity is

$$n = n_0 \exp(-\alpha \sigma + aP) = n_0 + \varepsilon_v$$

Because the volume strain  $\varepsilon_v$  is determined by the stress field  $\sigma_{ij}$ , so the permeability of soil mass can be expressed as a function of stress field, namely  $k = k(\sigma_{ij})$ . Thus it can be seen that the stress field affects the soil permeability by influencing the volumetric strain and porosity of the soil to, thereby affecting the seepage field.

Considering fluid and the effective stress principle of solid, the speed of the fluid particle is

$$V_f = V_r + V_s \quad (4)$$

The earth-rock aggregate skeleton continuity equation is shown:

$$\nabla \cdot [\rho_s(1-n)V_s] + \frac{\partial [\rho_s(1-n)]}{\partial t} = 0 \quad (5)$$

The continuity equation of pore fluid is shown:

$$\nabla \cdot [\rho_f n V_f] + \frac{\partial (\rho_f n)}{\partial t} = 0 \quad (6)$$

Based on equations (4) (5) (6), soil-rock-mixture continuity equation of fluid-solid coupling can be gotten:

$$-\nabla \cdot \left[ \frac{K}{\mu} (\nabla p - \rho_f g \nabla H) \right] + \frac{\partial \varepsilon_v}{\partial t} + \left( \frac{1-n}{E_s} + \frac{n}{E_f} \right) \frac{\partial p}{\partial t} = 0$$

### 4.3 Definite condition

#### 4.3.1 Seepage definite condition

Soil-rock-mixture boundary conditions can be divided into three categories, respectively

(1) The first category: head known boundary conditions

$$H|_{\Gamma_1} = H_1(x, y, z, t) \quad (x, y, z) \in \Gamma_1$$

(2) The second category: flow boundary conditions

$$\frac{\partial h}{\partial n} \Big|_{\Gamma_2} = -v_n / k = f_2(x, y, z, t)$$

(3) The third class: mixed boundary conditions

$$h + a \frac{\partial h}{\partial n} = \beta$$

Initial conditions is the function of coordinates and the time for the head, namely

$$H(x, y, z, t_0) = H_0(x, y, z, t_0)$$

#### 4.3.2 The stress field in definite condition

(1) The displacement boundary conditions

$$W \Big|_{\text{边界}} = W_r$$

(2) The stress boundary condition

$$\sigma_{ij} \Big|_{\text{边界}} = T_i$$

## V. CONCLUSION

For fluid-structure interaction of earth-rock mixture slope, this paper mainly introduces the characteristics of the fluid-structure interaction and its research progress. Mathematical model of the Fluid-Structure Interaction in the earth-rock mixture slope is given. It provides a theoretical basis for the further theoretical research and numerical simulation.

## REFERENCES

- [1] Dong Pingchuan, Xu Xiaohu, He Shunli. Research progress of the fluid-structure interaction [J]. Journal of Geomechanics, 1990, 3, 5(1),17-26.(In Chinese)
- [2] Zhang Xin. reservoir bank landslide stability analysis Based on ABAQUS fluid-structure coupling theory [D].Shan Dong University, 2005.(In Chinese)

- [3] Hu Yuanxin, Chai Hejun. Mechanism Study on Dynamic Instability of Roadbed along the Rivers of Mountainous Highway [J]. Journal of Chongqing Jiaotong University, 2007, 6, 26(3), 96-102. (In Chinese)
- [4] Zhang Lijuan, Wang Junjie, Chai Hejun. Influence of fluctuation of water level on stresses of roadbed along reservoir [J]. Rock and Soil Mechanics, 2007, 28(S1):863-867. (In Chinese)
- [5] Chen Ping, Zhang Youtian. coupling analysis of seepage/stress for jointed rock [J]. Chinese Journal of Rock Mechanics and Engineering, 1994, 04:299-308. (In Chinese)
- [6] Yang Linde, Yang Zhixi. Coupling analyses and numeric simulations on seepage flow in anisotropic saturated soils [J]. Chinese Journal of Rock Mechanics and Engineering, 2002, 10:1447-1451. (In Chinese)
- [7] Xu Cenghe, Xu Xiaohu. Liquid-solid coupled problem of radial flow through porous media under general plain stress condition [J]. Journal of Geomechanics, 1999, 01:14-18. (In Chinese)
- [8] Zhu Yanpeng, Xujiang. Analysis of Two-Way Fluid-Solid Coupling of Debris Flow Blocking Dam [J]. Journal of Gansu Sciences, 2015, 01:100-104. (In Chinese)
- [9] Xu Cida, Hua Bojie. Solid mechanics finite element theory, method and procedure [M]. China's Water Conservancy And Hydropower Press, 1983. (In Chinese)
- [10] Braja M. Das. Principles of Geotechnical Engineering [M], Boston: PWS Publishers, 1985.

## Multipath Rayleigh and Rician Fading Channel Simulation Using MATLAB

Md. Golam Sadeque, Shadhon Chandra Mohonta, Md. Firoj Ali

Lecturer, Dept. of EEE, PUST, Bangladesh

**ABSTRACT-** In this paper we present a simulation of multipath Rayleigh fading and Rician fading channel. We have used MATLAB software for simulation. Simulation was carried out for two different sample rate 20kb/s and 500 kb/s. This simulation process uses five path propagation models. The data is modulated, encoded and transmitted through a frequency selective and flat Rayleigh and Rician Multipath fading channel. Quadrature phase shift keying (QPSK) modulation technique is used to modulate the data. This paper compares the simulated result of Rayleigh and Rician fading channel.

**KEYWORDS-** Wireless Communication, Multipath, Fading Channel, Rayleigh Fading, Rician Fading

### I. INTRODUCTION

The wireless industry has developed and deployed an infrastructure for providing many services for the users [7]. Much of the current interest is in modeling and simulation of fading in mobile and indoor wireless communications. There has been significant research activity over the past 5-15 years into the performance of wireless channel models. Fading and Multipath occur in much radio communication systems. These effects were first observed and analyzed in troposcatter systems in the 1950s and early 1960s [17]. In a multipath situation, the signals arriving along different paths will have different attenuations and delays and they might add at the receiving antenna either constructively or destructively. If the path lengths and/or the geometry change due to changes in the transmission medium or due to relative motion of the antennas, as in the mobile case, the signal level might be subjected to wild fluctuations [17]. Although the fading mechanisms may be different in different environments, the general concepts of modeling and simulation remain the same. The design, production and deployment of technological infrastructure have high cost therefore manufacturers search for different alternatives to avoid high costs [7]. One of these alternatives is simulating a real wireless system. The advantage of simulation is that allows low-cost and low-risk environment. Simulation allows the designer to determine the correctness and efficiency of a design before the system is actually constructed. Consequently, the user may explore the merits of alternative designs without actually physically building the systems. Simulation helps us to forecast things that have never happened before and to run scenarios outside of historical bounds. In this paper we have simulated and tested multipath fading channel model for wireless communication. In wireless transmission system where a receiver is in motion relative to a transmitter with no line-of sight path between their antennas the Rayleigh fading is a good approximation of realistic channel conditions [7].

### II. MULTIPATH FADING CHANNEL

In any wireless communication system there could be more than one path over which the signal can travel between the transmitter and receiver antennas. The presence of multiple paths is due to atmospheric scattering and refraction, or reflections from buildings and other objects [17]. Multipath fading affects the signal in two ways: dispersion and time-variant behavior. If we transmit an extremely short pulse, ideally an impulse, over a time varying multipath path channel, the received signal might appear as a train of pulses [16]. Hence once characteristic of multipath channel is the time spread introduced in the signal that is transmitted through the channel. A second characteristic is due to the time variations in the structure of the medium. As a result of time variations, the nature of the multipath varies with time. That is, if we repeat the pulse-sounding experiment over and over, we shall observe the change in the receive pulse train, which will include changes in the size of the individual pulses, change in the relative delays among the pulses and quit

often, changes in the number of pulses observed in the received pulse train [p]. Moreover the time variations appear to be unpredictable to the user of the channel. Therefore it is reasonable to characterize the time variant multipath channel statistically.

We assume that there are multiple propagation paths. Associated with each path has a propagation delay and an attenuation factor. Both the propagation delays and the attenuation factor are time variant as a result of change in structure of the medium. Thus the received signal may be expressed in the form [p]

$$x(t) = \sum_n \alpha_n(t) s[t - \tau_n(t)]$$

Where,  $\alpha_n(t)$  is the attenuation factor of the signal received on the  $n$ th path and  $\tau_n(t)$  is the propagation delay for the  $n$ th path.

### III. FREQUENCY SELECTIVE AND NON SELECTIVE CHANNEL

The effect of fading can be expressed in terms of coherence bandwidth and coherence time. When an information bearing signal is transmitted through the channel, if the signal bandwidth is smaller than the coherence bandwidth, they will be affected by same type of fading then the channel model is called nonselective or flat fading model. On the other hand, if the signal bandwidth is larger than the coherence bandwidth, they will be affected by same type of fading the channel model is called frequency selective fading model

### IV. SYSTEM MODEL

When signal travels from transmitter to receiver due to fading effect of channel, the envelope of received signal follows Rayleigh or Rician distribution. When there is relative motion between mobile user and base station, the frequency of received signal changes and this phenomenon is called Doppler frequency shift.

#### (a) Rayleigh Distribution

This occurs when the envelope of the received signal follows a Rayleigh distribution. Rayleigh distribution is statistically used to model a faded signal, when there is no dominant LOS path. The envelope of the received signal with Rayleigh distribution has the probability density function (pdf) given by [5]

$$p_\alpha(\alpha) = \frac{\alpha}{2\sigma^2} \exp\left(-\frac{\alpha^2}{2\sigma^2}\right) \quad \alpha \geq 0 \dots \dots \dots (1)$$

Where,  $\alpha$  channel fades amplitude

$\sigma^2$  is the time average power of the received signal.

#### (b) Rician Distribution

The Rician distribution which also occurs as a result of multipath propagation is statistically used to model a distribution when a strong line of sight component is present along with the weaker components. It has the probability density function (pdf) given by [3] as:

$$P_\alpha(\alpha) = \frac{\alpha}{\sigma^2} \exp\left[-\frac{\alpha^2 + s^2}{2\sigma^2}\right] I_0\left(\frac{s\alpha}{\sigma^2}\right), \quad \alpha \geq 0 \dots (2)$$

Where,  $I_0(\dots)$  is the zero order Bessel function of the first kind.

$s$  is the peak amplitude of the dominant path.

$\alpha$  channel fades amplitude

$\sigma^2$  is the time average power of the received signal.

Rician distribution is often described in terms of a parameter,  $k$ , is known as the Rician factor and is expressed by [3] as:

$$k = 10 \log \frac{s^2}{2\sigma^2}$$

As  $s$  approaches 0,  $k$  approaches  $\infty$  dB and as the dominant path decreases in amplitude, the Rician distribution degenerates to a Rayleigh distribution.

#### (c) Doppler Frequency Shift

Doppler shift is the random changes that occur in a channel introduced as a result of a mobile user's mobility or movement. It is the apparent difference in frequency of the received signals from that of the transmitted signals when there is a relative motion between the transmitter and receiver. This Doppler frequency shift  $f_d$  is given in equation (3), where  $\theta$  is the angle between formed between the incident electromagnetic wave and the moving receiver,  $v$  is the mobile speed,  $f$  is the frequency of the carrier and  $c$  is the speed of light.

$$f_d = \frac{vf}{c} \cos\theta \dots \dots \dots (3)$$

V. SIMULATION PARAMETER

Transmitter transmit signal and receiver receive signal in different ways. The simulation process was carried out with random data source and following parameters by using MATLAB.

Table 1. Simulation parameter

Parameters	Variable
No of paths between Transmitter and receiver	05
Speed of light	$3 \times 10^8$ m/s
Delay of first path	0 $\mu$ s
Gain of the first path	0 dB
Second path larger than first path	1.2 km
Average Gain of the second path	-3 dB
Third path larger than first path	2.4 km
Average Gain of the third path	-6 dB
Fourth path larger than first path	3.6 km
Average Gain of fourth path	-9 dB
Fifth path larger than first path	4.8 km
Average Gain of the fifth path	-12 dB
Maximum Doppler shift of diffuse component	200 Hz
Doppler shift of the LOS component	100Hz
Modulation	QPSK
Sample rate	20 kb/s and 500 kb/s
Bits per frame	1000
Number of frames	20

Simulated result of Rayleigh Fading Channel at 500 kb/s sample rate

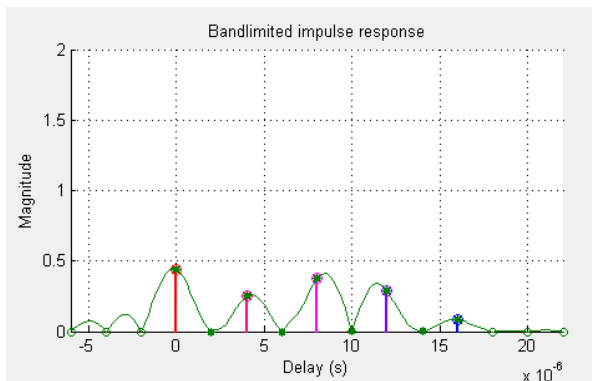


Fig. 1 Impulse Response

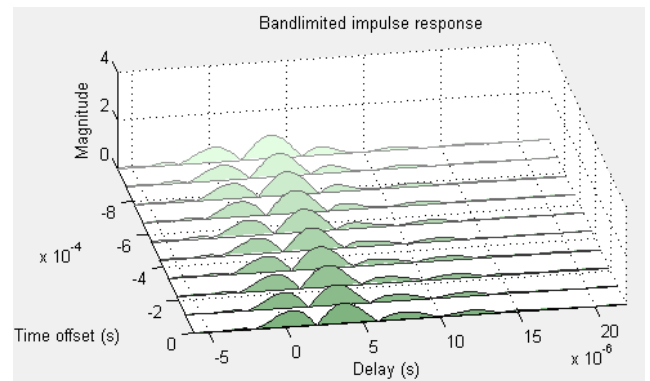


Fig. 3 Waterfall of impulse response

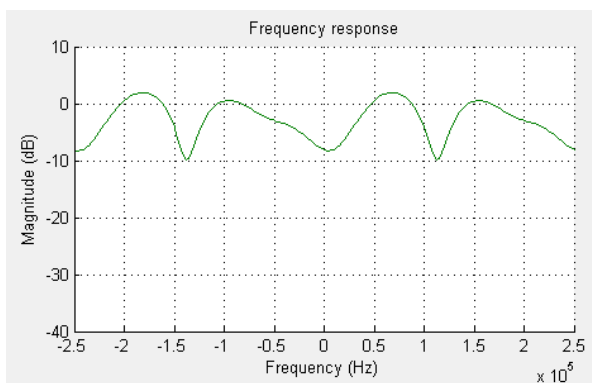


Fig. 2 Frequency Response

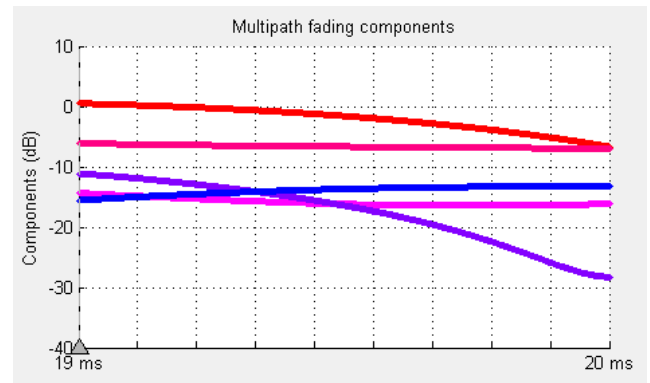


Fig. 4 Multipath fading component

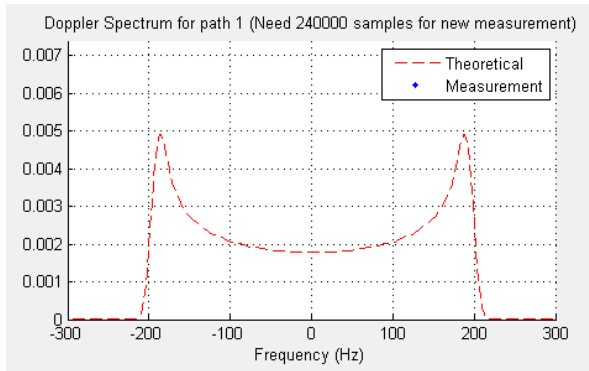


Fig. 5 Doppler spectrum

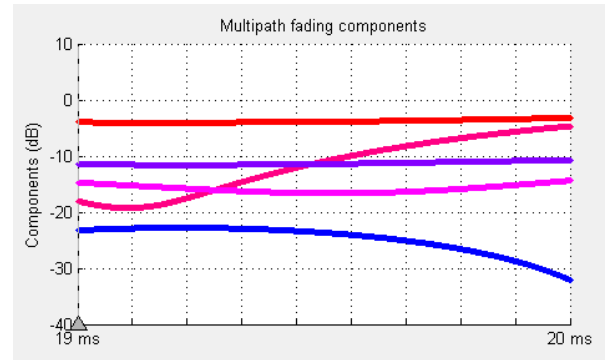


Fig. 9 Multipath fading component

Simulated result of Rician Fading Channel at 500 kb/s sample rate

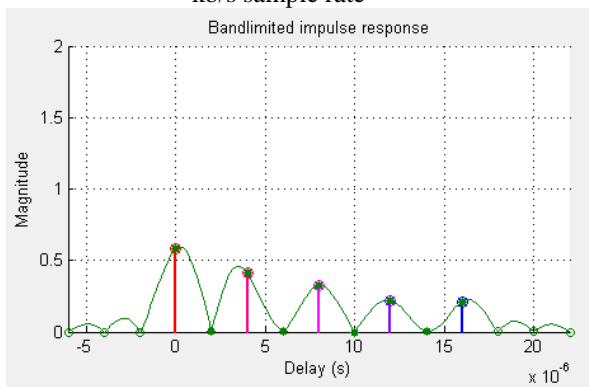


Fig. 6 Impulse Response

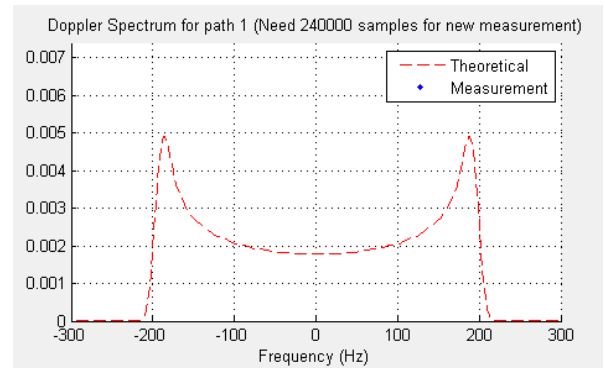


Fig. 10 Doppler spectrum

Simulated result of Rayleigh Fading Channel at 20 kb/s sample rate

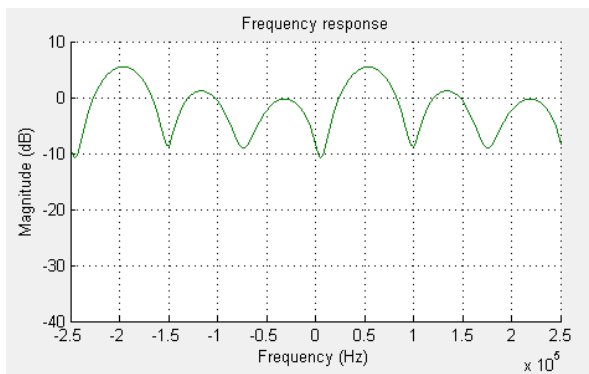


Fig. 7 Frequency Response

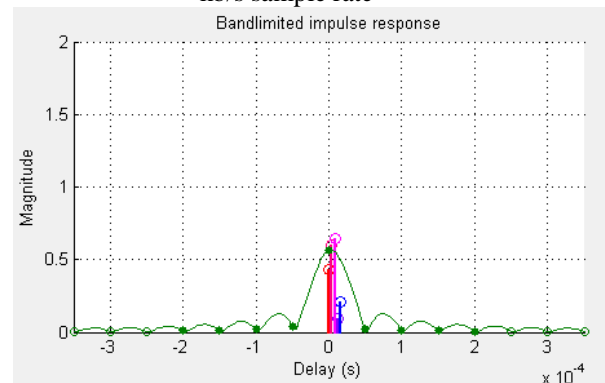


Fig. 11 Impulse Response

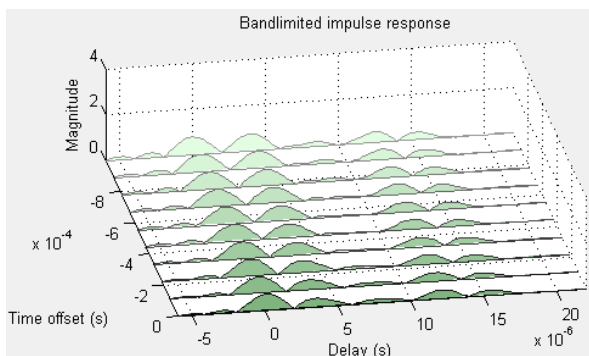


Fig. 8 Waterfall of impulse response

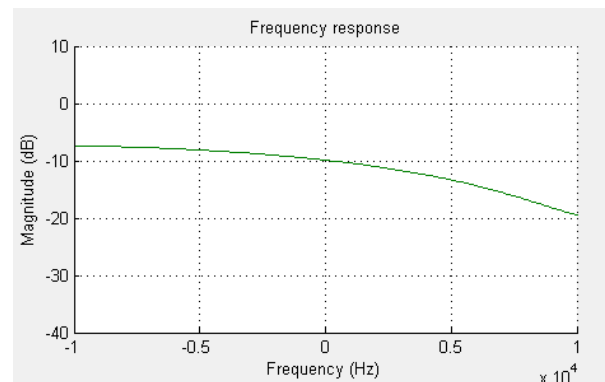


Fig. 12 Frequency Response

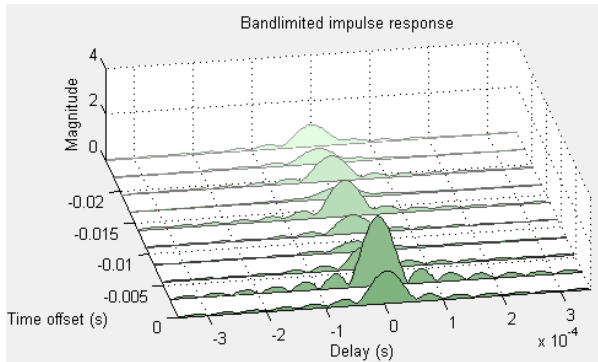


Fig. 13 Waterfall of impulse response

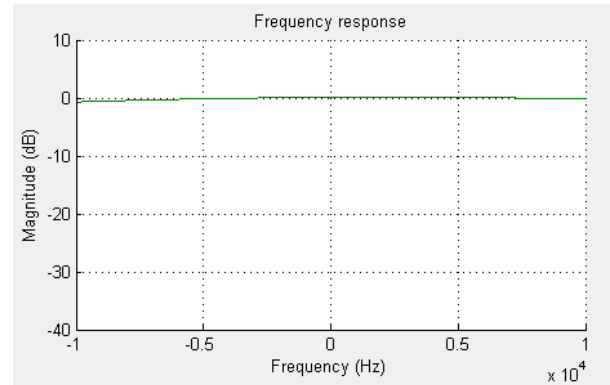


Fig. 17 Frequency Response

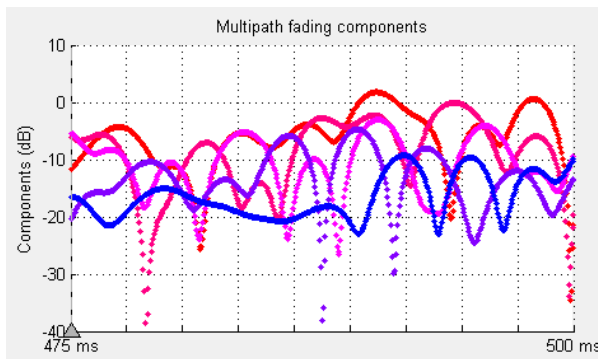


Fig. 14 Multipath fading component

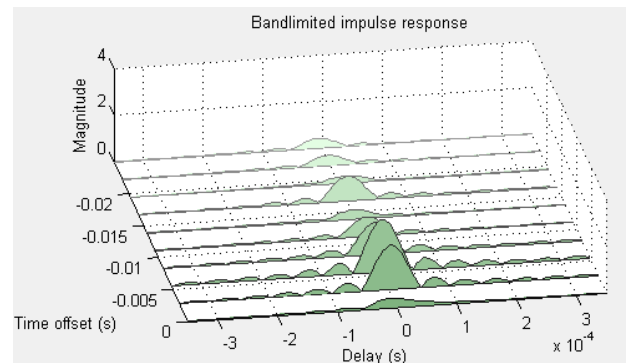


Fig. 18 Waterfall of impulse response

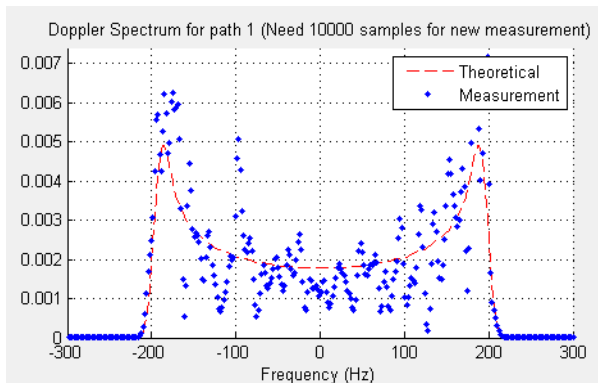


Fig. 15 Doppler spectrum

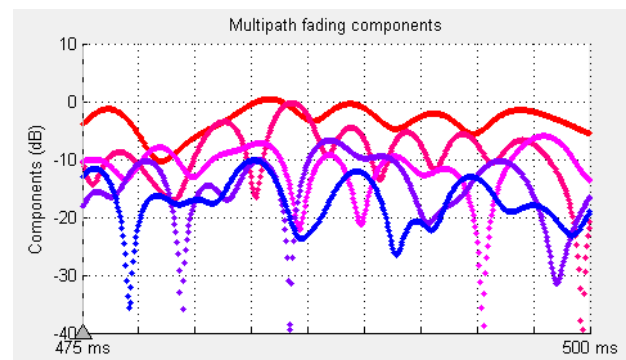


Fig. 19 Multipath fading component

Simulated result of Rician Fading Channel at 20 kb/s sample rate

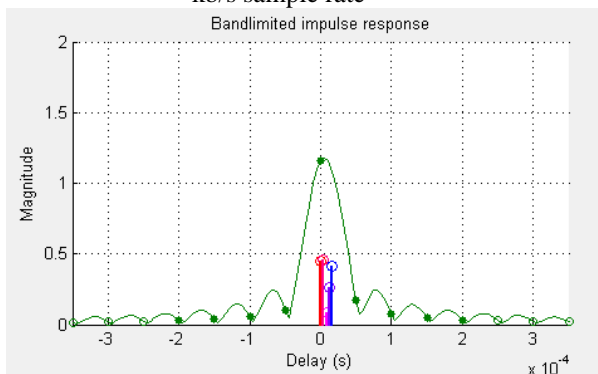


Fig. 16 Impulse Response

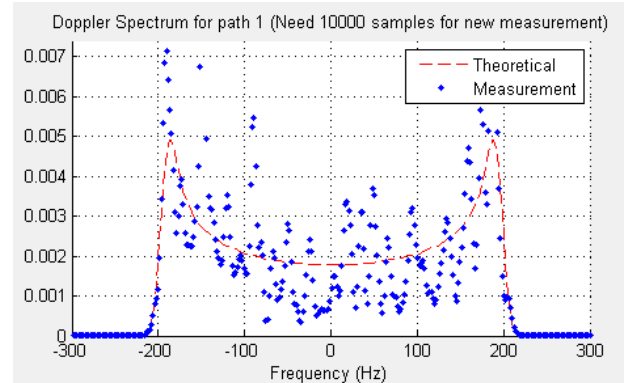


Fig. 20 Doppler spectrum

## VI. RESULT AND DISCUSSION

In this section, we have presented the simulation results using MATLAB for two sample rates are: 50kb/s and 20kb/s for Rayleigh and Rician fading channel. When the sample rate is 50kb/s then the frequency response of Rayleigh and Rician fluctuate shown in fig. 2 and fig. 7. This type of fading is called frequency selective fading. But when we use the sample rate is 20kb/s then the frequency response of Rayleigh and Rician fading channel are almost constant shown in fig. 12 and fig. 17. This type of fading is called frequency flat fading. For sample rate 20kb/s the multipath fading component fluctuate more than the 50 kb/s sample rate. Doppler spectrum for both types of fading channel for different sample rate are shown in fig.5, fig. 10, fig. 15 and fig. 16. From this figure we see that for sample rate 20kb/s the theoretical and measurement result Doppler shift are different. The response of the channel is time variant and unpredictable. All responses shown in figure are snapshot at the time. But their response will be different if run the program for different time. If the bandwidth is too small for the signal to resolve the individual components, the frequency response is approximately flat because of the minimal time dispersion caused by the multipath channel. This kind of low-dispersion multipath fading is often referred to as narrowband fading, or frequency-flat fading. When we increase the signal bandwidth to 500 kb/s, we see much greater distortion in the signal. This distortion is ISI that comes from time dispersion of the wideband signal. The channel's delay span (for fifth path 16 microseconds) is now larger than the QPSK symbol period (4 microseconds), so the resultant band limited impulse response is no longer well-approximated by a sinc pulse.

## VII. CONCLUSION

In this paper, multipath fading channel model has been simulated. We have used QPSK modulation to test the effect of fading channels to the received signal. There are various properties of the fading channel such as Doppler spread, path loss, time delay are taken into consideration while we simulate the characteristics of the channel. In this paper we have simulated mainly two types of fading environment. They are frequency selective fading and flat fading. For signal bandwidth 20kb/s channel act as flat fading and bandwidth 50kb/s channel act as a frequency selective fading. Among two types of fading the Rayleigh distribution is the best model to be adopted by communication systems.

## REFERENCE

- [1] Sanjiv Kumar, P. K. Gupta and G. Singh. Performance "Analysis of Rayleigh and Rician Fading Channel Models using Matlab Simulation", I.J. Intelligent Systems and Applications, 2013, 09, 94-102
- [2] Vinay Panwar and Sanjeet Kumar. "Bit Error Rate (BER) Analysis of Rayleigh Fading Channels in Mobile Communication", International Journal of Modern Engineering Research (IJMER) Vol.2, Issue.3, May-June 2012 pp-796-798
- [3] Z.K. Adeyemo D.O. Akande, F.K. Ojo and H.O. Raji. "Comparative evaluation of fading channel model selection for mobile wireless transmission system", International Journal of Wireless & Mobile Networks (IJWMN) Vol. 4, No. 6, December 2012
- [4] Cyril-Daniel Iskander and Hi-Tek Multisystems. "A MATLAB R-based Object-Oriented Approach to Multipath Fading Channel Simulation",
- [5] Niharika Sethy and Subhakanta Swain. "BER analysis of MIMO-OFDM system in different fading channel", IJAIEM, Volume 2, Issue 4, April 2013.
- [6] Pravindra Kumar, B.K.Kanaujia, and M. Gangadharappa. "BER Performance Analysis of Rake Receiver in Rayleigh Fading Channel for UMTS environment", International Journal of Engineering Science and Technology. Vol. 2(6), 2010.
- [7] M.S. Chavan, R.H. Chile and S.R. Sawant. "Multipath Fading Channel Modeling and Performance Comparison of Wireless Channel Models. International Journal of Electronics and Communication Engineering", Volume 4, Number 2 (2011), pp. 189-203.
- [8] Marvin K. Simon and Mohamed-Slim Alouini. "Digital Communication over Fading Channels", John Wiley & Sons, Inc
- [9] Mukesh Kumar Mishra, Neetu Sood and Ajay K Sharma. "Efficient BER Analysis of OFDM System over Nakagami-m Fading Channel", International Journal of Advanced Science and Technology. Vol. 37, December, 2011.
- [10] Abhishek Katariya, Amita Yadav and Neha Jain. "Performance Evaluation Criteria for OFDM under AWGN Fading Channel using IEEE 802.11a", International Journal of Soft Computing and Engineering (IJSC), Volume-1, Issue-3, July 2011.
- [11] Neetu Sood, Ajay K Sharma and Moin Uddin. "BER Performance of OFDM-BPSK and -QPSK over Generalized Gamma Fading Channel", International Journal of Computer Applications, Volume 3 – No.6, June 2010.
- [12] Gurpreet Kaur, and Partha Pratim Bhattacharya. "Performance Evaluation of an OFDM System under Rayleigh Fading Environment", Journal of Emerging Trends in Computing and Information Sciences, VOL. 3, NO. 3, March 2012.

- [13] Md. Noor -A- Rahim1 , Sheikh Md. Rabiul Islam , and Md. Nashid Anjum. "Performance analysis of Is estimated ofdm system over rayleigh fading channel", Daffodil international university journal of science and technology, volume 8, issue 1, january 2013.
- [14] Sabuj Sarkar and Mohammad Shaifur Rahman, "Optimal BER in MIMO Raleigh Fading Channel from QPSK Modulation: Modified MMSE Versus ML Equalizer Evaluation", International Journal of Electronics & Informatics, Vol. 2, No. 1, 2013
- [15] Hemchand Vashist, Arvind Pathak, Amarjeet Kaur, Sanjay Sharma, Ashish Sharma and Meenu Jangir. "Simulation and Modeling of Fading Channel and Improvement of Channel estimation using Artificial Neural Network", International Journal of Innovative Technology and Exploring Engineering, Volume-1, Issue-6, November 2012.
- [16] John J. Prokis and Masoud Salehi. "*Digital Communications*", 5<sup>th</sup> edition, McGraw-Hill, New- York, 2008.
- [17] Michel C. Jeruchim, Philip Balaban and K. Sam Shanmugan. "*Communication systems Modeling, Methodology, and techniques*", Kluwer Academic Publishers. New York.
- [18] Md. Sipon Miah, M. Mahbubur Rahman, T. K Godder, Bikash Chandra Singh and M. Tania Parvin. "Performance Comparison of AWGN, Flat Fading and Frequency Selective Fading Channel for Wireless Communication System using 4QPSK", IJCIT, VOLUME 01, ISSUE 02.
- [19] Pengda Huang, Dinesh Rajan, and Joseph Camp. "Weibull and Suzuki Fading Channel Generator Design to Reduce Hardware Resources".
- [20] T. S. Rappaport. "*Wireless Communica- tions: Principles and Practice*", Upper Saddle River, NJ: Prentice Hall, 1996.
- [21] Julian Cheng, Chinthananda Tellambura and Norman C. Beaulieu. "Performance of Digital Linear Modulations on Weibull Slow-Fading Channels", IEEE Transactions on communications, vol. 52, no. 8, August 2004.
- [22] George Tzeremes\* and C. G. Christodoulou. "Use of Weibull Distribution for Describing Outdoor Multipath Fading"
- [23] Julian Cheng, Chintha Tellambura, and Norman C. Beaulieu. "Performance Analysis of Digital Modulations o n Weibull Fading Channels"
- [24] Nikos C. Sagiasa and George S. Tombras. "On the cascaded Weibull fading channel model", Journal of the Franklin Institute 344 (2007).

## Soyabean Fibre – A Substitute to Silk Fibre

Sanjida Sultana<sup>1</sup>, Azmary Akter Mukthy<sup>2</sup>

<sup>1</sup>(Department of Textile Engineering, Primeasia University, Bangladesh)

<sup>2</sup>(Department of Textile Engineering, Primeasia University, Bangladesh)

**ABSTRACT :** The manufacturing process and the characteristics of soyabean fibre have been illustrated in this article. It is shown that this fibre has some characteristics which are as like as silk fibre. So, it can be said that this fibre can be used as a substitute to silk fibre.

**Keywords** -Soyabean fibre, Soya Glycine Max, Manufactured fibre, Dyeability, Comfortability.

### I. INTRODUCTION

Soybean protein fibres (SPF) are manufactured fibres, produced from regenerated soya *Glycine Max* soybean proteins in combination with synthetic polymer (polyvinyl alcohol) as a predominant component [1]. Polyvinyl alcohol is used for improving strength of fibre. It is a kind of reproducible plant protein fibre. At first the oil is extracted from soyabean, then a high polymer residual cake is found. Then a spinning solution of certain concentration is prepared and a filament bundle of single fibre is spun from the solution by wet spinning method. The fibre performance is stabilised through hydroformylation and then it undergoes winding, heat setting and cutting. In this way, soybean fibre of various lengths and specifications for spinning can be manufactured [2].

### II. CHARACTERISTICS OF SOYBEAN PROTEIN FIBERS

**2.1. Lusture:** The soya-bean protein fibre is lustrous like silk.

**2.2. Drape ability:** This fibre has also excellent drape ability.

**2.3. Comfortability:** Knitted fabric of soybean protein fiber has soft, smooth and light handle which is same as that of fabrics made from silk blended with cashmere and the fabric has the same moisture absorption as that of cotton and better moisture transmission than that of cotton, which make it comfortable [3].

**2.4. Color:** The color of soyabean fibre is light yellow as like as silk.

**2.5. Dyeability:** Weak acid dye, reactive dye and substantive dyes can be used for dyeing soyabean fibre while due to the low color fastness to wash, the substantive dyes are usually not used to soybean fiber except very few colors [3].

**2.6. Function of Health** [3]: Soybean Protein Fiber possesses many amino acids necessary to human's body, so this sole botanic protein fiber has the function of health that no other fiber processes. Meeting people's skin, the amino acid in soybean protein can activate the collagen protein in the skin, resist tickling and evaporate the skin. Bacteria resistant elements are integrated in fiber's molecule chain, which makes the fabrics keep the property of resisting *coli bacillus*, *staphylococcus aureus* and *candida albicans* permanently, this avoids the shortcoming of not permanent effect when the anti-bacteria function is added to the yarn when finishing.

**2.7. Breaking strength:** Breaking strength of the single soybean protein fiber is over 3.0cNdtex, which is higher than silk. By now, 1.27dtex fiber can be spun into 6dtex yarn with high quality, which can be used for high-quality and high-density fabrics [3].

**2.8. Elastic recovery:** Soyabean fibre has 55.4% elastic recovery [3].

**2.9. Resistance Properties to Alkali, Acid, Moth and Fungus [3]:**

Fibre Property	Soybean fiber	Silk
Resistance to acid	Resistant to thin- acid (good).	Resistant to thin- acid (good).
Resistance to alkali	Resistant to thin-alkali (soda), not resistant to caustic soda.	Resistant to thin-alkali (soda), not resistant to caustic soda.
Resistance to moth / fungus	Resistant to moth and fungus.	Resistant to fungus, not resistant to moth.

**2.10. Sanitarian property:**

Soybean fiber has good biocompatibility and is beneficial to the human health. Furthermore, the anti-bacterial agents, which were added to the soybean fiber in spinning process, can restrain the growth of colon bacillus, impetigo bacterial and sporothrix. Therefore, soybean fiber is a kind of sanitarian fiber [3].

**2.11. Some physical properties [3]:**

Property	SPF	Silk
Dry breaking extension (%)	18-21	14-25
Initial Modulus (kg/mm <sup>2</sup> )	700-1300	650-1250
Loop strength (%)	75-85	60-80
Knot strength (%)	85	80-85
Moisture regain (%)	8.6	11.0
Density (g/cm <sup>3</sup> )	1.29	1.34-1.38
Heat endurance	Yellowing and tacking at about 120° C (Bad)	Keep stable When temperature ≤148° C (Good)
Ultraviolet resistance	Good	Bad

**2.12. Wet Permeability and Moisture Vapor Transmission Characteristics [3]:**The wet permeability of Soybean is lower than that of PP and PE but higher than PAN, PA and silk; while the moisture vapor transmission property of soybean sample is better than silk, PP, PE, PA, PAN. Therefore, soybean fiber is a kind of comfortable fiber with relatively good wet permeability, excellent moisture vapor transmission property and dry touch.

**2.13. Frictional, flexural and draping properties[3]:****Frictional property:**

The sequence of the frictional property of some yarn is as below:

Silk>Soybean fiber/spandex >cotton>soybean>Chrysalis fiber

**Flexural property:**

The sequence of the soft handle property of some yarn is as below:

Chrysalis fiber >Soybean fiber> Silk > cotton

**Draping property:**

The sequence of the draping property of some yarn is as below:

Chrysalis fiber >Soybean fiber> Silk

**2.14.Light fastness property[3]:**

The light fastness of soybean fiber was tested under outdoor condition for two months. After the test, the color of soybean fiber fades a little, the strength decreases 11% and no mold fungus appears. Furthermore, the strength of soybean fiber decreases only 9.8% under the ultraviolet irradiation for 120 hours. The test results indicate that the soybean fiber has good light fastness property and good resistance to ultraviolet radiation, which is better than cotton, viscose and silk.

**III. CONCLUSION**

From the above discussions it is clear that soyabean protein fibre shows comparable lusture, comfortability, color, dye ability, breaking strength, resistance properties to acid, alkali, moth and fungus, light fastness property, sanitarian property, wet permeability and moisture vapor transmission, frictional, flexural and draping properties which are comparable to silk fibre. So it can be said that this fibre can be used as a substitute to silk fibre.

**REFERENCES**

- [1] TatjanaRijavec and ŽivaZupin,Soyabean Protein Fibres (SPF),[www.intechopen.com](http://www.intechopen.com), 501-522.
- [2] Li Yi-you, The Soybean Protein Fibre - A Healthy & Comfortable Fibre for the 21<sup>st</sup> Century, *FIBRES & TEXTILES in Eastern Europe*, 12(2), 2004, 8-9.
- [3] Dong Hua University, Department of Knitting Engineering, College of Textiles, Test Report of Comprehensive Properties of Soybean Protein Fibers.

## A Study on Overlay Design of Repeatedly Deteriorating Flexible Pavement

Mahendrakar Kiran Kumar<sup>1</sup>, D.Gouse Peera<sup>2</sup>, Konge Praveen Kumar<sup>3</sup>

<sup>1</sup>(M.Tech student, Civil Engineering, BITS Adoni, Kurnool District, Andhra Pradesh, India)

<sup>2</sup>(Associate Professor, Civil Engineering, BITS Adoni, Kurnool District, Andhra Pradesh, India)

<sup>3</sup>(M.Tech student, Civil Engineering, BITS Adoni, Kurnool District, Andhra Pradesh, India)

**ABSTRACT:** A factor, which causes further concern in India, is very high and very low pavement temperature in some parts of the country. Under these conditions, flexible pavements tend to become soft in summer and brittle in winter. Further increase in road traffic during the last one decade with an unduly low level of maintenance has contributed to accelerated deterioration of road surfacing. To prevent this deterioration process, several types of measures may be adopted effectively such as improved design, use of high performance materials and effective construction technologies. Over the last two decades, traffic volume and the percentage of heavy truck traffic have increased enormously on the National High Way No 18. This pavement is a Flexible pavement with bituminous surfacing. The high traffic intensity in terms of commercial vehicles, overloading of axles and significant variations in daily and seasonal temperature of the pavement have been always responsible for early development of distress symptoms like undulations, rutting, cracking, bleeding, raveling, shoving and potholing of bituminous surfacing.

**KEYWORDS** - Benkelman Beam, Bump Integrator, flexible pavement, integrator unit, pavement unevenness.

### I. INTRODUCTION

To conduct pavement unevenness tests on the selected stretch in Kurnool, Andhra Pradesh, India. Which is located at Longitude 78° 04' East of Prime Meridian and Latitude 15° 82' North of Equator in between Nandyal check post to towards G. Pulla Reddy Engg. College (550M) by using Bump Integrator. To evaluate strength on existing pavement and to design the thickness of overlay considering present traffic by using Benkelman Beam. The movement of agriculture and industrial loads on National Highway No.18 (369KM) is an important road which connects the city Kurnool with Chittoor via Nandyal and Kadapa is high. This road is a very important road to link three districts in Andhra Pradesh, where in the traffic and overloading of the commercial vehicles is on peak. Commercial activities in these districts are high and NH.18 plays a vital role by hooking these three districts. This road construction was undertaken during British rule. Temperature in this zone is very high during summer the pavement temperature reaches up to 50<sup>o</sup> C and improper drainage facilities this leads to lot of distress in this pavement. In this road from Nandyal Check Post (In Kurnool) to towards G. Pulla Reddy Engg. College constructed with plain bituminous concrete. Because of this agricultural, industrial traffic, Heavy Temperature Variations and improper drainage facilities, causing repeated deterioration of this Stretch of 550M, hence now is the time comes to find the causes to this repeated deterioration and the design of Overlay for this Repeatedly Deteriorating Pavement.

### II. DESCRIPTION OF FLEXIBLE PAVEMENT

Flexible pavements are those, which on the whole have low or negligible flexural strength and are rather flexible in their structural action under the loads. The layers of flexible pavement reflect the deformation of the lower layers onto the surface of the layer. The flexible pavement layers transmit the vertical or compressive stress to the lower layer by grain to grain transfers through the point of contact into each granular structure. A well compacted granular structure consisting of strong graded aggregate can transfer the compressive stress through a wider area and thus forms a good flexible pavement layer. The load spreading ability of this layer therefore depends on the type of the materials and the mix design factors. The vertical compressive stress is maximum on the pavement surface directly under the wheel load and is equal to the contact pressure under the

wheel. Due to the ability to distribute the stresses to a larger area in the shape of a truncated cone, the stress get decreased at the lower layers. Therefore by taking full advantage of the stress distribution characteristics of the flexible pavement may be constructed in a number of layers and the top layers has to be the strongest as the highest compressive stresses to be sustained by this layer, in addition to the wear and tear due to the traffic. The lower layers have to take up only lesser magnitudes of stress and there is no direct varying action due to traffic loads.

### III. BUMP INTEGRATOR

The roughness measurements of the whole length of the test sections were carried out using Bump integrator at the left wheel path. The left wheel paths were identified at a distance of 0.6m from the edge of the pavement. Bump integrator also known as Automatic road unevenness recorder gives speedily a quantitative integrated evaluation of surface irregularities on an electromagnetic counter. It comprises of a trailer of single wheel with a pneumatic tire mounted on a chassis over which on integrating device is fitted. The machine has a panel board fitted with two sets of electromagnetic counters for counting the uneven index value. The operating speed of the machine is 30 +/- ½ km/hr. A vehicle, usually a jeep, towed the machine and tire pressure is 2.1 kg/cm<sup>2</sup>. The calibration of BI unit was carried out by CRRI, New Delhi using Dip Stick. For calibration purpose, sections with a wide roughness range were covered to make the exercise meaningful. Sections of 100m long were selected for this purpose.

#### 3.1. Processing of results obtained with bump integrator

The results obtained with Bump integrator are the Integrator value of irregularities in inches (from BI counter reading), The number of wheel revolutions (from wheel revolution counter). Each set of are required to be converted to the unevenness index value (UI value) in terms of cms/km. The unevenness index value for the test section is arrived at by taking mean of UI values corresponding to the three sets of readings. The unevenness index value is calculated by dividing the BI counter values (in cms) by the distance traveled in kms.

$$\text{Unevenness Index UI} = \frac{\text{Integrator Counter Value (cms)}}{\text{Distance Traveled (km)}}$$

#### 3.2. Test results of bump integrator studies

##### 3.2.1. Left lane details

S.NO	CHAINAGE		TYPE OF LANE	BUMP INTIGRATOR READING			UNEVENNESS INDEX	RIDING QUALITY
	FROM	TO		OUT WARD	RETURN	AVERAGE		
1	0.0	0.1	DOUBLE	36	36	36.00	3600	VERY POOR
2	0.1	0.2	DOUBLE	67	33	50.00	5000	VERY POOR
3	0.2	0.3	DOUBLE	57	62	59.50	5950	VERY POOR
4	0.3	0.4	DOUBLE	41	33	37.00	3700	VERY POOR
5	0.4	0.5	DOUBLE	35	50	42.50	4250	VERY POOR
6	0.5	0.6	DOUBLE	25	64	44.50	4450	VERY POOR
7	0.6	0.7	DOUBLE	68	50	59.00	5900	VERY POOR
8	0.7	0.8	DOUBLE	92	42	67.00	6700	VERY POOR
9	0.8	0.9	DOUBLE	61	48	54.50	5450	VERY POOR
10	0.9	1.0	DOUBLE	55	76	65.50	6550	VERY POOR
11	1.0	1.1	DOUBLE	19	28	23.50	2350	POOR
12	1.1	1.2	DOUBLE	35	21	28.00	2800	VERY POOR
13	1.2	1.3	DOUBLE	58	35	46.50	4650	VERY POOR
14	1.3	1.4	DOUBLE	18	15	16.50	1650	POOR
15	1.4	1.5	DOUBLE	15	24	19.50	1950	POOR
16	1.5	1.6	DOUBLE	28	30	29.00	2900	VERY POOR
17	1.6	1.7	DOUBLE	15	15	15.00	1500	POOR

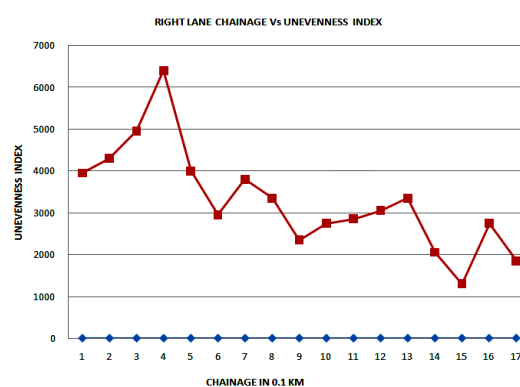
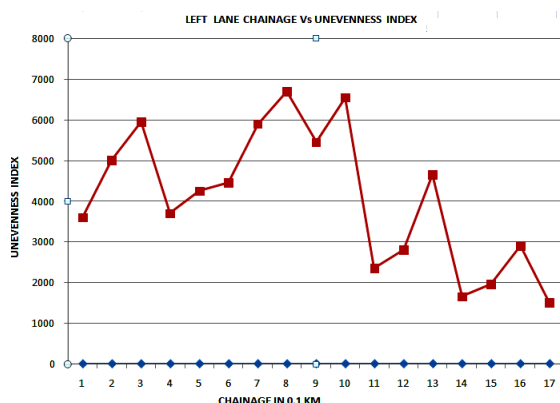
3.2.2. Right lane details

S.NO	CHAINAGE		TYPE OF LANE	BUMP INTIGRATOR			UNEVENNESS INDEX	RIDING QUALITY
	FROM	TO		OUT	RETURN	AVG		
1	0.0	0.1	DOUBLE	41	38	39.50	3950	VERY POOR
2	0.1	0.2	DOUBLE	46	40	43.00	4300	VERY POOR
3	0.2	0.3	DOUBLE	36	63	49.50	4950	VERY POOR
4	0.3	0.4	DOUBLE	55	73	64.00	6400	VERY POOR
5	0.4	0.5	DOUBLE	28	62	40.00	4000	VERY POOR
6	0.5	0.6	DOUBLE	12	47	29.50	2950	VERY POOR
7	0.6	0.7	DOUBLE	15	61	38.00	3800	VERY POOR
8	0.7	0.8	DOUBLE	22	45	33.50	3350	VERY POOR
9	0.8	0.9	DOUBLE	35	12	23.50	2350	POOR
10	0.9	1.0	DOUBLE	23	32	27.50	2750	VERY POOR
11	1.0	1.1	DOUBLE	27	30	28.50	2850	POOR
12	1.1	1.2	DOUBLE	10	51	30.50	3050	VERY POOR
13	1.2	1.3	DOUBLE	16	51	33.50	3350	VERY POOR
14	1.3	1.4	DOUBLE	19	22	20.50	2050	POOR
15	1.4	1.5	DOUBLE	07	19	13.00	1300	FAIR
16	1.5	1.6	DOUBLE	37	18	27.50	2750	VERY POOR
17	1.6	1.7	DOUBLE	19	18	18.50	1850	POOR

3.4. Recomendd roughness values in india in mm/km

UNEVENNES INDEX, MM/KM	RIDING QUALITY
In Old Pavements	
Below 950	Excellent
950 to 1190	Good
1200 to 1440	Fair
1450 to 2400	Poor (possible resurfacing)
Above 2400	Very poor (resurfacing required)
In New pavements	
Below 1200	Good (acceptable)
1200 to 1450	Fair (acceptable)
Above 1450	Poor (not acceptable)

3.5. Graphs chainage vs uneveness index



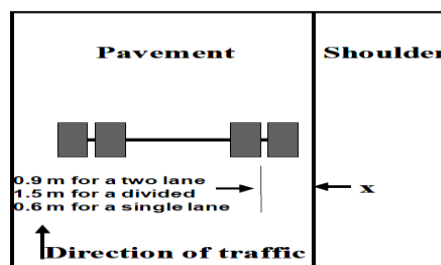
IV. DESIGN OF FLEXIBLE OVERLAY OVER RIGID PAVEMENTS

The overlay thickness required over a flexible pavement may be determined either by one of the conventional pavement design methods or by a non-destructive testing method like the Benkelman beam deflection method. The thickness of flexible overlay over rigid pavements is calculated using the following relationship  $h_f$  equal to  $2.5(F^*h_d - h_c)$ , where  $h_f$ ,  $h_c$ ,  $h_d$  and  $F$  are Flexible overlay thickness, Existing rigid pavement thickness, Design thickness of rigid pavement and Factor which depends upon modulus of existing pavement. For calculating thickness of bituminous overlay, the following relation is used  $h_b$  equal to  $h_f / 1.5$ , i.e.,  $h_b$  is equal to  $1.66 (F^*h_d - h_c)$ .

#### 4.1. Overlay design by benkelman beam deflection studies

Benkelman beam is a device which can be conveniently used to measure the rebound deflection of a pavement due to a dual wheel load assembly or the design wheel load. The Equipment consists of a slender beam of length 3.66m which is pivoted to a datum frame at a distance of 2.44 m from the probe end. The datum frame rests on a pair of front leveling legs and a rear legs and a rear leg with adjustable height. The probe end of the beam is inserted between the dual rear wheels of the truck and rests on the pavement surface at the center of the loaded area of the dual wheel load assembly. A dial gauge is fixed on the datum frame with its spindle in contact with the other end of the beam is twice the distance between the fulcrum and the dial gauge spindle. Thus the rebound deflection reading measured at the dial gauge is to be multiplied by two to get actual movement of the probe end due to the rebound deflection of the pavement surface when the dual wheel load is moved forward. A loaded truck with rear axial load of 8170 kg is use for the deflection study. The design wheel load is a wheel load assembly of gross weight 4085 kg with an inflation pressure of 5.6 kg/cm<sup>2</sup> and spacing between the rare tyre walls should be in between 30 - 40 mm. The stretch of road length to be evaluated is first surveyed to assess the general condition of the pavement with respect to the ruts, cracks and undulations. Based on the above pavement condition survey, the pavement stretches are classified and grouped into different classes such as good, fair and poor for the purpose of Benkelman beam deflection studies. The loading points on the pavement for deflection measurements are located along the wheel paths, on a line 0.9m from the pavement edge in the case of pavement of total width more than 3.5m; the distance from the edge reduce to 0.6m on narrower pavements. The number of loading points in a stretch and the spacing between them from for the deflection measurements are to be decided depending on the objective of the project and the precision desired. A minimum of 10 deflection observations may be taken on each of the selected stretch of pavement. The deflection observation points, the study is carried out in the following steps.

The truck is driven slowly parallel to the edge and stopped such that the left side rear dual wheel is centrally placed over the first point for deflection measurement. Probe end of the Benkelman beam is inserted between the gaps of the dual wheel and is placed exactly over the deflection observation point. When the dial gauge reading is reading is stationary or when the rate of change of pavement deflection is less than 0.025mm per min, the initial dial gauge reading  $D_0$  is noted. Both readings of the large and small needles of the dial gauge may be noted, the large needle may also be set zero if necessary at this stage. The truck is moved forward slowly through a distance of 2.7m from the point and stopped. The intermediate dial gauge reading  $D_i$  is noted when the rate of recovery of the pavement is less than 0.025mm per minute. The truck is then driven forward through a further distance of 0.9 m and the final dial gauge reading  $D_f$  is recorded as before.



Position of vehicle axle on road

#### 4.2. Correction for pavement temperature and subgrade moisture variations

When the pavement consist of relatively thick bituminous layers like the bituminous macadam or asphaltic concrete in the base/binder/surface course ,variations in temperature of pavement surface course cause variation in pavement deflection under the standard load. The IRC has suggested a standard temperature of 35°C and correction factor of 0.0065mm per °C to be applied for the variation from this standard pavement temperature. The correction will be negative when the pavement temperature is above 35°C and positive when it is lower. However it is suggested that deflection studies should be carried out when the pavement temperature is above 30°C, if this correction factor is to be applied. A seasonal variations cause variation is sub grade moisture. As it is always not possible to conduct deflection studies during monsoon season when subgrade moisture content is the highest the IRC has suggested that tentative correction factors of 2 for clayey soils and 1.2 to 1.3 for sandy subgrade soils may e adopted if the deflection observations are made during day seasons. The deflection under the worst subgrade moisture may therefore into be estimated by multiplying the summer deflection value by the appropriate correction factor.

4.3. Analysis of data

The rebound deflection values  $D_1, D_2, D_3$  are determined in mm after applying the leg corrections if necessary to the observed values of  $D_o, D_f$  and  $D_i$  in each case. The rebound deflection is calculated by taking the average of initial, intermediate and final readings and multiplying with the least count of dial gauge 0.025mm. The average deflection calculated by  $D = \frac{D_o+D_i+D_f}{3} \times 0.025$  mm, the mean value of the deflections at  $n$  points is  $\bar{D} = \sum \frac{D}{n}$  mm, standard deviation of the deflection values is  $\sigma = \sqrt{\frac{\sum(\bar{D}-D)^2}{(n-1)}}$ , characteristic deflection  $D_c = \bar{D} + t\sigma$ . Here the value of 't' is to be chosen depending upon the percentage of the deflection values to be covered in the design. When  $t = 1.0$ ,  $D_c = \bar{D} + \sigma$  covers about 84 percent of the cases; when  $t_o = 2.0$ ,  $D_c = \bar{D} + 2\sigma$  about 97.7 percent of the cases of deflection values on the pavement section, assuming normal distribution of rebound deflation values. The IRC recommends the former case, i.e.,  $D_c = \bar{D} + \sigma$ , whereas in many other countries they adopt the later case for overlay design. The necessary corrections for pavement temperature and sub grade moisture may be applied to the characteristic deflection value,  $D_c$  before designing the overlay thickness.

4.4. Benkle man beam test observations and results

S. No	Dial Gauge Reading			Deflection	Temp.	Deflection After temp. Correction	MC=2 After Deflection MC	Mean deflection	Standard deflection	Characteristic deflection
1	6	30	9	0.375	46	0.304	0.607	1.823	0.867	2.69
2	10	6	7	0.192	46	0.12	0.24			
3	48	65	68	1.508	46	1.436	2.873			
4	60	0	75	1.125	46	1.053	2.106			
5	82	2	63	1.225	54	1.101	2.202			
6	65	41	46	1.226	54	1.142	2.284			
7	42	1	92	1.125	54	1	2.002			
8	62	38	81	1.508	54	1.384	2.768			
9	20	23	25	0.566	54	0.442	0.884			
10	40	34	16	0.75	54	0.626	1.252			
11	48	49	45	1.183	54	1.059	2.118			
12	54	56	54	1.366	49	1.275	2.55			

V. OVERLAY THICKNESS DESIGN

The overlay thickness required  $h_o$  may be determined after deciding the allowable deflation  $D_a$  in the pavement under the design load. According to Ruiz's equation overlay thickness  $h_o$  in m is given by  $h_o = \frac{R}{0.434} \log_{10} \frac{D_c}{D_a}$  cm. Where  $h_o, R$  and  $D_a$  are the thickness of bituminous overlay in cm, deflection reduction factor depending on the overlay material (usual values for bituminous overlay range from 10 to 15, the average values that may be generally taken being 12) and allowable deflection which depends upon the pavement type and the desired design life values ranging from 0.75 to 1.25mm respectively. Which are generally used in flexible pavement for design of overlay thickness equivalent to granular material WBM layer. When superior materials are used in the overlay layer, the thickness value has to be suitably decreased taking "equivalent factor" of the material into consideration, then  $h_o = 550 \log_{10} \frac{D_c}{D_a}$  mm. where  $h, D_c$ , Thickness of granular of WBM overly in mm, pavement temperature and sub grade moisture  $\bar{D} + \sigma$  (after applying the corrections) respectively.  $D_a$  will be taken as 1.00, 1.25 and 1.5 mm if the projected design traffic A is 1500 to 4500, 450 to 1500 and 150 to 450 respectively, here

$$\begin{aligned}
 A &= \text{Design traffic} &= P[1 + r]^{(n+10)} \\
 r &= \text{Assumed growth rate} &= 7.5\% \\
 n &= \text{Construction period} &= 2 \text{ Years}
 \end{aligned}$$

When bituminous concrete or Bituminous Macadam with bituminous surface course is provided as the overlay, an equivalency factor of 2.0 is suggested by the IRC to decide the actual overlay thickness required, thus, the thickness of bituminous concrete overlay in mm will be  $\frac{h_o}{2}$  when the value of  $h_o$  is determined from above equation. According to R&B dept. present amount of traffic P is 700 CVPD, then design traffic is 1667 CVPD, therefore allowable deflection  $D_a$  is 1.00 for traffic in between 1500 to 4500. Here characteristic

deflection is greater than allowable deflection hence overlay design is required. Then  $h_0 = 550 \log_{10} \frac{D_c}{D_a}$  mm = 236mm, by considering equivalency factor 2.00 for bituminous concrete layer actual overlay thickness required  $= \frac{h_0}{2} = 11.8$  cm.

## VI. CONCLUSIONS & DISCUSSIONS

The designed overlay thickness for this repeatedly deteriorating pavement after conducting above tests is found to be 11.8cm, apart from this design the following conclusions are to be made. The growth of traffic on this stretch from last two decades are tremendously increased, increased traffic and heavy axle load vehicles are causing repeated deterioration of this road, hence the road stretch is redesigned for contemporary traffic condition, tonnage suitably. The drainage system both longitudinal and transverse on the selected stretch are inefficient and is not working properly especially at check post, leading to failures pertaining to improper drainage system, namely Pot holes, Stripping etc. Observing the nearest sites it is found that the ground water table at this site is very closer to ground surface, which leading to different types of pavement distress, hence it is necessary to take care to minimize this GWT by using techniques like Inverted sand filters, and by increasing the base course thickness, by observing the Benkelman Beam and Bump Integrator test results it is clear that on the road curve, the thickness of inner edge of the lane is very thinner than the outer edge, so the maximum deterioration is occurring on the inner edge, hence proper thickness of bitumen layer is provided on the inner edge of the road curve. Surface course has lack of binding with base course, which causing the keying hence necessary steps are taken while overlying is done to make good bond between surface course and base course.

## REFERENCES

- [1]. M.O.T (Road wings), "Manual for maintenance of Roads", Indian roads congress, 1983.
- [2]. Subba Raju, B.H. and Nanda, "Assessment of riding qualities of some of the roads in India", road research bulletin No. 5, Indian road congress.
- [3]. Khanna, S.K, Arora, M.G. and Nickwada,, "Use of Benkelman beam in the design of Flexible Overlays" National seminar, 20-years design and construction of roads and bridges, vol.1 , Ministry of Transport and shipping, Gov. of India, 1968.
- [4]. IRC, "Tentative guidelines for strengthening of flexible road pavements using Benkelman beam deflection technique". IRC: 81 - 1981, Indian roads congress.
- [5]. IRC Proceedings, "Seminar on Strengthening of Existing Road Pavements", Indian Roads Congress, 1971.
- [6]. S.K.Khana and C.E G. Justo, "Highway Engineering", Nem Chand & Bro's, publication 2001.
- [7]. IRC: 37-2001, Guide Lines for the Design of Flexible Pavements.
- [8]. IRC 81:1997 – Guidelines for Strengthening of Flexible Road Pavements Using Benkelman Beam Deflection Technique.
- [9]. Calibration report on "Axle Mounted bump integrator" By CRRI New Delhi Regional Laboratory PWD Kota, 1995.
- [10]. L.R. Kadiyali, Principles of Highway Engineering, Khanna Publications.
- [11]. MTAG (Maintenance Technical Advisory Guide) – Common Distresses on Flexible pavements.
- [12]. Justo C.E.G. and Ramadas,C.K., "Evaluation of Flexible Pavement and Design of Overlay Thickness",Seminar on Highway Design and Maintainance in Developing Countries,England,1979.

**MISSING HEART?...**  
**(“RAMANUJAM HEART”)**



**M.Arulmani, B.E.**  
**(Engineer)**



**V.R.Hema Latha, M.A., M.Sc.,**  
**M.Phil. (Biologist)**

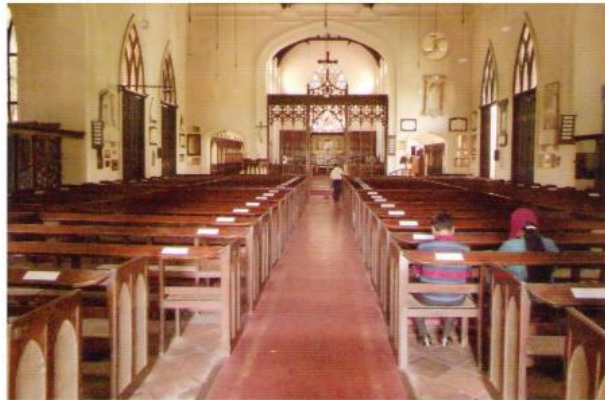
**GOD HAS STONY HEART?... HUMAN HAS FLESHY HEART?...** A scientific research article titled as “MISSING HEART” is brought out based on Historical facts of “SRI LANKA” based on Authors tour to Sri Lanka from **14.5.2015 to 18.5.2015**. This article focus that the stony heart of God has become fleshy heart by acquiring additional chambers in the **expanding universe**.

**I. FOREWORD:**

Sri Lanka is a secular country and most of the Sri Lankan population belong to “**BUDDHISM**”. It is apparently learnt that there is no “**CASTISM**” in Buddhism faith and having sense of **one family**. Christians, Muslims, Hindus are considered as Minorities in Sri Lanka. The name of international airport of Sri Lanka is called as **BHANDARANAYAKE** located at the place called **KATTUNAYAKE**.

In ancient epic **RAMAYANA** the land of Sri Lanka is much focused and concerned with **RAMA, SITA, RAVANA** and the author had a chance to visit that places where Hanuman landed first and the place where SITA was prisoned by Ravana concerned with this scientific research.

(i)



**St. Paul Church (1848)  
Kandy, Sri Lanka**

(ii)



**Sita Temple  
Nuwara Elia, Sri Lanka**

(iii)



**Buddha Temple  
Kandy, Sri Lanka**

(iv)



**Why we should take bath daily for the joy of Tourists?...**  
**(Elephant bath show, Sri Lanka)**

**II. ABSTRACT:**

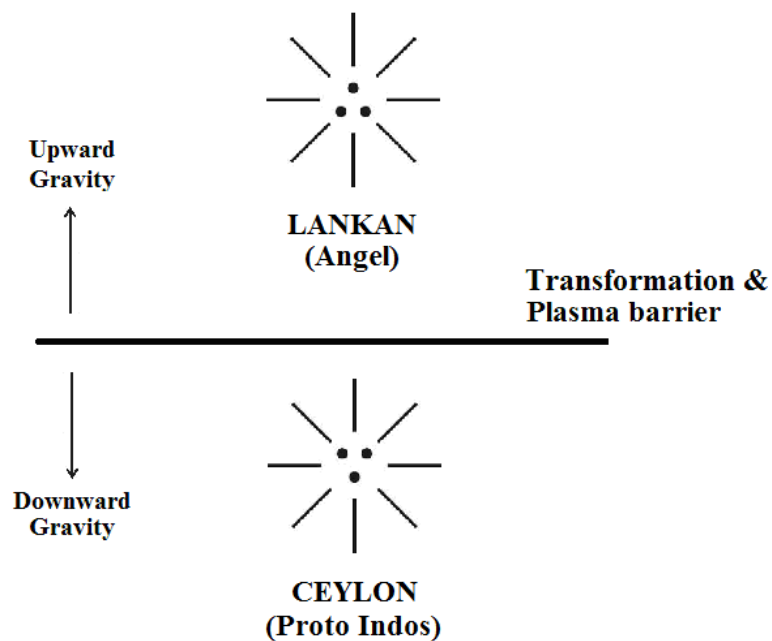
In the history of Sri Lanka, the Ancient land was called as "CEYLON". The total land are of Ceylon is focused about approximately 25,000 square mile and the total scattered populations is estimated about 2.0 Crores. The land of Ceylon is said to have ruled by British, Portuguese, French for about 350 years and ultimately got Independence on 4<sup>th</sup> February 1948.

- i) What does mean "CEYLON"?...
- ii) What does mean LANKAN?...
- iii) What does mean SRI LANKAN?...
- iv) What does mean BHANDARA NAYAKE?...
- v) What does mean KATTUNAYAKE?...
- vi) What does mean ABINAYAKE?...

... Author

It is further focused that the human ancestors lived on the land of "CEYLON" shall be considered as having only "SINGLE CHAMBER HEART". During the course of **expanding universe** human populations acquired genetic variation and become "THREE CHAMBER HEART" due to varied climatic conditions for **sustainability of Life**. CEYLONISH differs from LANKANS?...

It is further focused that "LANKAN" shall be considered as ANGEL POPULATIONS lived in MARS PLANET say around 5,00,000 years ago. The LANKAN shall also be called as BRAHMA (ARENKANAYAKA). During Plasma age the angel populations considered descended to "EARTH PLANET" having single chamber heart with distinguished genetic characteristics compared to Angel populations of "MARS PLANET". The philosophy of LANKAN, CEYLON shall be distinguished as below.



*GOD shall mean having STONY HEART. HUMAN shall mean having FLESHY HEART. Fleshy heart shall mean transformation of Stony heart into fleshy heart by acquiring additional chambers in the heart during expanding universe for sustainability of human due to varied environmental conditions.*

*...M. Arulmani, Tamil based Indian*

### III. Philosophy of "SRI LANKAN"?...

It is focused that "SRI LANKAN" shall mean genetically varied populations who considered have "THREE CHAMBER HEART" evolved from Ceylonish for sustainability of life say around 1,00,000 years ago. Further FOUR CHAMBER HEART human considered evolved just 10,000 years ago. In proto Indo Europe language root SRI LANKAN shall be called "THREE LANKAN". "Three Lankan" shall mean person having "Three chamber Heart".

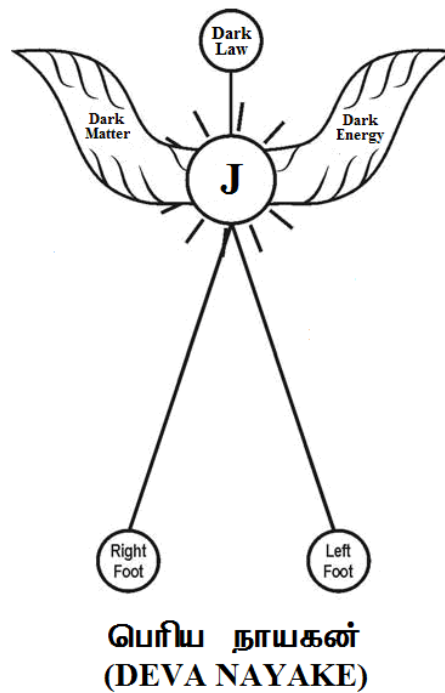
### IV. Philosophy of RAMANUJAM HEART?...

It is hypothesized that the entire cosmo universe shall be considered created by supernatural person called by name by author as "RAMANUJAM". Ramanujam shall be considered as have created everything through his "MOTHER JANAKI" (Souls) who shall be considered as **Integral** part of Ramanujam who consider have **SINGLE CHAMBER HEART (Stony Heart)**. The Philosophy of **RAMANUJAM, JANAKI** shall be described as below. The etymology of word **CEYLON** might be derived from the word J-Land (Lanther). J-Land shall mean **LAND OF JANAKI** or Land of **VIRGIN LIGHT**.

(i)



(ii)



#### V. BRAHMA had single chamber Heart?...

It is hypothesized that in Hindu mythology, the philosophy of Brahma, Ramakrishna, Shiva shall be considered as god of distinguished genetic populations having varied heart chamber in different phase of time in the expanding universe as described below:

- i) **RAMANUJAM (GOD)** - Single chamber heart
- ii) **JANAKI (SOUL)** - Single chamber heart
- iii) **BRAHMA (Ethics)** - Single chamber heart
- iv) **RAMA (Revolution)** - Broken heart (Plasma)
- v) **KRISHNA (Democracy)** - Single chamber heart
- vi) **SHIVA (Socialism)** - Three chamber Heart

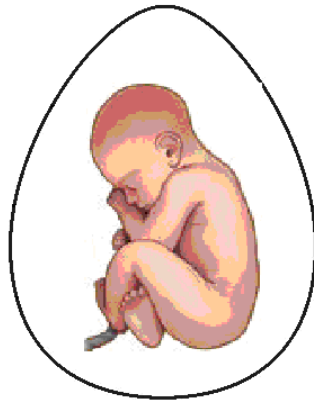
The philosophy of varied heart chamber shall be narrated as below for universal understanding.

(i)



**முதல்வர்  
(Ramanujam)  
(DEVA NAYAKE)**

(ii)



**விண்ணவர்  
(Brahma)  
(VIN NAYAKE)**

(iii)



**மண்ணவர்  
(Rama)  
(KATTU NAYAKE)**

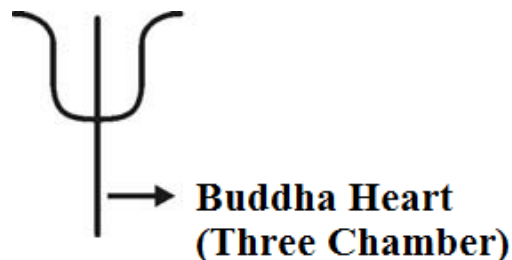
(iv)



மணீசர்  
(Krishna)  
(PANDARA NAYAKE)

#### VI. BUDDHA had three chamber heart?...

It is hypothesized that "BUDDHA" shall be considered as "MODERN SHIVA" (ABINAYAKE) having only three chamber and having the principle of "SOCIALISM" (Improved Democracy) eradicating the philosophy of "CASTISM" in human civilization and become "ONE FAMILY".



- i) **RIGHT CHAMBER - PROSPERITY** (Like Raksha mask)
- ii) **LEFT CHAMBER - WEALTH** (like Sanni mask)
- iii) **MIDDLE CHAMBER - PEACE** (Like kolam mask)

#### VII. JESUS CHRIST had four chamber Heart?...

It is hypothesized that JESUS CHRIST might have had four chamber heart in the expanding universe having the principle of "MARSISM" (Improved socialism) focusing improved life system of "ETHICS ORIENTED DEMOCRACY". It is hypothesized that JESUS CHRIST shall be considered as the father of four chamber heart generation.

#### VIII. "BRITISH" are Aliens?...

It is hypothesized that "BRITISH" shall be considered as the "SONS OF SOIL" of ancient "CEYLON" (Post Indos) rather than Aliens. The language "SINGHALISH" (Singha + English) of Sri Lanka shall be considered derived from ENGLISH of British (Ceylonish). The philosophy of Language evolution spoken by varied genetic human races shall be hypothetically narrated as below:

- i) **RAMANUJAM - JANGLISH** (Universal)
- ii) **BRAHMA - ANGLISH** (5,00,000 years ago)
- iii) **RAMA - TANGLISH** (3,00,000 years ago)
- iv) **KRISHNA - ENGLISH** (2,00,000 years ago)
- v) **SHIVA - SINGHALISH** (1,00,000 years ago)

*BRITISH (Ceylonish) shall mean ETHICIST. SRI LANKAN (Singhalish) shall mean SOCIALIST. The Philosophy of LIBERATION or INDEPENDENCE shall mean transformation of ethicisim to socialism in the expanding Universe for sustainability of human and betterment of life system.*

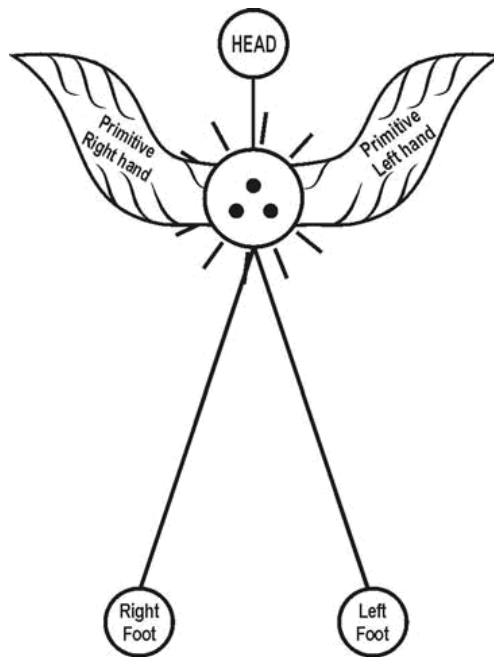
*...M. Arulmani, Tamil based Indian*

**IX. Philosophy of SINGHALISH Ethnics?...**

It is focused that during the course of time the populations of BUDDHA (Post Indos) shall be considered undergone three major ethnic divisions as described below:

- i) SINGHALISH ACHARIYA - (CHERA ELEPHANT)
- ii) SINGHALISH SANKARA - (PANDIYA TIGER)
- iii) SINGHALISH ADI SANKARA - (CHOLA LION)

**X. Can we see RAMA?...**



**MGR  
(KANDY)**

Why not?... RAMA (MINAVAR) shall be considered as “Super Scientist” capable of “FLYING” and effectively controlling the relative position of MARS, SUN, EARTH, MOON having Head quarters at “KANDY” (KACHCHA THEEVU) in the early universe. RAMA shall also be called as “MGR”. MGR shall mean “MARS GEO RULER”.

*MINAVAR (MEENAVAR) doesn't mean FISHERMAN. Minavar shall mean expert in Astronomy, Astrophysics. MINACHI shall mean ruler of Fundamental Neutrino particles.*

*...Author*

### XI. Tamilians (Black Indians) are Adventurers?...

It is focused that Tamilians shall be considered as strangers and adventurers. It is evident from recent incident happened at **SINGAPORE**. In the apartment (2<sup>nd</sup> floor) one **CHILD** was miraculously saved by two Tamilians by name Shanmuganathan and Muthukumar. It is apparently known that the mother instructed the child not to move anywhere in the locked house for the reason of sending the elder child to the school for short duration. By the time the child disobeyed the order of mother and gone to balcony and about to be fallen. So many peoples were crowded fearfully and watched the incident.

But the adventurers Shanmuganathan and Muthukumar immediately climbed to the upper floor through sanitary pipeline sacrificing their life (**NOT FOR GETTING ANY AWARD**). For appreciating this incident the **SINGAPORE GOVERNMENT** have honored these two adventurous Tamilians. The two Tamilians belongs to **PATTI** (Villiage). Shanmuganathan belong to Ammanpatti of Sivaganga district and Muthukumar belong to Puliya Rajakka Patti of Dindigul district.

Not only this incident but in many places, many child disobey the order of mother and fell into bore well and unnecessarily creating tension to the mother.

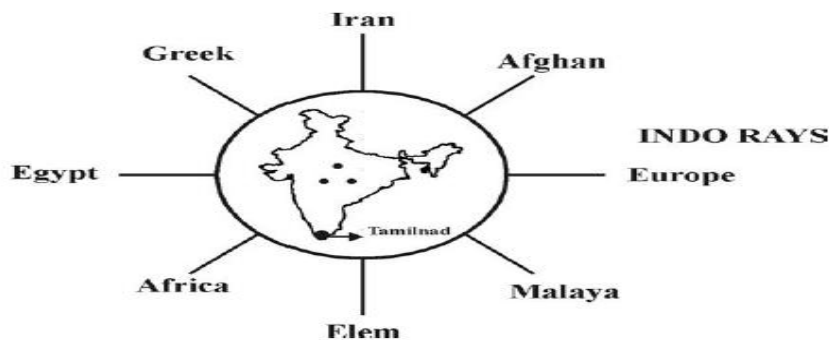
- Kumudam weekly report

*Tamilians like BLACK BRITISH.  
Singhalish like RED BRITISH.*

*...Author*

### XII. CONCLUSION

#### சுமர்ப்பணம்



“ இந்தியநாடு என் தாய்;  
தமிழ்நாடு என்தாயின் பாதஅடி.  
என் தாயின் பாத அடியில் இப்புத்தக அஞ்சலி ”

## புதுக்கவிதை

(மலரும் நினைவுகள்)

அந்தநாள் ஞாபகம்... வானொலியின் கம்பீர் ஒலி...  
சரியாக காலை ஏழுமணி... பதினைந்து நிமிடம்...  
கடிகாரம் தேவையில்லை... அந்த ஒலி மீண்டும் ஒலிக்குமா?...

பிறந்த நாள்... இன்று பிறந்த நாள்...  
நாம் பிள்ளைகள் போலே... தொல்லைகளெல்லாம்...  
மறந்த நாள்... இலங்கை வானொலியின் கம்பீர் ஒலி...

விண்ணைத் தொடும் K.S.ராஜா அப்துல்வஹீது கணீர் ஒலி...  
உலகநாடுகளையே ஒருங்கிணைக்கும் அந்த "தமிழ் ஒலி"...  
விண்ணை தொடுவதால் "வானொலி" என்று பெயர் வந்ததே?

இலங்கைக்கு இன்னொரு பெயர் கன்னி நாடு...  
முதல் மனித இனம் (Angels) வாழ்ந்த புனித நிலம்...  
செவ்வாய் கிரகம் எனும் தாய்கிரகம் (Mother planet)

தமிழர்கள் சிங்களர்கள், இந்தியர்கள்...  
உலகின் அனைவரம் கன்னித்தாயின் (Janaki) வாரிசுகள்...  
பூமியில் தோன்றிய ஒரே தாயின் (Sita) வாரிசுகள்...

**இந்தியாவும், திரிலங்கமும்... (Sri Lanka)**

**தொப்புள் கொடியால் இணைக்கப்பட்ட “தாய்சேய்”...**

**காலத்தால் தொப்புள்கொடி அறுந்துபோனது...**

**சிங்களத் தீவுக்கோர் பாலம் அமைப்போம்...**

**சேதவை மேடுகூந்தி பாதை அமைப்போம்...**

**பாரதியின் கனவு நனவாகுமா?...**



**Tamillan (Black Indians) with Singhalish (Red Indians)  
Kandy, Sri Lanka**

**-M. அருள்மணி  
தமிழ்ப்பேசும் இந்தியன்.**

**Previous Publications:**

1. YUGADI WISHES (IARA, March 2015)
2. TAMIL PUTHANDU!... (AJER, April 2015)
3. THEN MADURAI?... (IJERD, April 2015)
4. TAMIL NEW YEAR COOL DRINK?... (AJER, April 2015)
5. SCIENTIFIC RAMANUJAM?... (IJERD, April 2015)
6. ARENKA NAYAKI IS MOTHER OF RAMA?... (AJER, April 2015)
7. TRIVIDAITE?... (IJERD, April 2015)
8. THALI CULTURE OF ANGELS?... (AJER, April 2015)
9. UNIVERSAL POET?... (IJERD, April 2015)
10. "JANGLISH" IS CHEMMOZHI?... (AJER, April 2015)
11. RAMANUJAM PARLIAMENT?... (IJERD, May 2015)
12. CAN LORD JUDGE GOD?... (AJER, May 2015)
13. MAY DAY?... (IJERD, May 2015)
14. DEEMED UNIVERSITY?... (AJER, May 2015)
15. CAR FESTIVAL?... (IJERD, May 2015)

## On the Transmission Line Pulse Measurement Technique

X. Rodriguez<sup>1</sup>, M. Eduardo<sup>1</sup>, M. Harington<sup>2</sup>

<sup>1</sup>(Department of Physics, University of Barcelona, Spain)

<sup>2</sup>(Universidad AbatOliba CEU, Spain)

**ABSTRACT :** Transmission Line Pulse is a short pulse (25ns to 150ns) measurement of the current-voltage (I/V) characteristics of the ESD protection built into an integrated circuit. The short TLP pulses are used to simulate the short ESD pulse threats and integrated circuit must tolerate without being damaged. In this work the fundamental principles of how the TLP pulse is generated and used to create I-V characteristic plots will be explored. The measurement will be then used to characterize the I-V characteristics of some electronic parts to see how it can help arriving at accurate results.

**KEYWORDS**—Transmission Line Pulse, TLP, Device, Measurement

### I. INTRODUCTION

Transmission Line Pulse (TLP) measurement is an industrially accepted way for the characterization of ESD-protection devices in the high-current regime. In this technique a transmission line is charged up to an appropriate voltage and is used as a pulsed voltage source [1], [2], [3]. Once discharged a sharp pulse with very fast rise times down to 100 ps can be generated. The length of the used transmission line determines the pulse width. In 1985 Maloney and Khurana [4] introduced TLP measurements as method for characterization of ESD-protection devices in the high-current regime. Since then, TLP using a pulse width of 100 ns has become a standard practice for high-current measurements. In recent studies, the TLP method is used successfully to measure the reverse recovery phenomenon in power devices [5]. Later the method was further developed with generation of faster pulses, resulting in very fast TLP (vf-TLP) [6], which can produce pulse widths down to 1 ns.

Figure 1 shows a basic setup for a 50 ohm time-domain TLP system [4]. An approximately 10 m long 50 ohm coaxial cable, which can be charged to a high voltage, serves as the pulse source. A charged 50 ohm coaxial cable will create a rectangular pulse when discharged into a load. A switch is used to connect this transmission line to the test device. The voltage and current waveforms are monitored using high speed oscilloscopes and are sensed using special voltage and current probes.

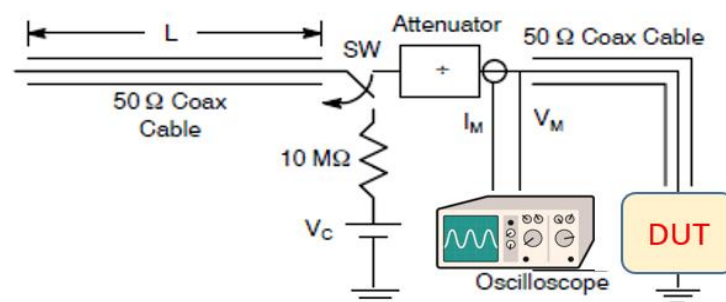


Figure 1. A 50 ohm basic TLP system

The way the TLP system works is as follows: The transmission will be charged while the switch is closed. The charged cable will act to create the voltage pulse. The pulse passes through the attenuator, travels down the coax cable to the DUT, reflects off the DUT and travels back toward the attenuator and into the pulse source transmission line. In this path, it is critical for the system to be impedance matched. Impedance matched refer to a state in which the impedance of different components of system is equal to one another. As mentioned earlier, often an oscilloscope is employed to monitor the signals during the measurement.

When a signal on a transmission line reaches a termination the reflected signal depends on the impedance of the termination as in the following equations, in which  $R_{DUT}$  is the resistance of the DUT and  $Z$  is the characteristic impedance of the transmission line.

$$V_{reflected} = V_{incident} = \frac{R_{DUT} - Z}{R_{DUT} + Z}$$

$$V_{reflected} = -V_{incident} = \frac{R_{DUT} - Z}{R_{DUT} + Z}$$

If the device has the same impedance as the measurement system then there is going to be no reflection. If the termination is open the reflected voltage is equal to the incident voltage while the reflected current is equal in magnitude but of opposite sign, since the charge is traveling in the opposite direction. For a short the reflected voltage is equal in magnitude to the incident voltage but is changed in sign. For a short the reflected current has the same magnitude and sign as the incident current. What is physically happening is that the reflected charge is traveling in the opposite direction from the incident pulse but because it was a short the charge is flowing back through the shield.

The pulse that the DUT finally sees is the sum of the incident and reflected pulses. For a TLP system with a characteristic time of 100 ns, the delay between the voltage and current probes and the DUT is much less than 100 ns, which means the incident and reflected pulses overlap at the point of the voltage and current probes. During the period of overlap between the incident and reflected pulses the oscilloscope is directly measuring what the DUT experiences. This is illustrated in Figure 2a, for an  $R_{DUT}$  with a resistance less than 50. For voltage we first see the incident pulse only, but after twice the transit time between the voltage probe and the DUT the reflected pulse arrives and adds to the incident pulse. Since  $R_{DUT}$  is less than 50 the reflected pulse is negative and the measured voltage is less than the incident pulse value. After the incident pulse has passed the voltage probe only the reflected pulse is measured and we see a negative going transient. The situation for current in Figure 2 is similar with an initial measurement of only the incident pulse, a period in which the incident and reflected pulses overlap, followed by the reflected pulse only. The major difference is that for current the reflected pulse for  $R_{DUT}$  less than 50 is positive, resulting in the measured current in the overlap region being larger than during the incident pulse only period.

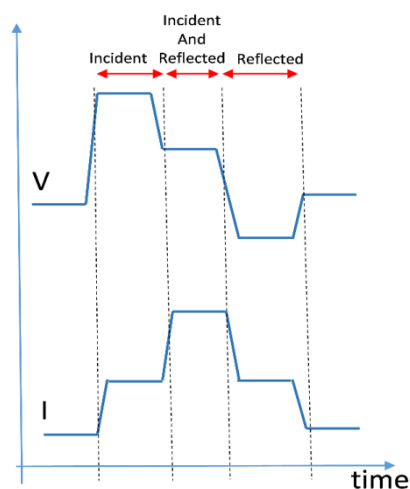


Figure 2. The incident and reflected current and voltage waveforms in the time domain

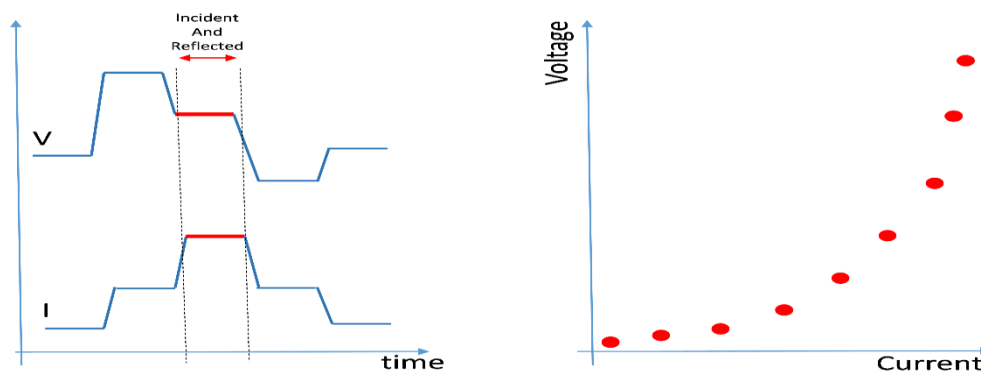


Figure 3. Demonstration of how an I-V plot is obtained from voltage and current waveforms

To obtain a current/voltage pair from the pulse measurements a measurement window is defined during the time period on the oscilloscope when the incident and reflected pulses overlap, usually toward the end of this overlap period. The voltage and current during the measurement window are plotted as a point on the I-V curve, as shown in Figure 3. To obtain a full I-V curve the process is repeated at a variety of charging voltages for the pulse source transmission line, usually starting at low charging voltages and progressing to higher voltages.

## II. MEASUREMENT RESULTS - TRANSIENT VOLTAGE SUPPRESSOR (TVS) DEVICE:

Figure 4 shows a TVS device measured in Reverse Bias using the TLP technique for a TVS diode in the reverse bias direction. In this case the TLP measurements indicate that over the measured range the TVS's properties are linear and can be represented by a linear least squares fit, as shown in Figure 4. The fit yields a dynamic resistance of  $1.35 \Omega$  and a voltage intercept of  $6.49 \text{ V}$ . (The dynamic resistance is the inverse of the slope of a current versus voltage curve over a limited range of current and voltage.) Note that the voltage intercept is not the low current breakdown voltage. The breakdown voltage of diodes is usually measured in the A or mA range, where the current is often still increasing exponentially with voltage. TLP measurements explore the high current range, which is precisely why the resistance and voltage intercept measured with TLP more accurately reflect the protection properties of a TVS device than measurements at longer time scales. Another important aspect that is demonstrated in this measurement is the suppression of the self-heating effect. During the DC measurements of power devices, the self-heating effect is always detrimental. This phenomenon can lead to erroneous results and needs to be avoided. As can be seen in the data set below, the self-heating effect is not present while the measurement is done in the pulsed form using the TLP setup. This is a great advantage of the TLP measurement over the ordinary DC measurements.

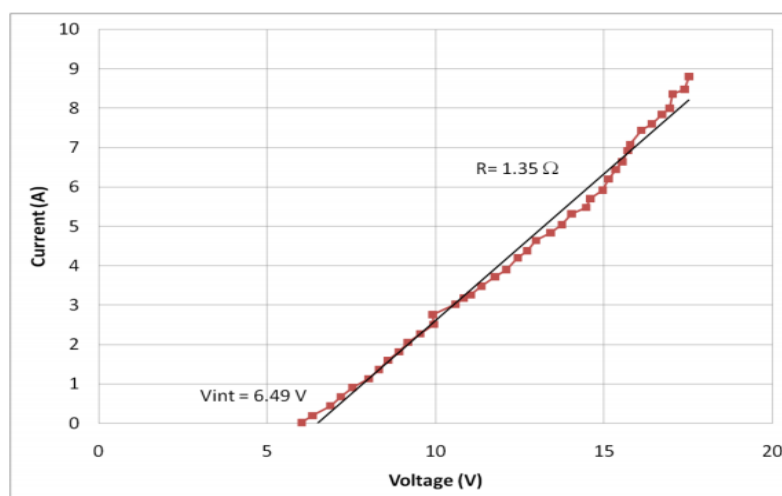


Figure 4. Sample TLP Curve of a TVS Diode

### III. CONCLUSION

The Transmission Line Pulse measurement was investigated and its fundamental mechanism was explained. The benefits of using the TLP measurement over DC measurement makes it a suitable choice for measuring ESD events and power devices. This is specifically true when the goal is to avoid effects such as self-heating. The standard 100 ns, 50 ohm TLP measurement was shown to be a suitable test for studying the I-V characteristics of TSV devices.

### REFERENCES

- [1] Q. Shi, Q.-Z. Xiao, Y. Liu, and Y.-F. En, "Notice of Retraction Measurement of ESD protection structure irradiation degradation using TLP method," in *2013 International Conference on Quality, Reliability, Risk, Maintenance, and Safety Engineering (QR2MSE)*, 2013, pp. 2029–2030.
- [2] Y. Xi, S. Malobabic, V. Vashchenko, and J. Liou, "Correlation Between TLP, HMM, and System-Level ESD Pulses for Cu Metallization," *IEEE Trans. Device Mater. Reliab.*, vol. 14, no. 1, pp. 446–450, Mar. 2014.
- [3] Y. Chung, H. Xu, R. Ida, and B. Baird, "Snapback Breakdown Dynamics and ESD Susceptibility of LDMOS," in *Reliability Physics Symposium Proceedings, 2006. 44th Annual., IEEE International*, 2006, pp. 352–355.
- [4] O. Semenov, H. Sarbishaei, and M. Sachdev, *ESD Protection Device and Circuit Design for Advanced CMOS Technologies*. Springer Science & Business Media, 2008.
- [5] A. ElhamiKhorasani, M. Griswold, and T. L. Alford, "Gate-Controlled Reverse Recovery for Characterization of LDMOS Body Diode," *IEEE Electron Device Lett.*, vol. 35, no. 11, pp. 1079–1081, Nov. 2014.
- [6] H. Gieser and M. Haunschild, "Very-fast transmission line pulsing of integrated structures and the charged device model," in *Electrical Overstress/Electrostatic Discharge Symposium, 1996. Proceedings*, 1996, pp. 85–94.

## Unsteady MHD flow and heat transfer of nanofluid over a permeable shrinking sheet with thermal radiation and chemical reaction

<sup>1</sup>, Srinivas Maripala, <sup>2</sup>, Kishan.N,

<sup>1</sup>. Assistant Professor, Dep.t of mathematics, SNIST, Hyd, Telangana, India, 501301.

<sup>2</sup> Associate Professor, Dep.t of mathematics, OU, Hyd, Telangana, India, 500007,

**ABSTRACT:** An analysis is presented to study the forced convection in unsteady magneto-hydrodynamic boundary layer flow of a nanofluid over a permeable shrinking sheet in the presence of thermal radiation and chemical reaction. A variable magnetic field is applied normal to the sheet. The nanofluid model includes Brownian motion and thermophoresis effects are also considered. The boundary layer equations governed by the partial differential equations are transformed into a set of ordinary differential equations the help of local similarity transformations. The coupled and nonlinear differential equations are solved by the implicit finite difference method along with the Thomas algorithm. We have explained the effect of various controlling flow parameters namely unsteadiness parameter  $A$ , magnetic parameter  $M$ , thermal radiation parameter  $R$ , Prandtl number  $Pr$ , Brownian motion parameter  $N_b$ , thermophoresis parameter  $N_t$  and Lewis number  $Le$  on the dimensionless velocity, temperature and nanoparticle volume fraction profiles are analyzed.

**KEY WORDS:** Nanofluid, Magnetic field, Thermal radiation, Chemical reaction, Shrinking sheet, implicit finite difference method.

### I. INTRODUCTION:

The flow over a shrinking surface is an important problem in many engineering processes with applications in industries such as the hot rolling, wire drawing and glass wire production. In nature, the presence of pure air or water is impossible. Some foreign mass may be present either naturally or mixed with the air or water. The present trend in the field of magnetic strength analysis is to give a mathematical model for the system to predict the reactor performance. A large amount of research work has been reported in this field. In particular, the study of heat and mass transfer with magnetic effect is of considerable importance in chemical and hydrometallurgical industries. Bhattacharyya and Gupta [1], Gupta and Gupta [2] and Cheng and Lin [3] studied the heat and mass transfer on nonlinear MHD boundary layer flow in various situations.

Magneto-hydrodynamic (MHD) mixed convection heat transfer flow in porous and non-porous media is of considerable interest in the technical field due to its frequent occurrence in industrial technology and geothermal application, high temperature plasmas applicable to nuclear fusion energy conversion, liquid metal fluids and power generation systems. A few representative fields of interest in which combined heat and mass transfer with chemical reaction play important role, are design of chemical processing equipment, formation and dispersion of fog, distribution of temperature and moisture over agricultural fields and groves of fruit trees, damage of crops due to freezing, food processing and cooling towers. Cooling towers are the cheapest way to cool large quantities of water. Chemical reaction can be classified as either heterogeneous or homogeneous processes. This depends on whether they occur at an interface or as a single phase volume reaction. This depends on whether they occur at an interface or as a single phase volume reaction. For example, formation of smog is a first order homogeneous chemical reaction. Consider the emission of  $NO_2$  from automobiles and other smoke-stacks. This  $NO_2$  reacts chemically in the atmosphere with unburned hydrocarbons (aided by sunlight) and produces peroxyacetyl nitrate, which forms an envelope of what is termed as photochemical smog.

The boundary layer flow over a shrinking surface is encountered in several technological processes. Such situations occur in polymer processing, manufacturing of glass sheets, paper production, in textile industries and many others. Crane [4] initiated a study on the boundary layer flow of a viscous fluid towards a linear stretching sheet. An exact similarity solution for the dimensionless differential system was obtained. Carragher and Carane [5] discussed heat transfer on a continuous stretching sheet. Afterwards, many investigations were made to examine flow over a stretching/shrinking sheet under different aspects of MHD, suction/injection, heat and mass transfer etc. [6–13]. In these attempts, the boundary layer flow, due to stretching/shrinking has been analyzed. Magyari and Keller [14] provided both analytical and numerical solutions for boundary layer flow over an exponentially stretching surface with an exponential temperature distribution. The combined effects of viscous dissipation and mixed convection on the flow of a viscous fluid over an exponentially stretching sheet were analyzed by Partha et al. [15], Elbashareshy [16] numerically studied flow and heat transfer over an exponentially stretching surface with wall mass suction. Madhu.M and Naikoti Kishan[17] studied the Two-dimensional MHD mixed convection boundary layer flow of heat and mass transfer stagnation-point flow of a non-Newtonian power-law nanofluid towards a stretching surface in the presence of thermal radiation and heat source/sink.

On the other hand, the flow over a shrinking sheet is a new field of research at present and few literatures is available on this area of research now. Wang [18] first studied a specific shrinking sheet problem. Recently, Miklavcic and Wang [19] obtained the existence and uniqueness of the solution for steady viscous hydrodynamic flow over a shrinking sheet with mass suction. Hayat et al. [20] derived both exact and series solution (using HAM) describing the magnetohydrodynamic boundary layer flow of a second grade fluid over a shrinking sheet. The problem of MHD viscous flow due to a shrinking sheet was solved by Sajid and Hayat [21] using HAM.

It is interesting to note that the Brownian motion of nanoparticles at molecular and nanoscale levels are a key nanoscale mechanism governing their thermal behaviors. In nanofluid systems, due to the size of the nanoparticles, the Brownian motion takes place, which can affect the heat transfer properties. As the particle size scale approaches to the nanometer scale, the particle Brownian motion and its effect on the surrounding liquids play an important role in the heat transfer. In view of these applications, Nield and Kuznetsov ([22, 23]) analyzed the free convective boundary layer flows in a porous medium saturated by nanofluid by taking Brownian motion and thermophoresis effects into consideration. In the first article, the authors have assumed that nanoparticles are suspended in the nanofluid using either surfactant or surface charge technology and hence they have concluded that this prevents particles from agglomeration and deposition on the porous matrix. Chamkha *et al.* [24] carried out a boundary layer analysis for the natural convection past an isothermal sphere in a Darcy porous medium saturated with a nanofluid. Nield and Kuznetsov [25] investigated the cross-diffusion in nanofluids, with the aim of making a detailed comparison with regular cross diffusion effects and the cross-diffusion effects peculiar to nanofluids, and at the same time investigating the interaction between these effects when the base fluid of the nanofluid is itself a binary fluid such as salty water. Recently, a boundary layer analysis for the natural convection past a horizontal plate in a porous medium saturated with a nanofluid is analyzed by Gorla and Chamkha [26], N. Kishan et.al [27], studied the unsteady MHD flow of heat and mass transfer of Cu-water and TiO<sub>2</sub>-water nanofluids over stretching sheet with a non-uniform heat/source/sink considering viscous dissipation and chemical reaction.

The effect of an applied magnetic field on nanofluids has substantial applications in chemistry, physics and engineering. These include cooling of continuous filaments, in the process of drawing, annealing and thinning of copper wire. Drawing such strips through an electrically conducting fluid subject to a magnetic field can control the rate of cooling and stretching, thereby furthering the desired characteristics of the final product. Such an application of a linearly stretching sheet of incompressible viscous flow of MHD was discussed by Pavlov[28] . In other work, Jafar et al.[29] studied the effects of magnetohydrodynamic (MHD) flow and heat transfer due to a stretching/shrinking sheet with an external magnetic field, viscous dissipation and Joule effects. Recently, Samir kumar at.el.[30] studied the forced convection in unsteady boundary layer flow of a nanofluid over a permeable shrinking sheet in the presence of thermal radiation.

It is now propose to study the effects of chemical reaction and the influence of magnetic field on the flow and heat transfer due to the unsteady two dimensional laminar flow of a incompressible viscous nanofluid caused by a permeable shrinking sheet with thermal radiation effects. The results are presented focus on how the chemical reaction parameter, thermal radiation, magnetic field, Brownian motion, thermophoresis effects of the heat transfer and characteristic of the flow.

## II. FLOW ANALYSIS:

Consider unsteady two-dimensional laminar boundary-layer flow of incompressible electrically conducting viscous nanofluid past a permeable shrinking sheet. The flow is subjected to a transverse magnetic field of strength  $B$  which is assumed to be applied in the positive  $y$ -direction, normal to the surface. It is

assumed that the velocity of the shrinking sheet is  $u_w(x, t)$  and the velocity of the mass transfer is  $v_w(x, t)$ , where  $x$  is the coordinate measured along the shrinking sheet and  $t$  is the time. It is also assumed that the constant surface temperature and concentration of the sheet are  $T_w$  and  $C_w$ , while the uniform temperature and concentration far from the sheet are  $T_\infty$  and  $C_\infty$ , respectively. Under these assumptions, the unsteady boundary-layer equations governing the flow, heat and mass transfer are

$$\frac{\partial u}{\partial x} + \frac{\partial v}{\partial x} = 0 \quad (1)$$

$$\frac{\partial u}{\partial t} + u \frac{\partial u}{\partial x} + v \frac{\partial u}{\partial y} = v \frac{\partial^2 u}{\partial y^2} - \frac{\sigma B^2}{\rho_f} u - \frac{\mu}{k\rho} u \quad (2)$$

$$\frac{\partial T}{\partial t} + u \frac{\partial T}{\partial x} + v \frac{\partial T}{\partial y} = \alpha_m \frac{\partial^2 T}{\partial y^2} - \frac{1}{\rho_f c_p} \frac{\partial q_r}{\partial y} + \tau [D_B \frac{\partial C}{\partial y} \frac{\partial T}{\partial y} + \frac{D_T}{T_\infty} (\frac{\partial T}{\partial y})^2] \quad (3)$$

$$\frac{\partial C}{\partial t} + u \frac{\partial C}{\partial x} + v \frac{\partial C}{\partial y} = D_B \frac{\partial^2 C}{\partial y^2} - \frac{D_T}{T_\infty} \frac{\partial^2 T}{\partial y^2} - k_c(C - C_\infty) \quad (4)$$

where  $u$  and  $v$  are the velocity components in the  $x$  and  $y$ -directions respectively,  $m$  is the kinematic viscosity,  $r$  is the electrical conductivity (assumed constant),  $\rho_f$  is the density of the base fluid,  $\alpha_m$  is the thermal diffusivity,  $D_B$  is the Brownian diffusion coefficient,  $D_T$  is the thermophoresis diffusion coefficient and  $C_p$  is the specific heat at constant pressure. Here  $\tau$  is the ratio of the effective heat capacity of the nanoparticle material and the heat capacity of the ordinary fluid,  $T$  is the fluid temperature and  $C$  is the nanoparticle volume fraction.

The term  $\frac{\sigma B^2}{\rho_f} u$  in the R.H.S. of Eq. (2) is the Lorentz force which arises due to the interaction of the fluid velocity and the applied magnetic field and  $\frac{\mu}{k\rho} u$  is permeability parameter. In writing Eq. (2), we have neglected the induced magnetic field since the magnetic Reynolds number for the flow is assumed to be very small. This assumption is justified for flow of electrically conductive fluids such as liquid metals e.g. mercury, liquid sodium, etc. Eq. (3) depicts that heat can be transported in a nanofluid by convection, by conduction and also by virtue of nanoparticle diffusion and radiation.

The term  $u \frac{\partial T}{\partial x} + v \frac{\partial T}{\partial y}$  is the heat convection; the term  $\alpha_m \frac{\partial^2 T}{\partial y^2}$  is the heat conduction; the term  $\tau D_B \frac{\partial C}{\partial y} \frac{\partial T}{\partial y}$  is the thermal energy transport due to Brownian diffusion; the term  $\tau \frac{D_T}{T_\infty} (\frac{\partial T}{\partial y})^2$  is the energy transport due to thermophoretic effect and  $\frac{1}{\rho_f c_p} \frac{\partial q_r}{\partial y}$  is the nanoparticle heat diffusion by radiation. Eq. (4) shows that the nanoparticles can move homogeneously within the fluid (by the term  $\frac{\partial C}{\partial x} + v \frac{\partial C}{\partial y}$ ), but they also possess a slip velocity relative to the fluid due to Brownian diffusion  $D_B \frac{\partial^2 C}{\partial y^2}$ ; the thermophoresis  $\frac{D_T}{T_\infty} \frac{\partial^2 T}{\partial y^2}$  and  $k_c(C - C_\infty)$  is chemical reaction parameter.

Here the boundary conditions are

$$u = u_w(x, t) = -\frac{cx}{(1-\lambda t)}, \quad v = v_w(x, t), \quad T = T_w, \quad C = C_w, \quad \text{at } y = 0,$$

$$u \rightarrow 0, \quad T \rightarrow T_\infty, \quad C \rightarrow C_\infty \quad \text{as } y \rightarrow \infty, \quad (5)$$

The wall mass transfer velocity then becomes

$$v_w(x, t) = -\sqrt{\frac{cv}{(1-\lambda t)}} s, \quad (6)$$

where  $s$  is the constant wall mass transfer parameter with  $s > 0$  for suction and  $s < 0$  for injection, respectively. Using Rosseland's (see Brewster [31]) approximation for radiation we can write

$$q_r = -\frac{4\sigma_1}{3K_1} \frac{\partial T^4}{\partial y}, \quad (7)$$

where  $\sigma_1$  is the Stefan-Boltzmann constant and  $K_1$  is the mean absorption coefficient. Assuming the temperature difference within the flow is such that  $T^4$  may be expanded in a Taylor series about  $T_\infty$  and neglecting higher order terms we get  $T^4 \approx 4T_\infty^3 T - 3T_\infty^4$ . Hence from Eq. (7), using the above result,

We have  $\frac{\partial q_r}{\partial y} = - \frac{16\sigma_1 T_\infty^3}{3K_1} \frac{\partial^2 T}{\partial y^2}$  (8)

to attain the similarity solutions of the Eqs. (1) – (4) with the boundary conditions (5), we take the transverse unsteady magnetic field strength applied to the sheet is of the form  $B = B_0/\sqrt{1-\lambda t}$ , where  $B_0$  is constant. This form of  $B_0(t)$  has also been considered by Vajravelu et al. [32] while analyzing the MHD flow and heat transfer over an unsteady stretching sheet. The stream function and dimensionless variable can be taken as

$\psi = \sqrt{\frac{cv}{(1-\lambda t)}} xf(\eta), \theta(\eta) = \frac{T-T_\infty}{T_w-T_\infty}, \varphi(\eta) = \frac{C-C_\infty}{C_w-C_\infty}, \eta = y \sqrt{\frac{c}{v(1-\lambda t)}}$  (9)

Where the stream function  $\psi$  is defined in the usual way  $u = \partial\psi/\partial y$  and  $v = -\partial\psi/\partial x$ . Substituting (9) into Eqs. (1)–(4), we obtain the following ordinary differential equations

$f''' + ff'' - f'^2 - A(f' + \frac{\eta}{2} f'') - Mf' - \delta f = 0$  (10)

$\frac{1}{Pr_{eff}}\theta'' + f\theta' - A\frac{\eta}{2}\theta' + Nb\theta'\varphi' + Nt\theta'^2 = 0$  (11)

$\varphi'' + Le(f - A\frac{\eta}{2})\varphi' + \frac{Nt}{Nb}\theta'' + Y\varphi = 0$  (12)

Where

$M = \frac{\sigma B_0^2}{\rho_f c}, \delta = \frac{\mu}{k_\rho} u, A = \frac{\lambda}{c}, Pr_{eff} = \frac{Pr}{1+4R/3}, R = \frac{4\sigma_1 T_\infty^3}{K_1 \alpha_m \rho_f c_\rho}, Pr = \frac{v}{\alpha_m}, v = \frac{\mu}{\rho_f}, Nb = \frac{\tau(C_w-C_\infty)D_B}{v}, Nt = \frac{\tau(T_w-T_\infty)T}{vT_\infty}, Le = \frac{v}{D_B}, Y = k_c(C - C_\infty)$  (13)

Here M is the dimensionless magnetic parameter, A is the unsteadiness parameter,  $\delta$  is permeable parameter,  $Pr_{eff}$  is the effective Prandtl number, R is the thermal radiation parameter, Pr is the Prandtl number,  $v$  is the kinematic viscosity of the fluid, Nb is the Brownian motion parameter, Nt is the thermophoresis parameter, Le is the Lewis number and Y is chemical reaction parameter. It is worth noting that the temperature actually does not depend on Prandtl number (Pr) and the thermal radiation parameter (R) independently, but depends only on a combination of them termed as effective Prandtl number  $Pr_{eff}$  which is directly proportional to the Prandtl number and inversely proportional to the thermal radiation parameter.

The corresponding boundary conditions are

$f(0) = s, f'(0) = -1, \theta(0) = 1, \varphi(0) = 1.$   
 $f'(\infty) = 0, \theta(\infty) = 0, \varphi(\infty) = 0.$  (14)

The physical quantities of interest are the skin friction coefficient  $C_f$ , the local Nusselt number  $Nu_x$  and the local Sherwood number  $Sh_x$  which are defined as

$C_f = \frac{\tau_w}{\rho_f u_w^2}, Nu_x = \frac{xq_w}{k(T_w-T_\infty)}, Sh_x = \frac{xq_m}{D_B(C_w-C_\infty)},$  (15)

Where  $\tau_w$  is the shear stress at the stretching surface,  $q_w$  and  $q_m$  are the wall heat and mass fluxes, respectively. Hence using Eq. (10) we get

$Re_x^{1/2} C_f = f''(0), Nu_x Re_x^{-1/2} = -\theta'(0), Sh_x Re_x^{-1/2} = -\varphi'(0)$  (16)

Where  $Re_x = u_w(x, t)x/v$  is the local Reynolds number based on the stretching velocity  $u_w(x, t)$ .

**III. RESULTS AND DISCUSSION:**

As the governing boundary layer equations 10-12 non linear, it is not possible to get the closed form solutions. Consequently, the equations with the boundary conditions (14) are solved numerically by the means of implicit finite difference scheme along with the Gauss-Sidel method. In order to investigate the flow quantities like velocity, temperature and concentration profiles and so forth a parametric study as taken to

illustrate the effects of the various physical parameters namely, magnetic parameter  $M$ , Unsteadiness parameter  $A$ , Prandtl number  $Pr$ , thermal radiation parameter  $R$ , Brownian motion parameter  $N_b$ , Thermophoresis parameter  $N_t$ , Lewis number  $Le$ , permeability parameter  $\delta$  and Chemical reaction parameter  $\gamma$ .

The numerical computations are carried out for velocity, temperature and concentration profiles and are presented in figures 1- 9. It is found that the system of equations have dual solutions. The solutions are called as first and second solutions. The variations of dimensionless velocity, temperature and concentration profiles with the effect of magnetic field parameter  $M$  is depicted in figure 1(a) – 1(c) respectively. It is seen in figure 1(a) that the effect of magnetic field  $M$  increases, the dimensionless velocity profiles increases for first solution while it decreases in the second solution and figure 1(b) the reverse phenomenon observed in the both cases of first and second solution. From figure 1(c), it can be seen that increase the magnetic field  $M$  effect is to decrease the concentration profiles in the first solution. The trends observed for the second solution as same as for the first solution but with a difference that the effect of  $M$  is more significantly in second solution.

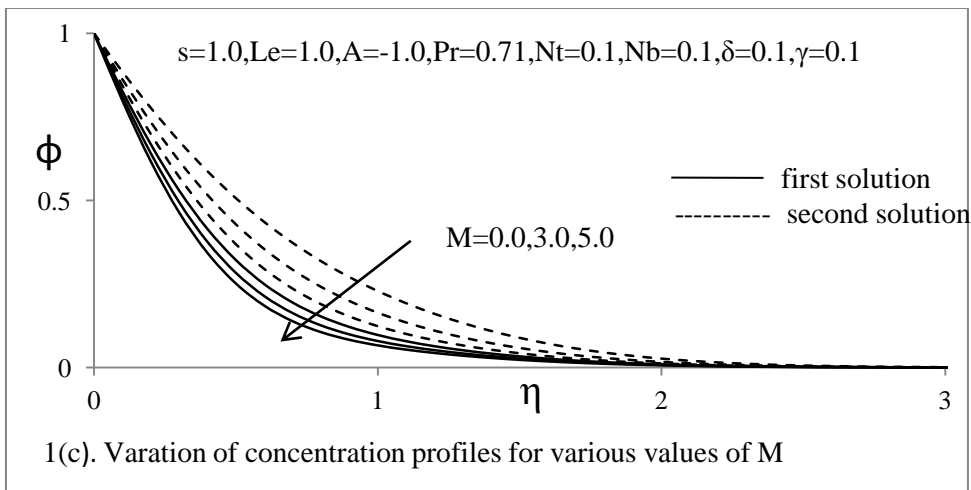
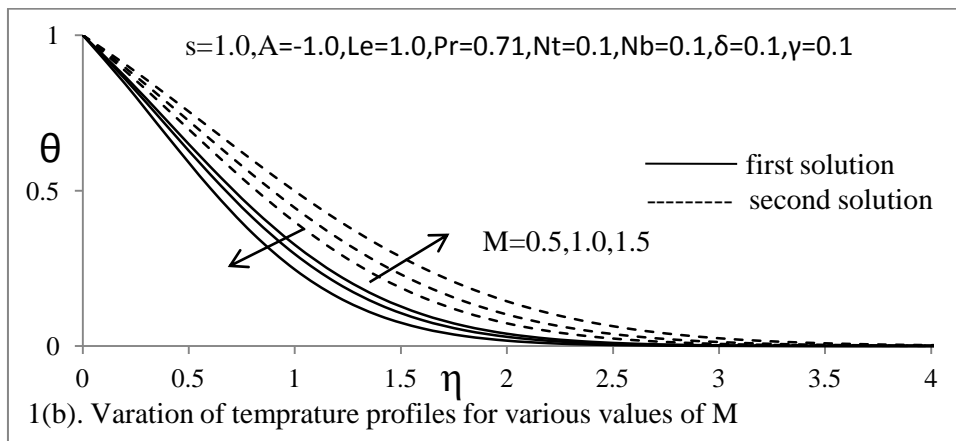
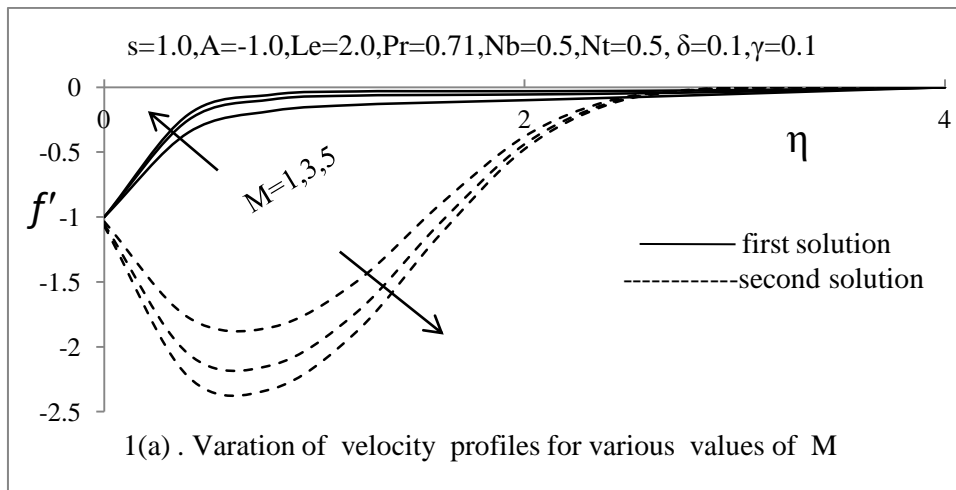
Figure 2(a) - 2(c) shows the variation of velocity, temperature and concentration profiles but different values of suction parameter  $s$  respectively. It can be seen in figure 2(a), for the first solution, if the increasing of suction parameter  $s$  the fluid velocity increases while the fluid velocity decreases with the increase of suction parameter  $s$  in the second solution. Figure 2(b) depicts that with the increase of suction parameter  $s$ , the temperature profiles decreases for both the solutions. The figure 2(c) depicts that the increasing in suction parameter  $s$  leads to enhance the concentration profiles both the solutions. Figure 3(a)-3(c) are drawn to analyze the influence of unsteadiness parameter  $A (<0)$  on 3(a) velocity profiles, 3(b) temperature profiles and 3(c) concentration profiles respectively. It can be seen that the velocity of a fluid increases with increase of unsteadiness parameter  $A$  in the vicinity of the boundary in both the solutions, the reverse trend is observed when it is away from the boundary. From figure 3(b) and 3(c) reveals that the temperature at a point decreases as the magnitude of the unsteadiness parameter  $A$  increases. This is due to the fact that the heat transfer rate increases with the increase of unsteadiness parameter  $A$  which in turn reduces the temperature of fluid. This same can be observing both the solutions. From the figure 3(c), it can be seen that the concentration profiles decreases as increasing as the magnitude of unsteadiness parameter  $A$  increases in both first and second solutions.

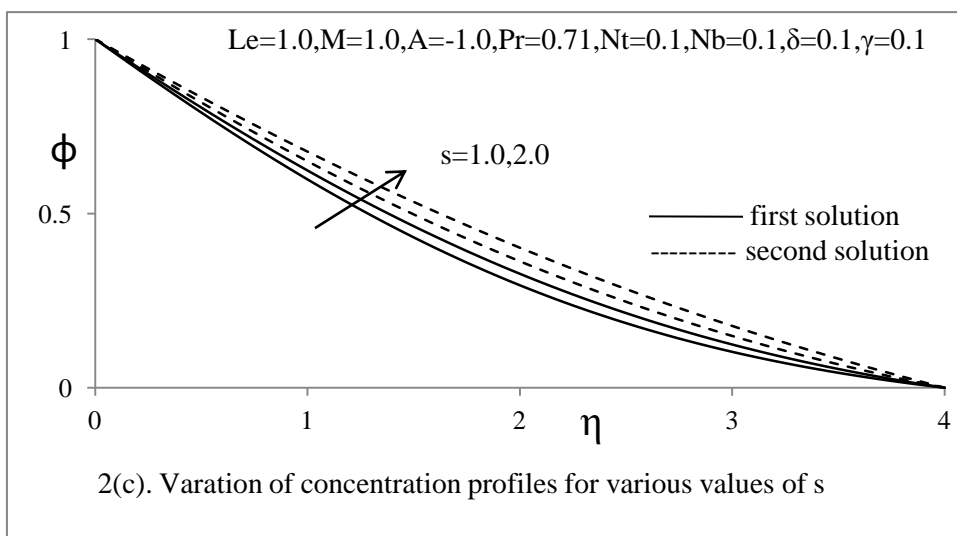
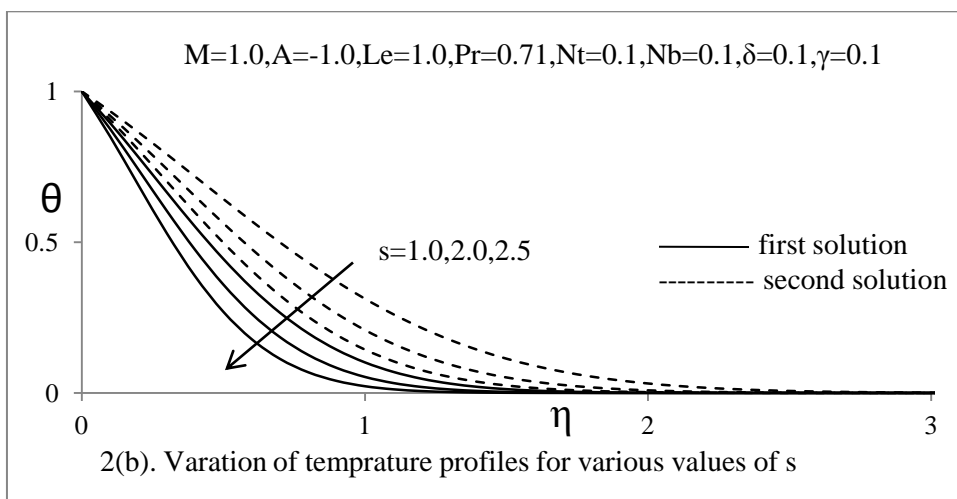
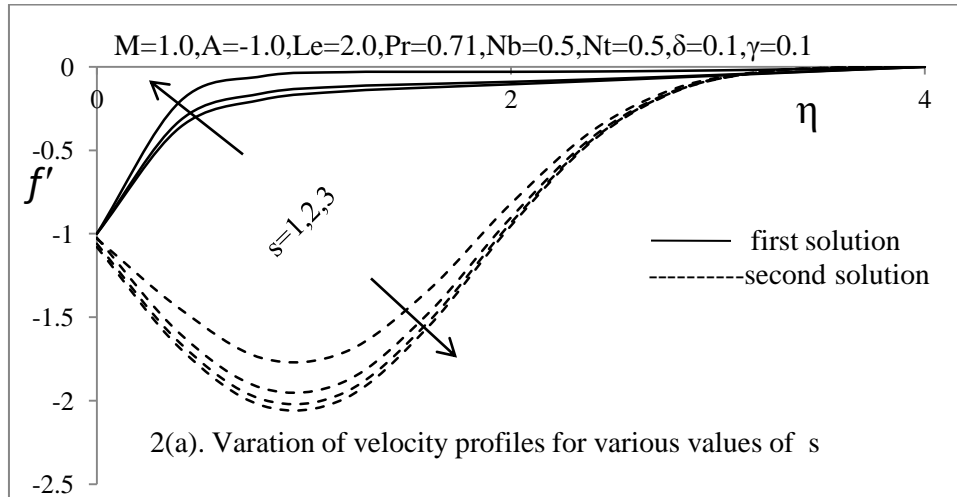
The effects of chemical reaction parameter  $\gamma$  on the dimensionless temperature and concentration profiles are illustrated in figure 4(a) and 4(b) respectively. It can be seen that the temperature of a fluid increases with the increase for restrictive chemical reaction parameter  $\gamma (>0)$  and it increases for generating chemical reaction parameter  $\gamma (<0)$  in both solutions. From figure 4(b) it is seen that the concentration profiles increase for generating chemical reaction parameter  $\gamma (>0)$ , while it decreases restrictive chemical reaction parameter  $\gamma (<0)$  in both solutions. The reaction rate parameter is a decelerating agent when  $\gamma (>0)$ . The concentration boundary layer decreases in case of restrictive chemical reaction. This is due to the conversion of the species takes place as a result of chemical reaction and thereby reduces the concentration boundary layer; actually chemical reaction causes to increase the rate of interference mass transfer.

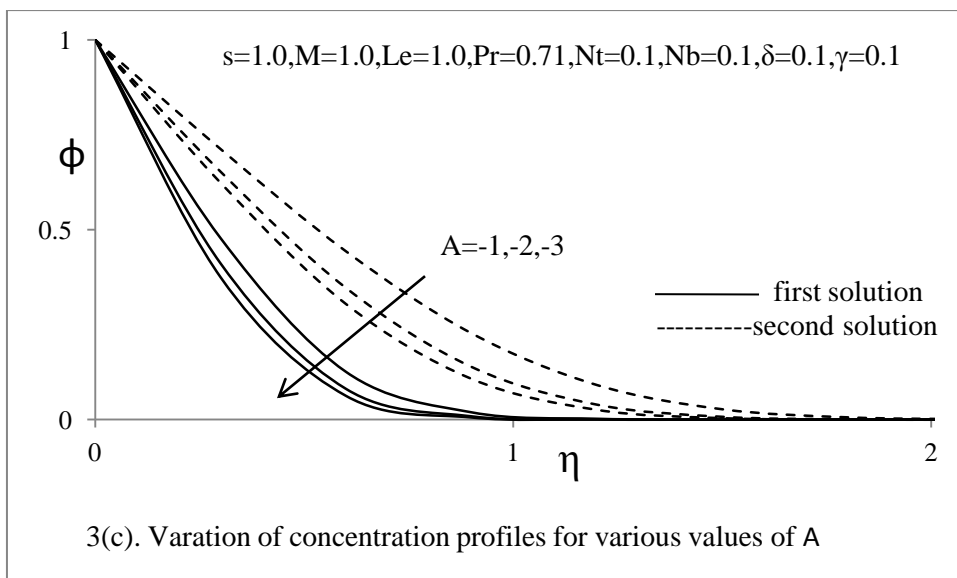
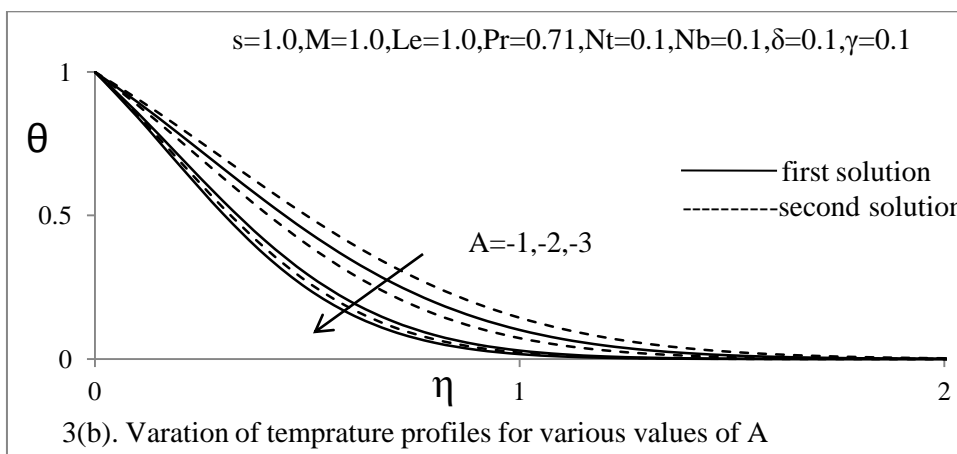
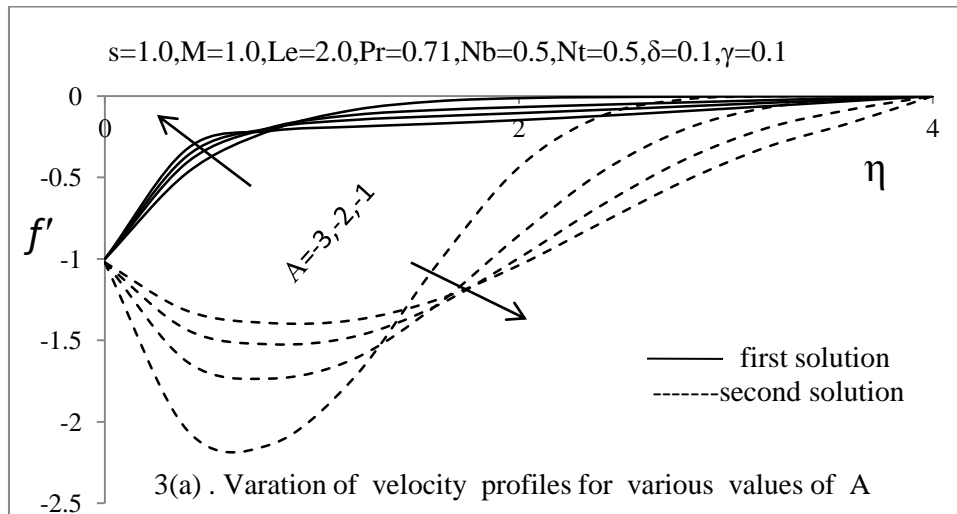
Figure 5(a) and 5(b) is plotted for the different values of Prandtl number  $Pr$  to the temperature and concentration profiles. It can be noticed from these figures. The temperature and concentration profiles decrease with the increase of Prandtl number  $Pr$  for both first and second solution. An increase in Prandtl number  $Pr$  reduces the thermal boundary layer as well as concentration boundary layer. Prandtl number  $Pr$  signifies the ratio of momentum diffusivity. As Prandtl number  $Pr$  decreases the thickness of thermal boundary layer becomes thickness of the velocity boundary layer. So the thickness of thermal boundary layer increases as Prandtl number  $Pr$  decreases and hence temperature profiles decrease with the increase of Prandtl number  $Pr$ . In heat transfer problems the Prandtl number  $Pr$  controls the relative thickness of momentum and thermal boundary layer hence Prandtl number  $Pr$  can be used to increase the rate of cooling in conducting flows.

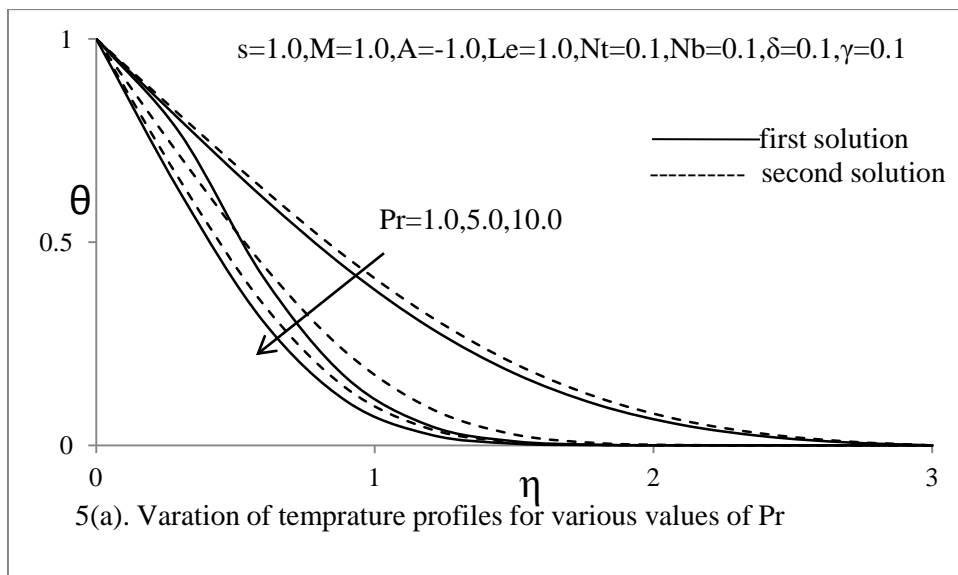
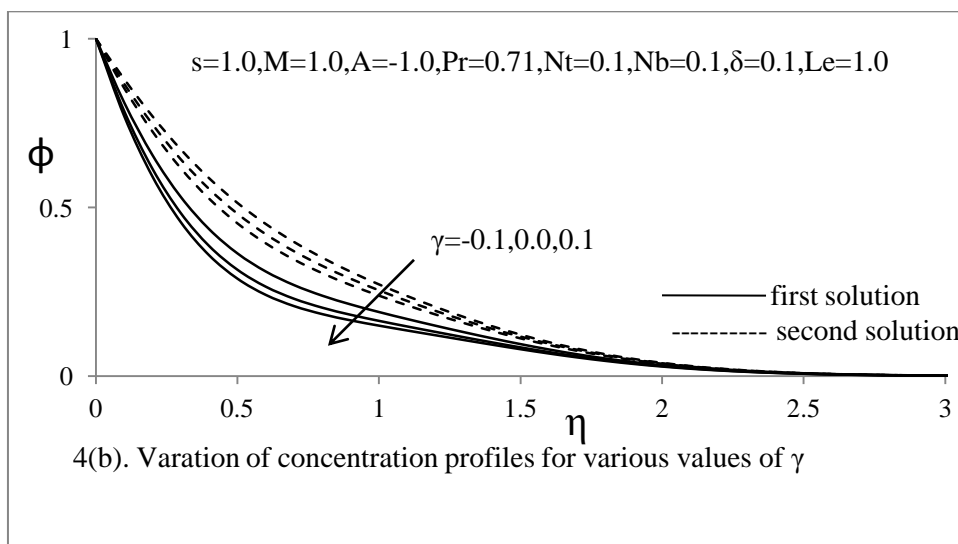
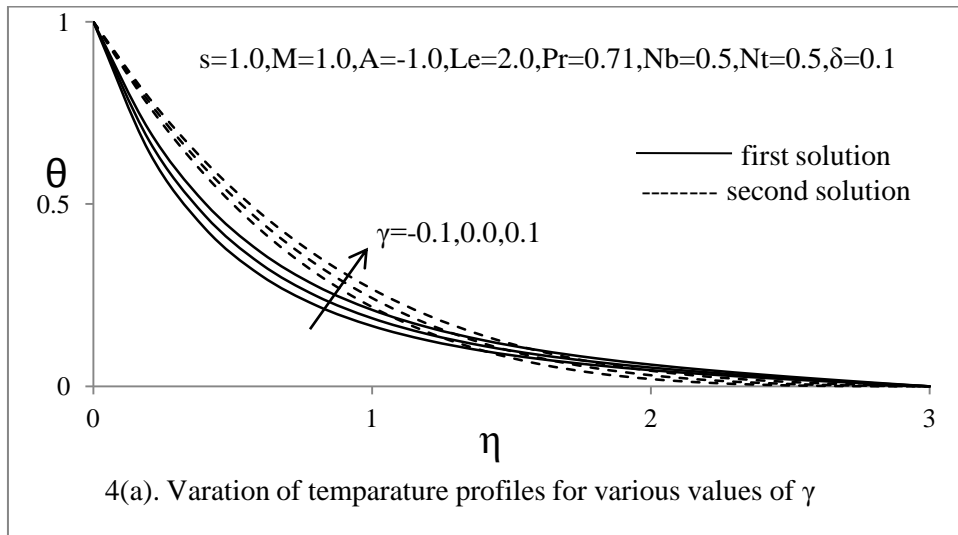
The effect of thermophoresis parameter  $N_t$  on temperature and concentration profiles are illustrated in figure 6(a) and 6(b). As the thermophoresis parameter  $N_t$  increases the temperature profiles increase and hence the thickness of thermal boundary layer with the increase of the thermophoresis parameter  $N_t$ . From figure 6(b) reveals that the concentration profiles increase with the increase of thermophoresis parameter  $N_t$  in both the first and second solutions. The thermophoresis parameter  $N_t$  phenomenon describes the fact that small micron size particles suspended in non-isothermal fluid will acquire a velocity in the direction of decreasing temperature. As increases of thermophoresis parameter  $N_t$  results in an increase of the temperature difference between sheet and the ambient fluid, consequently the thermal boundary layer thickness increases. Figure 6(b) reveals that the thermophoresis parameter  $N_t$  effects enhance the concentration profiles  $\phi$  in both solutions.

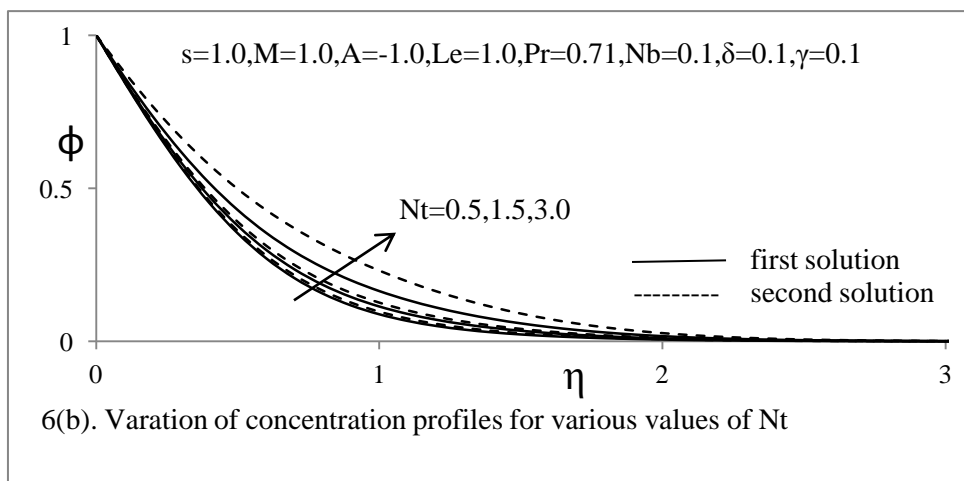
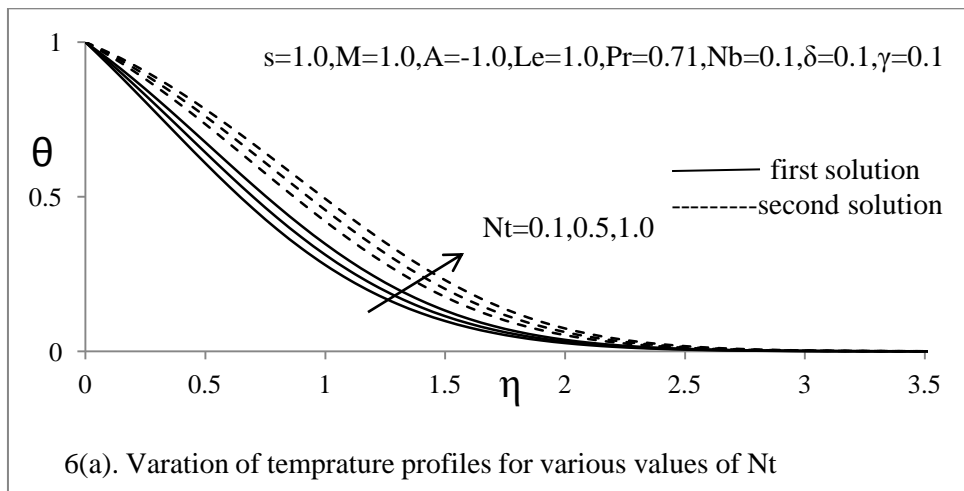
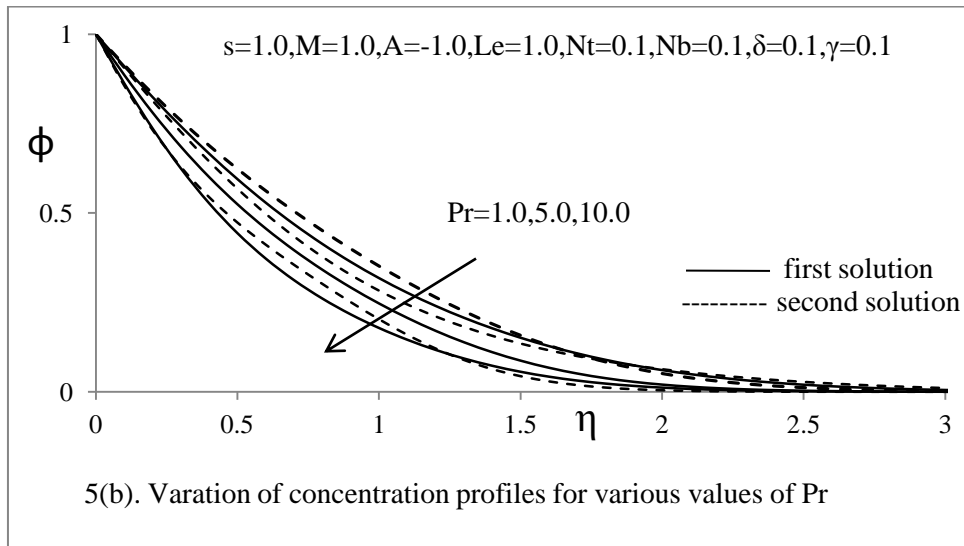
The figure 7(a) depicts for the effect of Brownian motion parameter Nb for the first and second solution respectively. The temperature profiles of nanofluid in the boundary layer region increase with the increase of Brownian motion parameter Nb. As Brownian motion parameter Nb the thickness of boundary layer increases. Figure 7(b) reveals that the impact of Brownian motion parameter Nb on concentration profiles decreases and hence the thickness of the concentration boundary layer decreases in both the solutions. From figure.8 observed that the permeability parameter  $\delta$  increases the dimensionless velocity profiles decreases for first solution while it increases in the second solution away from the boundary layer. Is the effect being on concentration profiles are shown in figure 9. The concentration profiles of the fluid decreases with increase of Lewis number Le, where the velocity and temperature profiles are not significances with the increase of Lewis number Le hence it is not shown.

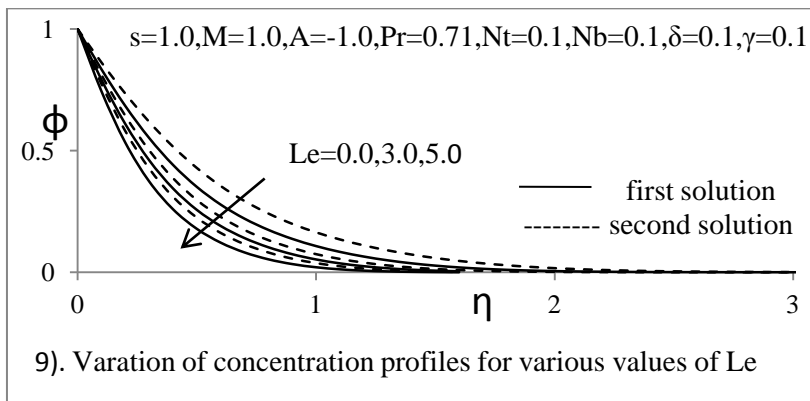
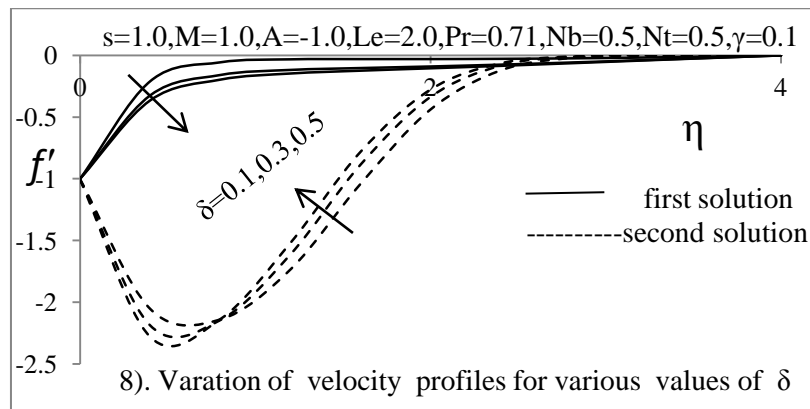
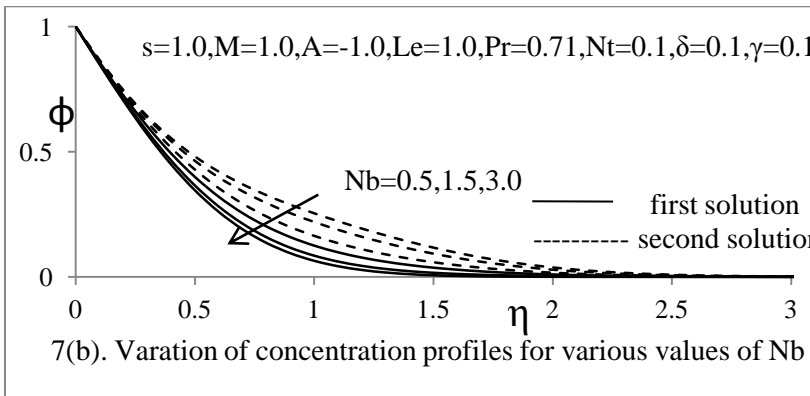
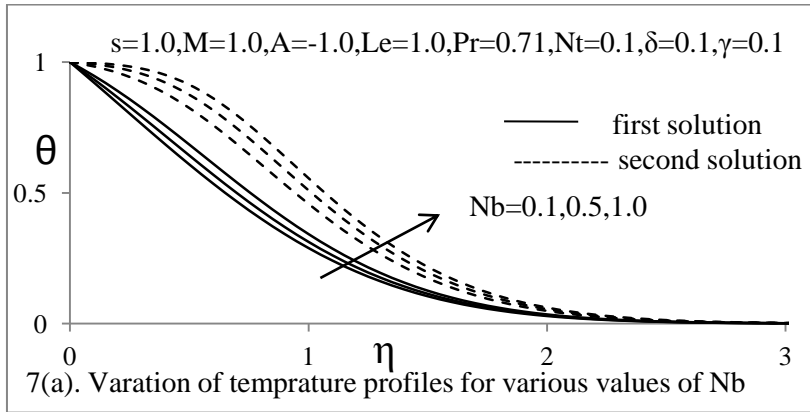












## REFERENCES:

- [1]. Bhattacharyya S.N and Gupta, A.S, 1985,"On the stability of viscous Flow over a stretching sheet", *Quarterly Applied Mathematics*, 43, pp. 359-367.
- [2]. Gupta, P.S and Gupta, A.S, 1977, "Heat and mass transfer on a stretching sheet with suction and blowing", *Canadian Journal of Chemical Engineering*, 55, pp. 744-746.
- [3]. Cheng, W.T and Lin, H.T, 2002, "Non-similarity solution and correlation of transient heat transfer in laminar boundary layer flow over a wedge", *International journal of Engineering Science*, 40, pp. 531 - 539.
- [4]. Crane, L.J. "Flow past a stretching plate", *ZAMP*, 21, pp. 645–655 (1970).
- [5]. Carragher, P. and Carane, L.J. "Heat transfer on a continuous stretching sheet", *Z. Angew. Math. Mech.*, 62, pp. 564–565 (1982).
- [6]. Ariel, P.D., Hayat, T. and Ashgar, S. "The flow of an elasto-viscous fluid past a stretching sheet with partial slip", *Acta Mech.*, 187, pp. 29–35 (2006).
- [7]. Nadeem, S., Hussain, A., Malik, M.Y. and Hayat, T. "Series solutions for the stagnation flow of a second-grade fluid over a shrinking sheet", *Appl. Math. Mech.*, 30(10), pp. 1255–1262 (2009).
- [8]. Nadeem, S., Hussain, A. and Khan, M. "Stagnation flow of a Jeffrey fluid over a shrinking sheet", *Z. Naturforsch.*, 65a, pp. 540–548 (2010).
- [9]. Hayat, T. and Qasim, M. "Radiation and magnetic field effects on the unsteady mixed convection flow of a second grade fluid over a vertical stretching sheet", *Int. J. Numer. Methods Fluids*, 66(7), pp. 820–832 (2010).
- [10]. Nadeem, S. and Faraz, N. "Thin film flow of a second grade fluid over a stretching/shrinking sheet with variable temperature-dependent viscosity", *Chin. Phys. Lett.*, 27(3), p. 034704 (2010).
- [11]. Ishak, A., Nazar, R. and Pop, I. "Heat transfer over an unsteady stretching permeable surface with prescribed wall temperature", *Nonlinear Anal. RWA*, 10, pp. 2909–2913 (2009).
- [12]. Hayat, T., Shehzad, S.A., Qasim, M. and Obaidat, S. "Steady flow of Maxwell fluid with convective boundary conditions", *Z. Naturforsch.*, 66a, pp. 417–422 (2011).
- [13]. Wang, C. and Pop, I. "Analysis of the flow of a power-law fluid film on an unsteady stretching surface by means of homotopy analysis method", *J. Non-Newtonian Fluid Mech.*, 138, pp. 161–172 (2006).
- [14]. Magyari, E. and Keller, B. "Heat and mass transfer in the boundary layers on an exponentially stretching continuous surface", *J. Phys. Appl. Phys.*, 32, pp. 577–585 (1999).
- [15]. Partha, M.K., Murthy, P.V. and Rajasekhar, G.P. "Effect of viscous dissipation on the mixed convection heat transfer from an exponentially stretching surface", *Heat Mass Transf.*, 41, pp. 360–366 (2005).
- [16]. Elbashbeshy, E.M.A. "Heat transfer over an exponentially stretching continuous surface with suction", *Arch. Mech.*, 53, pp. 643–651 (2001).
- [17]. MachaMadhu and Naikoti Kishan, "Magnetohydrodynamic Mixed Convection Stagnation-Point Flow of a Power-Law Non-Newtonian Nanofluid towards a Stretching Surface with Radiation and Heat Source/Sink". *Journal of Fluids* .Volume 2015, Article ID 634186, 14 pages .<http://dx.doi.org/10.1155/2015/634186>.
- [18]. Wang CY (1990). "Liquid film on an unsteady stretching sheet". *Quarterly of Applied Mathematics* 48, pp. 601-610.
- [19]. Miklavcic M, Wang CY (2006). "Viscous flow due to a shrinking sheet". *Quarterly of Applied Mathematics* 64(2), pp. 283-290.
- [20]. Hayat T, Abbas Z, Ali N (2008). "MHD flow and mass transfer of a upper convected Maxwell fluid past a porous shrinking sheet with chemical reaction species". *Physics Letters A* 372(26), pp. 4698-4704.
- [21]. Hayat T, Abbas Z, Sajid M (2007). "On the analytic solution of magnetohydrodynamic flow of a second grade fluid over a shrinking sheet". *Journal of Applied Mechanics, Trans. ASME* 74(6), pp. 1165-1171.
- [22]. D. A. Nield, and A. V. Kuznetsov, "The Cheng–Minkowycz problem for natural convective boundary-layer flow in a porous medium saturated by a nanofluid", *International Journal of Heat and Mass Transfer*, vol. 52, pp. 5792-5795, 2009a.
- [23]. D. A. Nield, and A. V. Kuznetsov, "Thermal instability in a porous medium layer saturated by a nanofluid", *International Journal of Heat and Mass Transfer*, vol. 52, pp. 5796–5801, 2009b.
- [24]. A. J. Chamkha, R. S. R. Gorla, and K. Ghodeswar, "Non-similar solution for natural convective boundary layer flow over a sphere", *Transport in Porous Media*, vol. 86, pp. 13-22, 2011.
- [25]. D. A. Nield, and A. V. Kuznetsov, "The Cheng–Minkowycz problem for the double-diffusive natural convective boundary layer flow in a porous medium saturated by a nanofluid", *International Journal of Heat and Mass Transfer*, vol. 54, pp. 374-378, 2011.
- [26]. R. S. R. Gorla, and A. J. Chamkha, "Natural convective boundary layer flow over a horizontal plate embedded in a porous medium saturated with a nanofluid", *Journal of Modern Physics*, vol. 2, pp.62-71, 2011.
- [27]. Hunegnaw Dessie, Naikoti Kishan, "Unsteady MHD Flow of Heat and Mass Transfer of Nanofluids over Stretching Sheet with a Non-Uniform Heat/Source/Sink Considering Viscous Dissipation and Chemical Reaction", *International Journal of Engineering Research in Africa*, Vol.14, pp. 1-12. 2015.
- [28]. Pavlov, KB: "Magnetohydrodynamic flow of an incompressible viscous fluid caused by deformation of a surface" *Magn. Gidrodin.* 4, 146-147 (1974).
- [29]. Jafar, K, Nazar, R, Ishak, A, Pop, I: "MHD flow and heat transfer over stretching/shrinking sheets with external magnetic field, viscous dissipation and Joule effects". *Can. J. Chem. Eng.* 99, 1-11 (2011).
- [30]. Samir kumar Nandy, Sumanta Sidui, Tapas Ray Mahapatra: "Unsteady MHD boundary layer flow and heat transfer of nanofluid over a permeable shrinking sheet in the presence of thermal radiation." *Alexandria eng. journal*(2014) 53,929-937.
- [31]. M.Q.Brewster, "Thermal Radiative Transfer Properties", Wiley, Newyork, 1972.
- [32]. K.Vajravelu, K.V.Prasad, P.S.Datti, B.T.Raju, "MHD flow and heat transfer of an Ostwald-de Waele fluid over an unsteady stretching surface." *Ain Shams Eng.J.5*(1)(2014) 157-167.

## Modelling Compressor's Initial Operating Conditions Effect on Turbine Performance in the Tropical Rainforest

Adumene Sidum<sup>1</sup>, Le-ol Anthony Kpegele<sup>2</sup>, Amadi Rex Kemkom Chima<sup>3</sup>

<sup>1</sup>(Department of Marine Engineering, Rivers State University of Science and Technology, Port Harcourt)

<sup>2,3</sup>(Department of Mechanical Engineering, Rivers State University of Science and Technology, Port Harcourt, Nigeria)

**ABSTRACT:** *The Gas Turbine performance in terms of power output and efficiency are often determined by many factors, among which the compressor inlet temperature and humidity are major factors. The research power plant is located in the tropical rainforest within the delta region of Nigeria and hence, its performance is highly influenced by compressor inlet temperature. It showed that the higher the compressor inlet temperature, the lesser the power output. And the lower the inlet temperature, the higher the output power of the plant. At the current average operational compressor inlet temperature of 31<sup>0</sup>C, the net power output of the plant is 125.5MW which is far less than the designed rated capacity of 138.29MW. However, at a lower temperature of 18<sup>0</sup>C, the power output was analysed to be 138.26MW which is quite close to the 138.29MW rated capacity, and at a much lower temperature of 10<sup>0</sup>C, a better output was obtained. It was also observed that the thermal efficiency of 33.1% at 31<sup>0</sup>C inlet air temperature improved impressively to 36.10 at 18<sup>0</sup>C. Analysis further showed that a reduction in temperature from 31<sup>0</sup>C to 18<sup>0</sup>C resulted to 0.78% increase in power output for every 1<sup>0</sup>C decrease compressor inlet temperature. Investigation of the effect of humidity on turbine performance revealed that at inlet air temperature of 31<sup>0</sup>C and a humidity of 80%, a power output of 128.406MW was generated. This represent an increase of 2.096MW or 1.67% above the 125.5 MW obtained at the same temperature without humidity effect consideration. The overall result indicates an inverse proportionality between the compressor inlet air temperature and the turbine power output and a proportional correlation between humidity and the power output.*

**KEYWORDS:** *Gas Turbine, Humidity, Compressor Work, Thermal Efficiency, Power Output, Turbine Work, Compressor Inlet Temperature.*

### I. INTRODUCTION

Gas turbine engine is a heat engine in which hot combustion gases, generated by burning a fuel, drives a turbine which generates power. It has basic configurations which consist of a compressor, combustor and a turbine. The turbine shaft is coupled to a generator which produces electrical energy through the rotary action of the shaft system. Gas turbine plays a very important role in aircraft, power generation and marine power plant usage [1].

Gas turbines are key components in combined cycle power plants. There are many economic advantages in using gas turbine for power generation. These include high reliability and flexibility in operation; they are compact, light weighted and efficient. Other unique features include its capability of rapid start-up and can be remotely operated.

Gas turbine compact size of high power-to- weight ratio and high reliability makes it the ideal power plant for use to drive aviation and marine systems, etc. Gas turbines use a wide variety of gaseous and liquid fuels, depending on the design and application. Fuel nature and ambient conditions of inlet air into the system also affect its power output. It has been shown that the cooler the compressor inlet air, the better the engine performance [2].

Despite the fact that gas turbines have many attractive features which makes it one of the most preferred power generations, one of the parameters that affect its performance is the ambient conditions of the inlet air into the compressor. Power output, which is directly dependent on the mass flow for a fixed cycle varies directly with air density which is a function of air pressure and temperature [3]. Variation in the initial operating conditions of the compressor affects the engine operating characteristics, especially the power output and efficiency which are some of the indices of engine performance. Previous works have revealed that the cooler the inlet air, the more the mass flow rate, and hence more power will be generated by the turbine. It has also been shown from research that a typical turbine plant experiences a capacity reduction of up to 1% for every 1°C rise in compressor inlet temperature above typical ISO conditions of 15°C and 60% relative humidity [4]. [1] Revealed that the power output can drop by about 0.5% to 1% rise in ambient temperature and an increase of about 0.623% for every 1°C rise in inlet air temperature.

The work of [5] revealed that the turbine power output decreases as the inlet air temperature increases. His conclusion was based on the experimental aero-derivative turbine, which showed that the power output of the turbine decreased by 73% when its inlet air temperature was increased from 15°C to 37.8°C. Also about 27% power loss was prevented when the temperature was reverted from 37.8°C to 15°C. In a similar investigation within Los Angeles vicinity, another turbine plant of 42MW output showed that temperature rise from 15°C to 17.8°C resulted to a power drop of 34.1MW, representing about 19% power loss [3].

According to [6] humidified air was injected into the air stream at the upstream of the combustor and downstream of the compressor. This improvement technique resulted into a tremendous power improvement without increasing the compressor work load. It also shows a double advantage by reducing the level of Nitrogen oxide compounds in the turbine system, and eliminates the possibility of compressor blades corrosion and distress. It was indicated that the mass flow rate of air entering into the gas turbine varies with their specific mass, which means that it depends on the temperature and the relative humidity of the ambient air [7].

Gas turbine performance is critically limited by the predominating ambient temperature, mainly in hot and dry regions. It occurs because the power output is inversely proportional to the ambient temperature [8]. The temperature drop provides an augment in the air density and consequently elevates air mass flow rate; this behavior increase the power output and efficiency by about 0.7% per degree Celsius for heavy duty gas turbine [9].

In the presentation by [10], the result from the study of combined cycle power plant operated from 35°C to ISO-rated condition which increases the power output of a gas turbine by 10.6% and the combined cycle power plant by 6.24% annually.

Further analysis has been carried out such as performance analysis and components irreversibility of a (25MW) gas turbine power plant modeled with a spray cooler. In this work the potentials benefits of improving the performance of the current gas turbine plant into a more advanced cycle with high efficiency and power output through inlet air cooling were analysed. In the study, performance characteristics were determined for a set of actual operational conditions including ambient temperature, relative humidity, and turbine inlet temperature and pressure ratio [11].

Investigate the temperature inlet effect on the gas turbine performance. And it show that during the summer in Saudi, the turbine suffer a 24% decrease in their capacity due to ambient temperature up to 50°C [12].

According to [12], it revealed that most turbines suffer as high as 50% capacity loss at 45°C by cooling the inlet air to as low as 15°C. He added that cooling the inlet air also lowers the heat rate by 10%, therefore saving fuel costs and reducing pollution. He further explained that for a combined cycle gas turbine plant operating at full load, with 45°C inlet temperature, the thermal efficiency is about 42%, while if the inlet air of the same plant was cooled to 15°C, a 53% thermal efficiency was achieved.

In the research work of [13], it was revealed that at high relative humidity, about 1.5 to 1.9 times higher cooling thermal loads was achieved than plants with low relative humidity of about 30% and below.

In this research modeling the initial operating conditions of the compressor in the tropical rainforest was carried out. Various procedures for the collation of data from service records, field measurement, simulation of systems and thermodynamic analysis of results were presented.

## II. MATERIALS AND METHODS

### 2.1 Theoretical Formulation

For this research, data collections were made by direct measurement via the human machine interface (HMI) and operational result from the log book for a period of two years. The data collection methods were designed to produce facts about some aspects of the research. The daily operational log data were used to determine those factors that influence the gas turbine performance.

In the treatment and collection of data, mean values of daily parameters were computed by the use of statistical method while the objective functions were modeled by MATLAB software, followed by monthly average and the overall average for the research period. Some of the phenomena of the operation of the set could not be investigated directly by field measurement, various thermodynamics theories were employed to model the performance of the plant under considerable conditions.

2.1.1 The Energy Model

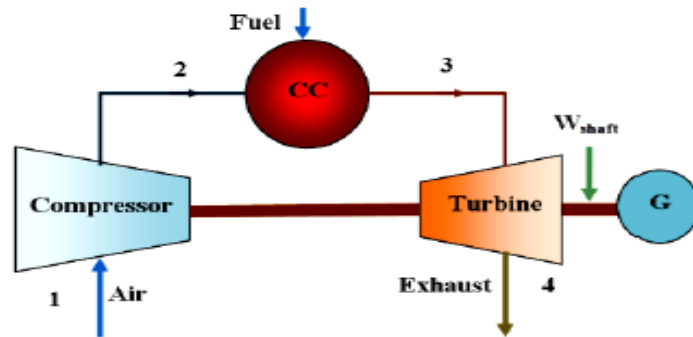


Figure 1: Schematic of the typical gas turbine cycle

The figure above represents a single shaft gas turbine engine and the expressions for the efficiency and work ratio of the Brayton Cycle was employed.

A simple cycle gas turbine is comprised of three major components, which are compressor, combustor and turbine as shown in figure 1. Air at ambient temperature and pressure enter the compressor. The ratio of the compressor exit pressure to the ambient pressure inlet defined the pressure ratio. For the compression process which is adiabatic, the temperature of the compressed air is higher than the ambient temperature of the inlet air.

The compressed air from the compressor enters the combustor, where it is mixed with high pressure gaseous fuel. The fuel and air are burned at constant pressure, and the high pressure, hot gases (product of combustion) enter the turbine. In the turbine, the gases are reduced in pressure, resulting in to a corresponding reduction in temperature. The heat removal process associated with expansion and cooling of the hot gases in the turbine, results in energy transfer from the gases to shaft work, leading to shaft rotation.

The compressor power can be modeled using the first law of thermodynamic as follows

$$\text{Compressor power transfer } \dot{W}_c = m_a c_{pa} (T_2 - T_1) \tag{1}$$

where  $m_a$  = air mass flow rate,  $c_{pa}$  = the specific heat of the dry air

$$\text{Turbine power output } \dot{W}_T = m_a c_{pg} (T_3 - T_4) \tag{2}$$

$$\text{Heat supplied during cycle } \dot{Q}_s = m_a c_{pg} (T_3 - T_2) \tag{3}$$

$$\text{Heat rejected by the cycle } \dot{Q}_r = m_a c_{pg} (T_4 - T_1) \tag{4}$$

where  $c_{pg}$  = the flue gas specific heat

$$\text{Thermal efficiency} = \frac{(T_3 - T_2) - (T_4 - T_1)}{T_3 - T_2} = 1 - \frac{1}{(r_p)^{\gamma-1/\gamma}} \tag{5}$$

where  $r_p$  is the pressure ratio.

2.1.2 The Humidity Function Model

Air contains water vapour in varying degrees, and at a very low partial pressure. At this low pressure and atmospheric temperature, the water vapour behaves like a perfect gas [4]. Humidity describes the amount of water vapour in the atmospheric air. Since air is essential in the burning of the fuel that is used for the production of gas turbine power, the quantity of water vapour contained in the air obviously affects its

characteristics as it is delivered to the turbine plant for fuel burning. This effect can be looked at from the laws governing humidity, and the relationship between humidity and gas turbine power output

The Gibbs-Dalton's theory is used to model the characteristic impact of humidity in this research.

The Dalton's Law relation show that

$$P = P_v + P_a \quad 6$$

Where P is the total pressure of the atmospheric air,  $P_v$ , the partial pressure of water vapour

$P_a$  is the partial pressure of the dry air in the mixture.

Applying the characteristic gas equation for the water vapour and dry gas gives

$$\frac{M_v}{M_a} = \frac{P_v}{P_a} \times \frac{R_a}{R_v} \quad 7$$

Where  $R_a$  = Gas constant for dry air = 0.287kJ/kgK

$R_v$  = Gas constant for water vapour = 0.462kJ/kgK

P = Barometric pressure of the atmosphere

$P_a$  = Partial pressure of dry air

$P_v$  = Partial pressure of water vapour

$M_a$  = Mass of dry air in kg

$M_v$  = Mass of water vapour in kg

$$\omega = 0.622 \frac{P_v}{P - P_v} \text{ or } \omega = 0.622 \left( \frac{P - P_a}{P_a} \right) \quad 8$$

Where  $\omega$  is the humidity

$$\text{The Relative humidity } \phi = \frac{P_v}{P_s} \quad 9$$

$$\text{Therefore } \omega = \frac{0.622 \phi P_s}{P - P_v} \quad 10$$

$$\text{The mass flow rate } M = m_a + m_v = m_a \left( 1 + 0.622 \phi \frac{P_s}{P_a} \right) \quad 11$$

Equation 10 shows that the specific humidity and relative humidity are directly proportional to each other, while other quantities remain constant. This represent an increase in one translates to an increase in the other

### III. RESULTS AND DISCUSSION

The parameters in table 1 were obtained from the installation manual of SIEMENS V94.2 gas turbine and its operational data. The application of the thermodynamics theories was used to model the objective parameters.

**Table 1: Design and average operational data**

S/NO	PARAMETER	DESIGN VALUE	OPERATIONS VALUE
1	Turbine Power Output	138.29kW	125kW
2	Exhaust Gas Flow	498kg/s	477kg/s
3	Fuel Flow Rate	12.4kg/s	9.3kg/s
4	Compressor Pressure Ratio	8.9	8.89
5	Turbine Pressure Ratio	9.68	8.89
6	Thermal Efficiency	36.2%	33.1%
7	Air Flow Velocity	200m/s	200m/s

### 3.1. Effect of Inlet –Air Temperature on Turbine Performance

The research was carried out in order to determine the effect of compressor initial operating conditions on turbine performance as well as the efficiency of the power plant. To do this, we set temperature at which the design net power output of 138.29MW could be attained, while we used operating values between 31<sup>0</sup>C and 10<sup>0</sup>C inlet air temperatures for numerical modeling of the various air mass flow rates, heat supplied, compressor power input, turbine power, net power output and the efficiency of the plant.

The research revealed that the lower the inlet air temperature, the higher the air mass flow rate, and therefore improve performance.

**Table 2: Impact of operating temperature on net power outputs and efficiencies without humidity consideration.**

Case	Inlet air temp. T <sub>1</sub> <sup>0</sup> C	Air mass flow rate (kg/s)	Compressor Power input P <sub>c</sub> (MW)	Turbine Power output P <sub>T</sub> (MW)	Turbine Net Power Output P <sub>N</sub> (MW)	Thermal Efficiency η (%)	% Increase in Net Power Output
1	31	467.70	125.50	251.50	125.50	35.44	-
2	25	478.04	124.27	256.55	132.28	35.93	5.4
3	20	486.66	124.39	261.18	136.79	36.06	9.0
4	18	490.04	124.41	263.18	138.07	36.10	10.44
5	15	495.27	124.39	265.80	141.41	36.19	12.68
6	10	503.9	124.40	270.43	146.03	36.30	16.36

**Table 3: Summary of inlet- air temperature impact on net power outputs at 70% relative humidity**

S/N	Inlet Air Temperature, T <sub>1</sub> <sup>0</sup> C	Mass flow rate (m) kg/s	Net Power output P <sub>N</sub> (MW)
1	10	505.59	146.59
2	15	497.34	142.10
3	18	443.03	139.61
4	20	486.47	136.76
5	25	483.83	133.89
6	31	477.17	128.04

### 3.2 Impact of Specific Humidity and Relative Humidity on the Turbine Performance at various inlet air temperatures.

Humidity has direct effect on gas turbine performance. This could be explained from the fact that when a moist inlet air passes through the compressor of the gas turbine, the water vapour in the air evaporates. In the process of evaporation, it takes its latent heat of vaporization from the air. This cools the air which in turn produces the effect of increasing the air mass flow rate into the system. Tables 3.4 – 3.5 show the results of the evaluation of specific and relative humidity on turbine performance at various inlet air temperatures.

**Table 4: Specific and relative humidity effect on turbine output at inlet air temperature of 31<sup>0</sup>C**

S/N	Relative Humidity (%)	Vapour Mass (kg)	Dry Air Mass (kg)	Total Mass Flow (kg)	Specific Humidity	Net Power Output (MW)
1	40	5.4251	467.7	473.12	0.01157	126.96
2	50	6.7653	467.7	474.47	0.01447	127.31
3	60	8.119	467.7	475.83	0.01736	127.68
4	70	9.470	467.7	477.17	0.02025	128.04
5	80	10.8240	467.7	478.52	0.02314	128.41

**Table 5: Specific and relative humidity effect on turbine output at inlet air temperature of 10<sup>0</sup>C**

S/N	Relative Humidity (%)	Vapour Mass (kg)	Dry Air Mass (kg)	Total Mass Flow (kg)	Specific Humidity	Net Power Output (MW)
1	40	1.539	503.9	505.44	0.00305	146.48
2	50	1.923	503.9	505.82	0.00382	146.59
3	60	2.308	503.9	506.21	0.00458	146.70
4	70	2.693	503.9	506.59	0.00534	146.81
5	80	3.077	503.9	506.99	0.00611	146.93

**3.3 Comparative Results of Net power Outputs and Efficiencies with and without Humidity Consideration**

The research analysed the turbine performance and efficiencies with humidity and without humidity. The comparative result from the analysis is shown in Table 6.

**Table 6: Turbine power output and efficiency with and without humidity effect**

S/N	Inlet Air Temp. (°C)	Turbine Net Power Outputs P <sub>N</sub> (MW) without Humidity	Turbine Net Power Outputs P <sub>N</sub> (MW) with Humidity	Thermal Efficiency η(%) without Humidity	Thermal Efficiency η(%) with Humidity
1	31	125.5	At φ =40% P <sub>N</sub> = 126.96 At φ =80% P <sub>N</sub> = 128.41	35.44%	At φ =80% η =35.51%
2	10	145.6	At φ =40% P <sub>N</sub> = 146.48 At φ =80% P <sub>N</sub> = 146.93	36.30%	At φ =80% η =36.85%

**IV. RESULTS AND DISCUSSION**

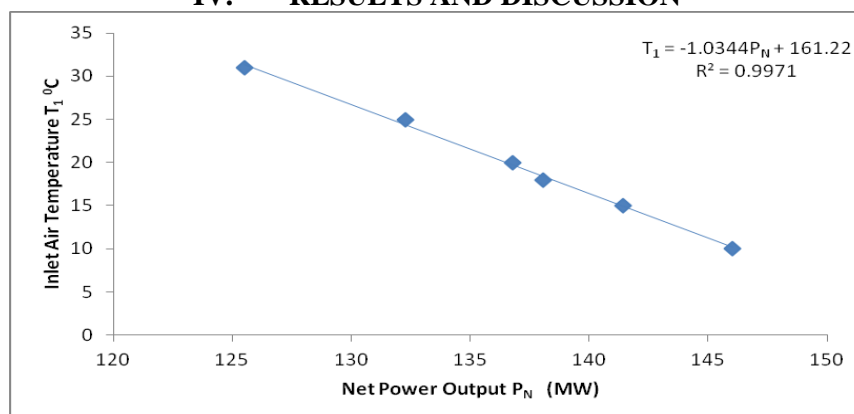


**Figure 2: Effect of inlet air temperature on power output**

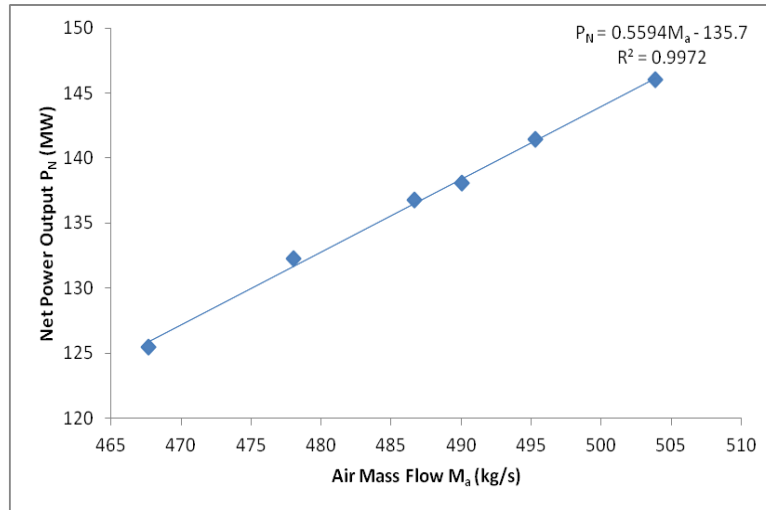


Figure 3: Effect of air mass flow on power output

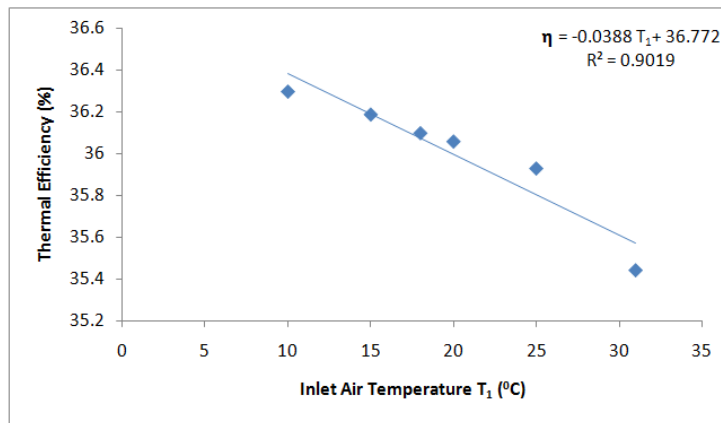


Figure 4 Effect of inlet air temperature on thermal efficiency

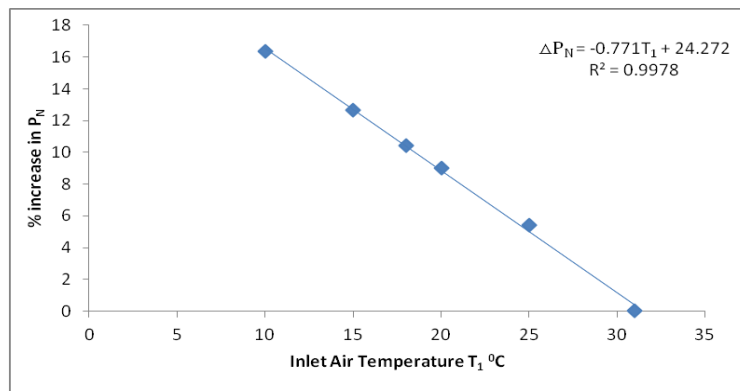


Figure 5: Effect of inlet air temperature on power drop

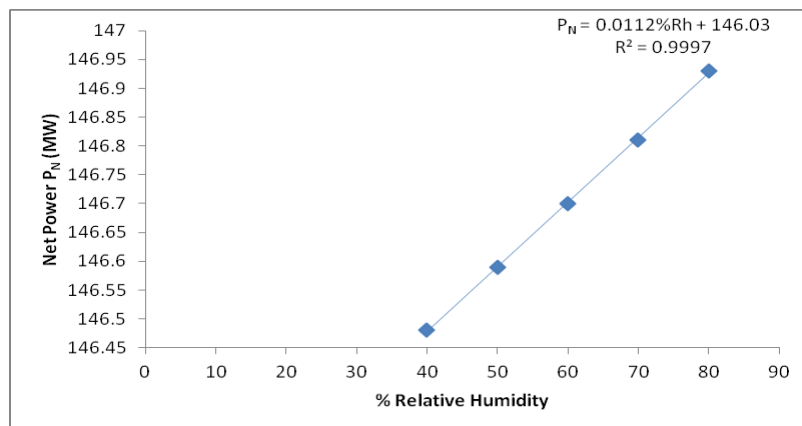


Figure 6: Effect of relative humidity on power output

Table 2 shows that between 31<sup>o</sup>C and 10<sup>o</sup>C the temperature difference is 21<sup>o</sup>C and there is a percentage increase in power output of about 16.36%. This represents an increase in power output of 0.78% for every 1<sup>o</sup>C reduction in the inlet air temperature. The analysis carried out which investigate the effect of inlet air temperature on power output shows that the cooler the inlet air entering the compressor, the more power output was obtained from the plant, this is clearly indicated in Table 2 and Figure 2

The research analysis was done within the range of 10<sup>o</sup>C and 31<sup>o</sup>C. This gave a corresponding net power output between 146.03MW and 125.50MW respectively. This is in line with the operational data of 125MW obtained at 31<sup>o</sup>C by the plant operator. From Figure 2, it can be seen that the plant rated capacity of 138.29MW design value could be achieved if the inlet air temperature is reduced to about 18<sup>o</sup>C. Also it can be seen that the plant efficiency progressively increased as the inlet temperature decreased. Figure 4 shows that at inlet air temperature of 18<sup>o</sup>C, the efficiency of 36.10% almost equal that of the designed value of 36.20%. On the whole the analyses showed that there is 0.78% power gain for every 1<sup>o</sup>C reduction in inlet air temperature.

The analysis carried out to investigate the effect of the humidity on the gas turbine power output and performance show the power output increase as humidity increases. At higher temperature and higher humidity of the inlet air, the power output was low compared with the result obtained when a lower inlet air temperature and same humidity was analysed. It shows that the best result was obtained at 80% humidity, 10<sup>o</sup>C inlet air temperature. This gave a power output of 146.92MW. On the other hand, the lowest power output was obtained when a humidity of 40% was used with the highest inlet air temperature of 31<sup>o</sup>C. This gave a power output of 126.96MW.

Table 3, 4, 5 and Figure 3-6 clearly illustrate these humidity effects on the turbine performance at various inlet air temperatures. A comparative analysis of power outputs at different humidity but at the same temperature was carried out at 10<sup>o</sup>C and 31<sup>o</sup>C inlet air temperatures respectively. The results show that at 31<sup>o</sup>C, 80% relative humidity, the power output obtained was 128.41. At the humidity of 40%, 10<sup>o</sup>C, the power output obtained was 146.48MW, and at the highest humidity of 80%, 10<sup>o</sup>C, the power output increased by 0.37% to 146.92MW. The above clearly establishes that the turbine power output and performance increases as the inlet air temperature decreases.

In the analysis, 138.26MW was obtained at 18<sup>o</sup>C, without humidity consideration, and 139.61MW power output was achieved when a relative humidity of 70% was applied at the same 18<sup>o</sup>C inlet air temperature condition. This represents an additional 0.97% increase power output. The result above affirmed clearly that the plant's designed net power output of 138.29MW could be achieved with the application of a higher relative humidity of the inlet air temperature.

In achieving the above application of higher relative humidity in a tropical weather where this plant operates, a suitable air temperature reduction system is employed. The process could be any of the evaporative cooling methods which include wetted media/ over-spraying, inlet fogging, wet compression and humid air injection.

## V. CONCLUSION

The research was to analyse the influence of the initial operating condition of the compressor on the turbine performance of V94.2 power plant. The research work was able to establish that at 18<sup>o</sup>C DBT, the plant's rated capacity of 138.29MW could be achieved and sustained. The low inlet temperature also increased the efficiency of the plant. It was established that there is an increase of 0.78% in power output for 1<sup>o</sup>C reduction in the inlet air temperature of the plant. The research analysis further established that the higher the relative humidity, the greater the net power output from the turbine as well as the performance. At 40% relative humidity and the inlet air temperature of 18<sup>o</sup>C, a power output of 138.37MW was achieved. This is greater than the output of 138.26MW obtained when the analysis was done at the same temperature but without humidity consideration. It also can be seen that the efficiency of 36.17% obtained at 18<sup>o</sup>C inlet temperature without humidity consideration increase to 36.21% at the same temperature on application of a relative humidity of 80%. This obviously shows a strong positive correlation between the compressor initial operating parameters and turbine power output.

## REFERENCES

- [1] Chaker M., Meher-Honiji C. R., and Mee T.R. (2002) Inlet Fogging of Gas Turbine Engines Part A: Droplet Thermodynamics, Heat Transfer and Practical Consideration. *Proceeding of ASME Turbo Expo*. 2002-GT-30562
- [2] Nag P. K (2001) Power Plant Engineering, 2<sup>nd</sup> Ed. Tata McGraw-hill. Pp96, 134-367
- [3] Al-Bortmany J. N., (2002) Assessment of Aqua-Ammonia Refrigeration for Pre-Cooling Gas Turbine Inlet Air. *Proceedings of ASME Turbo Expo*. Amsterdam, Netherlands
- [4] Abedin A., (1998) Integrated Combined Cycle Power Plant Design covering Conditioning of Gas Turbine Inlet Air for Part-Load Efficiency Enhancement coupled with Inlet Air Cooling for Increase in Peak Summer Capacity and Efficiency. *Proceeding of International Conference on Energy Research and Development*. 1: 390-397
- [5] Punawani D. V (2003) An Introduction to Turbine Inlet Cooling. *Energy Technology Magazine*. 4-5
- [6] Punawani D.V (2004) Hybrid systems and LNG for Turbine Inlet Cooling. *Energy Technology Magazine*. 18-19
- [7] American Society of Heating, refrigerating and Air-conditioning Engineers (2008). "ASHRAE Hand book-HVAC Systems and Equipment (SI)". CD-Rom, Atlanta, GA.
- [8] Nasser, A.E.M AND El-Kalay, M. A.,(1991) A Heat Recovery Cooling System to Conserve Energy in Gas Turbine Power Stations in the Arabian Gulf, *Applied Energy*. 38 (2). 133-142
- [9] Zuniga, M.O.V., (2005) Intake Systems for Industrial Gas Turbine, Cranfield University United Kingdom
- [10] Boonnasa, S (2006) Performance Improvement of the Combined Cycle Power Plant by Intake air Cooling using an Absorption Chiller. *Energy*. 31. 2036-2046
- [11] Rahman M.M., Thamir K. J. and Ahmed N. A., (2012). Thermodynamic Performance Analysis of Gas Turbine Power Plant. *Journal of Physical Sciences*. 6. 3539-3550
- [12] Al-Ibrahim, A. M and Varnham A. (2010) A Review of Inlet Air-Cooling Technologies for Enhancing the Performance of Combustion Turbines in Saudi Arabia, *Applied Thermal Engineering*.30 (14-15). 1879-1888
- [13] Amell A. A., and F.J Cadavid (2002). Influence of the Relative Humidity on the Air Cooling Thermal Load in Gas Turbine Power Output. *Applied Thermal Engineering*. 22: 1529-1533. DOI: 10.1016/S1359-4311(02)00063-7

## Design and Construction of a Prototype Gas Fired Kiln Using Nsu Clay Refractory Bricks

<sup>1</sup>, Oduagwu Ferdinand Azubuiké, <sup>2</sup>, Koreyo Victor Dorawa,

<sup>3</sup>, Azubuiké Thaddeus Chukwuemeka

*Department of Ceramics and Glass Technology*

*School of Industrial Technology*

*Akanu Ibiam Federal Polytechnic Unwana Afikpo, Ebonyi State*

*Nigeria*

**ABSTRACT:** *In the construction of a prototype gas fired kiln, plastic pressing method was used in producing the bricks. The bricks have a specific body composition of 48% of grog and 32% of uncalcined Nsu clay for dense bricks, 16% saw dust and 44% Nsu clay for insulating bricks. Test carried out to ascertain the quality of the bricks include the water absorption test (18.8% for dense bricks and 85% for insulating bricks), apparent porosity test (63.2% for insulating bricks and 23.2% for dense bricks) and crushing strength test (10.2N/mm<sup>2</sup> for dense bricks and 2.5N/mm<sup>2</sup> for insulating bricks). This constructed kiln has a total surface area of 0.54m<sup>2</sup> (54cm<sup>2</sup>) with volume of 0.00684m<sup>3</sup> and the kiln can fire up to the temperature of 1200<sup>o</sup>c it has a high efficiency for firing of ceramic wares and for low melting glasses.*

### I. INTRODUCTION

Kiln is any fixed structure of any shape or form built with insulation refractory materials used for the heat treatment of wares making them permanent object of usefulness. It is also used for roasting of ores and in cement production. In the production of ceramic wares, source of firing is the fact to be considered. Any article made with clay is said to be useful only when it undergoes heat treatment. The thermal efficiency of any kiln depends on the refractory wall of the kiln, damper system and heating element. Damper controls firing pressure and heating process of kiln. There is need for technological growth and economic development in our nation. Using our locally sources material kaolin which is available in building kilns, furnace for glass melting and in making ceramic wares. Due to high cost of importation of kiln, inadequate supply of electricity to operate electric kiln and power fluctuation, production of ceramic wares is been hampered. This discourages potters who are in the field. Gas kiln usually has high thermal efficiency which leads to high productivity level and varieties of colours which are absent in electric kiln can be achieved in gas kiln. This varieties of colours make's people to become more excited about ceramic wares since oxidation and reduction (redox reaction) can be done in gas kiln.

The motive behind this research is to embark on construction of prototype gas fired kiln using local material Nsu clay. This is a large clay deposit found in Nsu a town in Imo State, Nigeria. It is hereby imperative to facilitate construction of local kilns to meet increasing demand. Hence, the development of techniques for the construction of high efficiency kilns that are commercially viable and also meet required standard.

A kiln is expected to assume a temperature of not less than 600<sup>o</sup>c before it can be useful in ceramic. (Rhodes, 1973:16 and Fournier 200:184). The primary determination of use of any bricks, is their ability to withstand high temperature and prevent heat losses to acceptable limit (Fraser, 1979:1). Refractory bricks are made from a mixture of grog and fireclay or kaolin and or a combination of the three materials. According to Cardew (1969:162) this type of brick are heavy, resistant to cracking, wear and abrasion and do not crumble or disintegrate easily.

Insulating refractory brick are heat resistance suitable for inner brickwork of the kiln chamber. There are weak and less resistance to wear and abrasion because of their porous structure cause by the addition of pore creating substance (pore inducer). Searle (1956) say that the commonest among the insulating bricks are these made from refractory fire clays and kaolin with the addition of organic substance such as sawdust, peat, pulp, paper, waste flour or grass etc. the use of refractory insulation bricks is “a more recent development, coming into general use during the 1930s and has revolutionized the design of kilns furnaces of all sorts” (Rhodes, 1977:88). The bricks are fitted together to form framework using mortar, usually a heat resisting material of similar composition to the brick themselves. The construction is done to specification making sure that there is a workable relationship between the various parts of the kiln. The size of kiln chamber otherwise draught will be affected. This is necessary if the kiln is to give a maximum efficiency. Other composition of kiln include element, burners and temperature measuring instrument, kiln furniture such as shelves, props etc. used for setting wares inside the kiln. They are made from high firing refractory material that withstand high temperature without warping (Washaw 2006:223). Shelves and props like the bricks are highly refractory and give satisfactory service particularly those made from either high alumina materials such as silimanite, kyanite or silicon carbide, (Rado 1988:104, Cardew p. 158). Heat is introduced into the kiln through heating element for electric kilns or burners for oil, kerosene and gas fired kiln. Most modern kilns are fitted with temperature measurement such as pyrometer, although pyrometric cone can also be used. They are small pyramids made of ceramic materials which will melt and bend when desire temperature is reached and it is seen through spy hole. These materials and equipment are rather two expensive which accounts for the high cost of kilns.

**GAS KILN:** Gaseous fuel have become highly favoured among contemporary ceramist. This is because they do not require constant stocking and they create no unburned ash as residue that must be periodically removed. These fuels include propane, natural as, kerosene and oil. Modern kilns fired with these fuels greatly give room for ceramist to use a wide variety of glaze types and rich visual textures. A well fired and mature glaze with a reduce lusters can be produce in a gas kilns. Kilns fired with natural gas or propane do not have combustion problems, the burners used to fire these fuel are quit efficient and have only a moderate impact in the environment. When firing with gas it is important to avoid the direct impact of the flame on the ware. Therefore, kiln is constructed in such a way to leads the flame around the interior chamber and generally combustion is created, the wares can be fired in sagars or the kiln can have a full or muffle construction to protect against the direct heat of the flames. Gas kiln has the advantage that temperature can be controlled by reducing or increasing the fuel input. it is suited to reduce stoneware firing as the intake of air into the chamber can be reduced or some form of solid fuel can be introduced to create a reducing atmosphere. It gives a cheap easily burned and gives perfect result. Many gas kilns are downdraft designs which has fire box at the front or by the sides of the firing chamber. These kilns are very similar in design to those meant for firing solid fuel with the exception that since there is no unburned ash residue. Some gas kilns are updraft in design and employ very powerful blower-driven burners; these rely on the efficiency of the fuel and the power of the burners to reach high temperature.

## II. MATERIALS AND METHOD

### EXPERIMENTAL DETAILS

This chapter focuses on the experimental details of the production process in the construction of a prototype gas fired kiln using Nsu clay insulating and dense refractory bricks. In this study, the percentage composition of Nsu clay to combustibile material. (saw dust ) which will be used in producing insulation brick is 73.3% Nsu clay and 26.7% sawdust, and 40% unclained Nsu clay against 60% grog of Nsu clay for dense brick. The method selected for the kiln bricks production is pressing method.

### MATERIALS FOR THE CONSTRUCTION OF PROTOTYPE GAS-FIRED KILN

Dense brick made from Nsu clay, insulating brick made from Nsu clay, mortar, plume, Angle iron, saw and scraper

### METHOD FOR THE KILN'S BRICKS PRODUCTION AND KILN CONSTRUCTION

The procedure for the construction of a prototype gas fired kiln was carried out in different processes.

### GROG PREPARATON

Nsu clay is calcined at 1000<sup>0</sup>c, crushed and grounded to its finest form and sieved using 30 mesh in a plastic container from which it will be measured out for kiln's insulating brick production.

### PREPARATION OF SAW DUST

The saw dust is sieved using 30 mesh into a plastic container from which it will be measured out for the kiln's insulating brick production.

### III. PREPARATION OF NSU CLAY

NSu clay is crushed and grounded to a fine powder and then sieved using 100 mesh into a plastic container from which it will be weighed out during fabrication of both dense and insulating bricks for the kiln's construction.

#### 3.1 PROCEDURE FOR PLASTIC PRESSING METHOD OF KILN'S REFRACTORY BRICKS PRODUCTION

73.3% of Nsu clay is weighed out into a plastic container and the sieved saw dust of 26.7% is also weighed out and mixed with the Nsu clay and water to make the mix. The recipe was thoroughly mixed to obtain a uniform body mixture. It is allowed to age overnight and re-mixed again. The mixed batch is then gradually fed into the wooden mould and pressed to a considerable compression of uniform application of force using open ended pressing method. The fabricated brick is remolded and allowed to dry evenly by air drying, it is then moved into the drying cabinet to dry at the temperature of about 110<sup>0</sup>c, it is then removed and into the kiln for firing to obtain the required characteristics such as hardness, toughness, rigid and thermal shock resistance, sharp edges and corners.

The same procedure is equally applied in the dense brick production but excluding saw dust but addition of 60% of grog (calcined Nsu clay) and 40% Nsu clay (uncalcined). Both dense and insulating brick are fired at 1240c<sup>0</sup>.

#### 3.2 GAS – FIRED KILN CONSTRUCTION PROCEDURE

i. the fired bricks (insulating and dense brick ) is used in lining the kiln. At the inside of the kiln, dense brick forms the hot face while the insulating brick serve as back up brick to the dense brick, mortar, which is made up of 2% Nsu clay and 1% grog is used to hold the brick one after the other and to level the bricks.

ii. Metal casing is used to encase the kiln against surface abortion and to make the kiln portable and provide a well finished compatibility.

#### (INSULATING AND DENSE)

i. Test for water of absorption of the bricks

ii. Crushing strength of the bricks

iii. Porosity test of the bricks

#### 3.3 WATER ABSORPTION OF THE BRICKS USED IN KILN CONSTRUCTION

The brick samples (insulating and dense) were boiled at 100c<sup>0</sup> for five (5) hours to allow the brick samples to absorb water. Water absorption were calculated as a function of the samples weight difference prior to and after water submersion. The water absorption was computed using equation.

$$\text{Water absorption} = \frac{w_2 - w_1}{w_1} \times 100\%$$

Where  $w_2$  = boiled weight at 100c<sup>0</sup> for 5 hours

$w_1$  = dry weight of brick samples.

#### 3.4 APPARENT POROSITY TEST OF THE BRICK SAMPLES

The boiling method were used in which in the samples were weighted dry  $W_1$  and were subjected for boiling of 100c<sup>0</sup> for five (5) hours and then weighed  $W_2$ . The boiled samples were suspended from the beam of a balance in a used of water so arranged that the test piece under consideration was completely immersed in the water without touching the side of the used. The suspended samples in water were weighed as  $W_3$ . Porosity were calculate as a function of the samples weight difference between boiled weight and dry weight to samples against weight difference between boiled weight and suspended immersed weight. The results were abstained by the equation.

$$\text{Apparent Porosity (P)} = \frac{W_2 - W_1}{W_2 - W_3} \times 100\%$$

Where  $W_2$  = boiled weight

$W_1$  = dry weight

$W_3$  = suspended immersed weight

### 3.5 CRUSHING STRENGTH

The strength of the brick samples was investigated using a universal tensile testing machine in which it was used to carry out the falling load of the samples using formula.

$$\text{Crushing strength} = \frac{\text{Force (f)}}{\text{Area(A)}} \text{ N/mm}^2$$

Where f= farce (N)

$$A = \text{Area (length x width) (m}^2\text{)}$$

The crushing strength was determined using a universal tensile testing machine in the civil engineering workshop of Akanu Ibiam Federal polytechnic. Each of the samples was placed one after the other on the bearing edges of the compression machine. Load was then applied at the center of the samples uniformly.

The load at which the sample fails were calculated and recoded in kilo newton (KN). The length and width of the brick sample were measured and multiply by 2 to abstain the final result of the area of the brick samples.

### 3.6 HEAT PASSING THROUGH THE KILN STRUCTURE

Heat passing through brick structure is proportional to the cross – section area thought the structure from which it passing the temperature difference between the hot face and cold face and it is inversely proportion to the thickness of the brick wall.

$$Q \propto \frac{A\Delta T}{t}$$

$$Q = \frac{KA\Delta T}{t}$$

Where Q= heat passing per unit length ( $\text{w/m}^2$ )

K = thermal conductivity of the refractory brick ( $\text{W/mc}^0$ )

A = area of the brick ( $\text{m}^2$ )

$\Delta t$  = temperature difference between hot face and cold face of the brick ( $\text{c}^0$ )

T = thickness of the brick wall (m)

### 3.7 HEAT STORED IN THE KILN STRUCTURE

The quantity of heat stored in a kiln or furnace structure depends on refractory arrangement used in lining the structure. Quantity of heat stare in a brick wall is directly proportional to the muss of the refractory brick, thickness of the brick, and average temperature of the brick

$$Q \propto DtT$$

$$Q = SDtT \text{ (J/m}^2\text{)}$$

Where Q = quantity of heat store in the brick ( $\text{J/M}^2$ )

S =specific heat ( $\text{KJ/Kg/c}^0$ )

D = Density of the brick ( $\text{kg/m}^2$ )

t = thickness of the brick (m)

T = average temperature of the brick ( $\text{c}^0$ )

**THE INTERFACE TEMPERATURE**

This is the temperature between the dense refractory brick wall and insulating refractory brick wall, and which can be calculated as follow.

$$\text{Heat passing through the structure } \frac{Q}{A} = \frac{\Delta t}{\left(\frac{t_1}{k_1} + \frac{t_2}{k_2}\right)}$$

Where  $\frac{Q}{A}$  =heat passing through the structure (w/m<sup>2</sup>)

$\Delta t$  = temperature difference cold face of the brick wall (c<sup>0</sup>)

$t_1$  = thickness of the dense brick wall (m)

$t_2$  =thickness of the insulating brick wall (m)

$k_1$  = thermal conductivity of dense brick (W/ m c<sup>0</sup>)

$K_2$  = thermal conductivity of insulating brick (W/ m c<sup>0</sup>)

**BURNER**

The burners used in firing the kiln were locally constructed using 3inch pipe which is connected to a control gas tape. The tape has a nob which is used to control the amount of gas that flows from the tape to the 3inch pipe. The surrounding air entered the pipe through the opening along the side of which will mix with gas (petroleum liquefy gas) which will be ignited at the extreme end of the pip.

**BATCH COMPOSITION**

(i)DENSE BRICK BATCH COMPOSITION (KG)

TOTAL BATCH WEIGHT (60kg)

MATERIALS (KG)	CALCILATION	% COMPOSITION
NSU GROG FINE = 4.8	$\frac{4.8}{60} \times 100 = 8\%$	8%
COARSE = 24	$\frac{24}{60} \times 100 = 40\%$	40%
UNCALINE NSU CLAY = 19.2	$\frac{19.2}{60} \times 100 = 32\%$	32%
WATER = 12	$\frac{12}{60} \times 100 = 20\%$	20%
TOTAL = 60 Kg		TOTAL = 100%

(ii)INSULATING BRICK BATCH COMPOSITION (Kg)

TOTAL BATCH WEIGTH (60Kg)

MATERIALS (KG)	CALCILATION	% COMPOSITION
NSU GROG FINE = 26.4 (UNCALINE)	$\frac{26.4}{60} \times 100 = 44\%$	44%
SAW DUST = 9.6	$\frac{9.6}{60} \times 100 = 16\%$	16%
WATER = 24	$\frac{24}{60} \times 100 = 40\%$	40%
TOTAL = 60 Kg		TOTAL = 100%

**RESULTS AND DISCUSSION****(i) WATER ABSORPTION TEST OF DENSE REFRACTORY BRICKS**

BRICKS SAMPLE	DRY WEIGHT W <sub>1</sub> (kg)	WET WEIGHT W <sub>2</sub> (kg)	CHANGE IN WEIGHT (W <sub>2</sub> - W <sub>1</sub> ) kg	% WATER OF ABSORPTION $\frac{(W_2 - W_1) \times 100}{W_1}$
A	0.2285	0.2706	(0.2285 - 0.2706) = 0.0421	0.0421 X 100 = 18.4 <u>0.2285</u>
B	0.1166	0.1388	(0.1388 - 0.1166) = 0.0222	0.0222 X 100 = 19.0 <u>0.1166</u>
C	0.102	0.1215	(0.1215 - 0.102) = 0.0195	0.0195 X 100 = 19.1 <u>0.102</u>
TOTAL percentage water of absorption = 18.4 + 19.0 + 19.1 = 18.8% of dense bricks 3				

**(ii) WATER ABSORPTION TEST OF INSULATING BRICKS**

BRICKS SAMPLE	DRY WEIGHT W <sub>1</sub> (kg)	WET WEIGHT W <sub>2</sub> (kg)	CHANGE IN WEIGHT (W <sub>2</sub> - W <sub>1</sub> ) kg	% WATER OF ABSORPTION $\frac{(W_2 - W_1) \times 100}{W_1}$
A	0.1235	0.2287	(0.2287 - 0.1235) = 0.1052	0.1052 X 100 = 85.2 <u>0.1235</u>
B	0.1233	0.2287	(0.2287 - 0.1233) = 0.1036	0.1036 X 100 = 84.0 <u>0.1233</u>
C	0.1225	0.2276	(0.2276 - 0.1225) = 0.1051	0.1051 X 100 = 85.8 <u>0.1225</u>
TOTAL percentage water of absorption = 85.2 + 84.0 + 85.8 = 85.0% of the insulating bricks 3				

**CRUSHING STRENGTH OF THE BRICKS**

BRICK SAMPLE	FORCE(F) THAT CRUSH THE BRICK	AREA OF BRICK (L X W) X 2 (MM <sup>2</sup> )	CRUSHING STRENGTH = F/A (N/mm <sup>2</sup> )
DENSE BRICK	60000	64 X 46 X 2 = 5888	60000 = 10.2 5888
INSULATING BRICK	15000	64 X 46 X 2 = 5888	15000 = 2.5 5888

**4.3 APPARENT POROSITY TEST OF THE BRICKS**

$$\text{Porosity (P)} = \frac{W_2 - W_1}{W_2 - W_1} \times 100\%$$

Where W<sub>1</sub> = dry weight (kg)

W<sub>2</sub> = boiled weight (kg)

W<sub>3</sub> = suspended immersed weight (kg)

**INSULATING BRICK**

Porosity (P) = W<sub>1</sub> = 0.0593 (kg)

W<sub>2</sub> = 0.1109(kg)

W<sub>3</sub> = 0.1289 (Kg)

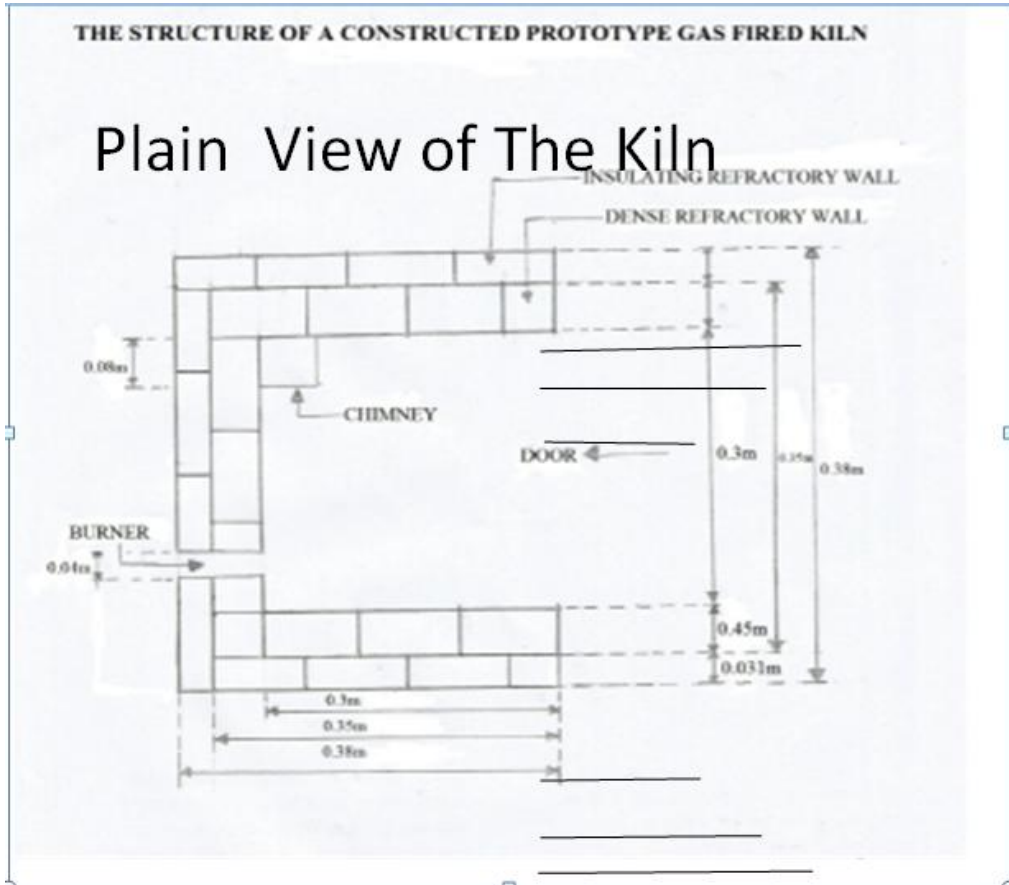
INSULATING BRICK

Porosity (P) =  $W1 = 0.0593(Kg)$   
 $W2 = 0.1109 (kg)$   
 $W3 = 0.1289(Kg)$   
 $P = \frac{W2-W1}{W2-W3} \times 100$   
 $= \frac{0.1109-0.0593}{0.1109-0.0293} \times 100$   
 $= \frac{0.0516}{0.0816} \times 100$   
 $= 0.0632 \times 100 = 63.2\%$   
 $P = 63.2\%$

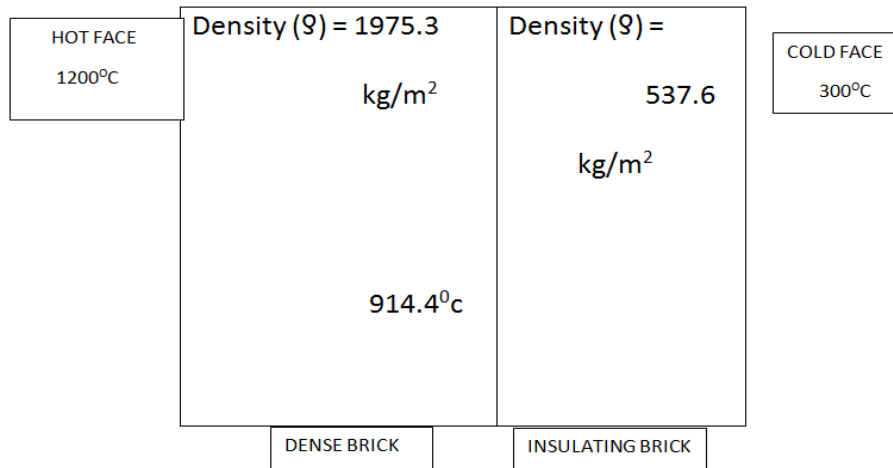
DENSE BRICK

Porosity (P) =  $\frac{W2-W1}{W2-W3} \times 100$   
 $= \frac{0.0951-0.0814}{0.0951-0.036} \times 100$   
 $= \frac{0.0137}{0.0591} \times 100$   
 $= 0.2318 \times 100$   
 $= 23.2\%$

THE STRUCTURE OF A CONSTRUCTED PROTOTYPE GAS FIRED KILN



HEAT STORED IN THE KILN STRUCTURE



HEAT STORED IN THE KILN STRUCTURE

BRICK SAMPLE	DENSITY OF BRICK WALL (kg/m <sup>3</sup> )	THICKNESS OF BRICK (m)	AVERAGE TEMPERATURE OF BRICK (°C) $\frac{HOT\ FACE + COLD\ FACE}{2}$	SPECIFIC HEAT OF BRICK (KJ/KG/°C)
DENSE BRICK	1975.3	0.045	$\frac{1200+914.4}{2} = 1057.2$	1.0
INSULATING BRICK	537.6	0.031	$\frac{914.4+300}{2} = 607.2$	1.0

Heat stored in the kiln structure  $Q = D \times t \times S \times T$

Where D = Density of brick (kg/m<sup>3</sup>)

t = Thickness of brick (m)

s = specific heat of brick (KJ/kg/°c)

T = average temperature of brick (°c)

Heat stored in dense brick wall  $Q = D \times t \times S \times T$

$$1975.3 \times 0.045 \times 1 \times 1057.2 = Q = 93972.9$$

$$Q = 94 \text{ KJ/m}^2$$

Heat stored in the insulating brick wall  $Q = D \times t \times S \times T$

$$Q = 537.6 \times 0.031 \times 1 \times 607.2$$

$$Q = 10119.4$$

$$Q = 10.1 \text{ KJ/m}^2$$

Heat stored in the kiln structure = heat stored in dense wall + heat stored in the insulating brick wall

$$= 94 + 10.1 = 104.2$$

$$= 104.2 \text{ kJ/m}^2$$

HEAT PASSING THROUGH THE KILN STRUCTURE

BRICK SAMPLE	AREA OF BRICK (L X W) (M <sup>2</sup> )	THICKNESS OF BRICKS (M)	TEMPERATURE DIFFERENCE OF BRICKS	THERMAL CONDUCTIVE OF BRICK (W/C)
DENSE BRICK	(0.3 X 0.3) = 0.09	0.45	1200 – 914.4 = 285.6	1.0
INSULATING BRICK	(0.3 X 0.3) = 0.09	0.031	914.4 – 300 = 614.4	0.32

Heat passing through kiln =  $Q = \frac{KA\Delta T}{t}$

$$Q = \frac{KA\Delta T}{t}$$

Where Q = heat passing per unit length (w/m<sup>2</sup>)

A = Area

$\Delta T$  = temperature difference between hot face and cold face of brick wall (°c)

K = Thermal conductivity of the bricks (w/m<sup>2</sup>)

Heat passing through the dense wall =  $\frac{KA\Delta T}{t}$

$$Q = \frac{1.0 \times 0.09 \times 285.56}{0.045}$$

$$= \frac{25.7}{0.045}$$

$$= 571.1$$

$$Q = 571.1 \text{ w/m}^2$$

Heat passing through the insulating wall =  $\frac{KA\Delta T}{t}$

$$Q = \frac{0.32 \times 0.09 \times 614.4}{0.031}$$

$$= \frac{17.69}{0.031}$$

$$= 572$$

$$Q = 572 \text{ w/m}^2$$

Heat passing through the kiln structure during firing = heat passing through the dense wall + heat passing

Through the insulating

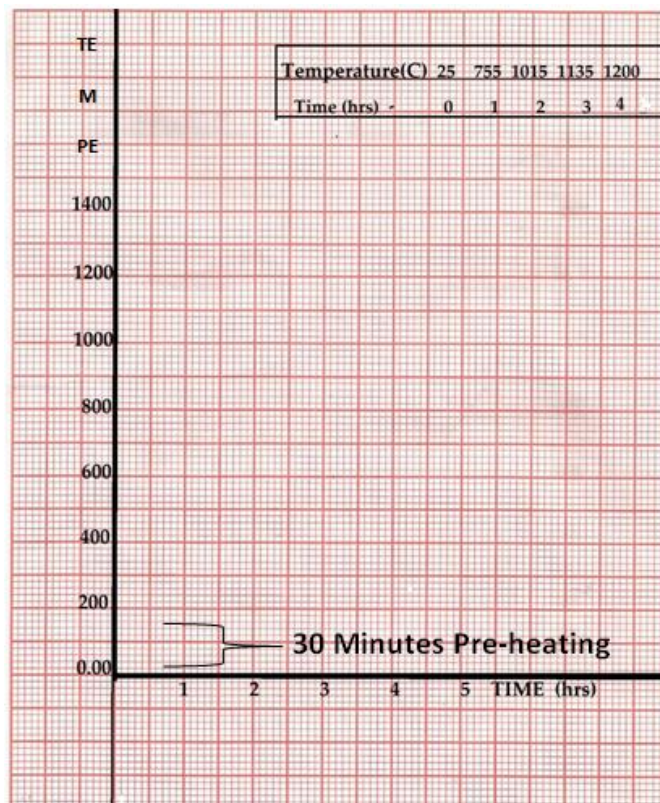
$$= 571.1 + 572$$

$$= 1143.1 \text{ W/m}^2$$

FIRING SCHEDULE OF PROTOTYPE GAS FIRED KILN (1200°C)

TEMPERATURE (C°)	TIME (sec)	REMARK
25	11:53	
74	12:23	
755	12:53	
810	12:56	Dark Red Colour
900	1:06	Cherry Red Colour
911	1:13	
942	1:20	
988	1:53	Cherry red-Orange Colour
1000	2:15	
1015	2:53	
1135	3:00	Orange Colour
1200	3:53	Light Orange Colour. Kiln off gas off end firing

THE GRAPH OF FOUR HOURS TEST FIRING OF PROTOTYPE GAS FIRED KILN



### V. DISCUSSION OF RESULT

The result of this research work shows that insulating bricks absorb more water up to 85% than that of dense brick which is 18.8%. This is because of the presence of large number of very small voids in the insulating which makes it lighter than the dense brick. The crushing strength of the dense brick is  $10.2 \text{ N/mm}^2$  and that of insulating is  $2.5 \text{ N/mm}^2$ . The quantity of heat store in this kiln is  $97.5 \text{ KJ/m}^2$ , this makes the kiln to fire high up to  $1200^\circ\text{C}$  within four hours with heat loss of  $1143.1 \text{ w/m}^2$ . However, this kiln can fire at faster rate than the laboratory test electric kiln.

#### THE BASE OF THE KILN



#### THE REFRACTORY WALLS OF THE KILN



#### THE KILN COVERED WITH CRO



**THE KILN WITH METAL REINFORCEMENT**



**FULLY CONSTRUCTED PROTOTYPE GAS FIRED KILN**



**TEST FIRING OF THE PROTOTYPE GAS FIRED KILN**



## VI. CONCLUSION

The research work on the design and construction of a prototype gas fired kiln using NSU clay refractory bricks was a success as shown in the result of test that was carried out. A well compatible and high efficiency gas fired kiln was construct having a total surface area of  $0.54\text{m}^2$  ( $54\text{m}^2$ ) and volume of  $0.00684\text{m}^3$ . This kiln can fire up to the temperature of  $1200\text{c}^0$  within four hours. The varieties of colours which are absents in electric kiln can be achieved using this kiln.

Base on this result, it shows that local source material (NSU clay refractory brick) can be used for building higher efficient kilns which will reduce the cost of importation of kiln and increase the nationally economic growthence reduce unemployment in this country. This study provide solution to irregular power change which have crippled the use of electric kiln. This local NSU clay bricks has composition of 48% grog (Calcined NSU clay) and 32% uncalcined NSU clay for dense brick. The dense bricks has water absorption of 18:8%, crushing strength of 10.2N/mm. The insulating brick has body composition of 16% saw dust and 44% NSU clay water absorption of 85% and crushing strength of  $2.5\text{ N/mm}^2$ .

## REFERENCES

- [1]. Adegoke, O.S. et al (1987) "Summary of Raw Materials Occurrence" Guid to Non – Metallic Industrial Potentials of Nigeria Vol 1, P. 180-195
- [2]. Cardew, M. (1969) Pioneer Potter (P. 162-170).
- [3]. Cooper, E. (1982) Electric kiln's Potter (P. 34-36) Echea, C (2001) "Gloss Firing: Beyond Thermosensor", CPAN Journal of Ceramics, Vol. 1, No 1 p, 14 -19.
- [4]. Fournier, R. (2000) Illustrated Dictionary of Practical Pottery. P.183-190 Fraser, H, (1979) Electric Kilns Firing (P. 84).
- [5]. Ossai A. A (2005) Introduction to Alumino-Silicate and Other Refractories (P. 128-134.) Rado, P. (1988). An Introduction to the Technology of Pottery. P 75-88
- [6]. Rhodes, D. (1977) Kilns, Design, Construction and Operation (P. 88-90).
- [7]. Rhodes, D. (1973) Clay & Glazes for the Potters (P. 16-34).
- [8]. kashim, I.B. (1999)" Manufacturing of Electric Kiln from Locally Derived Refractory Materials in Nigeria" Journals of Industrial Design and Technology, Vol.1, No 1., p. 64 – 70.
- [9]. "TheJournal of Liberal studies"(2012 - 2014) Improvisation in kiln Construction Materials, an Approach in a Depressed Economy. Vol 15, No. 1. Retrieved from editor @Jls. Online.

## Human Body Motion Detective Home Security System with Automatic Lamp and User Programmable Text Alert GSM Mobile Phone Number, Unique PIN to Allow Universal Users Using PIR Sensor

Oyebola B. O.

Department of Electrical/Electronic Engineering Technology  
Gateway (ICT) Polytechnic Saapade, Ogun State, Nigeria

**ABSTRACT:** Insecurity is not a credit to any responsible society, and the conventional use of watch-man has drawbacks of huge risk of life and cost intensive. The use home security system with user programmable text alert GSM mobile phone number with unique PIN to allow universal users with human body motion detective can overcome these limitations. This paper presents reliable security system that is able to recognize human body motion and send an alert message to inform the owner (at any location in the world where there is GSM mobile network coverage) of the house through an SMS alert when an unwanted visitor or thief enters the range of the sensor. The system design is in three main phases: the sensitivity, central processing and action. The sensitivity is the perception section that is done through PIR sensor mounted at watch-area, central processing is performed by a programmed microcontroller, and the action (task) is done through an interaction of an attached on-board GSM module to the processor (the microcontroller) which then send an SMS alert to the user or owner mobile phone number. This system is design to only detect only (or part of human) body motion.

**KEYWORDS** - Human, body, Motion, Sensor, Microcontroller, SMS, Alert, Lamp, Mobile, Phone

### I. INTRODUCTION

A high level of theft or insecurity calls for better security system. It is much safer to have a system that monitors and communicates to the device owner without putting human life to risk in the name of "Watchman". This insecurity has paved way to increasing rate of stealing packed cars, money and valuable things in the home even with security. In order to enhance an improved and life risk free security system, the purpose of this study is to aid a better security system of house with the use of GSM. This system monitors one's home against theft and has a text message sent to the house owner, telling him that there is an unauthorized person close to the house. The system will also notice what is happening around the building. With this home security system, the house is always protected. The total absence of sufficient security personnel in a house is a great discomfort to house owners.

This project has three basic modules along with a GSM module. GSM module is used to send the SMS whenever there are changes in any of the three modules. First module of this project detects the incidence of an intruder. This feature is helpful at night time or whenever we are out of our home. LED placed outside the house displays this status. And if person comes closer the more then the LED is turned on. Second part of project serves the functionality of the GSM network that quickly alerts the owner of the house through a sms sending this data to a GSM modem through serial port.

The new age of technology has redefined communication. Most people nowadays have access to mobile phones and thus the world indeed has become a global village. At any given moment, any particular individual can be contacted with the mobile phone. But the application of mobile phone cannot just be restricted to sending SMS or starting conversations. New innovations and ideas can be generated from it that can further enhance its capabilities. Technologies such as Infra-red[1,2], Bluetooth[3], and Global system for Mobile Communication[4] to mention a few, have been developed in recent years to show the very fact that improvements are in fact possible and these improvement have eased our life and the standard of living.

The system allows a greater degree of freedom to a house owner regarding its security. The need to employ a 'watchman' to guard a house is eliminated with the use of our system. The proposed approach for designing this system is to implement a microcontroller-based GSM module that sends notification from a GSM module over the GSM network to the user about the presence of an intruder in the house. The microcontroller then will carry out the issued commands and then communicate the status of an intruder.

### 1.2 Aims and Intended Users

*This work was highlighted into three main objectives as follows:*

- I. Develop a system that is capable to identify intruder and send information to user regarding a break-in at their resident.*
- II. The necessities of the home security system should have low cost, easy installation, fast response, and low power consumption and a better way of security.*
- III. To improve home security systems and eliminate the need of watchman to guard a house.*

*This system is aimed toward all the average users who wish to secure their household/office with a sensor that can be used to detect the presence of an intruder. This guarantees safety to the user.*

### 1.3 Limitations of the Project

*The system has certain limitations and a list of such is mentioned below;*

- [1] The receiver must be located in in a location where a signal with sufficient strength can be received from the GSM module.*
- [2] Operation of the SIM card in the GSM module when sending SMS is only achievable with the accessibility of credit on it.*
- [3] The GSM module users have to recharge the SIM card by removing it, via ATM or online.*

## II. TECHNOLOGY USED

The proposed system is concerned with the design and construction of a Home Security System with User Programmable Text Alert GSM Mobile Phone Number, Unique PIN to Allow Universal Users and Human Body Motion Detective through PIR Sensor system. The system design is in three main phases: the sensitivity, central processing and action. The sensitivity is the perception section that is done through PIR sensor mounted at watch-area, central processing is performed by a programmed microcontroller, and the action (task) is done through an interaction of an attached on-board GSM module to the processor (the microcontroller) which then send an SMS alert to the user or owner mobile phone number. This system is design to only detect only (or part of human) body motion.

### 2.1 The Motion Discernment (Detector) Circuit

A motion detector is contains a motion sensor and is either incorporated with or connected to other devices that alert the user of the pre-sense of body motion. An electronic motion detector contains a motion sensor that transforms the detection of motion into an electric signal. The electric signal can be connected to a burglar with lamp system which is used to alert the home owner or security service after it detects motion.

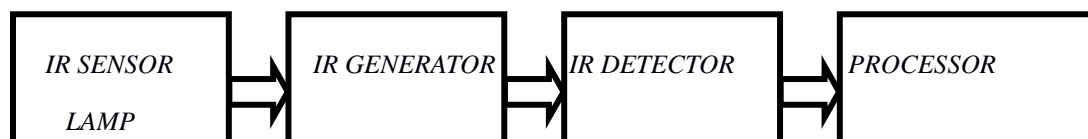


Figure 1: Block Diagram Motion Discernment (Detector) Circuit

In the Passive system each sensor consists of two housings. The first housing contains an infrared-emitting diode and an infrared-sensitive phototransistor as the infrared detector. The other housing contains an infrared reflector to reflect the infrared signal [7]. When positioned in front of an entrance to a protected area, the two housings establish an invisible beam.

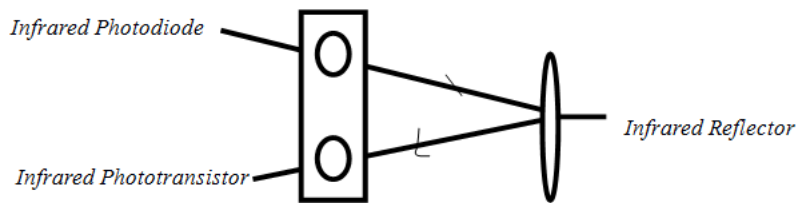


Figure 2: Passive infrared Motion detector for a Security System

The infrared motion detector circuit is based on two basic principles of passive infrared motion detector which are the infrared transmitter and infrared receiver as shown in Figure.3.

**Infrared transmitter**

For the infrared transmitter which is also known as emitter circuit, it is on a basic design of timer 555 astable operation. This means that the 555 timer can operate repeatedly; it will switch 'on' and 'off' continually to generate data for the infrared transmission

**Infrared receiver**

The infrared receiver which is also known as infrared detector receives the data transmitted by the infrared transmitter circuit. This infrared detector can be directly connected into the controller circuit to produce logic high '1' or low '0' from the output terminal thus activate or deactivate the controller system operation. The range of infrared detector components according to datasheet stated that the infrared detector can fully operates on detecting the infrared signal of 38 to 45 kHz.

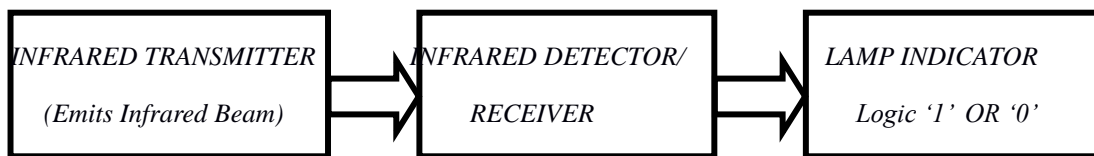


Figure 3: Block Diagram of Infrared Transmitter/ Receiver

**2.2 The Microcontroller circuit**

The controller systems that use to control the motion detector system and other electronic devices are the microcontroller PIC16F1508 – expended mode. In expended mode configuration, external ROM and RAM are used to add the data memory to be more than internal memory provided by the Intel manufacture. The purpose of using an expended mode for the project is to expend more data available on developing and designing an excellent operation of the security system[8].

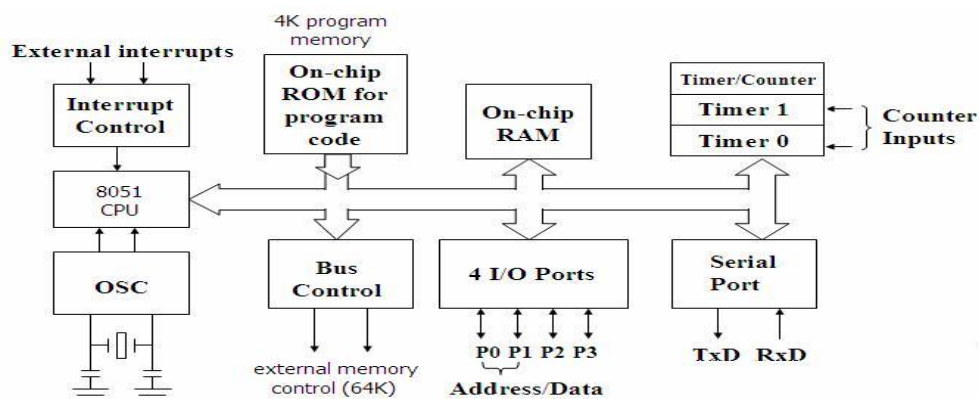


Figure 4: Internal Structure of a microcontroller

**2.3 GSM Module**

GSM module, Figure 5, is a specialized type of modem which accepts SIM card, and operates over a subscription to mobile operators. When the GSM modem and computer are interconnected, there is communication over the mobile network. Though these GSM modems are most frequently used to provide mobile internet connectivity, most of them can also be used for sending and receiving SMS and MMS messages. This device can also receive and process GSM signals from virtually all GSM bands.

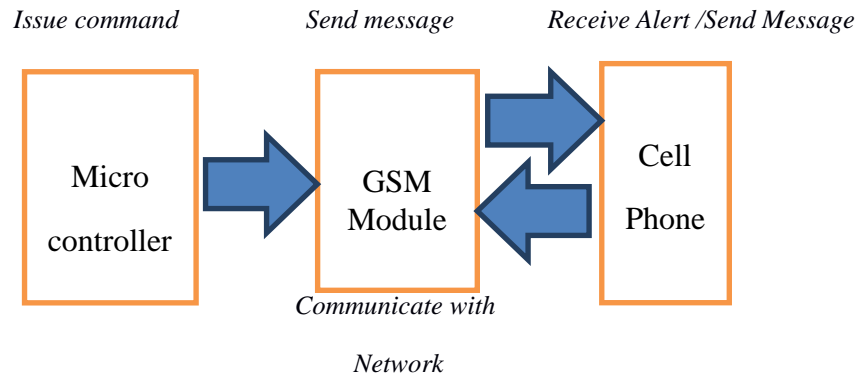


Figure 5: GSM Module Interaction

GSM module will then send Message to the user and also receive instruction from the user cell phone for reprogramming the phone number.



Figure 6: GSM module

Mechanical motion detection devices can be simple to implement, but at the same time, it can be defeated easily by interrupting the devices mechanics like “cutting the wire”.

#### 2.4 Short Message Service to Reprogrammed Alert Phone Number

SMS stands for Short Message Service. It is a technology that enables the sending and receiving of message between mobile phones. It was included in the GSM (Global System for Mobile Communication) standards right at the beginning. The reprogramming is done through the line 8 to 10 of the system processor algorithm in section 3.2 of this paper.

#### 2.5 Technology Considerations

The considerations for this system will include a choice of networks, communication protocols and interfaces. Serial I/O is considered as options for connection between the GSM receiver and the microcontroller. The proposed system is designed to detect motion of either authorized or non-authorized persons around a house. The system is designed with a GSM module, The GSM module system uses mobile network and is battery powered which makes home automation system safer from internet hacks.

### III. CIRCUIT DESIGN

In an attempt to implement the proposed system, it was divided into two parts which includes:

- a. Hardware design
- b. Software design

Figure 3.1 resembles the simple block diagram of the system.

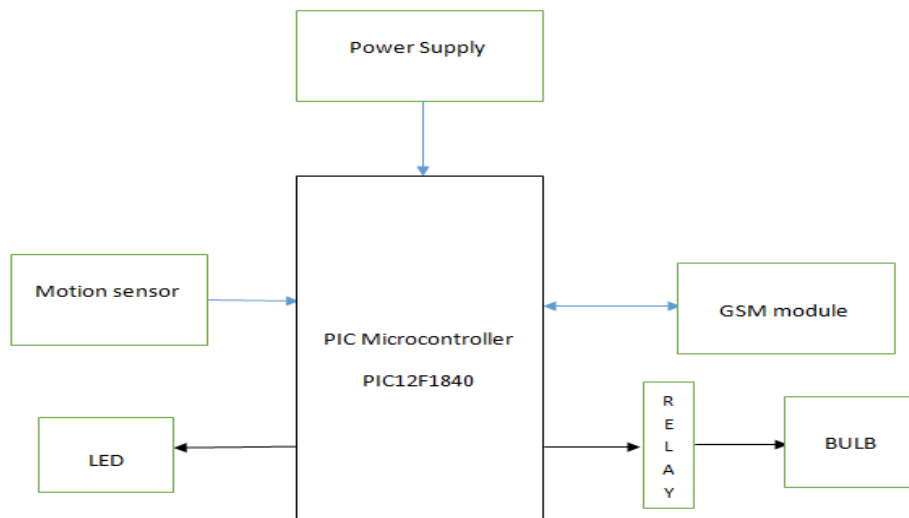


Figure 7: The System Block Diagram

**3.1 Hardware design Consideration**

**3.1.1 Microcontroller (IC2)**

This is the heart of the system wherein central processing of data takes place. The was developed with PIC12F1840 microcontroller; it collects the data or information from sensor and GSM module (with terminal Tx and Rx) for preprogrammed task.



Figure 8: Microcontroller

By receiving the sensor signals, it takes the corresponding course of action by sending commands to the output devices. It is the CPU (central processing unit) of system. It functions include reading of the digital input from infrared receiver, find out if person is within the house then, send the data to bulb or LED and GSM Module transmitter to eventually relay the alert to the owner mobile phone.

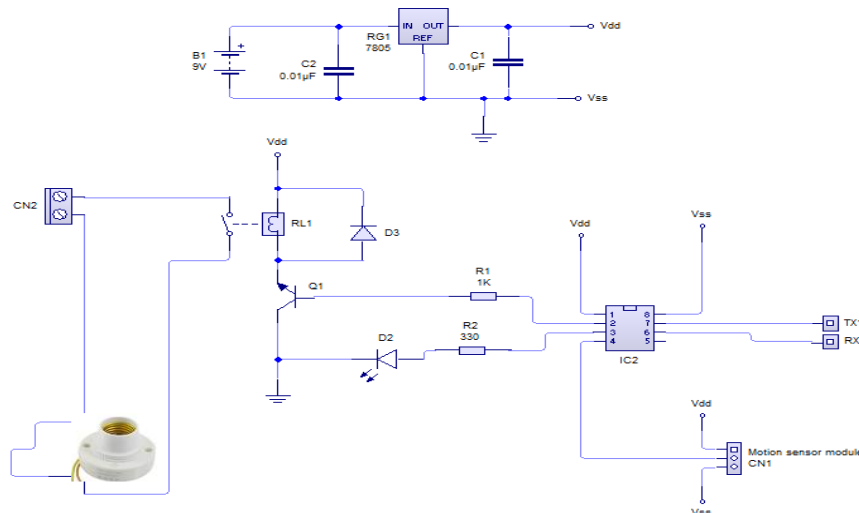


Figure 9: The System Microcontroller Circuit Diagram

**3.1.2 GSM Module:**

The GSM Module provides a remote GSM mobile to control the system using the SMS. The complete circuit diagram of the GSM Module is given in Fig. 2.6.

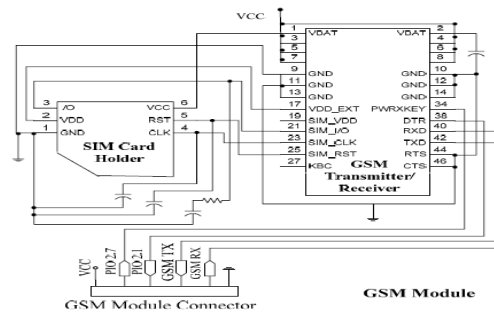


Figure 10: The Complete Circuit Diagram of the GSM Module

**3.1.3 Relay**

The relay acts as a mechanical switch to the SECURITY LIGHT either to ON or OFF.

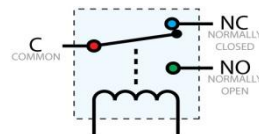


Figure 11: Relay Switch Connection

The relay driver is used to isolate both the controlling and the controlled device. The relay is an electromagnetic device, which consists of solenoid, moving contacts (switch) and restoring spring and consumes comparatively large amount of power. Hence the relay is used to switch the electrical supply to the Lamp indicator.

**3.1.4 Motion Sensor**

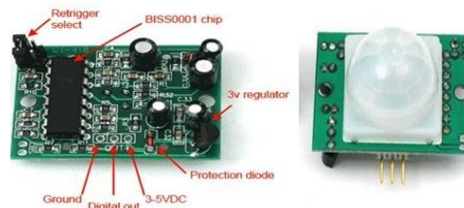


Figure 12: Motion Sensors

Motion sensors are used in a motion detector which is a device that contains a physical mechanism or electronic sensor that quantifies motion that can be either integrated with or connected to other devices that alert the user of the presence of a moving object within the field of view. They form a vital component of comprehensive security systems. The Motion sensors cannot detect still objects.

**3.1.5 Light Emitting Diode (LED)**

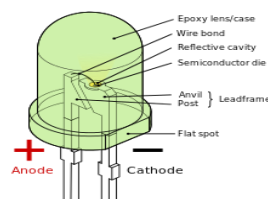


Figure 13: Light Emitting Diode

Light emitting diode is a two-lead semiconductor light source. It is a basic pn-junction diode, which emits light when activated. [5] When a suitable voltage is applied to the leads, electrons are able to recombine with electron holes within the device, releasing energies in the form of photons. An LED is often small in area (less than 1mm<sup>2</sup>) and integrated optical components may be used to shape its radiation pattern [6].

### 3.1.6 Lamp/Bulb



Figure 14: Bulb

*It's a device that produces light from electricity. Whenever a person is detected, it shines on the person to create awareness of being noticed.*

### 3.1.7 Power supply

*The power supply supplies electrical energy to the system.*

### 3.1.8 Voltage Regulator 7805

*RG1 7805 is voltage regulator. It brings the input voltage down to 5V the microcontroller needed.*

### 3.1.9 Transistor Q1

*The transistor acts as a driver for the bulb relay.*

## 3.2 Software Design Consideration

*The Processor Internal Control Program Algorithm is follows.*

1. Start
2. Microcontroller configuration
3. Interrupt Configuration
4. GSM module configuration
  - a. UART initialization
  - b. Baud rate negotiation
  - c. Issue Disable command echo
  - d. Set message type as TXT
  - e. Delete all messages(if any)
5. Blink the LED for 5 times
  - a. Read EEPROM for any saved number
6. Copy the saved number to microcontroller RAM
7. Begin infinity loop
8. Read if any message Received from GSM module
9. If "Pwd" received as message
  - a. Blink led for 7 times
  - b. Copy the phone number that sent the "Pwd" message to RAM of the microcontroller
  - c. Also saved the number to the EEPROM of the microcontroller
10. Send Acknowledge msg to the phone number.
11. If motion detected
  - a. LED off
  - b. SECURITY LIGHT is ON

- c. If the last message is over 30 seconds or thereabout
  - d. Send SMS message
  - e. Delay 10 seconds
  - f. LED is ON
  - g. SECURITY LIGHT is OFF
12. End an Infinity loop
13. End

#### IV. CONSTRUCTION

While constructing a microcontroller based system, it basically involves design and validation, veroboard implementation, testing and result and packaging.

##### 4.1 DESIGN AND VALIDATION

PIC12F1840, 8 bit, microcontroller was used to implement this work. In order for the microcontroller to be able to perform its function in the system, it was required to write code of program onto it. The MikroC was selected over assembly language based on its advantages: reusable, Code portability, easy to write, and High programmer efficiency. The program was run successfully.

##### 4.2 VEROBOARD IMPLEMENTATION

After proper verification, the design was transferred to a veroboard for permanent construction. The components were arranged and soldered on the veroboard such that each component can easily be identified. Before proper soldering, component layout plan was drawn paying particular attention to minimizing the distances involved between point to be connected and the prevention of the overcrowding.

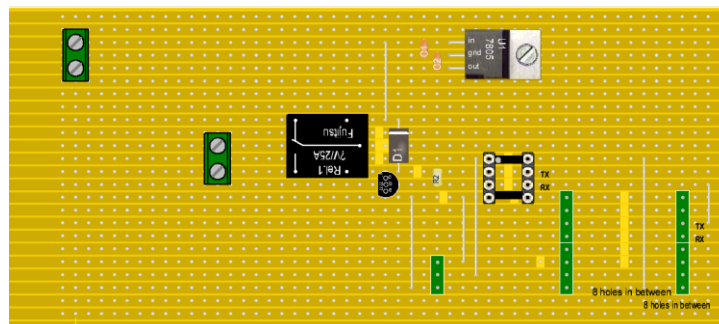


Figure 15: Vero board Layout of the System

##### 4.3 TESTING AND RESULT

It is of paramount importance to establish a highly efficient testing technique in other to minimize cost. The testing instrument used for examining logical signal, testing and troubleshooting application in the course of this project were: digital multimeter, logic probe and oscilloscope. Testing involves troubleshooting the hardware system to detect, isolate and correct internal or external fault such as malfunction in the internal circuitry, input or output shorted or  $V_{cc}$  input or output open circuited, short circuit between two pins broken wire, poor of dry connection, bent or broken pins, or an IC and faulty ICs socket.

The hardware system was properly tested because the software cannot work without the proper functioning of the hardware. The testing of the entire circuit was carried out in stages:

- i. Each of the components was first tested using the multimeter in order to check for their state of performance and accurate values.
- ii. In the connection, each component on the veroboard was then tested. This was done in other to carry out the continuity, which is meant for proper connection of the circuit and to detect any wrong connection.
- iii. The sensory unit circuitry was tested to ascertain the degree of sensitivity.

#### 4.4 PACKAGING

After proper testing was conducted, the packaging of the design into a model and casing was considered. The connecting wires were properly connected and well insulated; also the wires were well packed and bounded together.



Figure 16 : Constructed Human Body Motion Detective Home Security System with Automatic Lamp and User

Programmable Text Alert GSM Mobile Phone Number, Unique PIN to Allow Universal Users Using PIR Sensor

### V. APPLICATIONS

#### 5.1 Security Use

This project has its main application in security system. This project can be used in home as GSM based domestic security system. It can be used in our house for theft detection at night time. It can also be used for farm monitoring and automatic animal prevention.

#### 5.2 Industrial Use

Various parameters monitored in this project like theft detection and are also applicable for industrial purpose as well. So this system can also be used in industries as a GSM based industrial security system.

#### 5.3 Commercial Use

We can use this project in banks as well as other business organizations, since it has a sensor detector to detect any misconduct of persons. And, most importantly it's alert mobile phone number was flexible to change with a PIN.

#### 5.4 Remote indication

With the use of GSM technology owner of the house or industry get remote indication through SMS. So even if the user is away from home or industry, he/she will be informed of the presence of anyone within the house.

#### 5.5 Automation Use

The system is fully automated. So once this system is installed inside home or industry, then it does not require any human interaction to operate.

### VI. FUTURE IMPROVEMENTS

The future implications of the project are very great considering the amount of time and resources it saves. This system can be used as a reference or as a base for realizing a scheme to be implemented in other projects of greater level including audio-visual camera by sending the captured image to an e-mail instantly. The project itself can be modified to achieve a complete Home Automation System which will then create a platform for the user to interface between himself and his household.

### VII. CONCLUSION

The practical application of this developed system is immense with vast level of implementation. The model can be used in places such as banks, office and many other related places where continuous monitoring and regulation is needed.

It is definitely challenging to have implemented this work with tremendous applications and possibilities; the realization of a full automation, a real time system may be engaged and a biometric scanner that will provide an apt monitoring and security purposes. This makes it feasible for users to have a respite that their belongings are protected. A more effective and sensitive sensor is recommended for better performance.

## REFERENCES

- [1] Gill. K, S.H. Yang, F. Yao and X. Lu, "A Zigbee Based Home Automation system", *IEEE Transactions on Consumer Electronics*, Vol.55, No.2, (2009), pp. 422-430.
- [2] M. H. Jin, C. J. Fu, C. H. Yu, H.R. Lai and M. Whei, "IBM3 Zigbee Positioning Method for Smart Home Applications", *International Journal of Smart Home*, Vol.2, No. 2, (2008), pp.127-133.
- [3] Tajika. Y, T. Saito K. Termoto, N. Oosaka and M. Isshiki, "Networked Home appliance system using bluetooth technology integrating appliance control/monitoring with internet service", *IEEE Trans. Consumer Electron.*, vol. 49, no. 4, (2003), pp. 1043-1048.
- [4] Yuksekkaya. B, A.A. Kayalar, M.B. Tonsun, M.K.Ozean and A.Z. Alkar, "A GSM, Internet and Speech Controlled Wireless Interactive Home Automation System", *IEEE Transactions on Consumer Electronics*, Vol.52, No.3, (2006), pp. 837-843.
- [5] "LED" *The American heritage science dictionary*. Houghton Mifflin company.2015 led and LED
- [6] Moreno I; Sun c.c (2008). "modeling the radiation pattern of LEDs". *Optics express* 16(3): PMID 18542260
- [7] <http://www.google.com.ng/url?q=http://www.cse.iitm.ac.in/~vplab/courses/DVP/PDF/>
- [8] Mior Mohammad Hafizh Bin Abd. Rani "Active Infrared Motion Detector for House Security System." *Universiti Malaysia Pahang*

## Adaptation of compromise programming approach for multi-criteria material selection

A. D. Adeyeye<sup>1</sup>, G. O. Odu<sup>2</sup>, and O. E. Charles-Owaba<sup>3</sup>

<sup>1</sup>Department of Industrial and Production Engineering, University of Ibadan, Nigeria

<sup>2</sup>Faculty of Engineering, Delta State University, Abraka, Oleh Campus, Nigeria

<sup>3</sup>Department of Industrial and Production Engineering, University of Ibadan, Nigeria

**ABSTRACT:** Selection of proper materials for new products and continuous improvement of existing ones to meet the ever changing service requirements in order to gain and or maintain competitive edge is a challenging task. The material selected for a component determines its performance in terms of functionality, manufacturability, maintainability, environmental impacts and life cycle costs. Material selection requires multi-criteria decision analysis approach that is able to take the relative importance of each criterion and the deviations of the achievement levels of each criterion from their respective ideal values into account simultaneously. In this paper, the Minkowski distance metric as used in compromise programming is adapted to solve material selection problem. Two examples are presented to illustrate the potential of the proposed approach. The results show that the proposed method is effective for material selection and sensitive to the level of intensity of the designer's concern over the deviations of achievement levels from their respective ideal values and provides useful insights on optimal trade-offs among the alternative materials.

**KEYWORDS:** Compromise programming, Distance metric, Material selection, Multi-criteria decision making, Trade-off, Utopia

### I. INTRODUCTION

Material selection is an important element in product design. It is the task of identifying the material(s) that after being manufactured have the properties, dimensions and shape needed for the product to serve its purpose in the most effective and efficient manner and also at minimum costs to the manufacturer, user and the environment/society [1-4]. The material selected for a component or product determines its performance in terms of functionality, manufacturability, maintainability, environmental impact and life cycle costs [3,4-6]. Hence, it is crucial to select appropriate material for a particular design.

Material selection is not limited to the design of new products. Existing products are often redesigned in order to gain and/or maintain a competitive edge in the market and most of such redesigns necessitate the use of new materials. Service requirements of products are not static. They are ever changing; for instance, turbine discs for aero-engines developed in the 1950's were made of forged steel components when turbine gas temperatures were relatively low, typically 450°C. The steel disc met all requirements at this temperature, but strength and oxidation resistance fell rapidly at higher temperatures. Higher temperatures are needed in order to increase the thermodynamic cycle efficiency, induce fuel savings and reduce the emission of pollutants. To meet this requirement of higher temperature, Ni-Fe alloys replaced forged steel discs in the mid 1960's. With continuous improvement, the 1970's saw a further increase in the disc temperature to over 600°C where the stability of Ni-Fe alloys became inadequate. In order to extend disc capability above 600°C, Ni-based superalloys with increased precipitation hardening and higher thermal stability were introduced. Efficiency of aero-engine turbine is proportional to temperature; hence the research community in turbine machinery and power plants are seeking means to further drive temperature higher [7-9]. The operating temperatures of the rim sections of present day high-pressure turbine discs now approach 760°C and even as high as 815°C for some specialized military applications [10,11]. Hence, material selection is very crucial for new product design and the continuous improvement drive for existing products in order to gain technical and commercial benefits in the present day market [5].

Material selection presents a big challenge in product design and development for many reasons: (1) Material selection focuses on the entire product/component life cycle including manufacturing, operation and maintenance and product retirement. Manufacturing costs, total cost of ownership over the life of the product, including retirement and environmental impact are becoming increasingly important to manufacturers/business owners, customers/product users and regulatory agencies. The selection of materials that best meet the technical, economic and environmental criteria over the life of the product is not a trivial problem [3,12-17]. (2) Over 40,000 metal alloys and almost the same number of non-metals, ceramics, polymers and composites are at the designers' disposal. A plethora of new materials with varying degrees of properties improvements has been discovered by the research community in the last decade. Today, materials are developing faster than any other time in history and as a consequence the design space is ever expanding. It is difficult for designers, although educated in the fundamentals of materials and engineering, to still be able to make optimum decisions on materials to satisfy design problems given the vast range of materials available and new materials being developed [5, 17,18]. (3) The requirements the product/component is expected to meet are numerous and conflicting. For instance, the material must meet the service requirements and for a mechanical design, these may depend on many properties such as creep, wear resistance, ultimate tensile strength, toughness, etc... Since the material has to be processed to achieve the dimensions and shape needed for the component to serve its purpose in the most cost effective manner, other criteria such as manufacturability (weldability, castability, machinability, etc...) and economic factors (unit cost, cost-to-mass ratio, recoverability, etc...) must be considered. These requirements are of different degrees of importance and often incompatible because it is not possible to improved one requirement without reducing the satisfaction of one or more of the other requirements. (4) Apart from the conflict among the numerous requirements, there is also conflict among stakeholders. An instance is a case where the designer's interest is in composite light weight material with extreme strength-to-mass ratio while the interest of the recycler is in pure and easy-to-recycle material [19-23].

The challenge confronting the designer is how to choose from the vast number of materials, the one that best fulfill the numerous conflicting requirements. This requires systematic approach/mathematical tool to guide the designer in the material selection decision. Material selection is ultimately a multi-criteria decision making process involving assessment of trade-offs among various conflicting and divergent performance criteria [16,24]. Since it is not possible to achieve the ideal values of all the criteria simultaneously, the designer needs an approach that will give the best compromise solution [25,26].

An appreciable number of research works has appeared on material selection using different multi-criteria decision making (MCDM) methods. Athawale and Chakraborty [27] presented a review and comparative study of various MCDM methods such as VIKOR, ELECTRE, TOPSIS, PROMETHEE, simple additive weighting (SAW), Weighted product method (WPM), grey relational analysis (GRA), range of value method and graph theory and matrix approach. Various extensions of these methods either applied singly or in combination with other methods have also appeared in the literature [16,17,28]. Complex proportional assessment of alternatives (COPRAS) and its extensions, genetic algorithm with neural networks, desirability function, and multi-objective optimization on the basis of ratio analysis (MOORA) have also been used for material selection [6, 29-32].

These approaches mostly consider three characteristics of the material selection problem: (a) performance criteria (b) relative importance of each criterion and (c) alternatives. The alternatives are ranked and the one that gives the best compromise among the criteria is then selected for the given application. However, there is an aspect of performance criteria which has not been fully addressed in the literature. Criteria are assigned weights to reflect their relative importance, but the preferences of the designer concerning the deviations are often not taken into consideration. For instance, in some material selection situations it may be only the largest deviation that counts. In other words, the intensity of his concern over large deviations is high. In some other situations the designer may weigh all the deviations equally which implies the intensity of his concern over large deviations is low. He may also weigh the deviations in proportion to their magnitudes depending on his needs. Therefore, a fourth characteristic of material selection problem which is the intensity of designer's concern over deviations should be included in the material selection model. Although a plethora of multi-criteria methods has been proposed for material selection, there is still a need for simple as well as a systematic approach that incorporates the intensity of designer's concern over the large deviations and also provides opportunities for trade-off explorations based on these concerns. In this paper, an approach developed from the  $L_p$  - norm as used in the compromise programming (CP) method is proposed for the selection of most suitable material for a given engineering application.

## II. MATERIAL SELECTION PROBLEM

Material selection problem has the following characteristics; (i) there exist a finite set of performance criteria, usually conflicting, with non-commensurable units and different order of magnitudes (ii) the criteria are of varying degree of importance and weights are assigned to each to reflect their relative importance (iii) there exist a finite set of alternative materials from which the most appropriate/best is to be selected (iv) the intensity of the designer's concern over the large deviations. The problem is that of selecting the best material from the set of alternative materials while taking the existing situations into account such that there is a maximum realization of designer's objectives. The problem will be trivial if there exists a material that achieves the ideal performance levels of all criteria simultaneously. Unfortunately, it is often not feasible to get such material, so a compromise is needed to resolve the problem. A procedure for identifying the material that gives the best compromise is proposed in the following section.

## III. THE PROPOSED APPROACH

Compromise programming (CP) was first proposed by Zeleny [33,34] and has become one of the widely used multi-criteria decision making (MCDM) methods [25,26,36-38]. The basic idea in CP is to identify the utopian solution, which in our case is the material that achieves the ideal values of all criteria simultaneously. Achievement of utopia is not practically feasible because of the inherent conflict in the criteria but may be used as a base point. The designer therefore seeks a compromise solution. His decision is based on Zeleny's axiom of choice where the solutions that are closer to the utopian are preferred to those that are farther [33,34]. To achieve this closeness, Minkowski distance metric ( $L_p - norm$ ) is introduced into the analysis. The  $L_p - norm$  is used to calculate the distances between the achievement levels belonging to the solution set and the utopian point to identify the one that is closest to the utopia. We shall adapt the Minkowski distance metric as used in CP to material selection problem. The procedural steps on its adaptation are presented below:

### Step 1: Identification of performance criteria.

Identify the set  $\mathbf{I}$  of all performance requirements/criteria on which the evaluation of the materials will be based. The set  $\mathbf{I}$  has the following properties: (i) there is a set  $\mathbf{B} \subset \mathbf{I}$  of beneficial criteria for which higher values indicates better performance (ii) there also exist a set  $\mathbf{C} \subset \mathbf{I}$  of non-beneficial criteria of which lower values imply better performance (iii) observe that  $\mathbf{B} \cap \mathbf{C} = \Phi$  since a criterion is either beneficial or non-beneficial and not both.

### Step 2: Assignment of weight to criteria.

Assign weight ( $w_b, w_c \in [0,1]$ ) to each criteria  $b \in \mathbf{B}$  and  $c \in \mathbf{C}$  to reflect their relative importance using the appropriate method. Analytical hierarchy process (AHP) and entropy methods are commonly used for criteria weighting [28]. The authors have proposed a method for criteria weighting but its description is beyond the scope of this paper. Observe that;

$$\sum_{i \in \mathbf{I}} w_i = \sum_{b \in \mathbf{B} \subset \mathbf{I}} w_b + \sum_{c \in \mathbf{C} \subset \mathbf{I}} w_c = 1 \quad (1)$$

### Step 3: Assignment of aspiration levels and veto thresholds.

Assign aspiration levels and veto thresholds to each of the identified criteria. For each beneficial criterion, determine the largest/best performance value  $\{x_b^{\max} | b \in \mathbf{B}\}$  that is practically attainable and the smallest/worst performance value  $\{x_b^{\min} | b \in \mathbf{B}\}$  that is admissible. Recall that for beneficial criteria, larger values imply better performance. Hence,  $\{x_b^{\max} | b \in \mathbf{B}\}$  and  $\{x_b^{\min} | b \in \mathbf{B}\}$  are the aspiration levels and veto thresholds respectively. Similarly, for non-beneficial criteria, determine the smallest/best performance level  $\{x_c^{\min} | c \in \mathbf{C}\}$  that is practically achievable and the largest/worst performance value  $\{x_c^{\max} | c \in \mathbf{C}\}$  that is acceptable.  $\{x_c^{\min} | c \in \mathbf{C}\}$  and  $\{x_c^{\max} | c \in \mathbf{C}\}$  are the respective aspiration levels and veto thresholds for non-beneficial criteria. In order to adapt the  $L_p - norm$  as used in compromise programming to material selection, we shall call  $\mathbf{U}_{\mathbf{B},asp.} = \{x_b^{\max} | b \in \mathbf{B}\}$  and  $\mathbf{U}_{\mathbf{C},asp.} = \{x_c^{\min} | c \in \mathbf{C}\}$  the ideal/anchor values of the beneficial and non-beneficial criteria respectively while  $\mathbf{U}_{\mathbf{B},veto} = \{x_b^{\min} | b \in \mathbf{B}\}$  and  $\mathbf{U}_{\mathbf{C},veto} = \{x_c^{\max} | c \in \mathbf{C}\}$  are denoted as the

anti-ideal/nadir values of the beneficial and non-beneficial criteria respectively. Material that satisfies all criteria at their ideal/aspiration levels is the utopian. Observe that the utopian  $\mathbf{U}$  point is given by;

$$\mathbf{U} = \{\mathbf{U}_{\mathbf{B},\text{asp.}}, \mathbf{U}_{\mathbf{C},\text{asp.}}\} = \{x_b^{\max}, x_c^{\min} | b \in \mathbf{B} \text{ and } c \in \mathbf{C}\} \quad (2)$$

The utopian is practically not feasible, so according to Zeleny's axiom of choice we seek for a material whose performance rating on all the criteria is closest to it.

**Step 4: Sorting through material database.**

Sort through the material database to identify the set  $\mathbf{A}$  of alternative materials that meet these performance requirements. Any material whose achievement level on beneficial criteria falls below the veto threshold  $x_b^{\min}$  for any  $b \in \mathbf{B}$  is screened out while for non-beneficial criteria; a material is screened out if its achievement level is above the veto threshold  $x_c^{\max}$  for any  $c \in \mathbf{C}$ . Note that only the materials which fulfill the membership conditions as stated in Eq. (3) below are included in  $\mathbf{A}$ . The set  $\mathbf{A}$  may also be referred to as the solution set.

$$\text{Achievement level (AL)} = \{x_{ab} \geq x_b^{\min}, x_{ac} \leq x_c^{\max} | \forall (b \in \mathbf{B} \text{ and } c \in \mathbf{C})\}, a=1,2,\dots,m. \quad (3)$$

where  $x_{ab}$  is the achievement level of material "a" on beneficial criterion "b" and  $x_{ac}$  is the achievement level of material "a" on non-beneficial criterion "c". Next, the alternative materials are ranked in order to identify the best.

**Step 5: Developing the distance metrics.**

Develop the  $L_p$  - norm/Minkowski distance metrics. Let  $D_{ab}$  be the deviation/distance of the achievement of material "a" from the aspiration level,  $x_b^{\max}$  of beneficial criterion "b". Then  $D_{ab}$  is given by;

$$D_{ab} = x_b^{\max} - x_{ab} \quad (4)$$

Because of non-commensurable units and different order of magnitudes of the criteria, normalized distances are used rather than the absolute distances [25]. The normalized distance ( $D_{ab}^N$ ) is given by;

$$D_{ab}^N = \left( \frac{x_b^{\max} - x_{ab}}{x_b^{\max} - x_b^{\min}} \right); \text{ and } 0 \leq D_{ab}^N \leq 1 \quad (5)$$

Equation (5) above shows how far the performance rating of material "a" on criterion "b" is from the aspiration level. The degree of closeness,  $DC_{ab}^N$  to the aspiration level may be expressed as;

$$DC_{ab}^N = 1 - D_{ab}^N = 1 - \left( \frac{x_b^{\max} - x_{ab}}{x_b^{\max} - x_b^{\min}} \right) \quad (6)$$

Simplification of Eq. (5) gives,

$$DC_{ab}^N = \left( \frac{x_{ab} - x_b^{\min}}{x_b^{\max} - x_b^{\min}} \right) \text{ and } 0 \leq DC_{ab}^N \leq 1 \quad (7)$$

The degree of closeness  $DC_{ab}^N$  may also be express as percentage in which case the value of  $DC_{ab}^N$  lies between 0 and 100% (i.e.  $0 \leq DC_{ab}^N \leq 100\%$ ). If the level of achievement of criterion “b” is at the veto threshold, then  $DC_{ab}^N = 0$ , and  $DC_{ab}^N = 100$  if achievement is at the aspiration level. Note that while Eq. (5) expresses how far the achievement is from the aspiration level, Eq. (7) expresses how close it is to the aspiration level.

Similarly, the degree of closeness,  $DC_{ac}^N$  of the achievement of material “a” with respect to the non-beneficial criterion “c” is given by;

$$DC_{ac}^N = \left( \frac{x_c^{\max} - x_{ac}}{x_c^{\max} - x_{cb}^{\min}} \right) \quad (8)$$

The value of  $DC_{ac}^N$  also lies between 0 and 100%. Because of the divergent nature of the criteria, it is not feasible to get a material which achieves the aspiration levels of all performance criteria simultaneously. Hence, we seek for a material within  $\mathbf{A}$  whose overall achievement with respect to all criteria is closest to  $\mathbf{U}$ . So aggregate the normalized degrees of closeness to obtain the composite degree of closeness to  $\mathbf{U}$ . The degree of closeness of overall achievement of material “a” to  $\mathbf{U}$  is given by;

$$L_{p,a} = \left[ \sum_{b \in B \subset I} w_b \left( \frac{x_{ab} - x_b^{\min}}{x_b^{\max} - x_b^{\min}} \right)^p + \sum_{c \in C \subset I} w_c \left( \frac{x_c^{\max} - x_{ac}}{x_c^{\max} - x_{cb}^{\min}} \right)^p \right]^{\frac{1}{p}} \quad (9)$$

where  $p \geq 1$  and  $\sum_{b \in B \subset I} w_b + \sum_{c \in C \subset I} w_c = 1$

The properties of  $L_{p,a}$  are:

*Property i:* The weights  $(w_b, w_c \in [0,1])$  express the relative importance of each beneficial and non-beneficial criterion respectively.

*Property ii:* According to Eq. (9), it is obvious that  $L_{p,a} \geq 0$ . Since  $L_{p,a}$  is normalized by the exponent  $\frac{1}{p}$  it can be guaranteed that  $L_{p,a} \leq 1$ , hence,  $0 \leq L_{p,a} \leq 1$  for all  $a \in \mathbf{A}$ . If the degree of closeness is expressed as percentage then,  $0 \leq L_{p,a} \leq 100\%$ .

*Property iii:* the parameter p explicitly expresses the intensity of the concern of the designer over the deviations from the aspiration levels. The distance from  $\mathbf{U}$  decreases as p increases. On the other hand, the degree of closeness increases with increasing value of p. All the possible distances are bounded by  $L_{1,a}$  (i.e.  $p = 1$ ; Manhattan distance) and  $L_{\infty,a}$  (i.e.  $p = \infty$ ; Tchebycheff distance). Note that, the value of parameter p is chosen to express the designer’s preferences regarding the larger deviations. Manhattan distance is used when the deviations of the achievement from their respective aspiration values are of equal concern to the designer. If only the largest deviation counts to the designer, then the Tchebycheff distance is used and the problem becomes a mini-max problem. If the designer weighs each deviation in proportion to its magnitude, then the Euclidean distance ( $p = 2$ ) is used to rank the materials. The greater the concern of the designer over the maximum deviation the larger the value of parameter p; when  $p = \infty$  the largest deviation completely dominates the distance measure [25, 38, 39].

**Step 6:** find material “a” from the solution set A, so as to maximize  $L_{p,a}$ . To achieve this, compute  $L_{p,a}$  for each  $a \in A$  and rank the materials in descending order of  $L_{p,a}$  values. The material whose overall achievement (AL) corresponds to  $\max_a \{L_{p,a} | a = 1, 2, \dots, m\}$  is the closest to the utopia U.

**IV. NUMERICAL EXAMPLE**

In this section, material selections for some given engineering applications are used to demonstrate the feasibility of the proposed approach to evaluate and find the best material. Two examples will be used: (i) Material selection for non-heat-treatable cylinder cover from the literature [41] and (ii) material selection for armature shaft.

**Example 1: Non-heat-treatable cylinder cover material**

In this example, the problem of selecting the best material for non-heat-treatable cylinder cover is considered using the procedure described in section 3. Firstly, all necessary performance criteria were identified based on service requirements of the non-heat-treatable cylinder cover as well as the manufacturability and cost requirements. A total of twelve criteria were listed out of which eight were beneficial while four are non-beneficial. The criteria with their respective weights, aspiration levels and veto thresholds are presented in Table 1. Eight alternative materials that fulfilled the conditions of Equation (3) were selected (see Table 2) and their respective properties/achievement on each criterion is presented in Table 3.

**Table 1: Material Selection Data for Non-heat-treatable Cylinder Cover**

Criteria	Criteria Type	Aspiration Level	Veto threshold	Criteria Weight (%)
Density, D (Mg/m <sup>3</sup> )	Non-beneficial	2.67	8.95	5.3
Compressive strength, CS (MPa)	Beneficial	690	50	8.9
Ultimate tensile strength, UTS (MPa)	Beneficial	1030	210	7.3
Spring back index, SBI	Non-beneficial	0.08	1.55	10.3
Bending force index, BFI	Non-beneficial	1355	20317	10.3
Static load index, SLI	Beneficial	2916	260	8.7
Hardness, H (Vickers)	Beneficial	380	45	6.7
Yield strength, YS (MPa)	Beneficial	800	50	9.4
Elastic modulus, EM (GPa)	Beneficial	205	73.59	7.4
Thermal diffusivity, TD (cm <sup>2</sup> /h)	Beneficial	741	174	8.2
Thermal conductivity, TC (W/m K)	Beneficial	398	17	11.2
Cost of base material, C (CANS/kg)	Non-beneficial	1.04	18.64	6.5

Source: Shanian and Savadogo, (2006)

**Table 2: List of Alternative Materials**

Alternative materials	Code
Copper-2-beryllium (cast) UNS C82400	A1
Copper-cobalt-beryllium (cast) UNS C82000	A2
Electrolytic tough-pitch, h.c. copper, soft (wrought) UNS C11000	A3
Electrolytic tough-pitch, h.c. copper, hard (wrought) UNS C11000	A4
Wrought aluminum alloy 5052 H34	A5
Wrought austenitic stainless steel AISI 304, HT grade D	A6
Commercial bronze, cuzn10, soft (wrought) UNS C22000	A7
Carbon steel (annealed) AISI 1020	A8

Source: Shanian and Savadogo, (2006)

**Table 3: Material properties (achievement level for each criterion)**

Alt. Mat.	D	CS	UTS	SBI	BFI	SLI	H	YS	EM	TD	TC	C
A1	8.25	560	940	0.78	15183	2916	380	560	138	465	105	18.64
A2	8.65	460	600	0.71	12472	2395	220	460	125	465	205	13.99
A3	8.94	50	210	0.08	1355	260	45	50	122	460	398	3.00
A4	8.95	340	380	0.48	9218	1770	115	340	135	460	390	3.46
A5	2.67	190	295	0.25	20317	1966	87	191	73.59	741	152	2.81
A6	8.06	690	1030	1.55	5909	2174	350	800	190	189	17	5.99
A7	8.63	95	270	0.17	2711	520	63	100	116	174	185	3.22
A8	7.08	267	355	0.48	1957	720	110	265	205	329	50	1.04

Source: Shanian and Savadogo, (2006)

Using Equation (9), the degree of closeness to the utopian were computed for different values of parameter,  $p$  (i.e.  $p = 1, p = 2, p = 10$  and  $p = 100$ ). The degree of closeness as percentages and the ranking are presented in Table 4a below. For material selection situation where the deviations are of equal concern to the designer (i.e.  $L_1 - norm$ ) the ranking of alternative materials obtained was  $A6 \succ A1 \succ A4 \succ A2 \succ A8 \succ A3 \succ A5 \succ A7$ .  $A6, A1$  and  $A4$  are the 1<sup>st</sup>, 2<sup>nd</sup> and 3<sup>rd</sup> choice materials respectively. When the deviations are weighed in proportion to their magnitude (i.e.  $L_2 - norm$ ), the ranking was  $A6 \succ A3 \succ A1 \succ A4 \succ A5 \succ A8 \succ A2 \succ A7$ . The same  $A6$  remains the best choice but  $A3$  that ranked 6<sup>th</sup> when  $L_1 - norm$  was used is now 2<sup>nd</sup> and  $A1$  that ranked 2<sup>nd</sup> is now ranked 3<sup>rd</sup>. The ranking obtained with  $L_{10} - norm$  is  $A3 \succ A6 \succ A8 \succ A5 \succ A1 \succ A7 \succ A4 \succ A2$ . The  $L_{10} - norm$  expressed the increased concern (high intensity) of the designer over larger deviations, and alternative material  $A3$  that ranked 6<sup>th</sup> became the best choice instead of  $A6$  which is now 2<sup>nd</sup> and  $A8$  3<sup>rd</sup>. The  $L_{100} - norm$  shows that the intensity of the designer's concern over the large deviations is higher compared to his concern when the  $L_{10} - norm$  was used. The ranking of the alternatives with the  $L_{100} - norm$  is  $A3 \succ A6 \succ A1 \succ A8 \succ A5 \succ A4 \succ A7 \succ A2$ . The alternative materials  $A3, A6$  and  $A1$  are ranked 1<sup>st</sup>, 2<sup>nd</sup> and 3<sup>rd</sup> respectively when compared to the ranking obtained with the  $L_{10} - norm$  where  $A8$  is ranked 3<sup>rd</sup>. The suitability of this approach to reflect the preferences of the designer concerning the larger deviations is made clearer by Table 4b. The differences in the rankings at different intensity levels of the designer's concern show the necessity of incorporating the concern of the designer into the material selection process. It is clear that the level of designer's preferences regarding larger deviations determines the ranking of candidate materials. Hence rankings obtained without the incorporation of the intensity of designer's concern regarding the large deviations may be misleading.

Table 4a: Degree of Closeness ( $L_{p,a}$ ) and Ranking of alternatives

Alt. Mat.	$L_1 (p = 1)$		$L_2 (p = 2)$		$L_{10} (p = 10)$		$L_{100} (p = 100)$	
	Closeness (%)	Rank	Closeness (%)	Rank	Closeness (%)	Rank	Closeness (%)	Rank
A1	54.58	2	62.74	3	84.62	5	98.15	3
A2	49.55	4	52.13	7	64.15	8	78.44	8
A3	44.45	6	63.26	2	89.72	1	98.86	1
A4	53.22	3	59.08	4	80.24	7	95.78	6
A5	43.32	7	57.23	5	84.64	4	98.02	5
A6	57.99	1	71.34	1	89.13	2	98.65	2
A7	35.52	8	51.12	8	80.97	6	92.03	7
A8	45.97	5	57.20	6	85.87	3	98.07	4

Table 4b: Sensitivity of  $L_{p,a}$ 's to the intensity of designer's concern over deviations

Rank	Example 1: Non-heat-treatable Cylinder Cover			
	$L_1$	$L_2$	$L_{10}$	$L_{100}$
1 <sup>st</sup>	A6	A6	A3	A3
2 <sup>nd</sup>	A1	A3	A6	A6
3 <sup>rd</sup>	A4	A1	A8	A1

**Example 2: Armature shaft material**

Following the procedure of Section 3, ten criteria were identified out of which seven were beneficial and three were non-beneficial. The list of criteria with their respective aspiration level, veto threshold and weights is presented in Table 5. The list of materials that fulfilled the selection criteria of Eq. (3) are presented in Table 6 while Table 7 shows the properties or achievement levels of the alternative materials on each criterion. Next, Eq. (9) was used to compute the  $L_{p,a}$  values for ( $p = 1, 2, 10$  and  $100$ ) and the alternatives were ranked in descending order of  $L_{p,a}$  (see Table 8a).

**Table 5: Material Selection Data for Armature Shaft**

Criteria	Criteria Type	Aspiration Level	Veto threshold	Criteria Weight (%)
Ultimate tensile strength, UTS (MPa)	Beneficial	790	330	14.4
Yield strength, YS (MPa)	Beneficial	605	140	14.4
Elastic modulus, EM (GPa)	Beneficial	202	105	11.0
Ductility, DU (%)	Beneficial	55	10	8.4
Hardness, H (Vickers)	Beneficial	93	55	11.6
Density, D (Kg/m <sup>3</sup> )	Non-beneficial	7.80	8.44	6.2
Thermal conductivity, TC (W/m K)	Beneficial	120	16.2	9.2
Thermal diffusivity, TD (cm <sup>2</sup> /h)	Beneficial	415.4	127.3	6.8
Thermal expansion, TE ( $\mu\text{m} / \text{mK}$ )	Non-beneficial	11.5	15.7	8.8
Cost of base material, C (\$/Kg)	Non-beneficial	3.94	7.98	9.3

**Table 6: List of Alternative Materials (Armature shaft)**

Alternative materials	Code
Carbon Steel SAE 1006	B1
Carbon Steel SAE 1010	B2
Carbon Steel SAE 1020	B3
Carbon Steel SAE 1030	B4
Carbon Steel SAE 1070	B5
Carbon Steel SAE 1090	B6
Carbon Steel SAE 1117	B7
Carbon Steel SAE 1547	B8
Stainless Steel AISI 201	B9
Forging Brass, UNS C 37700	B10

**Table 7: Material properties (Armature shaft)**

Alt. Mat.	UTS	YS	EM	DU	H	D	TC	TD	TE	C
B1	330	285	200	20	55	7.872	64.9	171.4	12.6	5.90
B2	365	305	200	20	60	7.872	51.9	147.2	12.6	7.08
B3	420	205	200	15	73	7.872	51.9	135.7	11.9	5.59
B4	525	440	200	12	80	7.872	48.7	127.3	11.7	3.94
B5	640	495	201	10	91	7.872	51.2	132.7	12.1	4.57
B6	696	540	202	10	92	7.872	49.8	133.7	11.5	7.08
B7	475	400	200	12	86	7.872	51.2	135.2	11.5	7.67
B8	710	605	200	10	93	7.872	51.2	137.5	11.5	7.98
B9	790	380	197	55	90	7.80	16.2	415.4	15.7	4.60
B10	360	140	105	30	74	8.44	120	374.2	12.5	5.06

Source: MatWeb (Material Property Data) <http://matweb.com>

The ranking obtained for  $L_1 - norm$ ,  $L_2 - norm$ ,  $L_{10} - norm$  and  $L_{100} - norm$  as displayed in Tables 8a and 8b, reflect the sensitivity of this approach to the intensity of the concern of the designer over the deviations. For clarity, see the extract from Table 8a displayed in Table 8b showing the 1<sup>st</sup>, 2<sup>nd</sup> and 3<sup>rd</sup> best alternative materials for all the  $L_{p,a}$ 's. The best material for the armature shaft with  $L_1 - norm$ ,  $L_2 - norm$  and  $L_{10} - norm$  is **B9** while 2<sup>nd</sup> and or 3<sup>rd</sup> vary (Table 8b). With greater concern over the large deviations (i.e.  $L_{100} - norm$ ), **B8**, became the best material followed by **B9** and **B6** as 2<sup>nd</sup> and 3<sup>rd</sup> respectively, while **B1**, **B2** and **B3** are the worst with the same degree of closeness (95.80%) to the utopia Table 8a. Note that for the  $L_{100} - norm$ , **B8** was ranked 1<sup>st</sup> while **B9** is ranked 2<sup>nd</sup>. However, it may be expedient for the designer to choose alternative **B9** instead of **B8** since the difference between the closeness of **B8** and **B9** to the utopia is marginal (98.99% and 98.98%) and **B9** is ranked higher than **B8** for all the other distance metrics (see table 8a). This demonstrates another merit of this approach in that it provides opportunity for trade-off exploration with different values of parameter p in order to gain useful insights on optimal trade-offs among alternatives before making the final choice of material. The degree of closeness (Tables 4a and 8a) agrees with previous research that the distance from utopia decreases as the value of parameter p increases or conversely, the degree of closeness increases as value of p increases.

**Table 8a: Degree of Closeness ( $L_{p,a}$ ) and Ranking of alternatives for armature shaft**

Alt. Mat.	$L_1$ (p = 1)		$L_2$ (p = 2)		$L_{10}$ (p = 10)		$L_{100}$ (p = 100)	
	Closeness (%)	Rank	Closeness (%)	Rank	Closeness (%)	Rank	Closeness (%)	Rank
B1	39.27	8	51.70	8	80.37	8	95.80	8
B2	38.07	9	49.34	9	80.36	9	95.80	8
B3	44.36	7	55.26	7	82.21	3	95.80	8
B4	60.24	5	68.73	5	87.35	4	97.79	4
B5	66.70	2	74.26	4	86.48	5	96.82	7
B6	65.64	4	75.43	3	90.09	3	98.43	3
B7	51.51	6	62.47	6	85.62	6	97.74	5
B8	66.31	3	78.19	2	92.87	2	98.99	1
B9	72.13	1	81.17	1	93.11	1	98.98	2
B10	33.10	10	48.77	10	79.56	10	97.64	6

**Table 8b: Sensitivity of  $L_{p,a}$ 's to the intensity of designer's concern over deviations**

Rank	Example 2: Armature Shaft			
	$L_1$	$L_2$	$L_{10}$	$L_{100}$
1 <sup>st</sup>	B9	B9	B9	B8
2 <sup>nd</sup>	B5	B8	B8	B9
3 <sup>rd</sup>	B8	B6	B3	B6

## V. CONCLUSION

The proposed method for material selection has been shown to be a suitable tool for incorporating the intensity of designer's concern over larger deviations in the material selection process. The model ranked candidate materials from best to worst for each level of intensity of designer's concern over the deviations. Results of example problems demonstrate the sensitivity of the approach to the level of intensity of designer's concern and also provides useful insights on optimal trade-offs among the alternative materials.

## REFERENCES

- [1]. Gutteridge, P. A. and Waterman, N. A. Computer aided material selection. In Bever, M. D. (Eds): Encyclopedia of Materials Science and Engineering, Oxford 1986
- [2]. Sapuan, S. M., Mujtaba, I. M. and Wright, C. S. State of the art review of engineering selection methods. Multidiscipline Modeling in Materials and Structures, Vol.5, 2009, 263-268
- [3]. Ryan Michael J. Design for system retirement. Journal of Cleaner Production, Vol. 70, 2014, 203-210
- [4]. Shah Darshil U. Natural fibre composites: Comprehensive Ashby-type materials selection charts. Materials & Design, Vol. 62, 2014, 21-31
- [5]. Jahan Ali and K.L. Edwards. VIKOR method for material selection problems with interval numbers and target-based criteria. Materials & Design, Vol. 47, 2013, 759-765
- [6]. Sakundarini Novita, Zahari Taha, Salwa Hanim Abdul-Rashid, Raja Ariffin Raja Ghazila. Optimal multi-material selection for lightweight design of automotive body assembly incorporating recyclability. Materials & Design, Vol. 50, 2013, 846-857
- [7]. Tancret, F. and H.K.D.H. Bhadeshia. An affordable creep-resistant nickel-base alloy for power plant. Proc 6th Int Charles Parsons Turbine Conference, Engineering Issues in Turbine Machinery, Power Plant and Renewables, 2003
- [8]. Winstone, M.R. and J.L. Brooks. Advanced high temperature materials: aeroengine fatigue. Ciência e Tecnologia dos Materiais Vol. 20, No. 1 & 2, 2008, 15-24
- [9]. Caron, P. High  $\gamma'$  solvus new generation nickel-based superalloys for single crystal turbine blade applications. In T. M. Pollock, R. D. Kissinger, R. R. Bowman, K. A. Green, M. McLean, S. Olson, and J. J. Schirra (Eds): Superalloys (The Minerals, Metals & Materials Society), 2000; 737-746
- [10]. Total material. High Temperature Nickel-Based Superalloys for Turbine Discs: Part One 2011a <http://www.keytometals.com/page.aspx?ID=CheckArticle&site=ktn&NM=259> (accessed on July, 2014).
- [11]. Total material. High Temperature Nickel-Based Superalloys for Turbine Discs: Part Two 2011b <http://www.keytometals.com/page.aspx?ID=CheckArticle&site=KTN&NM=261> (accessed on July, 2014)
- [12]. Rao R.V and Patel B.K. A subjective and objective integrated multiple attribute decision making method for material selection. Materials and Design, 2010: Vol. 31, No. 10, 2010, 38-47.

- [13]. Zhao Rui, Gareth Neighbour, Pauline Deutz and Michael McGuire. Materials selection for cleaner production: An environmental evaluation approach. *Materials and Design*, Vol. 37, 2012, 429–434
- [14]. Peças P., I. Ribeiro, A. Silva and E. Henriques. Comprehensive approach for informed life cycle-based materials selection. *Materials and Design*, 2013; Vol. 43, 2013, 220–232
- [15]. Peças Paulo, Inês Ribeiro, and Elsa Henriques. Life Cycle Engineering for Materials and Technology Selection: Two Models, One Approach. *Proc CIRP 15*, 2014, 543–548
- [16]. Anojkumar L., M. Ilangkumaran and V. Sasirekha. Comparative analysis of MCDM methods for pipe material selection in sugar industry. *Expert Systems with Applications*, Vol. 41, 2014, 2964–2980
- [17]. Liu Hu-Chen, Jian-Xin You, Lu Zhen and Xiao-Jun Fan. A novel hybrid multiple criteria decision making model for material selection with target-based criteria. *Materials & Design*, Vol. 60, 2014, 380–390
- [18]. Rashedi, A., Sridhar, I. and Tseng, K.J. Multi-objective material selection for wind turbine blade and tower: Ashby's approach. *Materials & Design* Vol. 37, 2012, 521–532
- [19]. Beiter, K. A., James M. Cardinal and Kosuke Ishii. Preliminary Plastic Part Design: Focus on Material Selection and Basic Geometry While Balancing Mechanical Performance and Manufacturing Cost. *Journal of Reinforced Plastics and Composites* Vol. 16, No. 14, 1997, 1293-1302
- [20]. Vallbo, S. Material Selection Considerations for Polymer Composite Structures in Naval Ship Applications. *Journal of Sandwich Structures and Materials*, 2005; Vol. 7, 2005, 413-29
- [21]. Carruthers, J. J., Calomfirescu, M., Ghys, P. and Prockat, J. The application of a systematic approach to material selection for the light weighting of metro vehicles *Proc. IMechE Part F: Journal of Rail and Rapid Transit*, Vol. 223, 2009, 427-37
- [22]. Ziout A., Azab, A., and Atwan, M. A holistic approach for decision on selection of end-of-life products recovery options. *Journal of Cleaner Production*, Vol. 65, 2014, 497-516
- [23]. Cho, Jeonggil; Jeongseo Koo and Hyunseung Jung. A material selection method for a hybrid box-type bodyshell with cut-outs using an equivalent bodyshell model without cut-outs. *J Composite Mater*, Vol. 48, No. 14, 2014, 1767–1785
- [24]. Johnson Michael D. and Randolph E. Kirchain. Quantifying the effects of product family decisions on material selection: A process-based costing approach. *International Journal of Production Economics*, Vol. 120, 2009, 653–668
- [25]. Adeyeye A. D. and Oyawale F. A. Multi-objective methods for welding flux performance optimization. *RMZ-Materials and Geoenvironment*, Vol. 57, No. 2, 2010, 251-270.
- [26]. Odu, G. O. and O. E. Charles-Owaba. Review of Multi-criteria Optimization Methods – Theory and Applications. *IOSR Journal of Engineering*, Vol. 3, No. 10, 2013, 1-14
- [27]. Athawale, V. M. and Chakraborty, S. Material selection using multi-criteria decision-making methods: a comparative study. *Proc IMechE Part L: Journal of Materials Design and Application*, Vol. 226, No. 4, 2012, 266-285
- [28]. Caliskan Halil, Bilal Kursuncu, Cahit Kurbanoglu, Sevki Yılmaz Guven. Material selection for the tool holder working under hard milling conditions using different multi criteria decision making methods. *Materials & Design*, Vol. 45, 2013, 473–479
- [29]. Karande P, Chakraborty S. Application of multi-objective optimization on the basis of ratio analysis (MOORA) method for materials selection. *Materials & Design*, Vol. 37, 2012, 317–324.
- [30]. Chatterjee Prasenjit and Shankar Chakraborty. Gear Material Selection using Complex Proportional Assessment and Additive Ratio Assessment-based Approaches: A Comparative Study. *International Journal of Materials Science and Engineering* Vol. 1, No. 2, 2013, 104-111
- [31]. Karande Prasad, Susanta Kumar Gauri, Shankar Chakraborty. Applications of utility concept and desirability function for materials selection. *Materials & Design* Vol. 45, 2013, 349–358
- [32]. Zhou C-C, Yin G-F, Hu X-B. Multi-objective optimization of material selection for sustainable products: artificial neural networks and genetic algorithm approach. *Materials & Design*, Vol. 30, 2009, 1209–1215
- [33]. Zeleny, M. Compromise programming. In J. L. Cochrane and M. Zeleny (eds.): *Multiple Criteria Decision Making* (University of South Carolina, Columbia) 1973, 373-391
- [34]. Zeleny, M. A Concept of Compromise Solutions and the Method of the Displaced Ideal. *Computers and Operations Research* Vol. 1, No. 3, 1974, 479-496
- [35]. Romero C., Francisco Amador and Antonio Barco. Multiple Objectives in Agricultural Planning: A Compromise Programming Application. *American Journal Agricultural Economics* Vol. 69, No. 1, 1987, 78-86.
- [36]. Ballester, Enrique. Compromise Programming: A Utility-Based Linear-Quadratic Composite Metric from the Trade-Off between Achievement and Balanced (Non-Corner) Solutions. *European Journal of Operations Research* Vol. 182, No. 3, 1369–1382.

- [37]. Allouche, Mohamed Anis Belaïd Aouni, Jean-Marc Martel, Taïcir Loukil, and Abdelwaheb Rebaï. Solving Multi-Criteria Scheduling Flow Shop Problem through Compromise Programming and Satisfaction Functions. *European Journal of Operations Research*, Vol. 192, No. 2, 2009, 460–467.
- [38]. Beula, T. M. N. and Prasad, G. E. Multiple Criteria Decision Making With Compromise Programming. *International Journal of Engineering Science and Technology*, Vol. 4, no. 9, 2012, 4083-4086
- [39]. Jiang Jiang, Yu-wang Chen, Ying-wu Chen, Ke-wei Yang. TOPSIS with fuzzy belief structure for group belief multiple criteria decision making. *Expert Systems with Applications* Vol. 38, 2011, 9400–9406
- [40]. MatWeb (Material Property Data) <http://www.matweb.com> (accessed on August, 2013)
- [41]. Shanian, A. and Savadogo, O. A Material Selection Model Based on the Concept of Multiple Attribute Decision Making. *Materials & Design*, Vol. 27, 2006, 329-337

## Blood Donation Management System

K M Akkas Ali<sup>1</sup>, Israt Jahan<sup>2</sup>, Md. Ariful Islam<sup>3</sup>, Md. Shafa-at Parvez<sup>4</sup>

<sup>1,3,4</sup>Institute of Information Technology, Jahangirnagar University, Dhaka, Bangladesh

<sup>2</sup>Department of Computer Science and Engineering, Jahangirnagar University, Dhaka, Bangladesh

**ABSTRACT:** This paper is focused on Blood Donation Management System which is a web application with supporting mobile application aimed to serve as a communication tool between patients (who need blood) and blood donor. To become members of the system, donors need to create their profiles by providing fundamental information like name, blood group, email address, password, and exact location from "Google Map". In order to find out the exact location of a donor, Google Map is integrated with this application. The mobile application always updates the location of a donor. As a result, the system can automatically find a registered donor wherever he/she goes. Visitors can search blood donors from the home page by blood group and the place where blood is needed. The system will show the available donors along with their phone number, email address and mailing address through arranging them by nearest place and blood donation expire date. Visitors can send message to all donors through email but a member can send message using email and mobile phone. An appointment will be created only whenever a donor confirms that he/she will donate blood. Then the system will alert the donor before 12 hours of donation. Blood donors can also be searched from the mobile application, but this is only accessible for registered members. The goal of this paper is to reduce the complexity of the system to find blood donors in an emergency situation.

**KEYWORDS-** Online blood donation, Password, Smart phone, Administrator, Web application.

### I. INTRODUCTION

It is estimated that Bangladesh needs around 600,000 bags of blood every year. There are lots of communication gap among patients (accepting blood), donors (who donate bold), blood banks and hospitals in our country. Medical facility is not available equally in every part of the country. If someone needs blood, first of all he searches it within his family members, then nearest hospitals and blood banks. If they cannot manage blood in these ways, it is really hard for them to contact other people to collect blood in a short time. That is the problem we want to solve through our application, Blood Donation Management System in which electronic information about the donors and organizations related to donating the blood is created. Through this application, any person interested in donating blood can register himself as donor. Moreover if any general consumer wants to make request to have blood online, he can also take the help of this system. As soon as any update occurs in the blood database, the changes are reflected in all the interfaces used. So, the system provides a simple and quick interaction among various groups connected with the blood banks. It is designed to overcome the drawbacks of existing system. The main objective is to improve the efficiency of data communication within the supply chain to reduce response time for each blood demand request. We also focused on managing blood inventory at each blood bank effectively. The results have shown that the proposed system helps enhancing the communication among blood partners within the supply chain network. The recipient can get blood on emergency. The system also provides SMS facility to donors through smart phone so that they can reach to exact location.

Some existing applications of blood donation system are manual which cannot upload and download the latest update and there is no use of web services and remoting. There is no proper coordination between different applications and users. It consumes lot of manpower for better results. Retrieval of data takes lot of time and percentage of accuracy is less. It takes time to produce reports. To debug the existing system, remove procedures those cause data redundancy, make navigational sequence proper [1]-[2]. Chance of mismanagement of data

makes the system less secure. But the system we present here provides a lot of information about donors on different level and also reflects the current work status. User friendliness of the developed system is provided in the application with various controls. The system makes the blood management much easier and flexible. It provides high level of security with different level of authentication.

The Blood Donation Management System we present here is aiming for human welfare. The entire system has been developed keeping in view of the distributed client server computing technology, in mind. This web application allows you to access the whole information about Blood Donation Management Software, readily scalable and adaptable to meet the complex need of blood banks who are key facilitator for the healthcare sector. Aim of this paper is to provide user friendly and interactive services via web interface, mobile application and SMS. As soon as any update occurs in the blood database, the changes are reflected in all the mentioned interfaces. As a result, the system provides a simple and quicker interaction among various groups connected with blood bank.

## II. LITERATURE REVIEW

The system we present here is adequate for searching blood donors for available blood and thereby saving valuable time and money. This application provides necessary options to serve people on their emergency need making them free from worrying for blood by providing lot of donors at a single click. The options that are provided by this application are:

- ❖ Donor registration and blood collection
- ❖ Blood requisition/issue
- ❖ Discard accounting
- ❖ User access control
- ❖ Detailed donor database
- ❖ Maintain and update unique donor identification
- ❖ Search facilities by donor, patient, doctor, blood bag, and other recognizing factors
- ❖ Correlation and cross referencing between files
- ❖ Powerful search for donors by blood group, sex, location, telephone number.
- ❖ Exhaustive report formats and registers
- ❖ Interface with grouping and testing machine
- ❖ Sends various auto-SMS for alerting donor and reminding location and time
- ❖ Adequate security to protect users' potential information

Besides these, there are ample scopes to improve this application. Some more features can be added to establish this application for a social networking application.

Blood Donation Management System is a web enabled and mobile-based application to maintain day to day transactions in a blood bank. This application is to create an e-Information about the donor and organization that are related to donating the blood. This software help to register all the donors, Blood collection details, blood issued details etc [3]-[4]. When registration is completed, a user becomes a donor who will be able to open an account providing fundamental information with email ID and Password [5]-[7]. They can modify their account information by updating username, Facebook ID, mobile number and profile picture. If donors are eager to donate blood they can confirm the system [8]. They can remove their account from the system if they wish for. In this application, Admin is the main authority who can add, delete, and modify information if required. A user is able to search donor from the home page. This application provides search facilities by donor, patient, doctor, blood bag, and other recognizable factors. A dynamic search will show donor information by nearest place and blood donation expire date. It will make easier to find and contact with donors when needed. There is add on facility of printing available as an option [9]-[11]. Interface with grouping and testing machine provides user friendly communication. This application sends various auto-SMS for alerting donor and reminding location and time. Donor can send or receive message within this system. This system will automatically alert a donor before 24 hours of donating blood reminding the location and time by sending message when he/she is again eligible for donating blood after his/her previous donating. Donor can used this application through android based mobile phone. Donors login into the system with their e-mail Id and password. It allows donor to search others by location, blood group. They can get other donors details information. If they want to contact with donor, they can directly call to available donors.

We can say in short that Blood Donation Management System is an online centralized web portal which helps blood banks, hospitals and any other users to look for donors in their nearby area who will be available in quick time. This system helps the admin to check the database when he wants and it is very flexible for the hospital management, blood banks and any users to retrieve the data when they want and they can have the data according to the query given by the user from one particular date to another by the query given by admin.

### III. METHODOLOGY

#### A. Concept:

A Genuine person from the Administrator side will collect information about the blood donor like contact and address details for registration [12]. After filtering the invalid data, the Blood donor will be uploaded in Online Blood Bank System site for general users. Before uploading their details, the Administrator will give unique username and password to each donor. The Administrator can also add new donor who registered through site and allows him to create his own account. The administrator searches various donors details based on normal or map based search. The administrator can view the account information and can also view the suggestion (feedbacks) given by different users of this site. The administrator can view total report of the site.

Every donor will have their own e-mail address and password with which they will login to this site. After they logged on, he can search for other donors, view his own profile, and send message to other donors in the system. He can change and retrieve his password. General users are those who are new users in this site. They can view general information about the Blood Donation System details. They can give their suggestion about this site. They can register themselves and become a donor for the Online Blood Bank system. If a general user is registered as donor, he will be given user name and password with which he can maintain his own account. General user can act as recipient to blood if he requests for blood, he can search required donor based on location using Google Map and blood group. We have used Visual Studio 2010 for doing the implementation of Blood Donation Management System. We have used Microsoft SQL Server 2008 as database server. We use mobile with SMS facility, mobile which support such application.

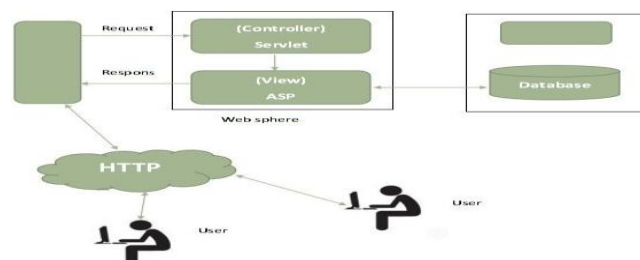


Figure1: Technical architecture of the proposed system

#### B. Method:

This paper is aimed to develop online blood donation information. The entire work has been developed keeping in view of the distributed client server computing technology, in mind. The system is to create an e-Information about the donor and organization that are related to donating the blood. Through this application any person who is interested in donating blood can register himself as a donor. Moreover if any general consumer wants to make request blood online, he can also take the help of this site. The work has been planned to be having the view of distributed architecture, with centralized storage of the database. The application for the storage of the data has been planned. Using the constructs of SQL Server, all the user interfaces have been designed using ASP.Net technologies. The database connectivity is planned using the “SQL Connection” methodology [13]. The standards of security and data protective mechanism have been given a big choice for proper usage. The application takes care of different modules and their associated reports, which are produced as per the applicable strategies and standards that are put forwarded by the administrative staff.

The system has been developed keeping in view of the distributed client server computing technology, in mind. The specification has been normalized up to 3NF to eliminate all the anomalies that may arise due to the database transaction that are executed by the general users and the organizational administration [14]. The user interfaces are browser specific to give distributed accessibility for the overall system. The internal database has been selected as SQL server 2008. The basic constructs of table spaces, clusters and indexes have been exploited to provide higher consistency and reliability for the data storage. The SQL server 2008 was a choice as it provides the constructs of high-level reliability and security [15]. The total front end was dominated using the ASP.Net technologies [12]. At all proper levels high care was taken to check that the system manages the data consistency with proper business rules or validations. The database connectivity was planned using the latest “SQL Connection” technology provided by Microsoft Corporation. The authentication and authorization was crosschecked at all the relevant stages. The user level accessibility has been restricted into two zones namely.

### IV. ANALYSIS

In this system, users can search donors and make request for blood. Donors can login to their own profiles and update information. They can search donor, request for blood and send message to other donors. Admin can maintain system management tasks. The use case diagram and class diagram of the system are shown in the Figure 2 and Figure 3 respectively.

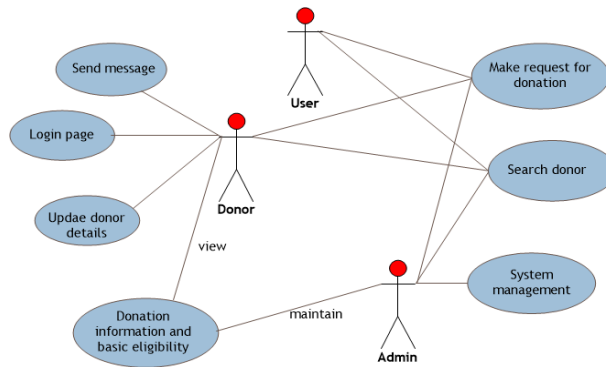


Figure 2: Use case diagram of the system

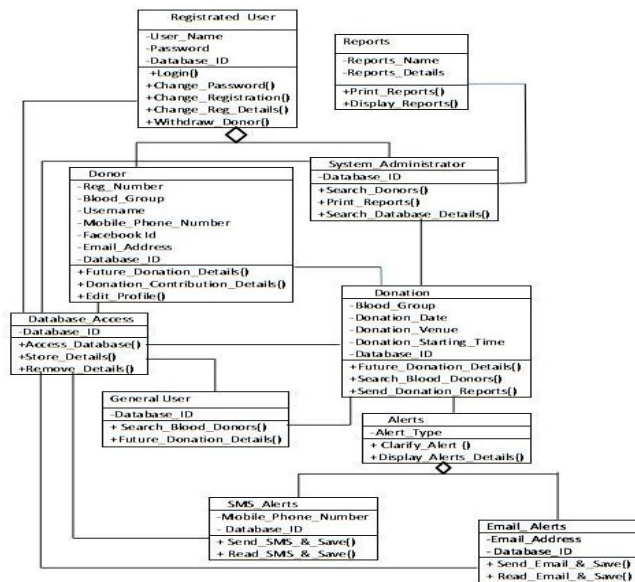


Figure 3: Class Diagram of the system

The database design of the system is presented in Table 1 to Table 7 below.

Attribute name	Data type	Constraints
Name	varchar(50)	Allow Null
Sex	varchar(50)	Allow Null
Phone_number	varchar(15)	Allow Null
Email_id	varchar(50)	Primary Key
Fb_id	varchar(50)	Allow Null
Blood_group	varchar(50)	Allow Null
Weight	varchar(15)	Allow Null
Height	varchar(15)	Allow Null
Location	varchar(15)	Allow Null
Latitude	varchar(15)	Allow Null
Longitude	varchar(15)	Allow Null
Religion	varchar(50)	Allow Null
Picture	image	Allow Null
Username	varchar(50)	Allow Null
Password	varchar(50)	Allow Null
Memorable Word	varchar(50)	Allow Null
Total_donation	varchar(15)	Allow Null
Last donation Date	varchar(15)	Allow Null

**Table 1: Member\_entry**

Table 1 contains donors' fundamental information which provides user expected result.

Attribute name	Data type	Constraints
Name	varchar(50)	Allow Null
Sex	varchar(50)	Allow Null
Phone_number	varchar(15)	Allow Null
Email_id	varchar(50)	Primary Key
Blood_group	varchar(50)	Allow Null
Weight	varchar(15)	Allow Null
Height	varchar(15)	Allow Null
Location	varchar(15)	Allow Null
Latitude	varchar(15)	Allow Null
Longitude	varchar(15)	Allow Null
Total_donation	varchar(15)	Allow Null
Last donation Date	varchar(15)	Allow Null

**Table 2: Donor\_search**

When we click donation form, donor's information will be removed from appointment table and stored in donation table. After 4 months, it is permanently remove from this table and return all information into Donor\_search table.

Attribute name	Data type	Constraints
Name	varchar(50)	Allow Null
Sex	varchar(50)	Allow Null
Phone_number	varchar(15)	Allow Null
Email_id	varchar(50)	Primary Key
Blood_group	varchar(50)	Allow Null
Weight	varchar(15)	Allow Null
Height	varchar(15)	Allow Null
Location	varchar(15)	Allow Null
Latitude	varchar(15)	Allow Null
Longitude	varchar(15)	Allow Null
Total_donation	varchar(50)	Allow Null
Last_donation_day	varchar(50)	Allow Null
Old_donation_day	varchar(15)	Allow Null
Last_donation_date	varchar(15)	Allow Null

**Table 3: Appointment**

When a user is appointed, his/her information will be removed from search table and store in this table (Table 3).

Attribute name	Data type	Constraints
Name	varchar(50)	Allow Null
Sex	varchar(50)	Allow Null
Phone_number	varchar(15)	Allow Null
Email_id	varchar(50)	Primary Key
Blood_group	varchar(50)	Allow Null
Weight	varchar(15)	Allow Null
Height	varchar(15)	Allow Null
Location	varchar(15)	Allow Null
Latitude	varchar(15)	Allow Null
Longitude	varchar(15)	Allow Null
Total_donation	varchar(50)	Allow Null
Last_donation_day	varchar(50)	Allow Null
Old_donation_day	varchar(15)	Allow Null
Last_donation_date	varchar(15)	Allow Null

**Table 4: Donated**

Table 4 contains donor's information that will be donated blood in future.

Attribute name	Data type	Constraints
Name	varchar(50)	Allow Null
Sex	varchar(50)	Allow Null
Phone_number	varchar(15)	Allow Null
Email_id	varchar(50)	Primary Key
Blood_group	varchar(50)	Allow Null
Weight	varchar(15)	Allow Null
Height	varchar(15)	Allow Null
Location	varchar(15)	Allow Null
Latitude	varchar(15)	Allow Null
Longitude	varchar(15)	Allow Null
Total_donation	varchar(50)	Allow Null
Last_donation_day	varchar(50)	Allow Null
Old_donation_day	varchar(15)	Allow Null
Last_donation_date	varchar(15)	Allow Null

**Table 5: Donation\_appoint**

Table 5 contains information of donors who were donated blood.

Attribute name	Datatype	Constraints
Name	varchar(50)	Allow Null
Phone number	varchar(50)	Allow Null
Blood_group	varchar(50)	Primary Key
Location	varchar(50)	Allow Null
Need_amount	varchar(50)	Allow Null
Need_date	varchar(50)	Allow Null
Donation date	varchar(50)	Allow Null

**Table 6: Acceptor**

Acceptor table (Table 6) contains information about blood donation.

Attribute name	Data type	Constraints
Name	varchar(50)	Allow Null
Sex	varchar(50)	Allow Null
Phone_number	varchar(15)	Allow Null
Email_id	varchar(50)	Primary Key
Blood_group	varchar(50)	Allow Null
Weight	varchar(15)	Allow Null
Height	varchar(15)	Allow Null
Location	varchar(15)	Allow Null
Latitude	varchar(15)	Allow Null
Longitude	varchar(15)	Allow Null
Total_donation	varchar(15)	Allow Null
Last donation Date	varchar(15)	Allow Null

**Table 7: Fixt\_donor**

Table 7 is used to show monthly report of the donor.

V. SCREENSHOTS

Figure 4 to Figure 21 illustrates some screenshots of the system.

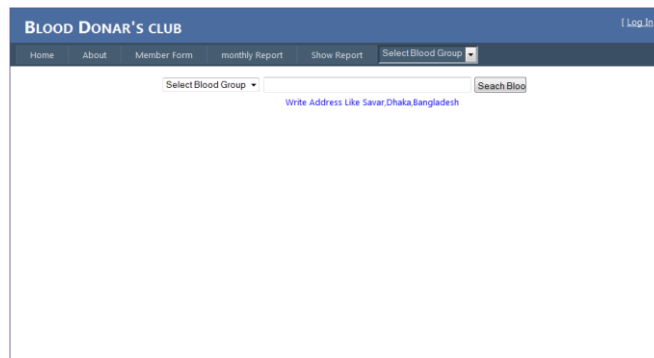


Figure 4: Homepage

In the homepage, the search box is placed for every visitor or member searching blood quickly. They can request donors to donate blood.



Figure 5: Search result page

The search page searches for donors who in turn can search other donors and send SMS including blood group, location of donation and date of donation to available donor.

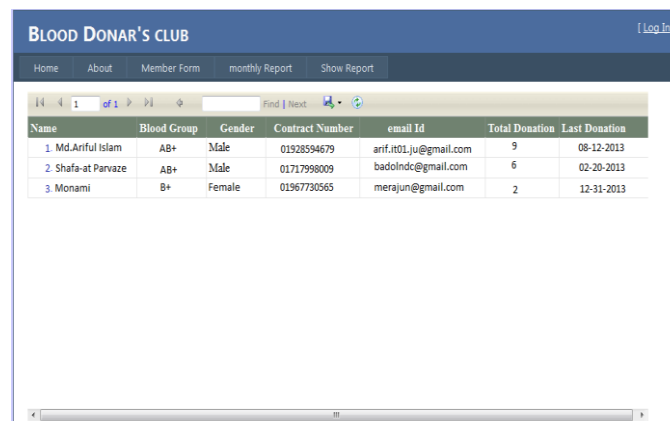


Figure 6: Report page

The report page of donation details can be shown in Microsoft Word, Microsoft Excel, and PDF format. User can download this report.

User can register by entering name, blood group, mobile number, username, date of birth, mail address, Facebook ID, total donation, last donate date, location, weight, height, memorable word using member entry form (shown in Figure 7 and Figure 8).

Figure 7: Member entry form 1

Figure 8: Member entry form 2

Donor can login to his own profile by entering valid email ID and password using User Login page (shown in Figure 9).

Using Profile page (shown in Figure 10), a donor can request other donors to donate blood. He can update his profile, change password, retrieve password and delete own membership. Donor can also cancel appointment for donation blood.

Figure 9: User login page

Figure 10: Profile page

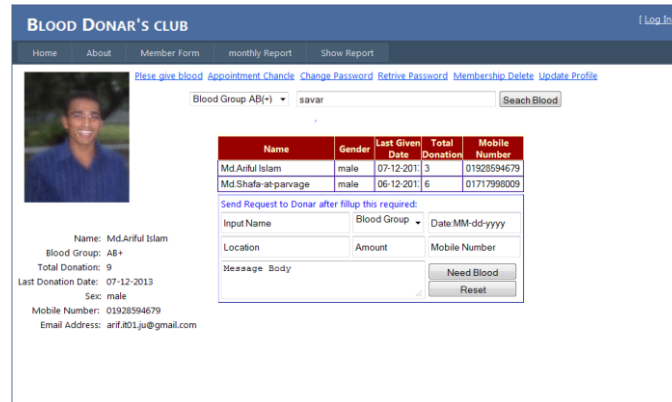


Figure 11: Donor search page

Donor can search donor (Figure 11) by blood group and location. They can send SMS including location, amount of blood, donation date to others donor for blood donation.



Figure 12: Donor confirmation page

Using donor confirmation page (Figure 12), a donor can easily send SMS to acceptor to confirm for blood donation.

Appointment cancel is the page (Figure 13), where donor can cancel any previous appointment. When donors insert name, mail address and donation date and press cancel button, the message sends to appointed donor to inform them that the appointment is canceled.

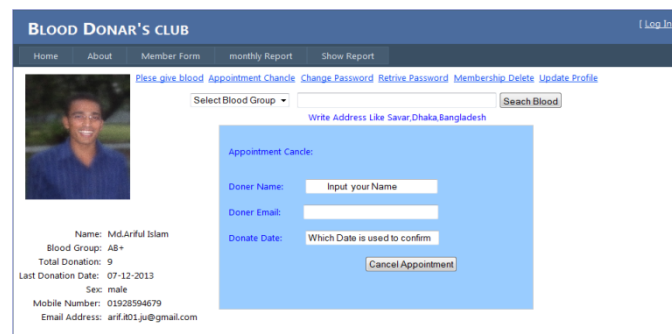


Figure 13: Donor appointment cancel page



**Figure 14: Donor change password page**

Donor can change password for better security using this page (Figure 14).



**Figure 15: Delete membership page**

Donors can cancel membership from this system using delete membership page (Figure 15) When they insert name, cause of delete membership and mobile number into name textbox, cause textbox and mobile number textbox respectively and press delete button, they are deleted from the system.

The statistical graph of donation details is shown in Figure 16. Y-axis of the graph is donor number and X-axis is blood group. By this graph, user can easily understand information of donor.



**Figure 16: Statistical Graph page**

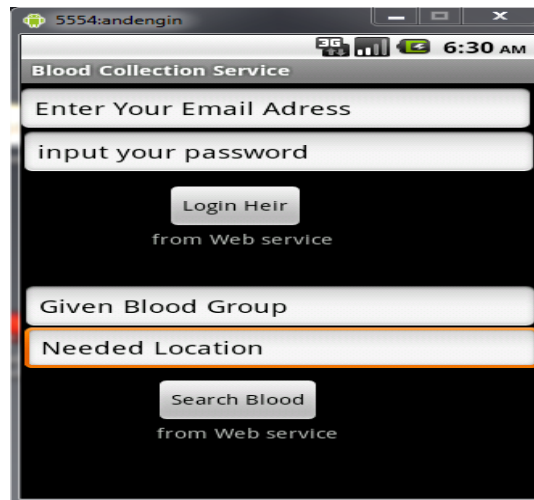


**Figure 17: Android home page**

This is the home page (Figure 17) for android application. Here, the member must login by valid mail address and password. Then, they can search donor by blood group and location where blood is needed. When donor visits from one location to another, location of donor is automatically updated. Donor is shown in current location list, while searching donor.

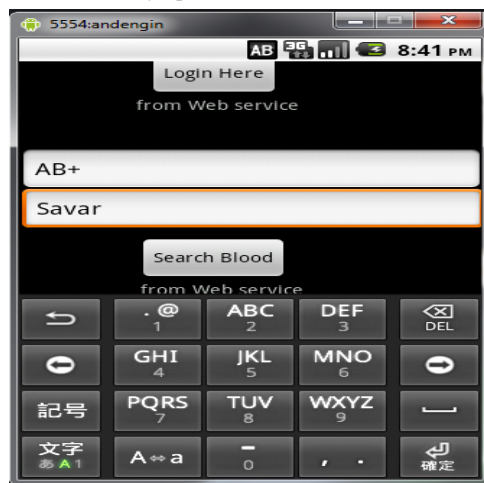


**Figure 18: Android search page**

Using the android search page (Figure 18), donor can searched other donors by blood group and location.

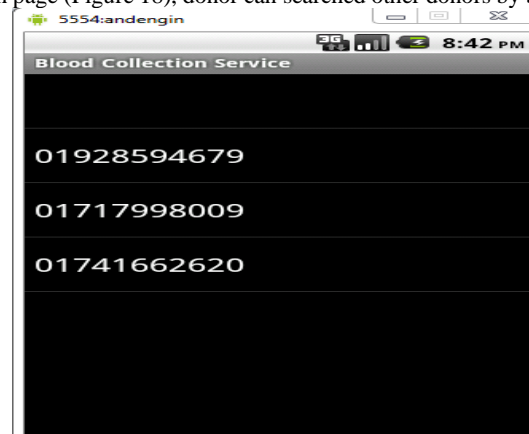


**Figure 19: Android search result page**

After searching, donor gets available donors in nearest location. The contact number of available donors is shown in android search result page (Figure 19).



Figure 20: Android contact page

When donors choose a contact number, they get details information of donor from contact page (Figure 20). They want to call donors; they press 'YES' button, otherwise press 'No'

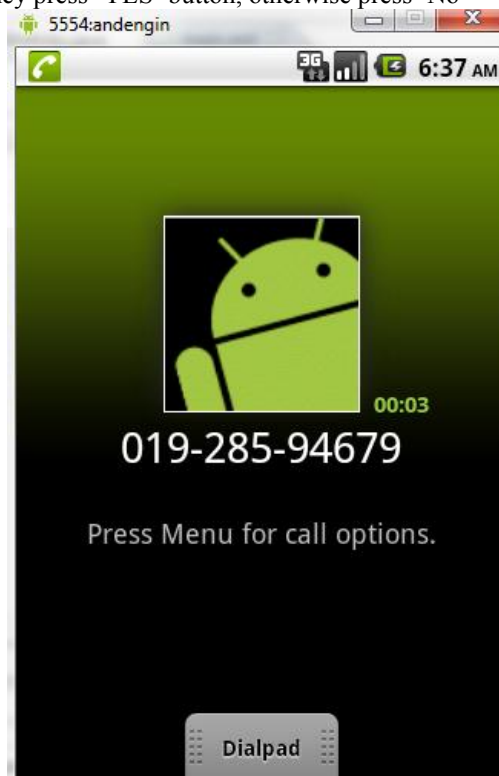


Figure 21: Android calling page

Here is the donor calling page (Figure 21). Donor can directly call others donor to appoint for blood donation.

## VI. CONCLUSIONS

The Blood Donation Management System is a 24×7 system which is essential for different kinds of people like blood donation system personnel, doctors, donors, recipients and other general users. Here any person who has undergone blood test can be registered in any authorized blood bank as donor. That person can get facilities like information about blood donation system, donors and recipients. This paper facilitates services like direct access to the site to get donor's information if there is an emergency. The goal of the paper is to present an online edge for bringing mutually giving blood donors and patients (blood requesters) who need blood. The primary objective of the paper is to create an interactive blood donors, blood requesters and blood bank clinics. This web application is to be conceived in its current form as a dynamic site requiring constant updates both from the blood donors as well as the blood requesters and is to enable blood donors (volunteer) to place their profile and blood requesters (patients) to publish their requests. In future, we will develop the mobile application which will provide the users (with multimedia cell phones) the service of finding a blood donor with map interface. Here the application will consist of a map which will highlight the various blood donors' locations and also it will give information about particular blood donors.

## REFERENCES

- [1] Michael Chau, Eddie Cheng and Chi Wai Chan. Data Analysis for Healthcare: A Case Study in Blood Donation Center Analysis. Proceedings of Sixteenth Americas Conference on Information Systems (AMICS), 2010.
- [2] Shyam Sundaram and T. Santhanam. Classification of Blood Donors using Data Mining. Proceedings of the Semantic E-Business and Enterprise Computing, pp. 145-147, 2009.
- [3] Bing Nan Li, Ming Chui Dong and Sam Chao. On decision making support in blood bank information systems. Expert Systems with Applications, Vol. 34, No. 2, pp. 1522-1532, 2009.
- [4] Ming Jiang, Ping Fu, Hexin Chen, Mianshu Chen, Bo Xing, et al. A Dynamic Blood Information Management System Based on RFID. Proceedings of the 2005 IEEE Engineering in Medicine and Biology 27th Annual Conference Shanghai, China, September 1-4, 2005.
- [5] Center for Biologics Evaluation and Research (CBER). Draft guidelines for the validation of blood establishment computer systems, <[www.fda.gov/cber/guidelines.htm](http://www.fda.gov/cber/guidelines.htm)>, 2005.
- [6] Glynn, S. A., Kleinman, S. H., Schreiber, G. B., Zuck, T., McCombs, S., Bethel, J., et al. Motivations to donate blood: demographic comparisons. Transfusion, 42(2), 216–225, 2002.
- [7] Li, B. N., & Dong, M. C. Banking on blood. Computing and Control Engineering (August–September), 22–25, 2006.
- [8] Roh, T. H., Ahn, C. K., & Han, I. The priority factor model for customer relationship management system success. Expert Systems with Applications, 28(4), 641–654, 2005.
- [9] Behrouz A. Forouzan, "Cryptography & Network Security", Special Indian Edition, Tata McGraw-Hill, ch. 1, ch. 14.
- [10] Self Study: Concepts of ASP.Net. Retrieved February 20, 2013, from <http://www.asp.net.com>
- [11] Insert data from textbox to sql database. Retrieved March 1, 2013, from <http://www.daniweb.com/software-development/csharp/threads/202614/>
- [12] Confirm to donate blood. Retrieved April 2, 2013, from <http://www.codeproject.com/Questions/531534/>
- [13] Self Study: Concepts of Android Application. Retrieved September 10, 2013 from <http://developer.android.com>
- [14] Android login. Retrieved September 12, 2013, from <https://developers.google.com/+/mobile/android/sign-in>
- [15] Dean Alan Hume. Tweaking ASP.NET Web Forms performance. Retrieved from <http://www.pdfol.com/ebook/fast-asp-net-websites>, 2012.

## Groundwater Resources Assessment For Joypurhat District Using Mathematical Modelling Technique

Md. Iquebal Hossain<sup>1</sup>, Md. Tarikul Islam<sup>2</sup>, Prof. Iqbal Matin<sup>3</sup>

<sup>1</sup>Executive Engineer, Barind Multipurpose Development Authority, Rajshahi, Bangladesh

<sup>2</sup>Senior Specialist, Irrigation Management Division, Institute of Water Modelling, Dhaka-1206, Bangladesh

<sup>3</sup>Professor, Department of Civil Engineering, Rajshahi University of Engineering & Technology, Rajshah, Bangladesh

**ABSTRACT:** In this study potential recharge as well as groundwater availability for 5 Upazillas (Akkelpur, Kalai, Joypurhat Sadar, Khetlal and Panchbibi) of Joypurhat districts has been estimated using MIKE SHE modelling tools. The main aquifers of the study area are dominated by medium sands, medium and coarse sands with little gravels. The top of aquifers ranges from 15 m to 24 m and the screenable thickness of aquifers range from 33 m to 46 m within the depth range from 57 m to 87 m. Heavy abstraction of groundwater for agricultural, industrial and domestic uses results in excessive lowering of water table making the shallow and hand tubewells inoperable in the dry season. The upazilawise potential recharge for the study area was estimated through mathematical model using MIKE SHE modelling tools in an integrated approach. The required data were collected from the different relevant organisations. The potential recharge of the present study varies from 452 mm to 793 mm. Maximum depth to groundwater table in most of the places occurs at the end of April. At this time, groundwater table in most of the part of Kalai, Khetlal, Akkelpur and Panchbibi goes below suction limit causing HTWs and STWs partially/fully in operable.

**KEYWORDS:** Groundwater, Specific yield, Recharge, DTW, STW

### I. INTRODUCTION

Groundwater is very important for agro-socio-economic development of Bangladesh. Supply of safe drinking water to 97% of the population and attaining self-sufficiency in rice production are the two major successes achieved with the utilization of groundwater. Easy availability, good quality and cheap development technologies make groundwater exploitation very popular all over the country and abstraction has increased manifold over the last 30 years. This increasing trend would remain unchanged for the years to come.

Despite of high dependence, accurate assessment of groundwater recharge potentials and its availability under various yield criteria has not been done for the most part of Bangladesh and consequently management of groundwater is not properly practiced.

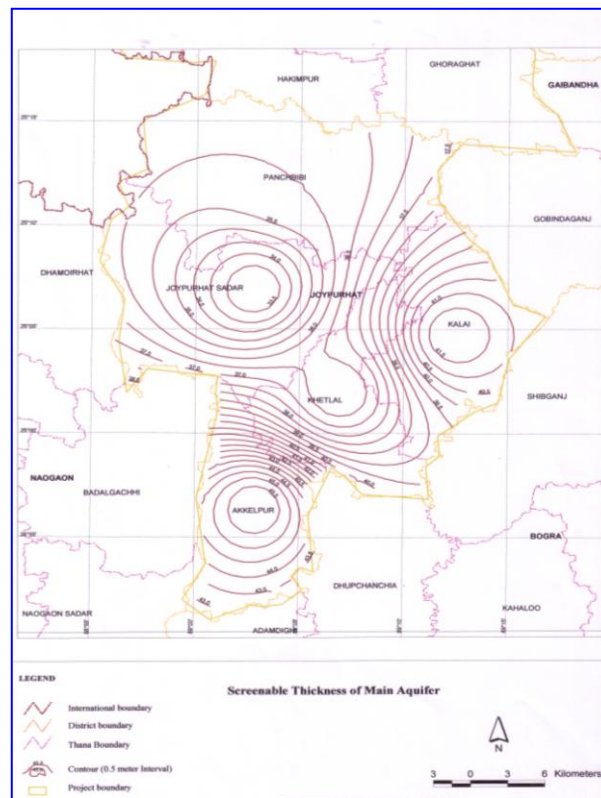


Figure 1: Screenable Thickness of Main Aquifer

This paper highlights the assessment of potential recharge as well as groundwater availability for 5 Upazillas (Akkelpur, Kalai, Joypurhat Sadar, Khetlal and Panchbibi) of Joypurhat districts using MIKE SHE modelling tools. Drought is one of the major problems of this area where groundwater is the only dependable source of drinking and irrigation purposes. Almost in all of the area, groundwater is being abstracted on an unplanned way and indiscriminately. Surface water sources are very limited for this area. In dry season, most of the hand tube wells (HTW) and shallow tube wells (STW) become inoperable.

The main aquifers of the study area ranges from 15 m to 24 m and the screenable thickness of aquifers range from 33 m to 46 m within the depth range 57 m to 87 m (Figure 1).

The survey indicated the existence of a 40 m thick aquifer at the depths varying from 20 m to 40 m in the study area (Depperman ,1956). Estimated the specific yield for the Bogra district including the area which varies between 8% and 18% (Karim, 1972). They recommended the hydraulic design parameters of aquifers, permeability ranges between 11 m/day to 32 m/day, transmissivity between 800 m<sup>2</sup>/day to 1350 m<sup>2</sup>/day and specific yield between 8% to 20%.

However, later on MacDonald (1980) revealed the transmissivity values of the aquifer ranges between 1000 m<sup>2</sup>/day and 2000 m<sup>2</sup>/day.

For general planning, a constant storage coefficient value of 13% was suggested in the report for typical water level fluctuations in the range of 5 to 9 m. In Khetlal, Joypurhat, Kalai, Panchabibi and Akkelpur upazillas of Joypurhat district transmissivity varies from 1240 m<sup>2</sup>/day to 1700 m<sup>2</sup>/day (IWM, 2009).

## II. APPROACH AND METHODOLOGY

Every modelling study involves the iterative development of a model. Model refinements are based on the availability and quality of data, hydrogeological understanding and modelling study scope. For this study purposes, the general approach has been adopted as shown in the Figure 2

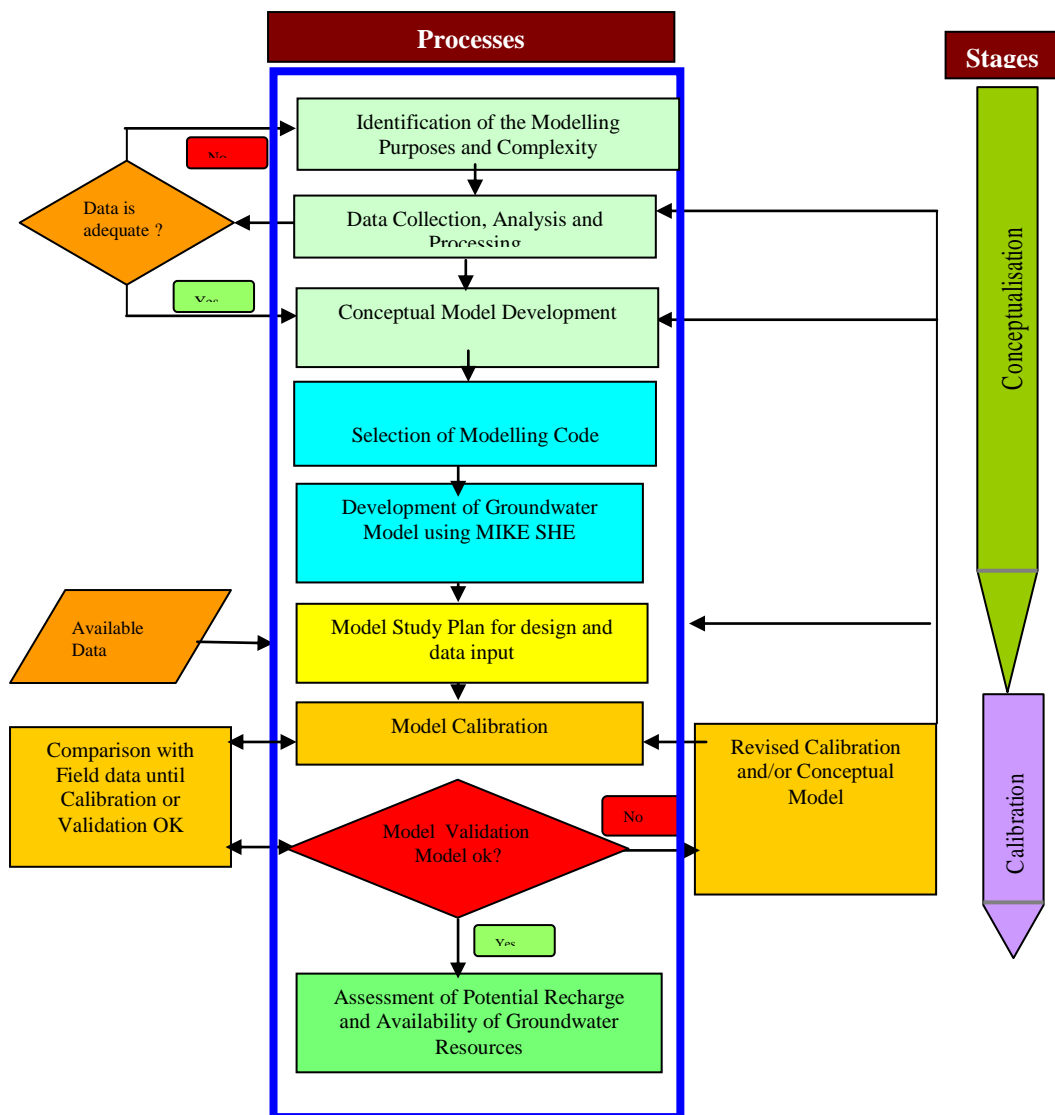


Figure 2 Flow chart of the general methodology for the study

### Data collection

The following data were collected from different sources:

- Rainfall and Evaporation data for the period of 1975 to 2009 for 9 stations.
- Groundwater level data from IWM and BWDB.
- Geological data from IWM.
- Land use and vegetation data from IWM.
- Upazilawise number of DTW and STW from BADC Report.

### Model Calibration

Calibration is the process in which the simulated result is matched with the observed data through adjusting the calibration parameter within a realistic limit. A set of 3 observation wells was selected for calibration matching. Due to the huge number of input data, the parameters are also numerous. During the calibration it is therefore important to adjust the parameters within acceptable ranges determined from field measurements, and also to minimize the number of adjustment of parameters. The model has been calibrated for the period 2001 to 2006. During calibration overland leakage co-efficient, soil properties, hydraulic conductivity and storage coefficient have been adjusted.

To measure the performance of the model, calibrated water levels were compared with the observed water levels for 3 observation wells. Sample calibration plot is shown in Figure 3. In general, the overall calibration of the present model is acceptable, but there is scope for further improvement. Some of the reasons of deviation between observed and simulated groundwater levels have been identified as follows.

- Insufficient irrigation information; the conceptual description of the irrigation abstraction might not be sufficient.
- Missing description of pumping systems close to the observation wells.
- There are considerable uncertainty in the crop water demand and the actual abstraction in the field.

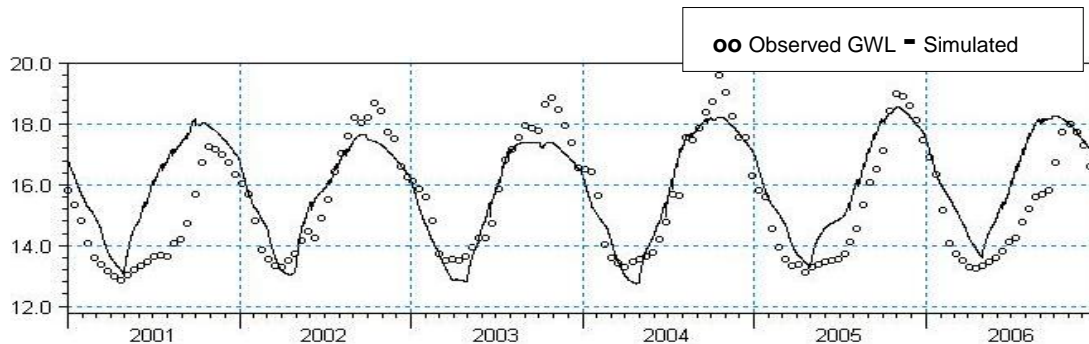


Figure 3: Calibration of groundwater level of BO-007 at Joypurhat

### Model Validation

To check whether the calibrated model is an adequate representation of the physical system or not, validation is carried out on the calibrated model. It is customary that the calibrated model should be verified outside the calibration period. As such verification has been done for a period 1995 to 2000. In validation all the calibration parameters were the same as for the calibrated model, only the input parameters were changed.

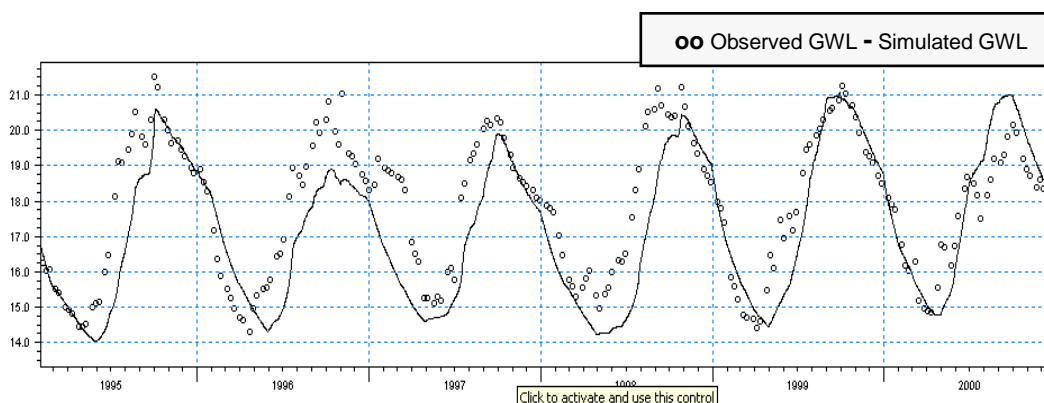


Figure 4: Validation of groundwater level of BO-008 at Panchbibi

In general the validation plots reveal a good correlation between the observed and the simulated values as shown in the Figure 4.

Overall validation results show similar trend of groundwater fluctuation and good matching of groundwater levels between observed and simulated values for both of the validation periods. From the results of the model validation, it can be concluded that the parameters used in the calibrated model are acceptable, thus the model can be used for prediction purposes.

### Selection of Design Year

Generally, irrigation projects are planned considering average hydrological conditions. In the present study, design year has been selected based on return period of mean annual rainfall of the study area. Observed annual rainfall for a period of 32 years(1975-2006) has been considered for statistical analysis. Data has been

fitted to Log Normal distribution to find out the average dry year. The statistical software HYMOS 4.0 has been used for this purpose. From the statistical analysis 2002 has been selected as the design year.

**Groundwater Resource Assessment**

Reliable assessment of groundwater resource is essential for effective irrigation management and preservation of environment. Groundwater resource of the study area has been assessed based on recharge characteristics, potential recharge and safe yield criteria. The starting of December has been chosen for the assessment of groundwater resources. To estimate groundwater resource, the availability of groundwater within the allowable depths are estimated based on available saturated thickness up to these depths multiplied by specific yield of the area:  $V_w = A \times \Delta h \times S_y$

Where  $V_w$  is the volume of water,  $\Delta h$  is the saturated thickness within allowable depths and  $S_y$  is the specific yield of the aquifer.

The availability of groundwater resources within the 7 m depths are estimated based on available saturated thickness up to 7 m depths multiplied by specific yield. Upazilawise resources under different yield criteria has been estimated.

**III. RESULTS AND DISCUSSION**

**3.1 Potential Recharge and Usable Recharge**

Upazilawise potential recharge has been estimated from model results simulated for average year (2002). The end of April is the end of irrigation period when the lowest water table generally occurs, after that water table starts rising due to recharge to groundwater from rainfall. The components that influence the groundwater storage after April are mainly rainfall, runoff, overland flow, overland storage, drain to river, evapo-transpiration, boundary inflow and outflow. Potential recharge for the study area has been estimated using the water balance obtained from model simulation. A sample water balance chart for Joypurhat Upazila is shown in Figure 5.

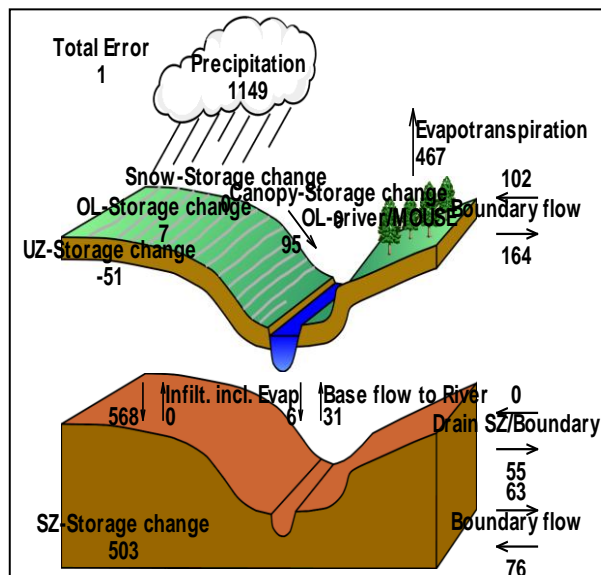


Figure 5: Water balance of Joypurhat Upazila

Potential Recharge = 503mm (SZ-Storage change)-51 mm (UZ-Storage change)= 452 mm.

Upazilawise estimated potential recharge has been shown in Table 1. According to the MPO and NWMP guideline, 75% of potential recharge has been taken as usable recharge for development consideration.

It is due to the fact that various uncertainties are inherent in different assumptions for the estimation of potential recharge.

**Table 1: Upazilawise potential recharge of the study area**

District	Upazila	Potential Recharge		Useable Recharge	
		mm	Mm <sup>3</sup>	mm	Mm <sup>3</sup>
Joypurhat	Akkelpur	516	76	384	57
	Joypurhat Sadar	452	111	339	83
	Kalai	793	130	595	98
	Khetlal	677	97	508	73
	Panchbibi	601	165	451	124
<b>Total</b>		<b>3039</b>	<b>579</b>	<b>2277</b>	<b>435</b>

The estimated potential recharge has been compared with the potential recharge of MPO, NWMP and IWM study. The comparisons indicate that present study result has good conformity and consistency with those of MPO, NWMP and IWM study. However, there are slight variations in Upazilawise estimation. Comparison of Potential Recharge obtained by the model study and other organization is shown in Table 2.

The potential recharge of the present study varies from 452 mm to 793 mm while the values of MPO study varies from 400 mm to 500 mm and the values of NWMP study varies 552 mm to 772 mm and the values of IWM studies ranges from 453 mm to 799 mm.

**Table 2: Comparison of potential recharge**

District	Upazila	Potential Recharge (mm) Estimated by			
		Present Study	MPO	NWMP	IWM
Joypurhat	Akkelpur	516	425	552	581
	Joypurhat Sadar	452	400	558	453
	Kalai	793	500	772	799
	Khetlal	677	400	746	677
	Panchbibi	601	450	636	635

The slight variation of results is due to variation in approaches and parameters used and boundary effect for comparatively small area. Distributed modelling approach and parameters were estimated through carefully data analysis. Furthermore, groundwater reserve has extensively been used over the recent years that create scope for higher recharge.

### 3.2 Available Groundwater Resources before Irrigation Period

Based on safe yield criteria, Upazila-wise available groundwater resources have been assessed considering the saturated thickness and the values of specific yield from the calibrated model. Upazila-wise available groundwater resources up to 7m from the surface is shown in Table 3.

It has been observed from the table that the potential recharge is lower than the available resource in Joypurhat Sadar. This is due to the fact that, potential recharge of this Upazila is less due to clay formation in upper geological layer. While the potential recharge is higher in other upazilas.

**Table 3: Upazilawise available groundwater resources up to 7 m depth**

District	Upazila	Available groundwater resource	
		(mm)	Mm <sup>3</sup>
Joypurhat	Akkelpur	365	53
	Joypurhat Sadar	587	144
	Kalai	621	102
	Khetlal	571	82
	Panchbibi	530	146
<b>Total</b>		<b>2674</b>	<b>527</b>

#### IV. CONCLUSIONS

The study aims to explore the modern technique for assessment of groundwater resources and its sustainable development. In this connection a dedicated groundwater model for the study area has been developed using the updated data and information collected from various secondary sources. The model has been calibrated for the period of 2001-2006 and validated for the period of 1995-2000. The calibrated and validated models have been applied for various scenarios. Based on the study findings, conclusions are summarized below:

- After developing, satisfactory calibration and validation of the model available groundwater resource for the study area has been determined for three safe yield criteria; (i) maximum groundwater table 7 m from ground surface, (ii) potential recharge and (iii) useable recharge . The usable recharge has been determined considering 75% of potential recharge as suggested by MPO.
- Groundwater resources for the entire study area for those yield criteria are found to be 527 Mm<sup>3</sup>, 579 Mm<sup>3</sup> and 435 Mm<sup>3</sup> respectively. Whereas the present irrigation requirement is 484 Mm<sup>3</sup>. This indicates that as a whole, if potential recharge is considered, there is no shortage of water to meet the present water demand.
- When usable recharge is considered, little shortage of water is observed in Joypurhat Sadar, Khetlal and Panchbibii Upazila. This is due to the fact that boro coverage is already more than 80% in these Upazilas which implies to higher water requirement.
- Maximum depth to groundwater table in most of the places occurs at the end of April. At this time, groundwater table in the most part of Kalai, Khetlal, Akkelpur and Panchbibi goes below suction limit causing HTWs and STWs partially/fully in operable.
- Based on the study findings, Irrigation Zoning Map has been prepared. Considering the depth to groundwater table, groundwater zone is divided into STW zone and DTW zone. Kalai, Khetlal, Akkelpur and Panchbibi upazilas are DTW zone and Joypurhat sadar upazila is STW zone. However STW zone is not restricted for STW use only, it is considered as a mixed zone of STW and DTW.

#### REFERENCES

- [1]. Depperman (1965): Geo electric resistivity survey for groundwater development in the northwest regions.
- [2]. IWM (2005): Groundwater Management and Zoning Study for repair and Rehabilitation of Deep Tubewell Project in Greater Dinajpur District under Post Drought Agricultural Rehabilitation Programme, Final Report, Volume-II.
- [3]. IWM (2009): Groundwater Resource Study and Decision Support System Development of Thakurgaon, Panchagarh, Dinajpur, Joypurhat Districts and also Remaining Districts of Rajshahi Division Through Mathematical Model Study, Volume-II.
- [4]. Karim M.A. (1972): Ground Water Potential in Northern Areas of Dinajpur and Rangpur Districts, Bangladesh Water Development Board.
- [5]. Mott. Mac Donald and Partners Ltd (1980): Groundwater modelling study for Tubewell project- North Bangladesh.
- [6]. Karim M.A. (1984): Upazilawise Groundwater Recharge Conditions of Bangladesh, Bangladesh Water Development Board.
- [7]. MacDonald (1977): BADC/IDA Tubewell Project, Vol. III, Groundwater, Bangladesh Agricultural Development Corporation.
- [8]. Mott. Mac Donald and Partners Ltd (1980): Groundwater modelling study for Tubewell project- North Bangladesh.
- [9]. MacDonald (1983): Water Balance Studies Bangladesh, Final Report.
- [10]. MPO (1986): Technical Report No. 5 on Groundwater.
- [11]. WARPO, Sir William Halcrow & Partners Ltd et al. (2000): National Water Management Plan Project Draft Development Strategy, Volume No. 4, Annex C: Land and Water Resources.
- [12]. Ministry of Water Resources, GOB.
- [13]. DHI (Danish Hydraulic Institute), August 2003: MIKE SHE Hydrological.
- [14]. Modelling System, Version 2003B for Windows 95 and Windows NT.

## Implementation of RSA Encryption Algorithm on FPGA

Amit Thobbi<sup>1</sup> ShriniwasDhage<sup>2</sup> Pritesh Jadhav<sup>3</sup> Akshay Chandrachood<sup>4</sup>

<sup>1234</sup>Department Of Electronics & Telecommunication, PVG's college of Engineering & Technology, Pune, India.

**ABSTRACT:** This paper presents a scheme for implementation of RSA encryption algorithm on FPGA. A 64 bit cipher text is accepted and using 128 bit public key RSA encryption technique, a 64 bit encrypted message is generated. Each block is coded using VHDL and the code is synthesized and simulated using Xilinx ISE Design Suite 14.7. Unlike previous approaches we have systematically provided timing, area and power measures for Spartan 3 and Virtex 6 FPGA using Pre and Post synthesis simulations. The design is optimized for either speed or power and a tradeoff is presented between speed, power and space. If the design is optimized for power then fewer resources are consumed but the maximum usable frequency is also reduced. Spartan 3 FPGAs are best suited for low power designs. As a major practical result we show that it is possible to implement RSA algorithm at secure bit lengths on a single commercially available FPGA.

**KEYWORDS:** RSA Encryption, Virtex6 FPGA, Spartan3 FPGA, Montgomery Algorithm

### I. INTRODUCTION

The art of keeping messages secure is Cryptography. Cryptography plays an important role in the security of data. It enables us to store sensitive information or transmit it across insecure networks so that unauthorized persons cannot read it. [5]

The RSA algorithm was introduced in the year 1978 by Ron Rivest, Adi Shamir, and Leonard Adleman. It is a public key cryptography algorithm. It is a secure, high quality algorithm. [5] It can be used as a method of exchanging secret information such as keys and producing digital signatures. However, the RSA algorithm is computationally intensive, operating on very large (typically thousands of bits long) integers. [2]

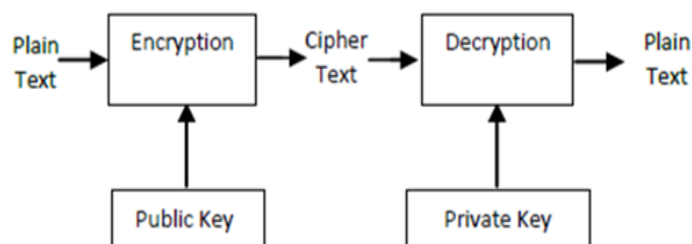


Figure 1: Public key cryptography

The rising growth of data communication and electronic transactions has made system security to become the most important issue. To provide modern security features Public key cryptosystems are used; one such cryptosystem is the RSA algorithm. A public key stored in the hardware, itself improves security greatly.



2. Generation of the Public Key modulus (n)

n is generated by multiplying the two 32 bit prime nos. 'a' and 'b' resulting into the 64 bit modulus 'n'. This multiplication is performed by the Booth's algorithm.

This is the U1 component. '13' and '17' are the inputs given and output generated is 221

3. Generation of the totient (t).

The totient is generated by multiplying (a-1) and (b-1), which gives a 64 bit totient. This multiplication is accomplished by Booth's algorithm.

This is accomplished by the U2 component. '12' and '16' are inputs and '192' is output generated.

4. Generation of public key exponential (e).

'e' is a 64 bit prime number which is co prime to 't'. The modular block checks this condition. Modular multiplication is carried out between e and t i.e. (e mod t) resulting into a 64 bit output denoted as 'o1'. The public key exponential is chosen by the user. Number '17' is chosen as the public key exponent. This is given to the U3 component and the public key condition is checked.

5. Encryption of the data.

In this stage the encryption of user data is carried out by modular and exponential operations i.e.  $outp = Cin^e \text{ mod } n$ .

This step results into a 64 bit encrypted message. The U4 component performs this operation. The public key exponent and modulus is given to the component and Cin is the user message. 'Outp' is the output generated. The public key exponent taken is '17' and public key modulus taken is '221'.

b) Functional verification of RSA Algorithm (Behavioral Simulation)

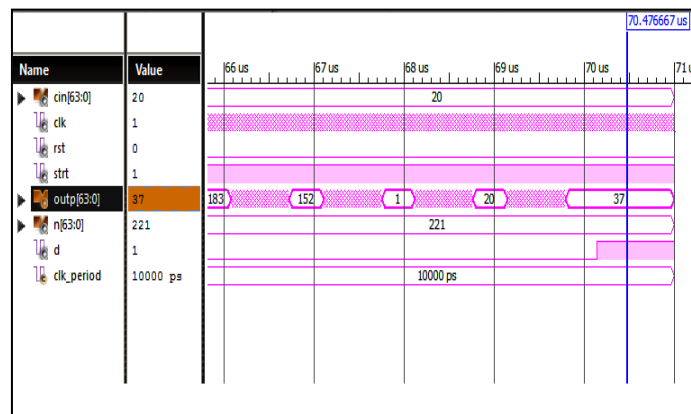


Figure 4: Behavioral simulation result of RSA Algorithm

Figure 4 shows the simulation results. Table I shows the parameters used for checking the correctness of the design i.e. behavioral simulation. The result is verified using theoretical calculation.

Parameter	Description	Value
cin	User input message	20
n	Public key modulus	221
e	Public key exponential	17
outp	Encrypted message output	37

Table I : Input Parameters for behavioral Simulation

Operation performed is  $outp = cin^e \text{ mod } n$

Substituting the values

$$outp = 20^{17} \text{ mod } 221$$

$$outp=37$$



Figure 5: Result verified using Wolfram Alpha

### III. TEST CONDITIONS

Device used : Spartan3 XC3s400fg320-4, Virtex6 XC6vlx75tff484-1  
 Design and Analysis Tool : Xilinx PlanAhead 14.7

Results were achieved for the following synthesis and implementation settings shown in Tables II and III.

Parameter	Spartan 3		Virtex 6	
	Power	Speed	Power	Speed
Opt mode	area	speed	area	speed
Opt level	1	2	1	2
FSM Encoding	gray	Speed1	gray	Speed1
lc	N.A.	N.A.	area	auto
Netlist hierarchy	As_optimised	Rebuilt	As_optimised	Rebuilt

Table II. Synthesis Settings

Parameter	Spartan 3		Virtex 6	
	Power	Speed	Power	Speed
pr	none	b	none	b
ir	off	off	off	off
cm	area	speed	N.A	N.A
Logic_opt	on	off	on	off
Global_opt	on	off	on	off
lc	on	off	on	off
Ol(map)	none	none	none	none
Mt(map)	N.A	N.A	on	on
Power(map)	on	off	on	off
Ol(par)	std	none	std	none
Power(par)	on	off	on	off

Table III: Implementation Settings

IV. RESULTS

a) Synthesis results

```

Selected Device : 3s400fg320-4

Number of Slices:          420 out of 3584 11%
Number of Slice Flip Flops: 425 out of 7168 5%
Number of 4 input LUTs:   714 out of 7168 9%
    Number used as logic:  710
    Number used as Shift registers: 4
Number of IOs:            196
Number of bonded IOBs:   196 out of 221 88%
Number of GCLKs:         1 out of 8 12%
    
```

Figure 6: synthesis result for spartan3 power optimized

```

Selected Device : 3s400fg320-4

Number of Slices:          625 out of 3584 17%
Number of Slice Flip Flops: 563 out of 7168 7%
Number of 4 input LUTs:   851 out of 7168 11%
    Number used as logic:  847
    Number used as Shift registers: 4
Number of IOs:            196
Number of bonded IOBs:   196 out of 221 88%
Number of GCLKs:         1 out of 8 12%
    
```

Figure 7: synthesis result for spartan3 speed optimized

```

Selected Device : 6v1x75tff484-1

Slice Logic Utilization:
Number of Slice Registers: 187 out of 93120 0%
Number of Slice LUTs:     241 out of 46560 0%
    Number used as Logic:  239 out of 46560 0%
    Number used as Memory: 2 out of 16720 0%
    Number used as SRL:    2
    
```

Figure 8: synthesis result for Virtex6 power optimized

```

Selected Device : 6v1x75tff484-1

Slice Logic Utilization:
Number of Slice Registers: 205 out of 93120 0%
Number of Slice LUTs:     253 out of 46560 0%
    Number used as Logic:  251 out of 46560 0%
    Number used as Memory: 2 out of 16720 0%
    Number used as SRL:    2
    
```

Figure 9: synthesis result for Virtex6 speed optimized

b) Maximum Frequency (PAR result)

The below figures show the PAR result i.e. the maximum usable frequency. A Timing score of zero indicates design has met all constraints. [6]

Name	Part	Constraints	Strategy	Status	Progress	Start	Elapsed	Util (%)	FMax (MHz)	Timing Score
synth_4	xc6v1x75tff484-1	constrs_1	PlanAhead Defaults (XST 14)	XST Complete!	100%	5/29/15 6:43 PM	00:00:28	0.000	228.595	
synth_5 (active)	xc6v1x75tff484-1	constrs_1	PlanAhead Defaults (XST 14)	XST Complete!	100%	5/29/15 4:13 PM	00:00:25	0.000	228.595	
impl_2 (active)	xc6v1x75tff484-1	constrs_1	ISE Defaults (ISE 14)	Implementation Out-of-date	100%	5/29/15 4:27 PM	00:01:52	1.000	224.568	0
synth_6	xc6v1x75tff484-1	constrs_1	implxsat (XST 14)	XST Complete!	100%	5/30/15 1:23 PM	00:00:38	0.000	228.595	
synth_7	xc6v1x75tff484-1	constrs_1	implxsat (XST 14)	XST Complete!	100%	5/31/15 2:10 PM	00:00:29	0.000	228.595	
impl_6	xc6v1x75tff484-1	constrs_1	impl4 (ISE 14)	PAR Complete!	100%	5/31/15 2:18 PM	00:02:05	1.000	203.046	0

Figure 10: PAR Result for Virtex6 speed optimized and power optimized design

Name	Part	Constraints	Strategy	Status	Progress	Start	Elapsed	Util (%)	FMax (MHz)	Timing Score
synth_4	xc3s400fg320-4	constrs_1	PlanAhead Defaults (XS...	Synthesis Out-of-date	100%	4/11/15 6:27 PM	00:00:25	9.000	71.355	
impl_4	xc3s400fg320-4	constrs_1	ISE Defaults (ISE 14)	Implementation Out-of-date	100%	5/28/15 5:47 PM	00:01:08	9.000	66.854	0
synth_5	xc3s400fg320-4	constrs_1	TimingWithIOBPacking (...)	Synthesis Out-of-date	100%	5/28/15 7:24 PM	00:00:32	11.000	86.730	
impl_5	xc3s400fg320-4	constrs_1	ParHighEffort (ISE 14)	Implementation Out-of-date	100%	5/28/15 7:57 PM	00:00:44	11.000	78.920	0
synth_6 (active)	xc3s400fg320...	constrs_1	synth4spartan (XST ...)	XST Complete!	100%	5/30/15 11:21 PM	00:00:28	9.000	71.355	
impl_6 (active)	xc3s400fg320...	constrs_1	impl4spartan (ISE 14)	PAR Complete!	100%	5/31/15 9:14 AM	00:01:18	9.000	67.696	0

Figure 11: PAR Result for Spartan3 speed optimized and power optimized design

c) Timing result

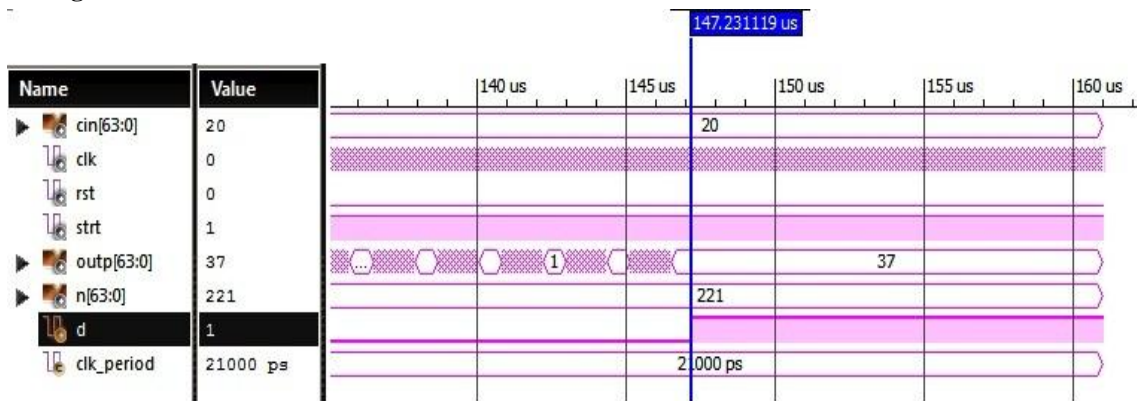


Figure 12: Timing result for Spartan3 power optimized design

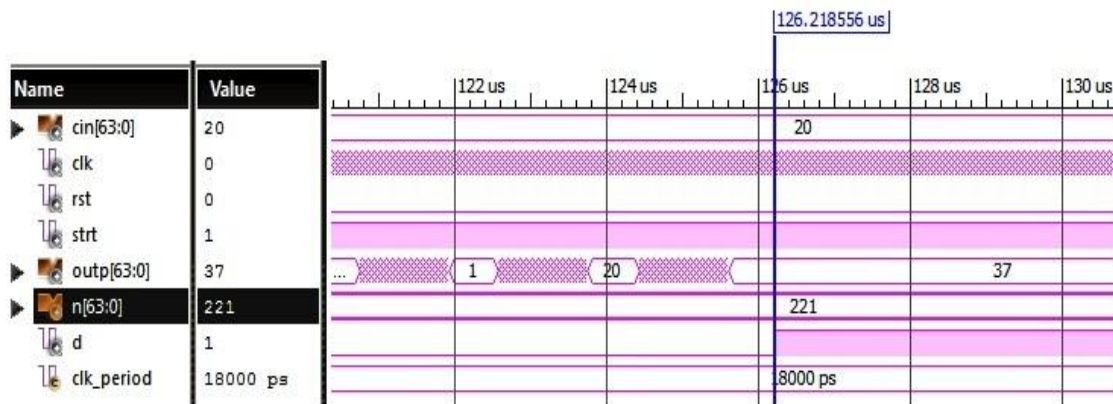


Figure 13: Timing result for Spartan3 speed optimized design

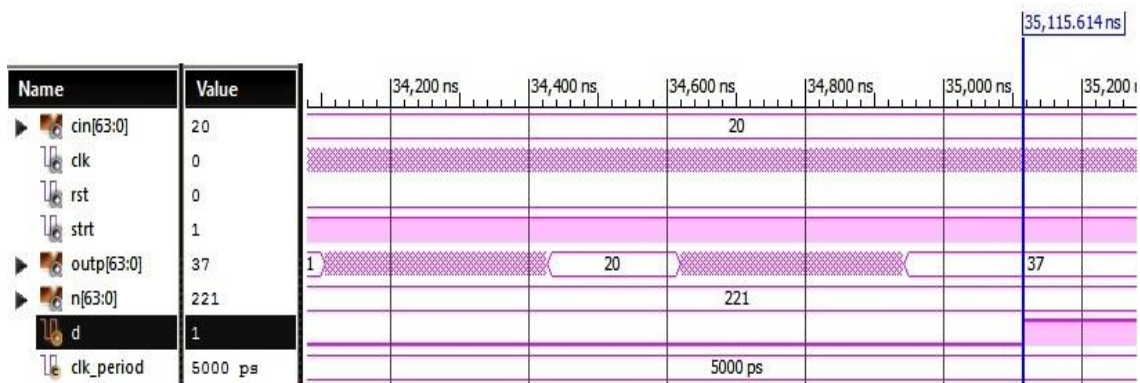


Figure 14: Timing result for Virtex6 power optimized design

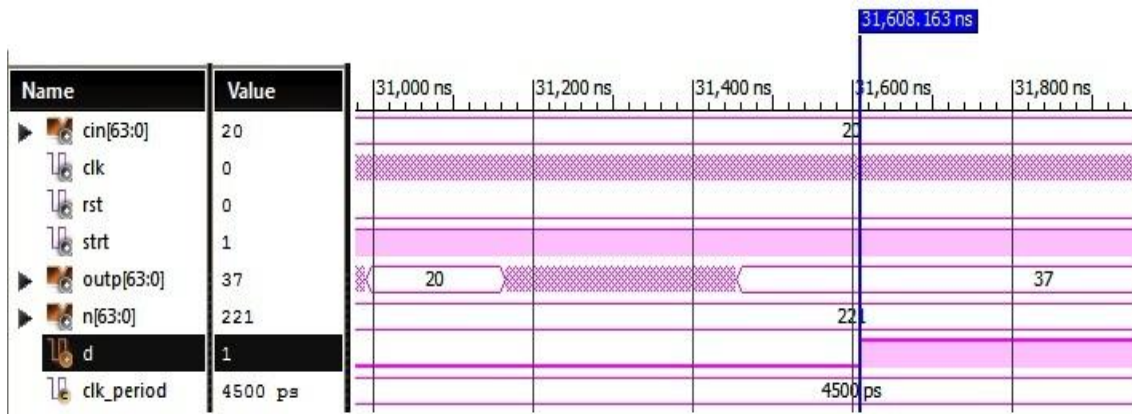


Figure 15: Timing result for Virtex6 speed optimized design

**d) Power analysis results**

Device		On-Chip	Power (W)	Used	Available	Utilization (%)
Family	Spartan3	Clocks	0.000	1	---	---
Part	xc3s400	Logic	0.000	774	7168	11
Package	fg320	Signals	0.000	974	---	---
Temp Grade	Commercial	IOs	0.026	196	221	89
Process	Typical	Leakage	0.060			
Speed Grade	-4	Total	0.086			

Figure 16: Power result forSpartan3 power optimized design

Device		On-Chip	Power (W)	Used	Available	Utilization (%)
Family	Spartan3	Clocks	0.000	1	---	---
Part	xc3s400	Logic	0.000	848	7168	12
Package	fg320	Signals	0.000	1247	---	---
Temp Grade	Commercial	IOs	0.037	196	221	89
Process	Typical	Leakage	0.060			
Speed Grade	-4	Total	0.097			

Figure 17: Power result forSpartan3 speed optimized design

Device		On-Chip	Power (W)	Used	Available	Utilization (%)
Family	Virtex6	Clocks	0.012	1	---	---
Part	xc6vx75t	Logic	0.001	208	46560	0
Package	ff484	Signals	0.002	338	---	---
Temp Grade	Commercial	IOs	0.040	196	240	82
Process	Typical	Leakage	1.294			
Speed Grade	-1	Total	1.349			

Figure 18: Power result for Virtex6 power optimized design

Device		On-Chip	Power (W)	Used	Available	Utilization (%)
Family	Virtex6	Clocks	0.013	1	---	---
Part	xc6vx75t	Logic	0.001	208	46560	0
Package	ff484	Signals	0.002	338	---	---
Temp Grade	Commercial	IOs	0.044	196	240	82
Process	Typical	Leakage	1.294			
Speed Grade	-1	Total	1.355			

Figure 19: Power result for Virtex6 speed optimized design

## e) Tabular description and comparison of results

Parameter	Spartan 3		Virtex 6	
	Power	Speed	Power	Speed
Number of slices used / Total Available	420/3584	625/3584	187/93120	201/93120
Number of LUTs used / Total Available	714/7168	851/7168	241/46560	251/46560
Utilization	9 %	11 %	0.51 %	0.54 %
Max Frequency	67.696MHz	78.920 MHz	203.046 MHz	224.568 MHz
Timing Simulation Result	147.2311 $\mu$ s	126.285 $\mu$ s	35.1156 $\mu$ s	31.6081 $\mu$ s
Power Consumption	0.086 Watts	0.097 Watts	1.349 Watts	1.355 Watts

Table IV: Results Summary

The synthesis reports show that when optimized for speed the number of slices and number of LUTs is increased. Virtex 6 FPGA has more resources compared to Spartan 3 and hence Virtex 6 should be used for larger designs. The PAR report shows maximum usable frequency [6]. Maximum Frequency has been achieved for Virtex 6 FPGA when optimized for speed.

Timing Simulation Results are obtained using Isim Simulator [6]. It shows the time required to obtain the final output. Virtex 6 is faster due to high clock frequency. Hence Virtex 6 FPGAs should be used to obtain faster results. The power reports are obtained using Xilinx Power Analyzer [6]. The reports indicate that Virtex 6 FPGAs consume more power. The clock frequency also consumes significant power. Increasing clock frequency increases power consumption. Hence for power conscious designs Spartan 3 FPGAs can be used.

## V. CONCLUSION

The RSA algorithm can be effectively implemented on FPGA. The arithmetical operations necessary for the RSA algorithm are time consuming as the number of bits used is usually large. However as the length of public key and message increases the utilization of FPGA resources also increases.

The design on FPGA can be optimized for power or speed but not both by changing synthesis & implementation settings. Optimizing design for power uses fewer resources but offers less speed. Optimizing design for speed uses more resources and offers more speed. Thus for large designs power optimized designs should be used. For better security, FPGAs with more resources should be used. Also a dedicated ASIC prototype can be developed which can be used to encrypt data in Communication equipments, Set Top Boxes, Personal computers.

## REFERENCES

- [1]. Sushanta Kumar Sahu and Manoranjan Pradhan "FPGA Implementation of RSA Encryption system", International Journal of Computer Applications, Volume 19- No.9,2011
- [2]. Perovic N.S; Popovic-Bozovic : "FPGA implementation of RSA crypto algorithm using shift and carry algorithm ",IEEE Telecommunications Forum (TELFOR), 2012 pages (1040-1043)
- [3]. Nibouche O. Nibouche M.Bouridane A. Belatreche A. : "Fast architectures for FPGA Architectures of RSA Encryption Algorithm",IEEE Conference Field programmable technology,2004 (pages 271-278)
- [4]. C-Chao Yang ; Tian-Sheuan Chang ; Chein-Wei Jen, "A new RSA Cryptosystem hardware design based on Montgomery's algorithm", Circuits and Systems II: Analog and Digital Signal Processing, IEEE Transactions on (Volume:45 No 7,2010 )
- [5]. Cetin Kaya Koc, High speed RSA algorithm, RSA laboratories, version 2, 1994
- [6]. Xilinx user guide 612- timing closure user guide 2012
- [7]. Xilinx user guide 625- constraints user guide 2012

## Improving Atm Security Check Using DNA Biometrics

<sup>1</sup>, Igwe, Agu Felix, <sup>2</sup> Eneh, I.I

<sup>1</sup>. Computer Engineering Dept, Abia State Polytechnic, Aba, Nigeria

<sup>2</sup>. Electrical/Electronic Engineering, Enugu State University of Science & Technology Enugu, Nigeria

**ABSTRACT:** This paper exposes how DNA can be used to identify account owner of a particular bank. DNA samples were obtained from body fluid. Buccal swab was used for sample collection. Buccal cell collection involves wiping a small piece of filter paper or a cotton swab against the inside of armpit in order to collect shed epithelial cells. The swab was then air dried or could be pressed against a treated collection card in order to transfer epithelial cells for storage purposes. The stored samples were later amplified and separated. The data generated from the samples were stored and saved in the database so that if a customer comes to claim money, the system checks whether it matches with what is stored in the database, if it matches with the one in the database, access is granted to the customer, if it does not match with what is stored in the database, access is denied from the customer.

**Keywords:** Buccal cell, Single nucleotide polymorphism (SNP), polymerase chain reaction (PCR), Database, ATM

### I. INTRODUCTION

The biometric authentication technologies, typified by fingerprint, face recognition and iris scanning, have been making rapid progress. Retinal scanning, voice dynamics and handwriting recognition are also being developed. These methods have been commercialized and are being incorporated into systems that require accurate on-site personal authentication. However, these methods are based on the measurement of similarity of feature-points. This introduces an element of inaccuracy that renders existing technologies unsuitable for a universal ID system. Among the various possible types of biometric personal identification system, deoxyribonucleic acid (DNA) provides the most reliable personal identification. It is intrinsically digital, and does not change during a person's life or after his/her death. This paper addresses three questions: First, how can personally identifying information be obtained from DNA sequences in the human genome? Second, how can a personal ID be generated from DNA-based information? And finally, what are the advantages, deficiencies, and future potential for personal IDs generated from DNA data (DNA-ID)?

### II. HUMAN IDENTIFICATION BASED ON DNA POLYMORPHISM

A human body is composed of approximately of 60 trillion cells. DNA, which can be thought of as the blueprint for the design of the human body, is folded inside the nucleus of each cell. DNA is a polymer, and is composed of nucleotide units that each has three parts: a base, a sugar, and a phosphate. The bases are adenine, guanine, cytosine and thymine, abbreviated A, G, C and T, respectively. These four letters represent the informational content in each nucleotide unit; variations in the nucleotide sequence bring about biological diversity, not only among human beings but among all living creatures. Meanwhile, the phosphate and sugar portions form the backbone structure of the DNA molecule. Within a cell, DNA exists in the double-stranded form, in which two antiparallel strands spiral around each other in a double helix. The bases of each strand project into the core of the helix, where they pair with the bases of the complementary strand. A pairs strictly with T, and C with G. [1]

Within human cells, DNA found in the nucleus of the cell (nuclear DNA) is divided into chromosomes. The human genome consists of 22 matched pairs of autosomal chromosomes and two sex-determining chromosomes, X and Y. In other words, human cells contain 46 different chromosomes. Males are described as XY since they possess a single copy of the X chromosome and a single copy of the Y chromosome, while females possess two copies of the X chromosome and are described as XX.

The regions of DNA that encode and regulate the synthesis of proteins are called genes; these regions consist of exons (protein-coding portions) and introns (the intervening sequences) and constitute approximately 25% of the genome [2]. The human genome contains only 20,000–25,000 genes [3]. Therefore, most of the genome, approximately 75%, is extragenic. These regions are sometimes referred to as ‘junk’ DNA; however, recent research suggests that they may have other essential functions. Markers commonly used to identify individual human beings are usually found in the noncoding regions, either between genes or within genes (i.e., introns).

### 2.1. Sort tandem repeat (STR)

In the extragenic region of eukaryotic genome, there are many repeated DNA sequences (approximately 50% of the whole genome). These repeated DNA sequences come in all sizes, and are typically designated by the length of the core repeat unit and either the number of contiguous repeat units or the overall length of the repeat region. These regions are referred to as satellite DNA [4]. The core repeat unit for a medium-length repeat, referred to as a minisatellite or VNTR (variable number of tandem repeats), is in the range of approximately 8–100 bases in length [6]. DNA regions with repeat units that are 2–7 base pairs (bp) in length are called microsatellites, simple sequence repeats (SSRs), or most commonly short tandem repeats (STRs) [7]. STRs have become popular DNA markers because they are easily amplified by the polymerase chain reaction (PCR) and they are spread throughout the genome, including both the 22 autosomal chromosomes and the X and Y sex chromosomes. The number of repeats in STR markers can vary widely among individuals, making the STRs an effective means of human identification in forensic science [8]. The location of an STR marker is called its ‘locus.’ The type of STR is represented by the number of repeat called ‘allele’ which is taken from biological father and mother. When an individual has two copies of the same allele for a given marker, they are homozygous; when they have two different alleles, they are heterozygous.

### 2.2. DNA sample collection

DNA can be easily obtained from a variety of biological sources, not only body fluid but also nail, hair and used razors [9]. For biometric applications, a buccal swab is the most simple, convenient and painless sample collection method. Buccal cell collection involves wiping a small piece of filter paper or a cotton swab against the inside of the subject’s cheek, in order to collect shed epithelial cells. The swab is then air dried, or can be pressed against a treated collection card in order to transfer epithelial cells for storage purposes.

### 2.3. DNA extraction and quantification

There are many methods available for extracting DNA. [10] The choice of which method to use depends on several factors, especially the number of samples, cost, and speed. Extraction time is the critical factor for biometric applications. The author has already reported the “5-minute DNA extraction” using an automated procedure [11]. The use of large quantities of fresh buccal cells made it possible to extract DNA in a short time.

In forensic cases, DNA quantization is an important step [12]. However, this step can be omitted in biometrics because a relatively large quantity of DNA can be recovered from fresh buccal swab samples.

### 2.4. DNA amplification (polymerase chain reaction: PCR)

The field of molecular biology has greatly benefited from the discovery of a technique known as the polymerase chain reaction, or PCR [13]. First described in 1985 by Kary Mullis, who received the Nobel Prize in Chemistry in 1993, PCR has made it possible to make hundreds of millions of copies of a specific sequence of DNA in a few hours. PCR is an enzymatic process in which a specific region of DNA is replicated over and over again to yield many copies of a particular sequence. This molecular process involves heating and cooling samples in a precise thermal cycling pattern for approximately 30 cycles. During each cycle, a copy of the target DNA sequence is generated for every molecule containing the target sequence. In recent years, it has become possible to PCR amplify 16 STRs, including the gender assignment locus called ‘amelogenin,’ in one tube [14].

## 2.5. DNA separation and detection

After STR polymorphisms have been amplified using PCR, the length of products must be measured precisely; some STR alleles differ by only 1 base-pair. Electrophoresis of the PCR products through denaturing polyacrylamide gels can be used to separate DNA molecules from 20–500 nucleotides in length with single base pair resolution [15]. Recently, the fluorescence labelling of PCR products followed by multicolour detection has been adopted by the forensic science field. Up to five different dyes can be used in a single analysis. Electrophoresis platforms have evolved from slab-gels to capillary electrophoresis (CE), which use a narrow glass filled with an cross-linked polymer solution to separate the DNA molecules [16]. After data collection by the CE, the alleles (i.e., the type or the number of STR repeat units), are analyzed by the software that accompanies the CE machine.

It takes around four hours, starting with DNA extraction, to obtain data from 16 STRs including the sex determination locus.

## 2.6. Single nucleotide polymorphism (SNP)

The simplest type of polymorphism is the single nucleotide polymorphism (SNP), a single base difference at a particular point in the sequence of DNA [17]. SNPs normally have just two alleles, e.g., one allele is a cytosine (C) and the other is a thymine (T). SNPs therefore are not highly polymorphic and do not possess ideal properties for DNA polymorphism to be used in forensic analysis. However, SNPs are so abundant throughout the genome that it is theoretically possible to type hundreds of them. Furthermore, sample processing data analysis may be more fully automated because size-based separation is not required. Thus, SNPs are prospective new bio-markers in clinical medicine [18].

### 2.2.1. SNP detection methods

Several SNP typing methods are available, each with its own strengths and weaknesses, unlike the STR analysis [19]. In order to achieve the same power of discrimination as that provided by STRs, it is necessary to analyse many more SNPs. 40 to 50 SNPs must be analyzed in order to obtain reasonable powerful discrimination and define the unique profile of an individual [20]. Importantly, however, we can count on the development of new SNP detection technologies, capable of high-throughput analysis, in the near future.

## III. DNA POLYMORPHISM FOR BIOMETRIC SOURCE

The most commonly studied or implemented biometrics are fingerprinting, face, iris, voice, signature, retina and the patterns of vein and hand geometry [21]. No one model is best for all situations. In addition, these technologies are based on the measurement of similarity of features. This introduces an element of inaccuracy that renders the existing technologies unsuitable for a universal ID system. However, DNA polymorphism information, such as STRs and SNPs, could provide the most reliable personal identification. This data can be precisely defined the most minute level, is intrinsically digital, and does not change during a person's life or after his/her death. Therefore, DNA identification data is utilized in the forensic sciences. On the negative side, the biggest problem in using DNA is the time required for the extraction of nucleic acid and the evaluation of STR or SNP data. In addition, there are several other problems, such as the high cost of analysis, issues raised by monozygotic twins, and ethical concerns.

This section describes a method for generation of DNA personal ID (DNA-ID) based on STR and SNP data, specifically. In addition, by way of example, the author proposes DNA INK for authentic security.

### 3.1. DNA personal ID using STR system

We will refer to repeat counts of alleles obtained by STR analysis as  $(j, k)$ . Each locus is associated with two alleles with distinct repeat counts  $(j, k)$ , one allele is inherited from the father, and the other from the mother. Before  $(j, k)$  can be applied to a DNA personal ID, it is necessary to statistically analyze how the distribution of  $(j, k)$  varies at a given locus based on actual data.

We can generate a DNA-ID,  $\alpha X$ , that includes allelic information about STR loci. The loci are incorporated in the following sequence. The repeat counts for the pair of alleles at each locus are arranged in ascending order.

**Step 1.** Measure the STR alleles at each locus.

Step 2. Obtain STR count values for each locus; express these in ascending order.

$$L_i: j | k, j \leq k \tag{1}$$

Depending on the measurement, the same person's STR count may appear as  $(j, k)$  or  $(k, j)$ . Therefore,  $j$  and  $k$  are expressed in an ascending order, i.e., using  $(j, k | j \leq k)$ , in order to establish a one-to-one correspondence for each individual. This step is referred to as a ordering operation.

Step 3. Generate a DNA-ID  $\alpha X$  according to the following series,  $L_i(j, k)$ :

$$\alpha X = L_1 | L_2 | L_3 | \dots | L_n \tag{2}$$

where  $L_i$  indicates the  $i$ th STR count  $(j, k)$ .

For example, suppose that Mr. M has the following alleles at the respective loci;

$$\alpha X = D3S1358 | D13S317 | D18S51 | D21S11 | \dots | D16S539 = (12,14) | (8,11) | (13,15) | (29,32.2) | \dots | (10,10) \tag{3}$$

The  $\alpha X$  was thus defined as follows.

$$\alpha X = 1214811131529322 \dots 1010 \tag{4}$$

When the STR number of an allele had a fractional component, such as allele 32.2 in D21S11, the decimal point was removed, and all of the numbers, including those after the decimal point, were retained.

Finally,  $\alpha X$  is generated number with several tens of digits, and becomes a personal identification information that is unique with a certain probability predicted by statistical and theoretical analysis.

**3.2. Establishment of the identification format**

Because

$\alpha X$  contains personal STR information, it must be encrypted to protect privacy. This can be achieved using a one-way function that also reduces the data length of the DNA-ID. This one-way function, the secure hash algorithm-1 (SHA-1), produces an ID with a length  $\delta X$  of 160 bits, according to the following transformation:

$$\delta X = h(\alpha X) \tag{5}$$

**3.3. Statistical and theoretical analysis of DNA-ID**

Probability  $p$  that the STR count at the same locus is identical for any two persons can be expressed as follows:

$$\text{When } j=k, \sum_{j=1}^m (p_j \cdot p_k)^2 \text{ When } j \neq k, \sum_{1 \leq j < k \leq m} (2p_j \cdot p_k)^2 : p = \sum_{j=1}^m (p_j)^4 + \sum_{1 \leq j < k \leq m} 4(p_j \cdot p_k)^2 \tag{7}$$

Here,  $m$  is the upper limit of  $j$  and  $k$ , and the information reported so far indicates  $m=60$ . Next, a determination is made of the DNA-ID matching probability  $p_n$ , where  $n$  loci were used to generate the ID. The probability that the STR counts at the  $i$ th locus will match for any two persons is denoted as  $p_i$ . When  $n$  loci are used, the probability  $p_n$  that the DNA-IDs of any two persons will match (the DNA-ID matching probability) is as follows:

$$p_n = \prod_{i=1}^n p_i \tag{8}$$

Here, it is assumed that there is no correlation among the STR loci.

**3.4. Verification using validation experiment (STR)**

As a validation experiment, we studied the genotype and distribution of allele frequencies at 18 STRs in 526 unrelated Japanese individuals. Data was obtained using three commercial STR typing kits: PowerPlex™ 16 system (Promega), PowerPlex SE33 (Promega), and AmpFISTR Identifier™. Information about the 18 target STRs is described in Table 1.

*Step 1.* Perform DNA extraction, PCR amplification and STR typing

*Step 2.* Perform the exact test (the data were shuffled 10,000 times), the homozygosity, and likelihood ratio tests using STR data for each STR locus in order to evaluate Hardy–Weinberg equilibrium (HWE). HWE provides a simple mathematical representation of the relationship among genotype and allele frequencies within an ideal population, and is central to forensic genetics. Importantly, when a population is in HWE, the genotype frequencies can be predicted from the allele frequencies.

*Step 3.* Calculate parameters, the matching probability, the expected and observed heterozygosity, the power of discrimination, the polymorphic information content, the mean exclusion chance, in order to estimate the polymorphism at each STR locus.

There are some loci on the same chromosomes (chr) such as D21S11 and Penta D on chr 21, D5S818 and CSF1PO on chr 5, and TPOX and D2S1338 on chr 2. No correlation was found between any sets of loci on the same chromosome, which means they are statistically independent. In addition, the statistical data for the 18 analyzed STRs, excluding the Amelogenin locus, were analyzed and showed a relatively high rate of matching probability; no significant deviation from HWE was detected. The combined mean exclusion chance was 0.999998995 and the combined matching probability was 1 in  $9.98 \times 10^{21}$ , i.e.,  $1.0024 \times 10^{-22}$ . These values were calculated using polymorphism data from Japanese subjects; it is likely that different values would be obtained using data compiled from different ethnic groups.

**Table 3.0 : Information about autosomal STR loci**

Locus	Chromosome	Location	Repeat Motif*	Locus	Chromosome	Location	Repeat Motif*
TPOX	2 q	25.3	GAAT	TH01	11 p	15.5	TCAT
D2S1338	2 q	35	TGCC/TTCC	VWA	12 p	13.31	TCTG/TCTA
D3S1358	3 p	21.31	TCTG/TCTA	D13S317	13 q	31.1	TATC
FGA	4 q	31.3	CTTT/TTCC	Penta E	15 q	26.2	AAAGA
D5S818	5 q	23.2	AGAT	D16S539	16 q	24.1	GATA
CSF1PO	5 q	33.1	TAGA	D18S51	18 q	21.33	AGAA
SE33	6 q	14	AAAG	D19S433	19 q	12	AAGG/TAGG
D7S820	7 q	21.11	GATA	D21S11	21 q	21.1	TCTA/TCTG
D8S1179	8 q	24.13	TCTA/TCTG	Penta D	21 q	22.3	AAAGA

\* Two types of motif means a compound or complex repeat sequence

**Table 3.1: Data Generated from sweat**

Locus1	Chromosome location1	Locus2	Chromosome location
TPOX	15.5	GAAT	10.5
FGA	12.5	PENTA E	8.25
SE33	8.4	AAAG	5.6
D7S820	4.8	GSTA	3.87

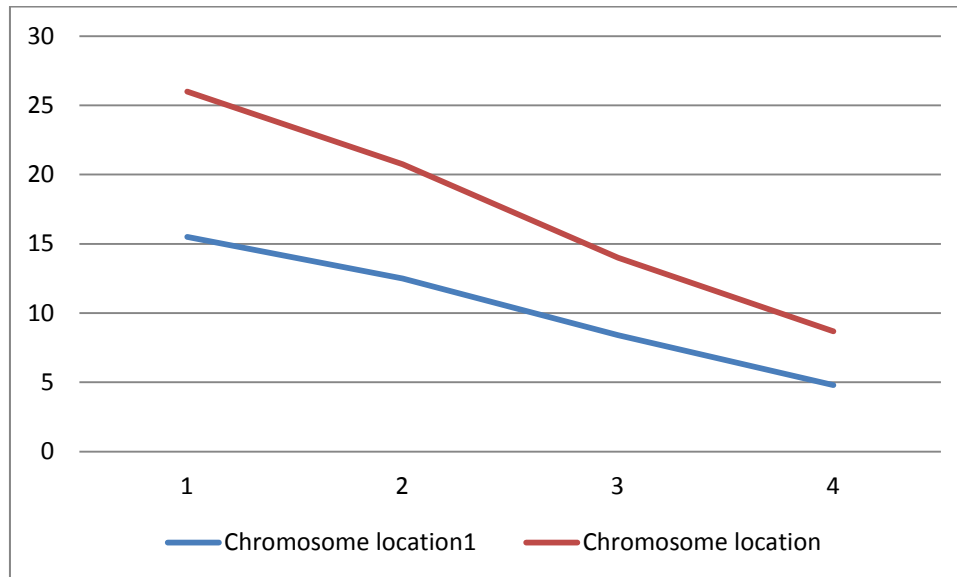


Fig.3.2: Graph of chromosome location

**3.3 Analysis of Data:** The graph above shows how the chromosome representation of rightful should be. If a customer comes to withdraw money, fluid will be extracted from the customer's armpit in order to ascertain whether he or she is the rightful owner of the money or not. The data gotten from the customer will be processed and matched with the graph in fig.3.2, if it matches with it, access is granted to the customer, in case it does not match with it, access is denied from the customer.

### 3.4. DNA personal ID using SNP system

The vast majority of SNPs are biallelic, meaning that they have two possible alleles and therefore three possible genotypes. For example, if the alleles for a SNP locus are R and S (where 'R' and 'S' could represent a A(adenine), G(guanine), C(cytosine) and T(thymine) nucleotide), three possible genotypes would be RR, RS (SR) or SS. Because a single biallelic SNP by itself yields less information than a multiallelic STR marker, it is necessary to analyze a larger number of SNPs in order to obtain a reasonable power of discrimination to define a unique profile. Computational analysis have shown that on average, 25 to 45 SNP loci are needed in order to yield equivalent random match probabilities comparable to those obtained with the 13 core STR loci that have been adopted by the FBI's DNA database (COMBINED DNA INDEX SYSTEM, CODIS).

The steps of creating a DNA-ID using SNPs are as follows;

*Step 1.* Define alleles 1 and 2 for each SNP locus. Since DNA has a double helix structure, the single nucleotide polymorphism of A or G is the same polymorphism of T or C, respectively (Fig. 4). In other words, it is important to specify which strand of the double helix is to be analyzed, and to define allele 1 and allele 2 at the outset.

*Step 2.* Analyze the SNP loci and place them in the following order.

$$L_i: \text{allele 1} \parallel \text{allele 2} \quad (9)$$

*Step 3.* Generate the DNA-ID  $\alpha X$  according to the following series of  $L_i$  (allele1, allele2):

$$\alpha X = L_1 \parallel L_2 \parallel L_3 \parallel \dots \parallel L_n \quad (10)$$

where  $L_i$  indicates the  $i^{\text{th}}$  SNP nucleotide (allele1, allele2).

For example, suppose that a person has the following alleles at the respective loci;

$$\alpha X = \text{SNP 1} \mid \text{SNP 2} \mid \text{SNP 3} \mid \text{SNP 4} \mid \dots \mid \text{SNP 50} = (A,A) \mid (C,T) \mid (T,C) \mid (C,C) \dots \mid (G,A) \quad (11)$$

Then  $\alpha_X$  would be defined as follows.

$$\alpha X = AACTTCCC \dots GA \quad (12)$$

Next, the four types of nucleotide, A, G, C and T, are translated into binary notation.

$$A=00, G=01, C=10, T=11 \quad (13)$$

Finally, the  $\alpha_X$  is described as a string of 100 bits (digits of value 0 or 1).

$$\alpha X = 0000101111101010 \dots 0100 \quad (14)$$

This  $\alpha_X$  must be encrypted for privacy protection using the secure hash algorithm-1 (SHA-1) for the same reasons as described above for STRs. The resulting DNA-ID (SNP) has a length  $\delta_X$  of 160 bits, according to the following transformation:

$$\delta X = h(\alpha X) \quad (15)$$

### 3.5. Verification using validation experiment (SNP)

As a validation experiment, the author analyzed 120 autosomal SNPs in 100 unrelated Japanese subjects using the TaqMan<sup>®</sup> method (Applied Biosystems), and built a Japanese SNP database for identification. Although several SNPs were located on the same autosomal chromosome, no correlation was found between alleles at any SNP loci. Furthermore, no significant deviation from Hardy–Weinberg Equilibrium (HWE) was detected. The matching probability (MP) of each SNP ranged from 0.375–0.465. The MP for 41 SNPs ( $3.63 \times 10^{-18}$ ), which have high MP in each loci, was very similar to the MPs obtained with the current STR multiplex kits, PowerPlex<sup>™</sup> 16 System (Promega) and AmpFISTR Identifier (Applied Biosystems), which were  $5.369 \times 10^{-18}$  and  $1.440 \times 10^{-17}$ , respectively in Japanese population.

### 3.6. Rapid analysis system of SNP

A reduction of the time required for DNA analysis is necessary in order to make practical use of DNA biometrics. In the STR system, it is difficult to decrease the analysis time because it is necessary to perform electrophoresis after PCR amplification. From DNA extraction to STR typing, the entire process takes 4–5 hours. However, there are many methods for analyzing SNPs that do not demand such a lengthy process. The author developed the SNP typing methodology using the modified TaqMan<sup>®</sup> method, which is capable of amplifying the DNA and typing the SNPs at the same time. The author modified the number of PCR cycles and the annealing/extension time, and selected SNP loci that yield successful results under the modified PCR conditions. This new method is capable of detecting and typing 96 SNPs within 30 minutes.

## III. IV PROBLEMS OF DNA BIOMETRICS

There can be no doubt that DNA-ID is potentially useful as a biometric. It has many advantages, including accuracy, strictness, discriminatory power (and ease of increasing this power), and the ability to use the same analysis platform all over the world. However, DNA polymorphism information is not widely used in biometrics at this point. The most serious flaw is that DNA analysis is time-consuming compared to other authentication methods. It takes at least 4 hours to get STR identification data by common methods used in forensic science. Most of the time required for DNA analysis is taken up by PCR amplification and electrophoresis. It is impossible to dramatically shorten the duration of these steps using existing technologies. SNP analysis may be faster, however: it is possible to analyze 96 SNPs within 30 minutes (Hashiyada, Itakura et al., 2009). Thus, a SNP system could use a specific usage, for example in passports or in very large-scale mercantile transactions

## IV. CONCLUSION

Development of biometric authentication technologies has progressed rapidly in the last few years. Personal identification devices based on unique patterns of fingerprints, iris, or subcutaneous veins in the finger have all been commercialized. All of these methods of verification are based on matching analog patterns or feature-point comparisons. Because they lack absolute accuracy, they have not yet achieved a universal standard. Among the various types of biometric information source, the DNA-ID is thought to be the most reliable method for personal identification. DNA information is

intrinsically digital, and does not change either during a person's life or after his/her death. The discriminatory power of the data can be enhanced by increasing the number of STR or SNP loci. The DNA-ID could be encrypted via the one-way function (SHA-1) to protect privacy and to reduce data length. Using the STR system, it is currently difficult to complete analysis within 3 hours; however, using the SNP system, it is possible to analyse 96 SNPs within 30 minutes. Both systems yielded verifiable results in validation experiments. The author also introduced the idea of DNA-INK as a practical application of DNA-ID.

DNA-ID has some disadvantages, as well, including long analysis time, ethical concerns, high cost, and the impossibility of discrimination of monozygotic twins. However, the author believes that the DNA-ID must be employed as a biometric methodology, using breakthrough methods developed in the near future.

## REFERENCES

- [1] Alberts, A. Jhonson, J. Lewis, M. Raff, K. Roberts, P. Walter, 2002 Molecular biology of THE CELL NY, USA: Garland Science. pp75-80
- [2] Anderson, et al. 1981 Sequence and organization of the human mitochondrial genome. *Nature*, 290(5806): pp.457- 465 .
- [3] T. D. Anderson, et al. 1999 A validation study for the extraction and analysis of DNA from human nail material and its application to forensic casework. *J Forensic Sci*, 44(5): 1053 1056 .
- [4] R. M. Andrews, et al. 1999 Reanalysis and revision of the Cambridge reference sequence for human mitochondrial DNA. *Nat Genet*, 23(2):pp. 147
- [5] A. J. Brookes, 1999 The essence of SNPs. *Gene*, 234(2): pp.177- 186 .
- [6] J. M. Butler, et al. 2004 Forensic DNA typing by capillary electrophoresis using the ABI Prism 310 and 3100 genetic analyzers for STR analysis. *Electrophoresis*, 25(10-11): pp.1397- 1412 .
- [7] J. M. Butler, 2010 Fundamentals of Forensic DNA Typing: ELSEVIER. pp.9-12
- [8] T. M. Clayton, et al. 1995 Identification of bodies from the scene of a mass disaster using DNA amplification of short tandem repeat (STR) loci. *Forensic Sci Int*, 76(1): pp.7- 15 .
- [9] F. S. Collins, et al. 2004 Finishing the euchromatic sequence of the human genome. *Nature*, 431(7011): pp.931- 945 .
- [10] P. Gill, 2001 An assessment of the utility of single nucleotide polymorphisms (SNPs) for forensic purposes. *Int J Legal Med*, 114(4-5):pp. 204- 210 .
- [11] E. Hagelberg, et al. 1991 Identification of the skeletal remains of a murder victim by DNA analysis. *Nature*, 352(6334):pp. 427- 429 .
- [12] F. N. Haque, et al. 2009 Not really identical: epigenetic differences in monozygotic twins and implications for twin studies in psychiatry. *Am J Med Genet C Semin Med Genet*, 151C(2): pp.136 141
- [13] M. Hashiyada, et al. 2009 Development of a spreadsheet for SNPs typing using Microsoft EXCEL. *Leg Med (Tokyo)*, 11 Suppl 1: pp.453 454 .
- [14] M. Hashiyada, Y. Itakura, T. Nagashima, M. Nata, M. Funayama, 2003a Polymorphism of [17] JSTRs by multiplex analysis in Japanese population. *Forensic Sci Int*, 133(3): pp.250 253 .
- [15] M. Hashiyada, Y. Itakura, T. Nagasima, J. Sakai, M. Funayama, 2007a High-throughput SNP analysis for human identification. DNA Polymorphism pp34-38 Official Journal of Japanese Society for DNA Polymorphism Research, 15 3
- [17] M. Hashiyada, S. Matsuo, Y. Takei, T. Nagasima, Y. Itakura, M. Nata, M. Funayama, 2003b The length polymorphism of SE33(ACTBP2) locus in Japanese population. *Practice in Forensic Medicine*, pp.46
- [18] M. Hashiyada, J. Sakai, T. Nagashima, Y. Itakura, J. Kanetake, S. Takahashi, M. Funayama, 2007b The birthday paradox in the biometric personal authentication system using STR polymorphism-Practical matching probabilities evaluate the DNA personal ID system-. *The Research and practice in forensic medicine*, 50: 5
- [19] J. Hedman, et al. 2008 A fast analysis system for forensic DNA reference samples. *Forensic Sci Int Genet*, 2(3): pp.184- 189 .
- [20] A. Jasinska, W. J. Krzyzosiak, 2004 Repetitive sequences that shape the human transcriptome. *FEBS Lett*, 567(1): pp.136- 141 .
- [21] A. J. Jeffreys, et al. 1985 Hypervariable 'minisatellite' regions in human DNA. *Nature*, 314(6006):pp 67- 73 .
- [22] A. J. Jeffreys, et al. 1992 Identification of the skeletal remains of Josef Mengele by DNA analysis. *Forensic Sci Int*, pp. 56(1): 65 76 .

## Biomedical Waste Treatment: A Case Study of some Selected Hospitals in Bayelsa State, South-South, Nigeria

Zekieni R. Yelebe<sup>1</sup>, Revelation J. Samuel<sup>2</sup> and Blessing Z. Yelebe<sup>3</sup>

<sup>1,3</sup>(Department of Chemical/Petroleum Engineering, Niger Delta University, Bayelsa State, Nigeria)

<sup>2</sup>(Department of Chemical Engineering, University College London, WC1E 7JE, United Kingdom)

**ABSTRACT :** *The treatment and disposal of solid medical waste from hospitals in Nigeria has been of growing concern in recent times. This is due to the hazardous nature of these wastes and the potential threat to spread deadly diseases to humans and other living organisms. To characterise and quantify these wastes, a study was carried out to ascertain the generation of biomedical wastes from ten hospitals in Bayelsa State, South-South, Nigeria. The hospitals were categorised into Tertiary, Secondary and Primary health institutions, and grouped into Public and Private owned facility. The result revealed that all the hospitals involved disposed their generated waste into municipal waste dumpsites without any form of treatment, leading to unhealthy and hazardous environment around the health institutions, affecting patients and staffs and the well-being of the general public. The study also showed that about 4330 kg total waste was generated per month by all ten hospitals of which 69% and 31% were generated by Public and Private hospitals respectively. The Tertiary, Secondary and Primary hospitals generate 69%, 28% and 3% of the total waste respectively and the average biomedical waste generated per bed per day was 0.18 kg. The study was concluded with recommendations for improvements on biomedical wastes handling and treatment in order to render proper and adequate waste disposal system in health institutions of Nigeria.*

**KEYWORDS:** *Biomedical wastes, health institutions, infectious waste, incinerator, segregation*

### I. INTRODUCTION

Good medical care is vital for life, health and general well-being and hospitals are health institutions that provide these services. Wastes generated from the hospitals, health care centres, medical research institutions, blood banks, medical laboratories, etc. [1], usually include sharps, human tissue or body parts and other infectious materials and is referred to as "Health care waste", "Hospitals solid waste", and or "Biomedical solid waste" [2, 3].

While waste management has become a critical issue which has taken a central place in the national health policies of developed nations and is attracting considerable interest, in most developing countries like Nigeria, the handling and treatment of municipal solid waste (MSW) or domestic waste have not received sufficient attention [4]. In most developing countries like Nigeria, the management, treatment, and handling of medical waste is often very poor as medical wastes are still handled and disposed together with municipal solid waste into landfills and/or open municipal dumpsites at various locations within the cities [5]. Yet only about 75-90% of the waste is non-risk while the remaining 10-25% of medical waste is hazardous, creating a variety of health risk for the municipal workers, the general public and the environment, because of the presence of infections biological, hazardous and radio-active waste materials [6].

In Nigeria, for example, this unwholesome medical waste disposal practices may be attributed to ignorance, lack of awareness of the potential dangers this poses to the health of the people and the environment, including ground water, the high cost of effective and efficient management and handling of the waste by the authorities concerned, lack of strict laws and policies or enforcement of the laws governing the disposal of the medical waste by government agencies. Another important factor that may be responsible for this poor waste management practice is the problem of corruption, generally affecting all section of government agencies and parastatals. Furthermore, valuable information's on the definitions, nature, classification, generation rate, method of collection, storage and disposal of medical waste is very scarce.

The aim of this study therefore, is to evaluate the actual situation of medical waste management in Bayelsa State, South-South, Nigeria, with a view of:

- (i) Quantitatively determining the types and quantity of medical waste generated,
- (ii) Examining the existing waste management practices and its compliances with standard international produces for biomedical waste management and
- (iii) Making useful contribution and suggestion to Government and hospital authorities were necessary on how best to handle the waste so as to minimize risk and protect human lives and the environment from pollution.

## II. METHODOLOGY

### 2.1 Study Area

Bayelsa State with its capital, Yenagoa, is located in the Niger Delta Region, South-South of Nigeria. The state has a population of about 2 million people [7]. Presently, the State Government through the Bayelsa State Environmental Sanitation Authority is responsible for the collection and disposal of municipal solid waste through private companies contracted to carry out these services. Disposal of the municipal solid waste mixed with the medical waste with no treatment at all is carried out, in open municipal dumpsites along Tombia-Amassoma road, and this has led to serious environmental and social problems in Yenagoa, the state capital.

### 2.2 Sampling and Data Collection

A general survey of the operating procedures practiced in the handling, treatment and disposal of medical waste was carried out on some government and private hospitals present in the state with the capacity to handle simple to fairly complicated health problems. These hospitals, which may be classified as secondary health care centres, were examined to determine the nature and quantity of wastes generated, including their waste management practice.

Table 1: Inventory of Health care facilities sampled

Hospitals	Category	Hospital Type	Number of Beds
A	Tertiary	Public	154
B	Tertiary	Public	102
C	Tertiary	Private	82
D	Secondary	Public	74
E	Secondary	Private	54
F	Secondary	Private	48
G	Secondary	Private	38
H	Primary	Public	24
I	Primary	Public	20
J	Primary	Public	15
Total		10	611

Detailed information was collected from each ward/department/labouratory by means of structured questionnaires administered on the appropriate category of staff in the wards and departments of each hospital. Each field worker engaged during the study was fully kitted with protective wears.

Polythene bags were provided for each ward/department/depending on the expected waste generation rate. The waste were sorted out into different components and measured after every 24 hours. Waste generation rates were obtained on weight basis as described by Sangodoyin and Coker [8] and Silva et al [9]

The waste generated in the hospital kitchen and restaurants, and the soiled clothes sent to the laundry were not included in the study.

## III. RESULT AND DISCUSSION

### 3.1 Assessment of Operating Procedures

During this study, it was observed that majority of the hospitals investigated had no waste management department or plan. There is also no training programme for the sanitary workers. Only hospital C and E has a pit used for burning some waste.

### 3.2 Segregation

The best way to reduction and effective management of biomedical waste is segregation and identification of waste. This can be achieved by sorting the waste into colour coded polythene bags of containers. Investigation revealed that all ten hospitals gave priority to segregation of sharps, biohazardous and infectious wastes. These wastes are segregated at the point of generation in the wards/department using cylindrical sharp aluminium containers fitted with polythene bags inside, for easy disposal. However, these segregated wastes are mixed together with other types of waste generated in the hospitals at the external waste storage facility during collection and disposal at municipal dumpsites, thereby endangering the lives of the sanitary workers, general public and the environment. It was also observed that the collection of these wastes from the external storage facilities within the hospital premises and subsequent disposal at the municipal dumpsites by the contracting firms is not regular.

### 3.3 Waste Generation

Investigation revealed that none of the hospitals had records of volume and kind of waste they generate making this the most difficult aspect of evaluation during this survey. Table 2 presents the details of various kinds and quantity of biomedical waste generated by each of the ten hospitals investigated. The results are presented with average values on a weight basis (kg/day).

Table 2: Waste Generation Rate (Average values)

Nature of waste	Hospitals										Cumulative	
	A	B	C	D	E	F	G	H	I	J	Kg/d	%
Infectious waste	24.67	11.79	8.45	8.23	4.04	2.80	2.70	0.43	0.30	0.32	63.73	44.74
Sharps	5.31	1.12	0.90	1.90	0.88	0.88	0.65	0.51	0.48	0.20	12.83	8.88
Pharceutical	3.20	2.02	1.30	-	1.02	1.12	0.35	-	-	-	9.01	6.24
Radiological waste	3.26	1.01	1.00	-	0.98	0.89	0.29	-	-	-	7.43	5.14
Non-infectious waste	19.62	8.58	6.72	5.45	3.72	3.07	2.15	0.50	0.42	0.28	50.51	34.99
Total Generation	56.06	24.52	19.20	15.58	10.64	8.76	6.14	1.44	1.20	0.80	144.34	100
Total Generation/bed/day	0.36	0.24	0.23	0.21	0.20	0.18	0.16	0.06	0.06	0.05	0.18 kg/bed/Day	

The data presented in Table 2 summarizes the average quantity of biomedical waste generated by all ten hospitals. The result shows that these ten hospitals cumulatively generate approximately 4330 kg of medical waste per month, of which only about 35% is non-infectious. Which means that, the remaining 65% is hazardous and about 44.74% is infectious, and while the remaining 20.26% (consisting of sharps – 8.88%; pharmaceutical waste – 6.24%; and radiological waste – 5.14%) is also harmful to human and the environment. Hence, 65% of biomedical waste generated by these hospitals is infectious and harmful to humans and the environment.

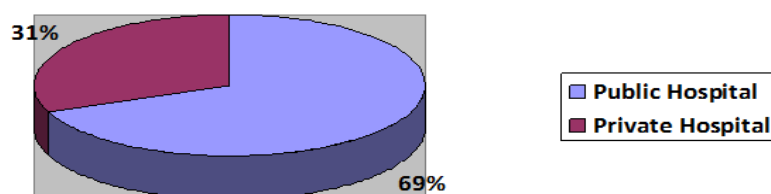


Figure 1: Percentage waste distribution by Hospital type

Fig. 1 shows that the public hospitals generate more wastes than the private hospitals. This shows higher patronage in the public hospitals, maybe due to low costs and proximity to residential homes especially in the rural areas. The average biomedical waste generation for the public hospitals is 0.16 kg/bed/day whereas that of the private hospitals is 0.19 kg/bed/day. This means that more waste is generated per bed in the private hospitals and potentially more severe cases are handled in the private hospitals.

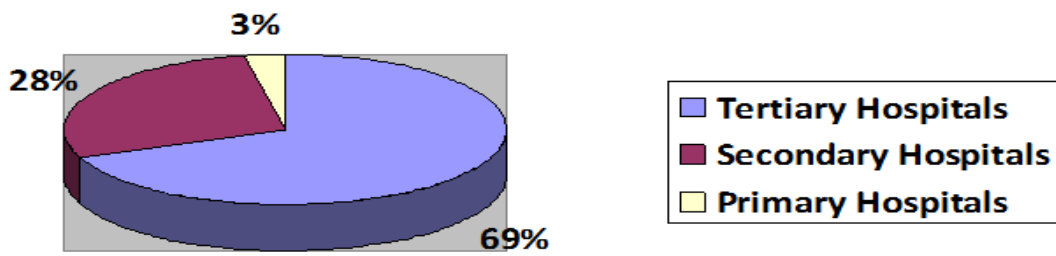


Figure 2: Percentage Waste distribution by Hospital Category

Fig. 2 shows the percentage biomedical wastes distribution based the hospital’s category. Tertiary hospitals generates an average 0.27 kg/bed/day approximately 69% of the total wastes generated by all ten hospitals whereas the secondary and primary hospitals generate an average 0.19 kg/bed/day and 0.06 kg/bed/day respectively. This distribution might be due to the location of these hospitals as the tertiary hospitals are all located in highly populated areas and the primary hospitals are mainly situated in the rural sparsely populated areas.

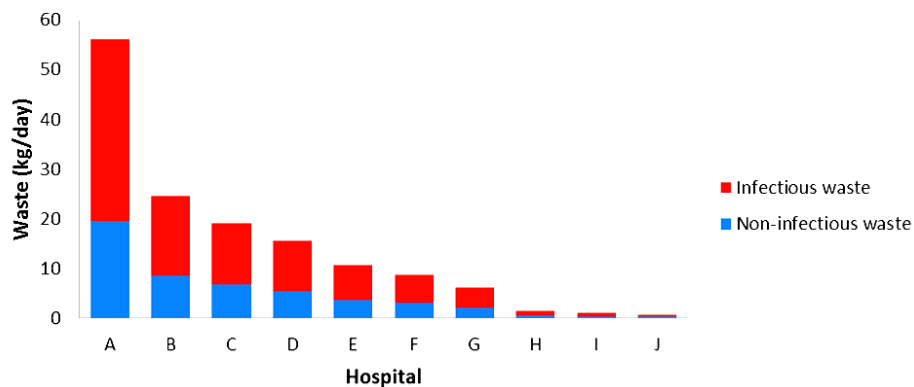


Figure 3: Hospitals Infectious/Non-infectious Waste distribution

Fig. 3 illustrates the daily distribution of infectious and non-infectious waste for all ten hospitals. All hospitals showed higher values of infectious wastes due to the classification of sharps, pharmaceutical waste and radiological waste as infectious wastes. The results also follow a descending order according the number of beds each hospital contains. The private hospital generated more pharmaceutical and radiological wastes compared with the public hospitals.

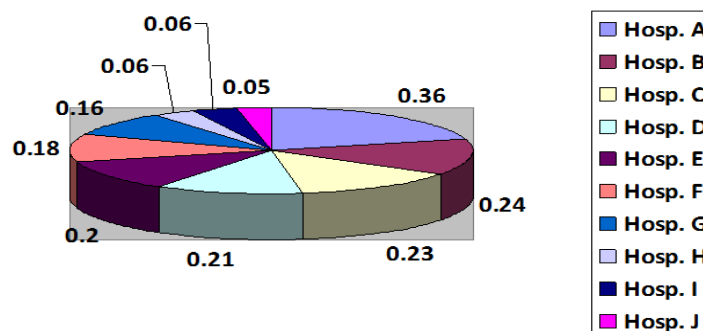


Figure 4: Hospitals waste distribution in Kg/bed/day

The result shown in Fig. 4 gives the average rate of biomedical waste generation for the ten hospitals as 0.18 kg/bed/day with (A – 0.36 kg/bed/day; B – 0.24 kg/bed/day; C – 0.23 kg/bed/day; D – 0.21 kg/bed/day; E – 0.20 kg/bed/day; F – 0.18 kg/bed/day; G – 0.16 kg/bed/day; H – 0.06 kg/bed/day; I – 0.06 kg/bed/day; J – 0.05 kg/bed/day) generated by the individual hospitals.

The average biomedical waste generation 0.18 kg/bed/day obtained in this study is relatively low compared with 1.27 kg/bed/day and 5.4 kg/bed/day for similar hospitals in Ibadan, Nigeria and Frieberg, Germany [5, 8]. It is also low relative to 6.6 kg/bed/day for a typical US hospital [10]. This low waste generation rate may be as a result of poor patronage of these hospitals due to the poverty, preference to alternative/traditional medicine, and religious beliefs and practices by the people living in the study area.

### 3.4 Final Disposal

This study showed that the present waste management practice employed by the sampled hospitals in Bayelsa State is poor. There are no incinerators in any of the health facilities for burning infectious wastes, and no form of treatment is carried out on the waste before disposal, except hospitals C and E, where there is an open pit used for burning some of the waste considered extremely harmful by the hospital authorities.

A visit to the municipal dumpsite along Tombia-Amassoma road revealed nothing more than open dumping and burning of these wastes, with human scavengers having a filled day looking for what they can pick, reuse or refurbish and possibly resell to the public without considering the health implications of their actions. This open burning practice and the leachate produced at these dumpsites poses a serious environmental problem to the atmosphere, underground water, surrounding rivers and the general well-being of the people.

## IV. CONCLUSION

Management of biomedical waste is a serious environmental problem in developing countries like Nigeria. This present study has shown that the hospital administrations, the state governments and indeed the government of the Federal Republic of Nigeria currently pay little or no attention to the management of biomedical waste in Bayelsa State and Nigeria at large. It is shown that hospitals in Bayelsa State generate an average of 0.18 kg/bed/day of medical waste leading to about 4330 kg/month, of which more than 65% is both infectious and hazardous to health.

From the investigations carried out, the following suggestions are made:

- (i) Every health care facility should have a waste management unit to seriously handle the waste management practice.
- (ii) Cleaners, Nurses and sanitary workers handless should be properly trained.
- (iii) Sorting of wastes at source using the colour-coded system being practiced in countries like UK, India etc. should be introduced.
- (iv) Government should formulate and enforce laws on good waste disposal practices.
- (v) Government should ensure that health care facilities have good and functioning incinerators or provide a central incinerating facility where these waste could be taking to and treated before final disposal.

## REFERENCES

- [1] Patil G.V., and Pokhrel K., (2004) "Biomedical solid waste management in an Indian hospital: a case study. *Waste management* 2(5),592-599.
- [2] Baveja G., Muralidhar S., and Aggawal P., (2000) "Hospital waste management-an overview. *Hospital today* 5(9), 485-486.
- [3] Manohar D., Reddy P.R., and Kotaih B., (1998) "Characterization of solid waste of a super specialty Hospital a case study. *Ind. J. Environ. Health* 40(4),319-326.
- [4] Yelebe Z.R., and Puyate Y.T., (2012) "Effect of Bioaugmentation on aerobic digestion of biodegradable organic waste", *J. Appl. Technol. Environ Sanit.* 2(3)165-174.
- [5] Da Silva C.E., Hoppe A.E, Ravanello M.M., and Mello N.,(2005) "Medical wastes management in the South of Brazil". *Waste management vol.25, Issue 6*, pp.600-605.
- [6] Pruess A., Giroult E., and Rush Brook P., (1999) Editions: Sage Management of waste from health care activities, Geneva, WHO.
- [7] Report on Bayelsa State of Nigeria. [http://en.wikipedia.org/wiki/Bayelsa\\_State](http://en.wikipedia.org/wiki/Bayelsa_State)
- [8] Sangodoyin A.Y., and Coker A.O., (2005) "Case study Evaluation of Health care solid waste and pollution aspects in Ibadan, Nigeria" *Journal of Applied Science, Engineering and Technology*, vol.5, No.1&2: 27-32.
- [9] Da Silva C.E., Hoppe A.E, Ravanello M.M., and Mello N., (2007). "Medical Waste Generation in the Vacacai river basin-RS. In: *Proceedings of the sixth national seminar on solid waste, Gramado, RS, Brazil* pp. 1-15.
- [10] Rutala, W.A., Odette, R.L and Samsa, G.P., (1989) Management of infectious waste by US hospitals, *JAMA*, 262, 1635-1640.

## Development of Roofing Sheet Material Using Groundnut Shell Particles and Epoxy Resin as Composite Material

Jacob Olaitan AKINDAPO<sup>1</sup>, Umar Alhaji BINNI<sup>1</sup>, Olawale Monsur SANUSI<sup>2</sup>

<sup>1</sup>Mechanical Engineering Department, Nigerian Defence Academy, Kaduna, Nigeria

<sup>2</sup>Mechanical Engineering Department, Federal University Oye-Ekiti, Nigeria

**ABSTRACT:** *The present work is on the development of roofing sheet material using groundnut shell particles and epoxy resin as composite material. Three different samples of roofing sheets "A", "B" and "C" were prepared and produced from three different weight particle length sizes of 0.5mm, 1mm and 1.5mm at a weight ratio of 70:30 between epoxy and groundnut shell. The sample roofing sheets were cast manually and the rate of water absorption, tensile strength, impact and flexural strength due to bending and deflection were all experimentally evaluated. The sample specimen A with a particle length of 0.5mm have the lowest rate of water absorptivity value of 8.3% ,with the highest impact value of 29.65KJ/m<sup>2</sup>. Likewise sample B with a particle length of 1mm have the highest ductility and tensile strength of 2.356mm and 8.25N/mm<sup>2</sup> respectively. The results revealed that Groundnut shell particles can be used as reinforcement for polymer matrix for the production of roofing sheets. Sample "A" was adopted in this work because of its excellence performance properties.*

**Keywords:** *Composites, reinforcements, fibres, matrix, groundnut, roofing sheets.*

### I. INTRODUCTION

Emphasis on the development of new materials and technology for the building industry has been there for the past few decades, especially in developing countries or third world, so that the overall cost of construction becomes affordable by the people. If overall economy in the construction of shelter is to be achieved, then, economy in each major component of shelter to the extent possible has to be realized. Roof is one of the main building elements which constitute about 8% of the total cost of construction [1]. Asbestos cement based roofing and other light roofing materials such as long span Aluminum, Aluminium-Zinc, are very commonly used in the construction of houses and industrial buildings in all developing countries of the world or third world. In spite of the fact that asbestos based roofing elements and products pose health hazards, ban on their use has not been effectively enforced [2].

Composite materials are made by combining two or more materials to give a unique combination of properties, one of which is made up of stiff long fibres and the other a binder or matrix which holds the fibres in place [3].

Kelly [3] clearly stated that the composite should not be regarded as a mere combination of two materials. In the broader significance, the combination has its own distinctive properties in terms of strength or resistance to heat or some other desirable quality. It is better than either of the component along or radically different from either of them.

Beghezan [4] defined composite as compound materials which differ from alloys by the fact that the individual components retain their characteristic but are so incorporated into the composite as to take advantage only of their attributes and not of their short comings in order to obtain improved materials.

De S.K. *et al* [5] defined composite materials as heterogeneous materials consisting of two or more solid phase, which are in intimate contact with each other on a microscopic scale. They can also be considered as homogeneous materials on a microscopic scale in the sense that any portion of it will have the same physical property.

In the present study, Epoxy Resin is being considered as matrix material. Epoxy resin is a polymer containing two or more epoxy groups and has high mechanical properties due to its low shrinkage and relatively unstressed structures. Epoxy resin system exhibits extremely high resistance to alkali, good acids and solvent. It has good electrical properties over a range of frequencies and temperature. The cured epoxy systems generally exhibit good dimensional stability, thermal stability and exhibit resistance to most fungi.

They are self- excellent moisture barriers exhibiting low water absorption and moisture transmission [6].

Natural organic fibres have a very important role in the alleviation of the housing problem. They not only occur in luxurious abundance in many parts of the world, but can also lead directly to energy savings, conservation of the world's most scare resources and protect human and environment [7]. Natural and vegetable plants and fibres have thus a unique irreplaceable role in the ecological circle. Despite the fact that natural fibres generally have poor mechanical properties compared with synthetic fibres their use as reinforcement material has been adopted by mankind to make straw reinforced huts and other articles [8]. Their natural abundance, plentiful supply, relative cheapness and swift replenish ability are the strongest arguments to utilize them in the construction industry [9].

Groundnut botanically belongs to arches hypogea Linn of leguminous family. It is a self-pollinated, annual and herbaceous legume crop. A complete seed of groundnut is called pod and contain up to five Kermis, which develop underground in a needle like structure called peg, which grow into the soil and then converts into a pod. Groundnut has taproot system which has many nodules contain Rhizobium bacteria which are symbiotic in nature and focus atmospheric nitrogen. [41]

The outer layer of groundnut is called groundnut shell. The shell constitute about (25-35%) of the pod. Nigeria is one of the foremost producers of groundnut in the world, producing up to about 2.699 million matrix tones in 2008. Groundnut shell is found in large quantities as agricultural farm wastes in Northern part of Nigeria such as Sokoto, Kebbi, Kaduna, Borno and Yobe States [2].

Over the years, groundnut shell constitutes common solid waste especially in the developing part of the world. It's potentiality as a useful engineering material has not been investigated. The utilization of groundnut shell will promote cleanliness and increase the economic base of the farmer when such wastes are sold. This work therefore investigates the possibility of using groundnut shell matrix composites for the production of roofing sheets.

Previous research works by Khalid et al, Ngala and Nwankwo, Raju, Gaitondi and Kumarappa, Naidu et al, Iducula et al, Agrawal et al, Alsina, et al, Sada, Amartey and Bako, Chanakan A., Bensely A., Sanjay K., Sangita M., Dixit S., Brian George et al., [5 – 19] have been reviewed in this work.

## II. MATERIALS, EQUIPMENT AND EXPERIMENTAL PROCEDURES

### 2.1 Materials

The materials used for this research work were all sourced locally. These include:

- i. Groundnut shell
- ii. Epoxy resin (Bisphenol-A-Co-Epichlorohydrine)
- iii. Tetraethylenepentamine (Hardener)
- iv. Sodium hydroxide solution (NaOH)
- v. Distilled water
- vi. Wax

### 2.2 Equipment

The major items of equipment used for this work are as follows:

- i. Impact Testing Machine 100kg (Norwood)
- ii. Monsanto Tensometer serials No. 9875, UK (200KN)
- iii. Universal Material Testing Machine (100KN)
- iv. Thermal conductivity testing machine (Norwood)
- v. Metallic sieve of size 0.5mm, 1mm and 1.5mm.
- vi. Mixing Sterilizer
- vii. Metal Mould

## 2.3 Experimental Procedures

### 2.3.1 Specimen Preparation

The strength of the composite largely depends on the preparation of the shell. The groundnut shells were collected and sun dried. The dried groundnut shells were washed with water to take away the sand and other impurities. The washed shells were later treated with 10% sodium-hydroxide (NaOH) solution for two (2) hours and then washed with distilled water until the sodium hydroxide (NaOH) in the groundnut was eliminated. Subsequently, the shells were solar dried and hammer milled to reduce its size to smaller ones and then grinded in a machine and particles were sieved through 0.5mm, 1mm and 1.5mm BS sieves to obtain fine uniform shapes and get different sizes of groundnut shell particles. The three (3) different fine sieved particles were used as reinforcement material in the polymer matrix.

The low temperature curing epoxy resin (Bisphenol-A-Co-Epichlorohydrine) was dissolved in acetone and then mixed with tetraethylenepentamine in ratio of 10:1 by weight as recommended [20]. A prototype of a gerrad roofing sheet was used to design a metallic mould for the production process. The mould made of Aluminium was constructed for producing the sample roofing sheets. Aluminum material was chosen due to its availability, relatively low cost and resistance to corrosion.

### 2.3.2 Production Technique

Each composite consist of 30% groundnut particles and 70% epoxy resin (weight ratio 30:70). The designations of these composites are given in Table 1 below. A layer of wax was applied to the mould so that the specimen can be easily taken out of the mold. Measured quantities of groundnut shell particles and resin were taken in a plastic container and stirred thoroughly to get homogenous mixture. After adding a suitable quantity of hardener, the mixture was again stirred for ten minutes. The prepared composite was placed in the mould and compressed uniformly. Compression is done carefully to avoid buildup of air gap within the sample, the set up was allowed to cure for 8 hours at room temperature and then the sample roofing sheet was taken out from the mould, it was taken to an electric oven for 48 hours at 38<sup>0</sup>C for further curing. This procedure was repeated for each of the three specimens.

**Table 1: Specimen Composition**

Specimen	Composition
A	70% wt Epoxy + 30% wt shell particles (particles length 0.5mm)
B	70% wt Epoxy + 30% wt shell particles (particles length 1mm)
C	70% wt Epoxy + 30% wt shell particles (particles length 1.5mm)

## 2.4 Mechanical Tests

In the present study, tests were conducted to determine the following characteristics of the sample groundnut reinforced roofing sheets:

- i. Water absorptivity test
- ii. Flexural strength
- iii. Tensile Strength
- iv. Impact strength.

### 2.4.1 Water Absorptivity Test

The test quantifies the water absorptivity of the sample roofing sheets, this test is pertinent to measure its response to water leakage from the roof after or during down pour (rainfall). This test was carried out in accordance with international method for determination of water absorptivity test ASTM D 570 for all composite [21]. Three samples were cut from each mass fraction, weighted and soaked in water, cleaned, dried and re-weighted. The obtained data were recorded against each mass fraction and the mean value obtained. The percentage water absorptivity was calculated and recorded against each mass fraction. The percentage increase in weight during immersion was calculated using the following equation.

$$m = \frac{w - w_0}{w_0} \times 100\%$$

Where m, w, w<sub>0</sub> are the moisture absorption content, weight of dried and wet composite material respectively [21].

### 3.4.2 Flexural Test

This test was carried out in accordance with international method for determination of flexural test ASTM D654 [22], the sample sheets were subjected to a central line load over a sample supported span of 115mm. The sample roofing sheets were all tested in natural dry conditions and the load was measured using a 100KN proving ring load which was gradually applied till failure of specimen occurs.

### 2.4.3 Tensile Test

This test was carried out in accordance with international method for determination of tensile test ASTM D638 [22], on sample roofing sheets due to direct loads (gradually applied). A point load was applied along the center of the span of the corrugation. The maximum load at the point was noted, which gives the splitting load for the corrugated specimen.

### 2.4.4 Impact Test.

This test was carried out in accordance with international method for determination of impact test ASTM D256 [21]. Corrugation portion of a size 220mmx250mm was cut from the sample roofing sheet and used for the impact test.

The projectile was so arranged such that the impact took place exactly on the crown of the specimen. For each sample sheet, the number of blows required for the appearance or initiation of first crack at the Crown Point and the number of blows required for complete propagation of the crack along the line of the specimen were noted. The height of fall was fixed at 60mm which was based on a few initial trials conducted. The weights of the ball used were maintained constant throughout the test for all specimens.

## III. RESULTS, ANALYSIS AND DISCUSSION

### 3.1 Test Results

#### 3.1.1 Result of Water Absorptivity Rate Test

The results obtained from the Water Absorptivity Rate Test are indicated in table 1 below:

**Table 1: Rate of Water Absorptivity**

Specimen	Dry Pieces Weight (gm)	Weight of the Water Content (gm)	Average % of Water Absorption (%)
Specimen A	3.0	3.25	8.3
Specimen B	5.6	6.8	21.43
Specimen C	5.6	6.9	23.21

### 3.2 Flexural Test: Bending & Deflection

The result of the flexural test obtained for sample A, B, C are indicated in table 2 below:

**Table 2: Results of Flexural Tests**

Specimen A	width(mm)	Thickness (mm)	Load (KN)	Deflection (mm)
A1	52.0	5.5	130	1.941
A2	50.6	4.2	140	2.019
A3	53.6	4.7	160	2.192
Average A	52.06	4.8	143	2.051
<b>Specimen B</b>				
B1	54.8	4.0	90	2.128
B2	53.4	4.4	130	2.637
B3	53.0	4.7	130	2.304
Average B	53.7	4.4	117	2.356
<b>Specimen C</b>				
C1	52.0	3.7	80	1.748
C2	52.0	4.5	130	1.591
C3	53.4	3.6	130	2.387
Average C	52.5	3.9	113	1.907

### 3.3 Tensile Test

The results obtained for the tensile test is shown in table 3 below:

**Table 3: Result of Tensile Tests**

Specimen A	Width (mm)	Thickness (mm)	Cross Area (mm <sup>2</sup> )	Load (N)	Tensile Strength (N/mm <sup>2</sup> )
A1	11.4	4.1	46.74	400	8.56
A2	10.6	10.6	112.36	350	3.11
A3	10.6	10.6	112.36	300	2.67
Average A	10.9	9.8	30.9	350	4.78
<b>Specimen B</b>					
B1	10.3	2.5	25.76	160	6.21
B2	10.5	6.0	63	684	10.86
B3	10.2	5.2	53.04	408	7.96
Average B	12.3	4.6	47.3	584	8.25
<b>Specimen C</b>					
C1	10.0	2.7	27	276	10.22
C2	10.3	3.8	39.14	360	9.20
C3	10.0	5.5	55	228	4.15
Average C	10.1	4	40.4	228	7.86

### 3.4 Impact Test Result

The results obtained from the impact test is indicated in table 4

**Table 4: Result of Impact Tests**

Specimen A	Load KJ	Cross Section Area m <sup>2</sup>	Impact Value KJ/m <sup>2</sup>
A1	220	0.4674	10.28
A2	350	0.11236	39.33
A3	350	0.11236	39.33
<b>Average</b>	306.7	0.2307	<b>29.65</b>
<b>Specimen B</b>			
B1	300	0.02576	7.73
B2	350	0.063	22.05
B3	450	0.05304	23.87
<b>Average</b>	367	0.0473	<b>17.88</b>
<b>Specimen C</b>			
C1	200	0.027	5.4
C2	220	0.03914	8.61
C3	250	0.055	17.75
<b>Average</b>	223	0.0404	<b>10.58</b>

## IV. DISCUSSION OF THE RESULTS

### 4.1 Water Absorptivity Test

The purpose of water absorptivity test is to determine the amount of water that the roofing sheet can absorb during raining season or down fall in relation to its weight.

The percentage of water absorbed was computed to be 8.3% for specimen A with 0.5mm particle length, while specimen B and C with 1mm and 1.5mm particle length had 21.43% and 23.21% respectively, when soaked for 17hours.

Figure 1 below depicts the results graphically, from the result obtained, specimen A with 0.5mm particle length had the lowest percentage mean water absorptivity with a value of 8.3% followed by sample B with 1mm particle length had a value of 21.43%. Then sample C with 1.5mm particles length had a value of 23.27% respectively. The smaller the grain size, the better the bond, the lower is the water absorptivity ratio.

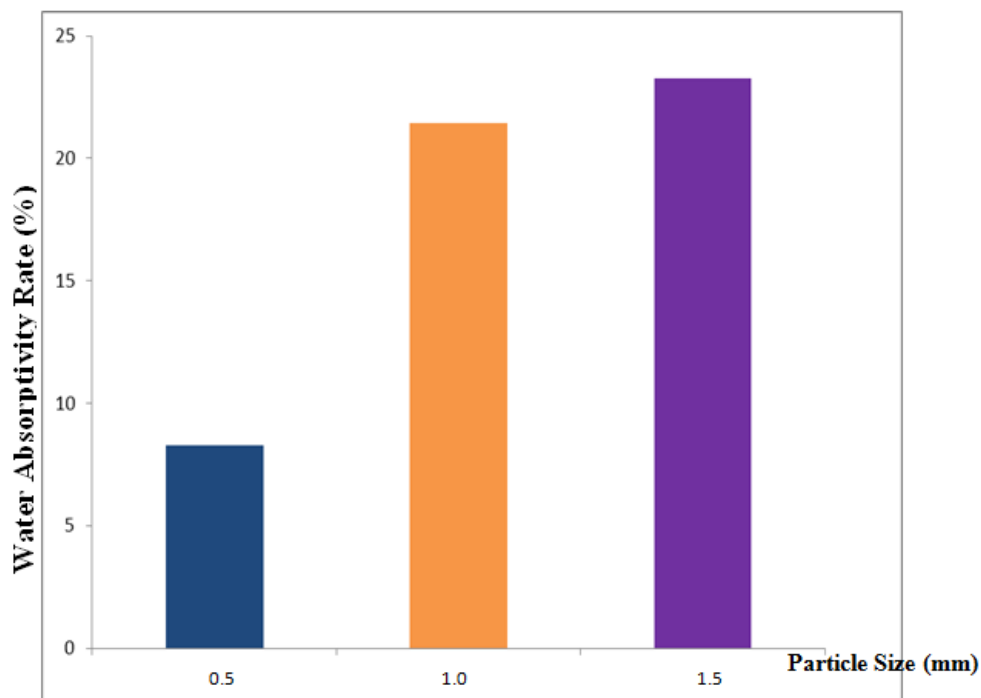


Fig1: Water Absorptivity Rate of Groundnut Shell Composite

## 4.2 Flexural Test

### 4.2.1 Flexural Test (Bending)

The flexural load is the minimum load the composite can bear before fracture during flexure or bending test. Figure 2 depicts the results graphically. Specimen B with 1mm particle length showed excellent ability to withstand the load before fracture with value of 140N. While specimen A and C with particle length of 0.5mm and 1.5mm had strength ability values of 117N and 113N respectively. Therefore the bending strength initially increase for grain size 0.5mm to 1.0mm before it latter dropped to 113N for 1.5mm where the bond turned out to be weak and brittle decreases as the grain size increases.

### 4.2.2 Flexural Test (Deflection)

Figure 3 below shows the mid-span deflection and toughness of each of the specimen. The specimen (B) with 1mm particles length showed the greatest deflection with value of 2.356mm signifying that it possessed the highest ductility followed by the specimen (A) with 0.5mm particle length with value of 2.05mm, specimen C with 1.5mm particle length had the lowest value of 1.907mm showing that it had a poor ductility and hence, most brittle of all the specimens. Therefore, ductility increases with grain size up to a maximum of 1mm beyond which it reduces.

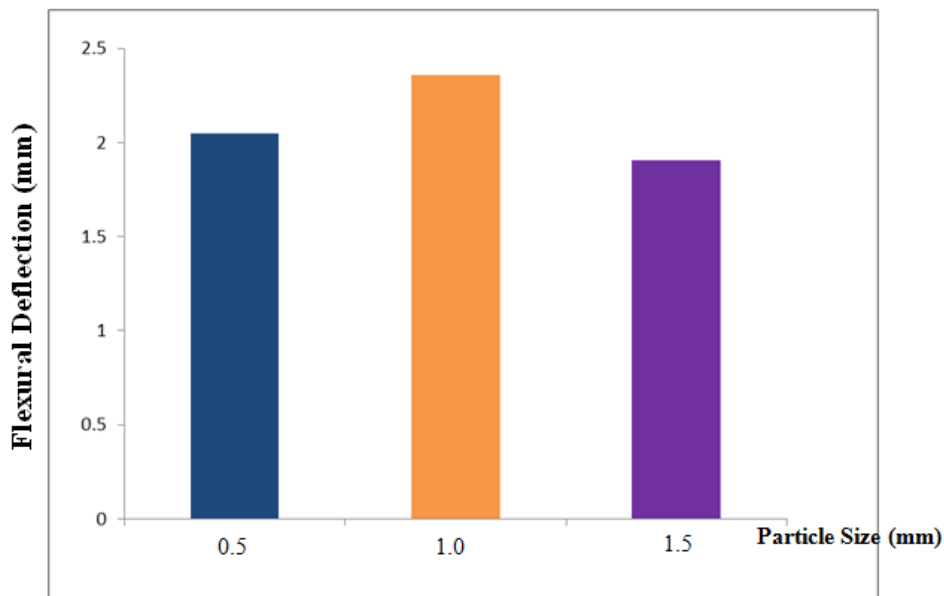


**Fig3: Flexural Deflection Strength of Groundnut Shell Composite**

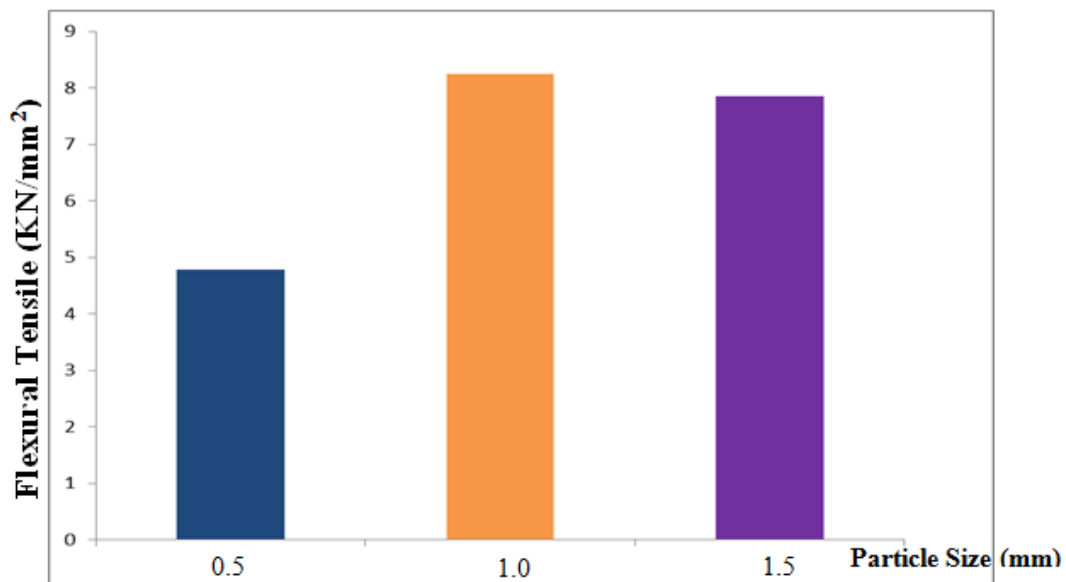


**Fig4: Flexural Tensile Strength of Groundnut Shell**

#### 4.2.3 Flexural Strength (Tensile)

Figure 4 above depicts the tensile test result graphically. Specimen B with 1mm particle length followed by specimen C with 1.5mm particle length had the highest strength of 8.25 N/mm<sup>2</sup> and 7.86 N/mm<sup>2</sup> respectively. While specimen A with 0.5mm particle length had 4.78 N/mm<sup>2</sup> strength value, therefore the strength increases with grain size up to maximum of 1.00mm beyond which the strength decreases.

#### 4.2.4 Impact Test

Figure 5 depicts the result of impact strength graphically. The impact energy absorbed by specimens A with 0.5mm particle length had a value of 29.65 KJ/m<sup>2</sup> followed by sample B with 1.0mm particle length which had a value of 17.88 KJ/m<sup>2</sup> while sample C with 1.5mm particle length had a value of 10.58 KJ/m<sup>2</sup>. Thus these indicate that sample A with 0.5mm particle length had the highest impact strength while sample C with 1.5mm particle length had the lowest impact strength.

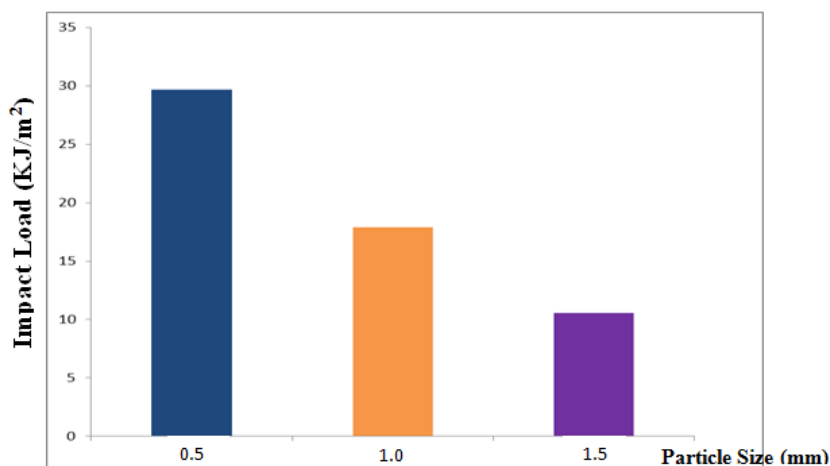


Fig5: Impact Strength of Groundnut Shell Composite

## V. CONCLUSION AND RECOMMENDATION

### 5.1 Conclusion

The aim of this work is to develop roofing sheet material from groundnut shell polymer matrix composite.

Three different grades of sample roofing sheets were produced, the samples differ from one another by varying the composition, epoxy resin proportion and particle sizes during production.

Based on the experimental investigation carried out on the produced sample roofing sheets, the results and analysis of the data obtained shows that:

- i. Sample A with 8.3% water absorption rate had the best and lowest rate of water absorption followed by sample B with 21.43% While C had the highest of 23.27% respectively.
- ii. Sample A with 140N had the highest strength before bending occurred while sample A and C fracture at the lowest values of 117N and 113N respectively.
- iii. Likewise sample B had the highest ductility value of 2.356mm followed by sample A with 2.05mm value, while sample C is the lowest with value of 1.907mm.
- iv. Sample B also had the highest tensile strength of 8.25 N/mm<sup>2</sup> followed by sample C and A with 7.86 N/mm<sup>2</sup> and 4.78 N/mm<sup>2</sup> respectively.
- v. Sample A had the highest impact value of 29.65 KJ/m<sup>2</sup> followed by sample B and C with 17.88 KJ/m<sup>2</sup> and 10.58 KJ/m<sup>2</sup> respectively.

Sample A and B have the best possible proportion to be taken into consideration for the production of commercial roofing sheets. Sample "A" was adopted in this work because of its excellence performance properties. The results revealed that Groundnut shell particles can be used as reinforcement for polymer matrix for the production of roofing sheets.

### 5.2 Recommendation

Further research work should be carried out on the design of the produced sample roofing sheets especially on the manufacturing process and finishing process. This could result in improved mechanical properties of the composite and reduce the cost of production. Further work in the following area is hereby recommended;

- i. Selection of other manufacturing processes other than hand layer up techniques.
- ii. The use of other types of polymer resins such as vinyl ester, polyester or other locally available bonding agent is to be investigated further and compare the result with the existing ones.
- iii. There is need for further study on how to control biochemical and environmental pollution in order to safe guard the life span of roofing sheets.
- iv. Coating should be carried out on the sample roofing to prevent corrosion.

## REFERENCES

- [1]. Ramakrishna, G., Sundararajan, T., and Kothandaraman, S., (2011), "Strength of Conjugations of a Roofing Sheets Reinforced with Sisal Fibres", ARPN Journal of Engineering and Applied Sciences, Asian Research Publishing Network (ARPN), Vol 6, No 12, Pg 24 – 32.
- [2]. Oladele, I.O., Akinwekomi, A.D., Aribi, S., and Aladenika, A.K., (2009), "Development of Fibre Reinforced Cementitious Composite For Ceiling Application" Journal of Minerals and Materials Characterization and Engineering, JMMCE.org Printed in USA, Vol 8, No 8, Pg 583 - 590.
- [3]. Kelly, A., (1967), "The Nature Of Composite Material", Sciences American Magazine, Kluwer Academic Publishers, No 217, Pg 161.
- [4]. Beghezan, C.T., (1990), "Fabrication and Performance of Natural Reinforced Composite Materials", Journal of Polymer Engineering and Science, Vol 35, No 35, Pg 970 - 978.
- [5]. Van S., (2012), "Coir Fabre Reinforcement and Application in Polymer Composites", Journal Of Polymer Engineering And Sciences, Vol 4, No 6, Pg 263 – 276.
- [6]. Raju, G.U., Gaintonde, V.N., and Kumarappa, S., ( 2012 ), "Experimental Study on Optimization of Thermal Properties of Groundnut Shell Particle Reinforced Polymer Composite", International Journal of Emerging Sciences, Vol 2 No 3, Pg 433 - 454.
- [7]. Aji, I.S., Ngala, G.M., and Nwanko, H., (2007), "Investigation of Groundnut Shell as a Composition Material", Continental Journal of Engineering Sciences, Wilolud online Journal, Vol 2, Pg 8-14.
- [8]. Al-Quresh, H.A., (1999), "The Use of Banana Fiber Reinforced Composites for the Development of a Truck Body", Second International Wood And Natural Fibre Composites Symposium, Kassel/Germany, Pg 1- 8.
- [9]. Swamy, R.N., ( 1990 ), "Vegetable fibre Reinforced Cement Composites-A False Dream or a Potential Reality"; Proceedings of Second International RILEM Symposium, 1st edition, Chapman and Hall London (ed. H.S Sobral), Pg 3 - 8.
- [10]. Mohanty, A.K., Misra, M., and Drzal, L.T., (2001), "Surface Modification of Natural Fibres And Performance of the Resulting Biocomposites: An Overview", International Journal of Emerging Sciences, IJES Publishing, Pg 313 - 343.
- [11]. Mohanty, A.K., Misra, M., and Hinrichsen, G., (2000), "Biofibres, Biodegradable polymers And Biocomposites : An Overview", Journal of Macromolecular Material And Engineering, JMME Publishing, No 276, Pg 1-24.
- [12]. Moji, A.B., (2001 ), "Polymers", The Chemistry And Technology of Modern Materials, First Edition, Concept Publications Limited, Pg 9 - 265.
- [13]. Khalid, A.A., Sahabi, B., and Khalid, Y.A., ( 1998 ), "Environmental Effects On The Progressive Crushing OF Cotton And Glass Fibre /Epoxy Composite Cones", Proceeding Of The Fourth International Conference On Advances In Materials And Processing Technology, The Arabian Journal For Sciences And Engineering, Vol 28, No 2B, Pg 268 - 275.
- [14]. Luo, S., and Netravali, A.N., (1999), " Mechanical And Thermal Properties Of Environmentally Friendly Green Composites Made From Pineapple Leaf Fibres And Poly Resin", Industrial Engineering Chemical Product Research And Development , Arabian Journal, For Sciences And Engineering, Vol 20, No 3, Pg 367-378.
- [15]. Smith, W.F., (1985), "Principles of Material Science And Engineering", Second Edition (2ed), Mcgrawhill Book Company, Pg 743 - 794.
- [16]. Naidu, A.L., Sudarshan, B. and Hari, K. K., (2013), "Study On Mechanical Behaviour of Groundnut Shell Reinforced Polymer Metal Matrix Composites", International Journal Of Engineering Research And Technology (IJERT), Asian Research Publishing Network (ARPN), Vol 2, No 2, Pg 1 - 6.
- [17]. Ragu, G.U., Gaitonole, V.N., and Kumarappa, S., (2013), "Experimental Study On Optimization of Thermal Properties of Groundnut Shell Particle Reinforced Polymer Composite", International Journal Of Emerging Sciences, Asian Research Publishing Network (ARPN), Vol 2, No 3, Pg 433- 454.
- [18]. Naidu, A.L., Sudarshan, B., and Krishna, H.K., (2013), "Study On Mechanical Behavior of Groundnut Shell Reinforced Polymer Metal Matrix Composites", International Journal Of Engineering Research And Technology (IJERT), Asian Research Publishing Network (ARPN), Vol 2, No 2, Pg 1 - 6.
- [19]. Agrawal, R., Sharma, N., Thomas, S., and Pothan, L. A., ( 2003 ), "Thermal Conduction and Diffusion Through Glass-Banana Fibre Polyester Composites", Indian Journal Of Pure Applied Physics, Asian Research And Publishing Network (ARPN), Vol 41, No 6, Pg 448 - 458.
- [20]. Raju, G.U., Kumarappa, S., (2011), "Experimental Study on Mechanical Properties of Groundnut Shell Particles Reinforced Epoxy Composites", Journal Of Reinforced Plastics And Composites, International Journal Of Emerging Sciences Publishing, Vol 30, No 12, Pg 1029 - 1037.
- [21]. Raju, H.U., Gaintonde, V.N., and Rumarappa, S., (2012), "Experimental Study on Optimization of Thermal Properties of Groundnut Shells Particle Reinforced Polymer Composite", International Journal Of Emerging Sciences , IJES Publishing, Vol 2, No 3, Pg 433 - 454.
- [22]. IS: 654-1997. Clay Roofing Tiles, Mangalore Pattern-Specification. BIS, India.
- [23]. Ramakrishna, G., and Sundaragan T., (2005), "Impact strength Of A Few Natural Fine Reinforcement Mortar Slabs", A Comparative Study Of Cement And Concrete Composite, Journal Of Engineering And Applied Sciences (ARPN), Asian Research Publishing Network, Vol 27, No 5, Pg 554 - 564.

## Problem Prevention Method for Product Designs Based on Predictive Technical Evaluation: A Study of Bolt-loosening Mechanisms in Automobiles

Ryota Nomura<sup>1</sup>, Kimihiro Hori<sup>2</sup>, Kakuro Amasaka<sup>3</sup>

<sup>1</sup>(Graduate School of Science and Engineering/ Aoyama Gakuin University, Japan)

<sup>2</sup>(Graduate School of Science and Engineering/ Aoyama Gakuin University, Japan)

<sup>3</sup>(School of Science and Engineering/ Aoyama Gakuin University, Japan)

**ABSTRACT :** This research investigates the mechanisms that cause bolt loosening, which is a concern for automobile manufacturers. Specifically, experimental analysis is conducted in order to ascertain stress distribution patterns when bolts loosen under vibration testing conditions. The insights gained from this analysis are then used to reproduce actual machine tests in a simulator based on a technical element model for highly accurate CAE analysis. Looking at pressure distribution on the nut seating surface (the trigger for thread loosening), the authors were able to clearly and rationally clarify the degree to which this pressure distribution impacted the contact points between nut and bolt threads. The results can contribute to the formulation of problem prevention methods for product design based on a predictive technical evaluation process that does not rely on actual machine testing.

**Keywords** -CAE, bolt-loosening, thread portions of nuts and bolts

### I. INTRODUCTION

In recent years, the authors have been conducting research on the establishment of highly accurate Computer Aided Engineering (CAE), which improves the reliability of product development and design. This research investigates the mechanisms that cause nut loosening in solid axle rear suspension, which is a matter of concern for automobile manufacturers around the world. Ultimately, actual machine tests revealed that the primary cause of loosening was due to uneven surface pressure distribution between the chassis nuts and the welded base (at the point where surface pressure was the weakest). Next, the authors used CAE Finite Element Modeling (which incorporates actual phenomena, modeling, algorithms, theory, and computers) to come up with a highly accurate numerical simulation that was then reproduced through actual machine tests. This made it possible to identify the key factors that cause loosening which were difficult to observe (visually confirm) through experimentation. Specifically, the causal relationship between (1) stress distribution (dynamic behavior) at the engaged thread portions of nuts and bolts, and (2) surface pressure distribution (dynamic behavior) at the contact point between the seating surface of the nut and the welded base, which directly contacts the area described in (1). The insights gained from these investigations were then successfully used to improve product development and design through highly accurate numerical simulations that do not rely on real-world testing.

### II. THE TECHNICAL ELEMENT MODEL

#### 1.1 A Highly Reliable CAE Analysis

Highly reliable CAE analysis refers to CAE analysis that produces results that do not deviate from those obtained during actual machine testing. Accuracy is further improved by taking the mechanisms discovered during actual machine testing and entering them into the CAE software. This helps achieve intelligent development design as well as shorter development times.

## 1.2 The Technical Element Model

This section focuses on bolt loosening. In order to more accurately reproduce actual machine test results with the aim of setting up a highly reliable CAE analysis, the authors developed the technical element model in figure 1 based on six principal factors. This model addresses the failure mechanism through steps (1.2.1) to (1.2.6) below.

### 1.2.1 Phenomenon

Based on the insights obtained through previous research, it was critical to logically identify the mechanism triggering the bolt-loosening phenomenon in bolted parts and to identify a physical phenomenon that could be numerically simulated.

### 1.2.2 Problem

Prior research on “the mechanism that loosens threads” indicates that uneven pressure on the nut seating surface has a major impact on the loosening of bolted parts. As a point for further research, note that it has not yet been determined how the fit between male and female threads, which is a source of stress, influences fluctuations in seating surface pressure values. For this reason, the authors chose to define the problem here as clearly determine the impact of stress generated from thread contact areas identified during actual machine testing. In order to research the problem, the authors visually represented the dynamic behavior of thread loosening and its mechanisms by assigning, the authors assigned actual measured values for parameters like thread dimensions, coefficient of friction for thread contact points, and load torque.

### 1.2.3 Model

In the modeling stage, the shape and dimensions of the target structure, Young’s modulus, the modulus of rigidity, and other material characteristic values were used to reproduce the phenomenon as a 3D model. In order to create a highly realistic reproduction during the analysis, the authors generated a fine mesh for the thread area, seating surface, and other critical contact points when applying the finite element method to break down the elements of the model. Since it was important to determine element size which convergence properties were taken into account for reason to prevent diversion of the output, the minimum element size for contact points in the model was set to 0.08 mm. Faithfully reproducing contact points between components also required that a valid contact force be defined for each contact surface. Augmented Lagrangian methods were implemented to avoid overlap with the model when element node loads for the fit between thread portions. Because the authors determined the properties and response phenomena of structures targeted by this modeling stage, numerical value settings and applied definitions could be precisely implemented—laying the groundwork for highly accurate CAE analysis.

### 1.2.4 Computer

Although computer technologies are largely reliant on the hardware and software used, it was necessary to select optimal settings from the perspective of the CAE model being employed in order to ensure analytical precision and realistic calculation times. The penalty method was used so that the non-linear analysis of bolted parts could be treated as a linear problem, while Augmented Lagrangian methods were employed in areas where generating highly accurate output was particularly important.

### 1.2.5 Theory

In order to accurately and faithfully replicate the identified phenomena in the numerical simulation, it was critical to logically identify the physical phenomena involved. The primary theoretical formulas used to assign selected actual measurement values as parameters were structural mechanics, the equation of equilibrium, and the coefficient of friction calculation method.

### 1.2.6 Algorithm

The finite element method is widely applicable, and was therefore used to analyze physical phenomena affecting complex structures. The thread contact portion between two screws has a complex shape, but the authors were able to calculate an accurate approximation by developing a model with minute element units and using it as the basis for their computations.

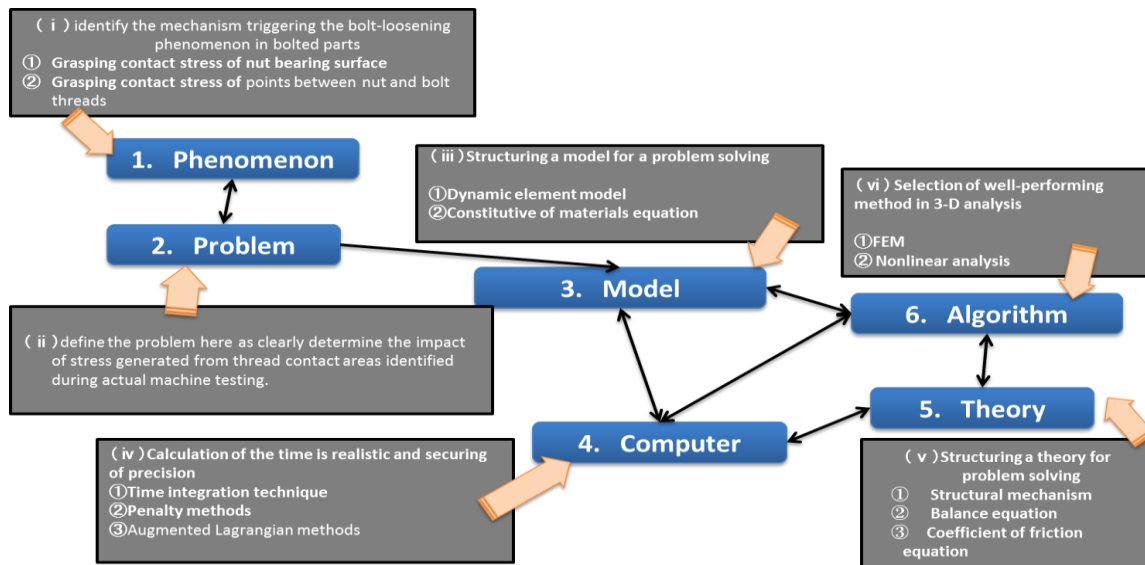


Fig.1The technical element model

### III. SAMPLE APPLICATIONS : USING CAE TO ANALYZE THE LOOSENING MECHANISM FOR BOLTED PARTS IN AUTOMOBILES

The authors next applied their predictive technical evaluation model in order to analyze the mechanism triggering loosening between bolt-tightened automotive parts. Specifically, they used the knowledge gained from their previous study indicating that uneven stress on the nut seating surface causes structures fastened with a nut and bolt to loosen. This allowed them to focus the current study on the thread contact areas between the nut and bolt.

#### 3.1 Actual Machine testing

Actual machine testing involved subjecting threads of different pitches to vibrational tests under the same conditions to see whether different thread specifications had an impact on the loosening of bolted parts.

To start, a six-sided nut and bolt with a flange were manufactured at the smallest (1.75 mm, figure 2) and largest (0.50 mm, figure 3) pitches and vibrational testing was conducted.

A strain gauge was first attached to the bolt axis and the test piece was tightened to a load of 80 N m. To estimate the amount of load to use during the vibration test, the authors applied static external force at a right angle to the axis and measured the load at which slippage occurred on the seating surface.



Fig.2 1.75mm pitch



Fig.3 0.50mm pitch

Next, a vibration load equivalent to  $\pm 90\%$  of the static extraction load was applied at a right angle to the axis, which is the primary trigger for loosening. The authors identified the phenomenon that triggered bolt loosening and measured the displacement trends in the bolt axial force relative to vibration time. Figures 4 and 5 below show the results of these tests. The figures indicate that the 1.75-mm pitch test bolts showed a loss of axial force at fewer repetitions than the 0.50-mm pitch test bolts. In other words, the length of the thread pitch impacts the way seating surface slippage is triggered, and was demonstrated to be a factor in the reduction of axial force.

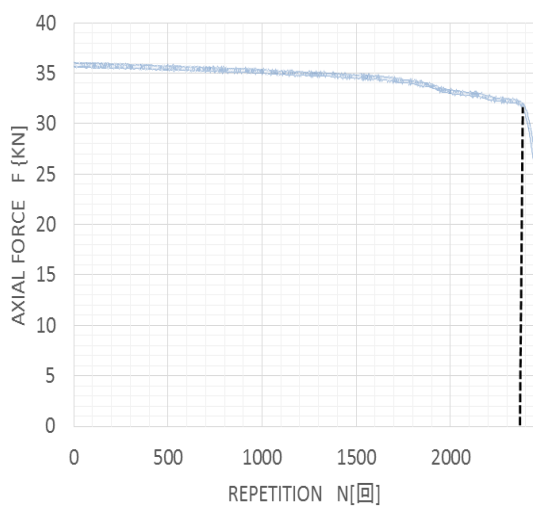


Fig.4 1.75mm pitch

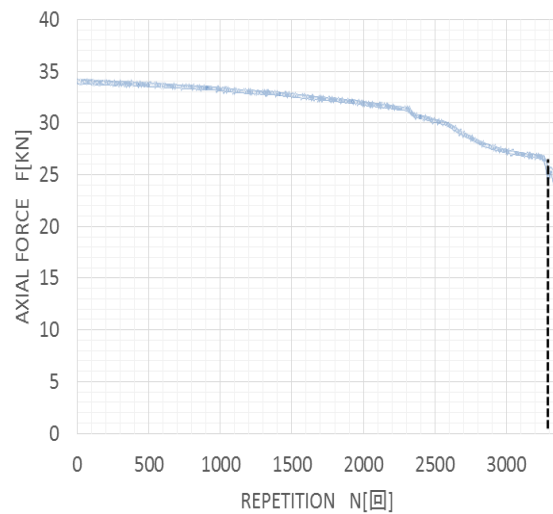


Fig.5 0.50mm pitch

**3.2 Numerical Testing**

Here, numerical testing were carried out under the same conditions as actual machine testing applying the technical element model in the last section. The analysis procedure had three steps. First, the fastened objects (two base plates) were placed between the nut and bolt. Second, the test pieces were subjected to the same loads during the test. Third, a vibration load equivalent to  $\pm 90\%$  of the static extraction load was applied at a right angle to the bolt axis. In this way, factors that could not be seen during actual machine testing (nut surface pressure distribution and distribution of stress on thread contact areas) could be ascertained.

Analysis results indicating the stress distribution on bolted parts are shown in figures 6 through 9 below. The test piece with a pitch of 1.75 mm caused surface pressure on the outside nut seating surface to drop significantly, and stress was found to be locally concentrated at the starting point of the thread. The piece with a 0.50-mm pitch (shallower thread angle) showed a stronger distribution of thread stress along the inside of the seating surface, but stress deviation was not particularly pronounced.

When we focus on the results of analyzing the thread contact surface, we see that the larger thread dimensions (the 1.75-mm piece instead of the 0.50-mm piece) experiences greater stress on each thread, and also shows a wider deviation in stress values along the seating surface. Using this information, the authors were able to clearly and rationally determine that different thread angles and thread dimensions were a factor in triggering uneven stress on the nut seating surface.

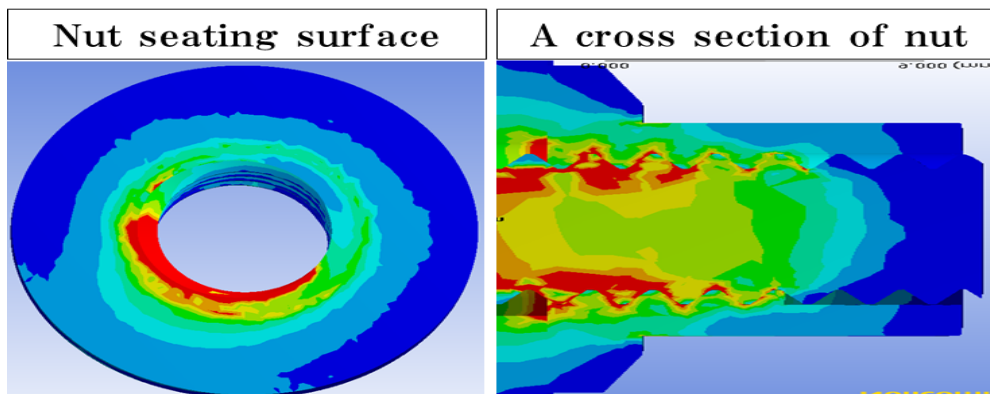


Fig.6 An analysis results: 1.75mm pitch

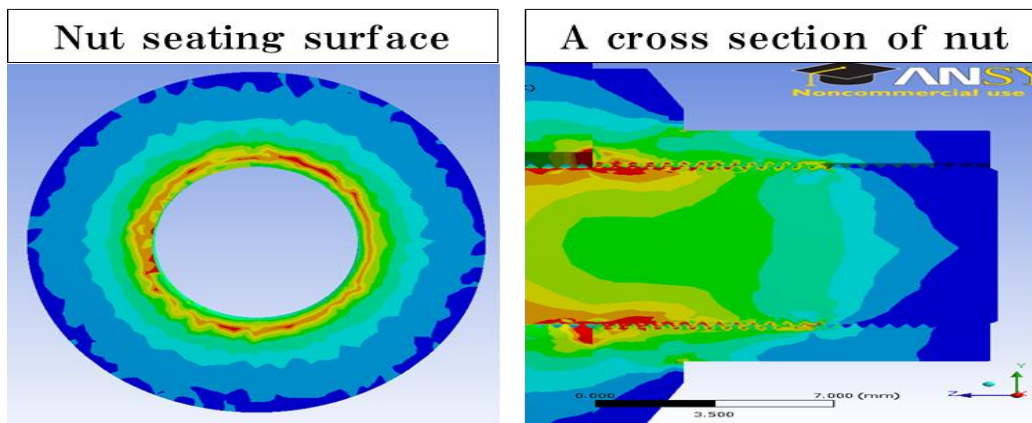


Fig.7 An analysis results: 0.50mm pitch

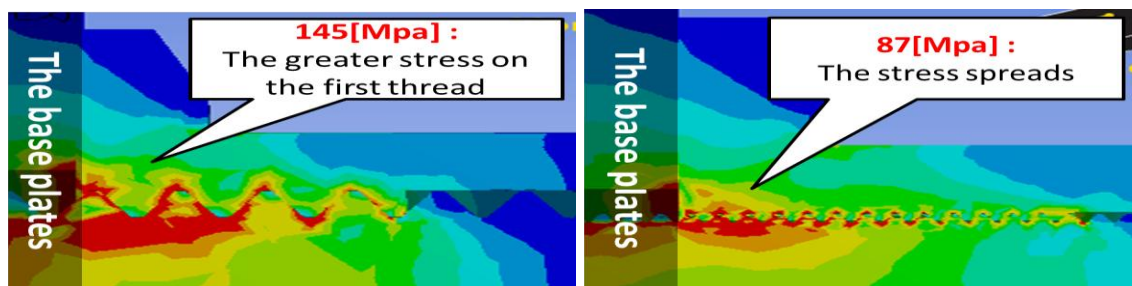


Fig.8 An enlarged drawing: 1.75mm pitch

Fig.9 An enlarged drawing: 0.50mm pitch

#### IV. CONCLUSION

In prior research, the authors clearly and rationally identified the mechanism that loosens bolts, and were able to visually represent a phenomenon that is difficult to observe in actual machine testing; namely, stress distribution along the nut seating surface. Here, the authors take the next step and visually represent the dynamic behavior of the thread contact points that generate stress during tightening, clarifying the causal relationship that determines how much impact the starting point of the thread affects stress distribution along the nut seating surface. The given results can be used to help establish product designs based on predictive technical evaluation.

#### REFERENCES

- [1] K. Amasaka, Proposal and Effectiveness of a High Quality Assurance CAE Analysis Model: Innovation of Design and Development in Automotive Industry, Current Development in Theory and Applications of Computer Science, *Engineering and Technology*, 2(1/2), 2010, 23-48.
- [2] K. Amasaka and M. Yamaji, CAE Analysis Technology for Development Design Utilizing Statistical Sciences, *The Open Industrial and Manufacturing Engineering Journal*, 1, 2008, 1-8.
- [3] K. Amasaka and T. Onodera, Developing a Higher-cycled Product Design CAE Model: The Evolution of Automotive Product Design and CAE, *International Journal of Technical Research and Applications*, 2(1), 2012, 17-28.
- [4] K. Hashimoto and K. Amasaka, Researching Technical Prevention Measures for Development and Design Utilizing Highly-Accurate CAE Analysis: Automotive Nut loosening Mechanism, *IOSR Journal of Mechanical and Civil Engineering*, 11(4), 2013, 24-27.
- [5] T. Onodera and K. Amasaka, Automotive Bolts Tightening Analysis using Contact Stress Simulation: Developing An Optimal CAE Design Approach Model, *Journal of Business Research Mechanical*, 10(7), 2012, 435-442.
- [6] T. Onodera T. Kozaki ,and K. Amasaka, Applying a Highly Precise CAE Technology Component Model: Automotive Bolt-Loosening Mechanism, *China-USA Business Review*, 12(6), 2013, 597-607.
- [7] T. Ueno, M. Yamaji, H. Tsubaki, and K. Amasaka, Establishment of Bolt Tightening Simulation System for Automotive Industry Application of the Highly Reliable CAE Model, *International Business & Economics Research Journal*, 8(5), 2009, 57-67.
- [8] H. Yamada and K. Amasaka, Highly-Reliable CAE Analysis Approach-Application in Automotive Bolt Analysis, *China-USA Business Review*, 10(3), 2011, 199-205.
- [9] S. Kasei, W. Yoshida, H. Ishibashi, and M. Okada, Bearing Surface Slip and Self-loosening of Threaded Fasteners, *Proc. JSME Annual Meeting*, Japan, 2003(4), 67-68.
- [10] M. Zhang and Y. Jiang, Finite Element Modeling of Self-Loosening of Bolted Joints, *Analysis of Bolted Joints*, *ASME Journals of Mechanical Design*, 478, 2004, 19-27.
- [11] E. Alba, *A New Class of Algorithms* (Parallel Metaheuristics, London: Addison Wihey, 2005).
- [12] R. C. Whaley, A. Petitot, and J.J. Dongarra, Automated Empirical Optimization of Software and the ATLAS Project, *Parallel Computing*, 27(1-2), 2001, 3-7.

## Impact of rejection of non-industrial wastewater treated origin: savex case in batambo district of second Bangui

Koyassambia Marcel Landry<sup>1</sup> Prof Li Jiang Feng<sup>2</sup>, Dr Zaguy Raoul G<sup>3</sup>Poungo Nicole Elizabeth<sup>4</sup>, Nzoussi Hilaire Kevin<sup>5</sup>, Bangala Yamokito Sandrine<sup>6</sup>.

*School of Public Administration, China University of Geosciences, Wuhan*

**ABSTRACT:** For many years, cities around the world in general and the CAR (Central African Republic) in particular have seen a very alarming pollution problem sometimes sparking fears. This pollution is due both to industrial activity than human activity in the case of deforestation for agricultural reasons. The growth of the urban population of the city of Bangui foreshadows an increase in demand for goods and services at all levels of environmental pressures resulting from the activities of the latter. The degradation of the urban environment in Bangui is the corollary of several factors that require adequate resources to cope. Which implies the establishment of a suitable environmental policy in order to save not only the wells for the consequences of pollution are many factors and other waterborne diseases but also people of the dangers against pollution.

**KEYWORDS:** Impacts, Wastewater, Industrial, Savex, Bangui.

### I. INTRODUCTION

Environmental Protection requires special attention with regard to industrial activities which, because of the processes of manufacturing and processing of raw materials into finished products, use a significant amount of water. (Arnaud, 1998)

Wastewater chemical composition some of which may possibly have a toxic character more or less marked, and contribute to the deterioration of the quality of groundwater percolation into the ground.

The growing success of industrialization corollary of diversity including the pollution of surface water and groundwater. Today, the use of water is more than necessary in the manufacture of various products including the residual waste (solid, liquid or gaseous) are dangerous for the environment such as air, water and soil. (Balkiabiya, 2008)

The protection of the environment in African cities in general and in particular in Bangui poses enormous problems. The establishment of the plant in an urban setting generates unprecedented degradation of the urban environment populations Batambo in the second district of Bangui.

Faced with damaging consequences to the environment caused by the discharge of industrial effluents on processing defined by the WHO, it is necessary to analyze the need for treatment of effluent prior to discharge into nature to realize the harmful nature of the effects they produce on the environment. (Diawara, 2010)

However, industrial development in the city of Bangui, and implementation of SAVEX soap in the second district specifically Batambo the neighborhood, which pours its liquid toxic waste in the canals and kouanga Dékongo directly pollute surface and ground water causing danger and nuisance's effects for the well being of the residents of that neighborhood.

In Bangui, the high filling of wetlands and stagnant sewage in living environments, floors and drains reflect the dysfunction of sanitation of solid and liquid waste and the difficulty to maintain wellbeing. (Dorier - April, 2002)

Water, a natural resource essential to life, has become directly or indirectly, the leading cause of death and disease in the city of Bangui in general and in particular, Batambo. Water stocks on earth should be able to renew themselves naturally, but unfortunately, some human activities (domestic, industry and agriculture) seriously pollute ground water, *sources 'potable water.*( Miras C, .2010)

In general, the Man eats and drinks about 80% of water and in developing countries, 80% of diseases are caused by water. According to the WHO 1.6 million children (21% of infant mortality) die each year due to unsafe water, lack of basic sanitation and poor hygiene.

Two decades after the United Nations Conference on Sustainable Development held in Rio de Janeiro (Brazil) in 1992, the world is always striving to achieve the ambitious goals that have been set. An estimated 1.5 billion people still lack access to safe drinking water and 2.5 billion lack access to sanitation services. Also, nearly one billion people live in slums, a figure expected to double over the next 30 years

1. <http://www.eau-artois-picardie.fr/article.php3?idarticle=p14>

The industry is characterized by considerable use of water, and therefore rejects a significant amount of waste water, carrying different manufacturing residues which chemicals are associated. In this context, our study will focus on determining the impacts of wastewater discharged by SAVEX that seeping into the soil and contaminate well water.

## 2. Study area

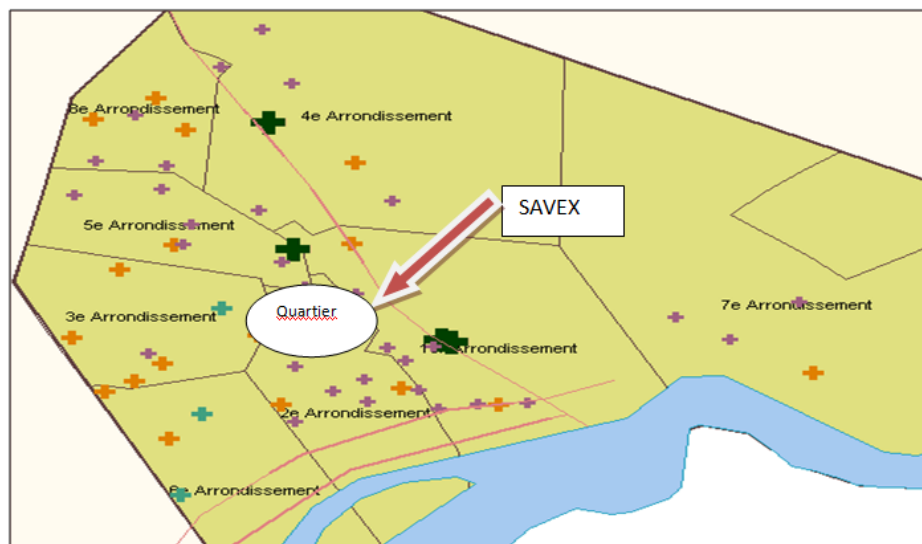


*Photo 1: SAVEX plant Bangui*

Bangui (CAR) covers an area of 623,000 km<sup>2</sup>. According to the General Census of Population and Housing 2003 (RGPH03) and projection 2012, the RCA has 4,663,731 inhabitants.

Bangui, CAR capital, covers an area of 67 km<sup>2</sup>. It has a population of 778,989 inhabitants, with a density of 11,059 inhabitants per km<sup>2</sup> (RGPH 2003) projection 2012. The climate is Guinean forest with the alternation of two seasons: a rainy season from March to mid December, with a strong involvement in the pollution of waters swamp and a dry season from January to February. Bangui is divided into eight district which in turn include several neighborhood .These districts are divided into 16 groups and 205 districts.

The second district has been created by Ordinance No. 88/006 of 12 February 1988. It is composed of two groups erected in 26 districts, including the Batambo district is in the second group with a population of 5436 inhabitants according to the general census of 2003. The area is between 04 ° 21.9'58 'north latitude and 18 ° 33.5'75' east longitude.

It is bounded to the east by the Bordeaux area (1 and 2), to the west by the district Yapélé and Bakongo, to the north by Sica 2 district, south by the district and M'bélé Kingoma.

## II. POLLUTION

Pollution is defined as "an adverse change in the natural environment that appears in whole or in part, as a byproduct of direct or indirect human actions, altering the criteria for distribution of the flow of energy from the production level of the constitution physicochemical natural environment and abundance of living species. The changes can affect humans directly through agricultural resources, water and all organic elements. They can also affect by altering physical objects it owns. »

In 1994, RCA began a participatory and decentralized process of preparing its strategy for the management of natural resources and protection of the environment. At the level of policy formulation and the development of environmental programs, the National Environmental Action Plan (NEAP) is the strategic reference framework for environmental planning. As such, it gives a high priority to the integration of environmental considerations into macroeconomic planning. Also, the industrial sector is it arrested in the first place, to the impacts caused on the environment and natural resources, both in construction and by their use. Once again, we do not see the applicability and feasibility of this law by the state.

### 4.1 The pollution of well water in the neighborhood Batambo

Pollution of water from wells in the area Batambo comes from two distinct factors:

- ✓ The first factor is related to the poor state of waste water pipe containing toxic products from the factory SAVEX and its location relative to the inhabitants of Batambo neighborhood.

### 4.2. Water pollution

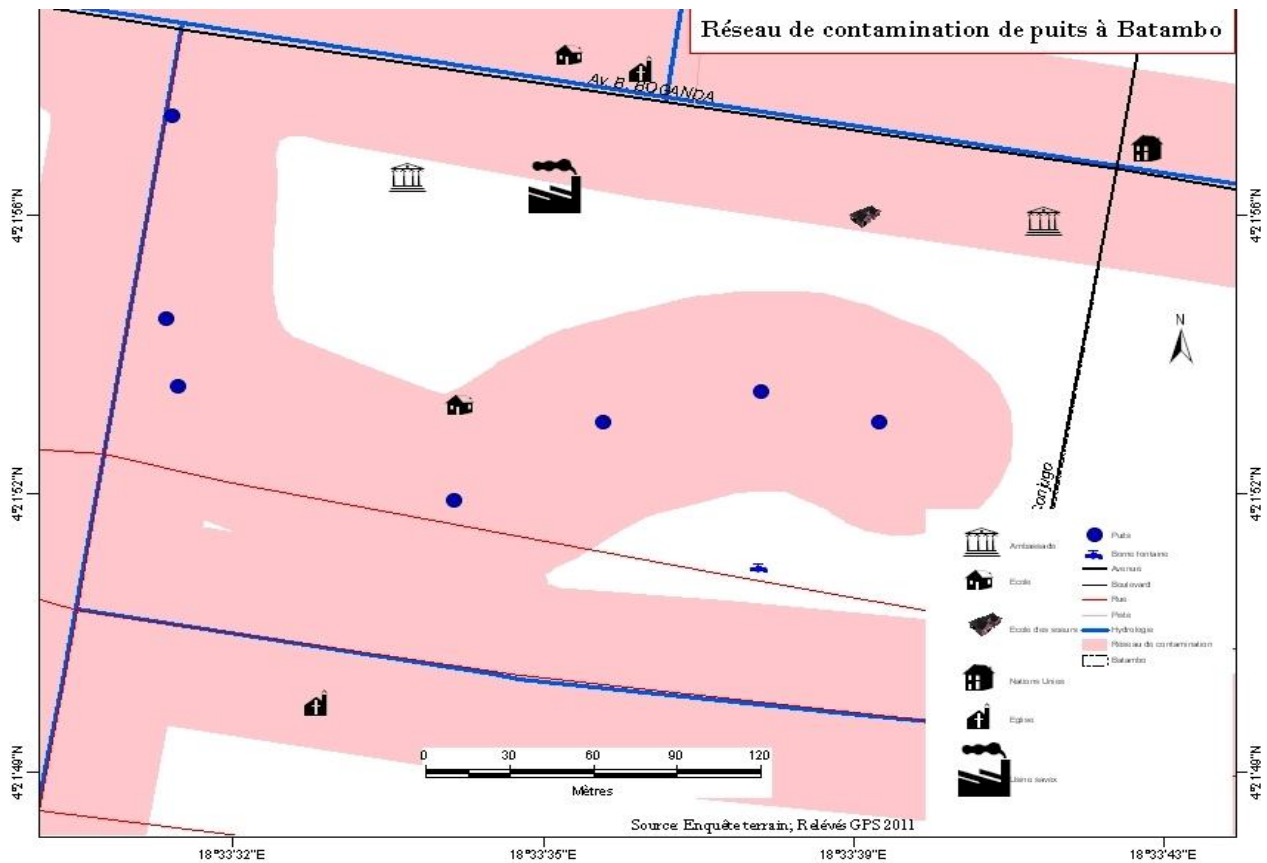
*In general, the Man eats and drinks about 80% of water and in developing countries, 80% of diseases are caused by water.* According to the WHO 1.6 million children (21% of infant mortality) die each year due to unsafe water, lack of basic sanitation and poor hygiene. Two decades after the United Nations Conference on Sustainable Development held in Rio de Janeiro (Brazil) in 1992, the world is always striving to achieve the ambitious goals that have been set. An estimated 1.5 billion people still lack access to safe drinking water and 2.5 billion lack access to sanitation services. Also, nearly one billion people do they live in slums, a figure expected to double over the next 30 years. In 2006, diarrheal diseases and malaria were respectively 1.5 million and 1.3 million deaths. (UN-Water / WWAP, 2006). In 2002, about 2.6 billion people lack adequate sanitation and 80% of these people live in sub-Saharan Africa and Southeast Asia. This situation is exacerbated by poverty, which is a major barrier to access to adequate sanitation services. In fact, two out of three people do not have access to clean water survive on less than two dollars a day. Reduce the vulnerability of these populations by giving them better access to water and sanitation services is thus a factor in the fight against poverty and reduce waterborne diseases.

The water supply for agriculture is sometimes insufficient in many parts of the globe; the reuse of untreated wastewater in irrigation poses serious health risks because the untreated sewage is a factor conveying pathogens and chemicals hazardous to the human body and all of nature. (Diawara, 2010)

Monitor the quality of water consumed therefore has a fundamental importance for the life of man on earth. Water should be preserved from all stain, not what becomes a disease vector for humans. According to the World Health Organization (WHO) in the world, one billion people lack access to safe drinking water and three-quarter (3/4) live on the African continent.

Such is the case in Central African Republic in general and particularly in Batambo area in the second district of Bangui, which he is the object of our study. Statistics taken from the field show those 75 surveyed households, 50 households or 66.66% are in danger because they use well water to meet most of their daily needs. However, the wells of this district are polluted.

Figure 2: Network contamination of wells



Source: Laboratory of Geographic and Cartographic Climatological Studies (The ACCEG)

The residues of products used for the manufacture of soaps are made in the shallow drainage channel which is located on the Avenue Bartholomew BOGANDA. (ATEUKENG 2012) In 2002, about 2.6 billion people lack adequate sanitation and 80% of these people live in sub-Saharan Africa and Southeast Asia. This situation is exacerbated by poverty, which is a major barrier to access to adequate sanitation services. In fact, two out of three people do not have access to clean water survive on less than two dollars a day. Reduce the vulnerability of these populations by giving them better access to water and sanitation services is thus a factor in the fight against poverty and reduce waterborne diseases.

The image below shows the discharge channel wastewater from Savex (Figure 4)



Photo 4: discharge channel wastewater from SAVEX (Source: ML Koyassambia, 2010)

A less rain, the canal waters containing residues of toxic products of plant SAVEX beyond his usual bed and walks in plots adjacent to it and create flooding. These flood waters, their towers and flow into the wells of the area that are Batambo plant downstream. Therefore, the well water of this town takes the yellowish color.

- ✓ The second factor is related to the construction of wells that are still in the traditional way and does not take into account the rules of hygiene and sanitation required by WHO.

The wells in this area are in circular shape, surmounted by a drum cut in half and build a curb which consists of a few pieces of scrap metal recovery that is consolidated with the earth. This artisanal construction does not guarantee a true seal the wells, as shown in this figure below.



**Photo 3:** Water color and without the disorder (SOURCE: Landry KOYASSAMBIA)

In some wells, we observed a lack of coping. They are in constant contact with the outside world: water runoff, dust, leaves etc.

Furthermore, the container used to draw water from the well is always put on the ground after use. By this way, impurities and pathogens are introduced into the wells.

In France for example, the volume of waste water produced is 150l / person / day, ecological damage caused by their release into the wild is now punishable by law, and after, the polluter pays principle, polluters must pay compensation for damage to the environment at the level of the injury. (CROIX ROUGE FRANÇAISE 2009)

Also in South Asia, sanitation coverage for 40% of the poorest households did not increase from 1995 to 2008. ( Zhongguo Qingnian Bao,2007) Between 1953 and 1960 MINAMATA in Japan, 111 people died or were severely intoxicated following the absorption of fish and shellfish that contain high levels of organic mercury. Then followed the disease-ITAI-OUCH OUCH ITAI or resulting from contamination by cadmium. Chemical contamination of the water can also be natural. Thus, according to a survey by the British Geological Survey in 2001, contamination of groundwater by arsenic in the bedrock of the Brahmaputra basin in Bangladesh threatens the lives of nearly 75 million people. Since the idea of chronic poisoning caused by heavy metals originated among toxicologists and toxicologists (Idem)

Same in Africa South of the Sahara, according to a UNDP report, 63% of the African population has no access to basic sanitation. Furthermore, only 10% of wastewater is treated before their return to the wild. Thus, a two Africans suffering from waterborne disease which 90% are children under 5 years (WASTE, 2006).

According to a study by the United Nations Environment Programme (UNEP) published in March 2011, approximately 51 million people in the Democratic Republic of Congo (DRC), or three-quarters of the population do not have access to the drinking water, even if the country holds more than half of Africa's water supply. Conflict, environmental degradation, urbanization and lack of investment in infrastructure have seriously affected the availability of drinking water.

Many deaths have been reported in Lagos, Port Harcourt and Kaduna in Nigeria due to industrial pollution around some chemical manufacturing plants that have accidentally spilled toxic chemicals in surface water lying near them.

As a result, wastewater is discharged directly or in river beds or in the sea and cause huge health and environmental problems. Their treatment is low due to the dilapidated state of treatment infrastructure. Thus, to support himself, he uses the raw wastewater in irrigation as additional water resources. This is a factor to adverse effects on the health status of the population and not only the environment application area but also in all of entire cities.

To this end, a physicochemical analysis allowed us to determine the organoleptic aspect of poor water quality of some wells, the Batambo neighborhood.

**4. PHYSICO-CHEMICAL ANALYSIS OF WELL WATER DISTRICT BATAMBO**

For this analysis, ten wells were taken.

**4.1. Checks the quality of well water**

Given the objective assigned to our work, only a few analyzes deemed important physicochemical parameters were performed in order to have an idea about the quality of well water in the study area. These parameters are: temperature, hydrogen potential, color, conductivity, suspended matter and dissolved oxygen.

**4.2. Organic and chemical composition**

Liquid wastes include dissolved solids and settleable solids and non-settleable suspended. Organic matter concentration is obtained by analyzing the Biochemical Oxygen Demand (BOD5) and Chemical Oxygen Demand (COD). First, BOD5 represents the amount of oxygen required by microorganisms for five (5) days to break down organic matter in sewage 200C. While the COD is the amount of oxygen required to oxidize the organic material using the dichromate in an acid solution to convert it into carbon dioxide (CO2) and water (H2O). ( French development Agency,2011)

The value of COD used to test the strength of non-biodegradable waste water is always higher than that of the BDO5 used to test the strength of treated municipal wastewater or not. (14) In general, the types domestic wastewater contained 50% carbohydrate, 40% protein and 10% fat, with a pH of 6.5 to 8.0 (14).

The industries release into the environment chemical pollutants such as heavy metals (cadmium, lead, etc.), nutrients (nitrogen, phosphorus), artificial chemicals (pesticides, hydrocarbons, etc.) and natural chemicals (chloride, sodium, fluorine, arsenic, etc.) for adverse effects on the ecology and human health and in some cases toxic phenomena.

**4.3 Health risks**

The combined presence or one of these organic chemicals above is likely to result in the individual being exposed to various conditions. The following table lists the different risks that can have adverse effects on human health and the environment.

**Table 1: Table of different risks of contamination**

Types of hazards		Enes pathogenic agents
infectious	Bacterial Second	Vibrio cholerea Salmonella typhi Shigella Leptospira legionellosis
	viral	Ent erovirus Adenovirus Rotavirus Hepatitis A Virus
	parasitic	Historica Entamoeba, and Giardia lamblia Balantidium coli. Bilharzia Intestinal parasites (roundworms, pinworms, hookworm ...)
	Fungal	Mycoses (pool)
Chemicals	Min 'meeting	Normally pr ESENT but harmful in excess: calcium, sodium ... Abnormal presence: mercury, arsenic, chromium, Lead ...
	physical	
	organic	
	thermal	Pheating of the water
	radioactive	center near nuclear

*Source: "The health and environmental risks of wastewater discharge in Ngoa-Ekellé neighborhood in Yaounde." FEUDJEU DEFO Paul Ines 2011. [9bis]*

Wastewaters have impacts on human health but also its living environments.

#### 4.4 On the environment

To appreciate the magnitude of the problem and its consequences on the lives of the population, it is significant to watch, sewage flowing in the streets, garbage everywhere present, habitat types, clogged gutters waste, excreta in public places, the state of the roads, and environmental management infrastructure.

This lack of processing infrastructure management has significant impacts on the quality of the natural environment (contamination of groundwater, degradation of ecosystems) (WASTE, 2006). These impacts can be observed on several types of waters.

##### ✓ Surface water

When wastewater is discharged directly into the natural environment, we notice the excessive presence of phosphates; in particular, promote eutrophication, which can ultimately lead to death of fish and other aquatic organisms that live there. (Ateukeng, 2011)

##### ✓ Groundwater

The quality of the ground water can be degraded by sewage, if the sealing of the wastewater treatment plant or lagoon is defective or when the individual sewerage system is dysfunctional.

#### 4.5 On the human health

Sanitation is strongly related to public health because of the many diseases observed in humans living in an unhealthy environment. In Batambo area, proximity to populations with sewage can cause diseases faecal-oral transmission. Wastewater conveys a large number of micro-organisms (viruses, bacteria, protozoa, helminths etc.). These more or less pathogens that pose a real danger to health. (Mouchili Mfome, 2008) If this untreated wastewater directly discharged into water courses, lagoon or spread on the floor, they can cause contamination of crops, surface water and groundwater. These are also the discomforts associated with traditional latrines that favor the proliferation of mosquitoes, cockroaches and bad odors in the living environment of the people. The first category of diseases related to water quality (cholera, typhoid, hepatitis, polio) results from the contamination of water by human waste, chemicals or animal and can be avoided by simple treatment of water. The second category is derived from aquatic organisms such as worms that spend part of their life in water and another as parasites.

The most known diseases identified at Batambo are typhoid, and schistosomiasis. Next come the diseases due to water-related vectors such as malaria, trypanosomiasis, yellow fever, filariasis and dengue fever, which are most prevalent in the world. Finally, we can note serious social consequences (modest rate of access to the small school) and economic (rising care costs, loss of the number of actual working days). (Mouchili Mfome, 2008)

### 5 DISCUSSIONS

These analyzes are performed simultaneously in different circumstances, because the first was made directly after the rain while the second was conducted without any rain; but all analyzes gave almost similar results we try to demonstrate. The water quality depends on the nature of its environment. The middle of the geological and hydraulic training can have influence on the water. In our study area, we worked in a sandy and clayey formation because the area is swampy. Groundwater is a victim of runoff threats and sometimes infiltration of various elements: The distance between latrines and wells is not respected; deposits of household garbage, wastewater discharges by the nearby factory houses affect well water. That's the reason for the contamination of wells Batambo area waters.

Before any discussion we have referred to European standards of raw water and drinking water recognized by the Central African state to assess the quality of the analyzed well water. The waters are classified into three grades: A1, A2, A3, and a class off class (HC)

Poor water quality; disturbed fish life; use for cooling water for navigation, water for irrigation. Water of very poor quality; cannot be used for the processing of drinking water. At the end of our analysis, we assessed the results based on campaigns carried out by the graph below:

The temperature is not in itself a water potability parameter as it depends on the nature of the water which is to be analyzed. Well water and drilling elevated temperatures compared to that of the water surface; because they constitute what is called "groundwater". The temperature values are slightly higher than that fixed by the standards discussed as well water, these values are acceptable.

PH influence on the most chemical and biological mechanisms in the water, for example carbon dioxide is present in the water in various forms in equilibrium. Thus, pH-meter, the dominant form is the bicarbonate ion; carbon dioxide is only found at acidic pH (companion report of well water in the 5<sup>e</sup> and 8<sup>e</sup> district, "water team Hydro Lavoisier Laboratory Science" 2007). These values correspond to the nature of the

deep shallow aquifer that feeds the water of traditional wells. According to the standards, the pH value is between 6.5- 9 for drinking water, our tables give us an alternative value of 5.72 - 6.81 it shows that almost all of the examined wells of acidic water .

As we mentioned earlier, the color of water depends on the material contained in this water, and then it is well water that are not even protected, our results demonstrate that three quarter ( $\frac{3}{4}$ ) analyzed wells have the color that does not meet the standards set at 15mg / l of Platinum in reference to the scale Platinum / Cobalt.

Well n° 2 has a water stain that far exceeds the values of European standards. This is due to discharges of wastewater from the factory, as well as the household rubbish dumps. The lack of roads in this area causes a large-scale pollution of well water. The conductivity measurement for assessing quickly but about the overall mineral water and to monitor progress.

The guideline value of the mineralization is set to a value less than 600 $\mu$ s / cm. The results of our analysis show that the wells in the vicinity of the plant contain many minerals that we see during our two companions. During these three well companions (P2, P3, and P4) have extremely high values, indicating the presence in the wells of considerable mineralization. These minerals are not highlighted because all physicochemical parameters characterizing pollution have not been carried out.

**Comment:** all the wells studied, turbidity has much higher standards; as shown on the above curves. This high turbidity could be explained by the fact that water wells analyzed in our study, are used by lots of people for lack of hydrants in the countered. High turbidity is often a sign of pollution. This setting prevents the propagation of light, the intensity decreases and it causes eutrophisation phenomena in certain cases.

Regarding the dissolution of oxygen, there is no ambiguity because the results obtained in our analyzes show that the standards are met. This standard is 3 mg / l O<sub>2</sub>.

As for total suspended solids (TSS), following the state are the wells and from the nature of the use of water in these wells, MY far exceed the standards (0 mg / l); because most of these wells are not covered or sometimes covered by old sheets.

As a partial conclusion, the study that has been conducted basically involves the illegal occupation of industries (SAVEX) from the ground and planning gaps in the major part of the city of Bangui, particularly in study area were causing the degradation of not only the human living environment, but also water from traditional wells in the Batambo neighborhood. This motif abundantly justifies the proliferation of traditional wells as the main mode of household food, depending on the network of water whose access is limited and conditioned. Unfortunately, the quality of this widely used resource problem for the local population because of the implications for public health that it induces.

Merely the degree of pollution which these wells have can be classified in class A2; Average quality water that requires normal physical treatment, chemical treatment and disinfection;

## 6. CONCLUSION AND RECOMMENDATIONS

Through this study we showed that the city of Bangui in general and especially Batambo district faces several environmental problems. At this stage, we can affirm the hypothesis that SAVEX would be partly the cause of the pollution of water wells nearby. A soil and geological study of the area and is located Batambo Savex the plant would also be necessary to determine if the soil quality is also a source of pollution of wells in the area.

To improve the water quality and saving of the dangers linked to pollution of the water, a few suggestions are necessary: Users must reduce the use of this well water. The plant must be sealed rejection network of these effluents. NGOs working in the field of water must conduct a development wells and regular disinfection of the wells. The government facilitated access to water SODECA. Prohibit anarchic settlements factories in the city center. Build roads that meet international standards while taking into account the quality of the rocks on the ground. Increase the budget allocated for mayor of the city while avoiding the financial mismanagement which is a blockage in the management of the urban structure responsible to clean up the city. (Arnaud, 1998) All this implies a rational management of well-trained human resources and dynamic.

## REFERENCES

- [1]. Arnaud M, 1998 Dynamics of urbanization in Africa south of the Sahara, Paris, MAE and ISTE
- [2]. Anonym 2009 general report of the International Workshop of training of national actors in the management of municipal wastewater in coastal cities of Cameroon, Buea, from June 29 to July 03, 2009, p 5.
- [3]. ATEUKENG M René, 2012, court treatment of wastewater and concept structures, EITMS-GS Yaoundé,
- [4]. Balkiabiya K.D.S, 2008, Spatial dynamics and environmental problems of the city Brazzaville, UMNG, memory CAPES
- [5]. Diawara A.B, 2010 Solid Waste in Dakar. Environment, society and sustainable management, University of Bordeaux III, PhD thesis
- [6]. Dorier - April E, 2002, Management of the urban environment and municipalization in West Africa; If Mopti (Mali) in other hand
- [7]. Feudjeu D. P. I., 2011, Environmental release of wastewater district Narayanan-Ephraim in Yaoundé and health risks. Memory
- [8]. French Development Agency 2011, water in Cameroon sector: issues and lessons,;
- [9]. French Red. Cross, Water, 2009, Hygiene and sanitation a challenge to improve the standard of living of populations
- [10]. MFOME (BW), 2008, Impact environmental and health of the pollution of the Abiergue River at a place called 'market coal of Mokolo; 2nd promotion facilities engineering of reform,
- [11]. Miras C. 2010, urban services drinking water and sanitation in Morocco or the requirements of the emergency in Geocarrefour, vol.85/2.pp119-126
- [12]. <http://www.eau-artois-picardie.fr/article.php3?idarticle=p14>
- [13]. Zhongguo Qingnian Bao, 2007, "the Yellow River transformed into garbage dump," in mail international No. 853, from 8 to 14 March 2007, p. 34

## Effect of variation of pick density on the properties of jute fabric samples woven in S4A loom and a comparative study with the standard fabric (IS 12650: 2003 2nd revision)

Prof. Swapan Kumar Ghosh<sup>1</sup>, Mr. Rajib Bhattacharyya<sup>2</sup>, Mr. Chinmoy Dey<sup>3</sup>

<sup>1</sup>(Professor, Department of Jute and Fibre Technology, University of Calcutta, India)

<sup>2</sup>(Senior Research Fellow, Department of Jute and Fibre Technology, University of Calcutta, India)

<sup>3</sup>(Junior Research Fellow, Department of Jute and Fibre Technology, University of Calcutta, India)

**ABSTRACT :** The variation of pick density of the jute fabric samples, woven in multiphase, shuttleless S4A loom, effecting the physical, mechanical and hydraulic properties of those fabric samples have been investigated in this article. An attempt has been made in this work to make a comparative study between the properties of jute fabric samples woven in S4A loom with respect to that of the standard fabric used to manufacture jute bags for packing 50 kg of foodgrains as per Bureau of Indian Standards (IS 12650: 2003 2nd revision).

**Keywords** –pick density, breaking strength, bursting strength, apparent opening size, BIS.

### I. INTRODUCTION

Textile products play a vital role in meeting man's basic needs [1]. The backdrop of growing global concern for environment concomitant with the alarming danger of carbon foot-print generation amalgamated with non-biodegradability and higher toxicity generation from the use of synthetic fibres have created an urge to come back to natural fibres, thereby opening new market opportunities [2]. The growing disinclination to use artificial fibres and an increasing preference for natural fibres is reviving the importance of the latter like jute, cotton, flax, sisal, hemp, coir etc. [3]. The Textile Industry should attempt to play a pathfinder's role to facilitate natural fibre competitiveness in a global context. For orienting natural fibres from its present status of struggle against other alternatives, mainly synthetics, in the area of packaging to a positively prospering commodity having diverse applications, the Industry shall have to appreciate the versatility and all the positives of natural fibres, overcoming their deficiencies and evolving commercially viable product lines for their use in the future. To meet the dynamics of ever-changing demand-driven market the Textile Industry will have to orient and sensitize the manufacturers, researchers, technologists, end-users, stake-holders towards new design, products and technological innovation [4]. That would require not only the identification of the potential products made out of natural fibres but also urges development of specifications in consultation with manufacturers and end-users. Good quality fabrics and high weaving efficiency cannot be achieved unless a suggested woven fabric construction is weavable and does not exceed the limit, that is, the maximum number of ends and picks per unit length that can be woven with given yarns and weaves [5]. When trying to weave a fabric with construction close to the limit or higher than the limit, the fell of the cloth would creep beyond the reed's furthest forward position and bumping would occur. This is because the fabric would build up more rapidly at the fell of the cloth than the take-up motion could accommodate. Obviously with such unrealistic fabric constructions, the loom parts may be overstressed and damaged, and frequent warp end breaks may occur due to excessive wear and high beat-up forces, resulting in low weaving efficiency and poor fabric quality [6]. Since the last century, many researchers have been attracted to the subject of maximum constructions. Extensive empirical investigations have derived relationships expressing the maximum ends and picks per unit length in terms of warp and filling yarn counts and weaves design [7]. An additional concurrent objective of the earlier work was to develop a numerical dimensionless parameter that describes a woven cloth relative to a standard or reference fabric. The ultimate goal behind this development was to relate the degree of tightness to fabric properties [8].

This correlation between tightness and fabric properties could be used to construct comparable fabrics that might vary in one or more fabric parameters and, equally important, to predict fabric properties and hence develop structures to fit specified end uses. The production of modern woven fabrics demands developing strategies considering new structures. It is clear that a new fabric structure should have the desired quality at minimum production costs, and the highest possible weaving efficiency. Fabrics are designed to fit different projected demands in order to be suitable for their end use [9]. For a fabric constructor it is essential that the relationships between the constructional parameters of fabrics and their individual properties, i.e. those that should fit the desired quality, are well defined. The mechanical properties are of considerable importance to fabric end use, so a lot of research has been dealt with them and there have been a number of efforts to try to define different models. Usually, several types of looms are used in factories. It was noticed that, properties of fabrics with the same setting parameters, but woven with various looms in various companies are different. It is well-known that the woven fabric's qualities are closely dependent on its structure. The tensile qualities of woven fabric have been researched by Nikolic [10] and others. He has proposed investigating woven fabric's strength as a function of thread strength, fabric density and thread strength coefficient. It was established that as thread strength increases, the woven fabric's strength also increases. While investigating woven fabrics of different weaves, it was established that plain weave has the maximum strength. Frydrych [11] et al. investigated the influence of woven fabric finishing, weft setting and raw materials on the elongation at break.

## II. MATERIALS AND METHODS

Both the warp yarns, weft yarns have been procured from a reputed commercial Jute Mill of West Bengal, India. The fabric samples have been manufactured from these procured yarns in the S4A loom in the Department of Jute and Fibre Technology, University of Calcutta. The specification of the S4A loom that has been employed in this study has been provided in the table 1. Two number of fabric samples i.e. Fabric Sample - 1 (FS-1) and Fabric Sample - 2 (FS-2) have been produced. The particulars of the fabric samples have been given in the table 2.

**Table 1: Particulars of the Loom used in the study**

Loom Type	Shuttleless multiphase curvilinear rapier loom
Make	ZHEJIANG GOLDEN EAGLE CO. LTD.
Speed of the loom	710 ppm
Type of weft carrier	Semi-circle tube type rigid rapier
Picking mechanism	Both side double weft insertion picking

**Table 2: Particulars of the Woven Fabric Samples**

Fabric samples	Warp Count (lbs/spy)	Weft Count (lbs/spy)	Warp Crimp (%)	Weft Crimp (%)	Ends/dm	picks/dm	Converted gsm at 20 % M.R.	Thickness (mm)	Total Fabric Cover factor	Moisture Regain %
FS-1	14.43	14.98	5.33	3.40	47.01	62.99	618.60	2.32	82.28	11.00
FS-2	14.43	16.60	4.76	3.20	46.77	54.88	620.00	2.53	81.34	10.50

### 2.1. Conditioning of test fabric samples

The entire range of woven fabric samples were conditioned using standard temperature ( $21^{\circ}\text{C} \pm 2^{\circ}\text{C}$ ) and humidity ( $65\% \pm 2\%$  relative humidity) for 24 hours before commencement of any testing work.

### 2.2. Selection of fabric samples for testing work

Small size samples used for normal textile testing cannot generally be regarded as appropriate for technical textile testing. These small samples have only a limited usefulness in assessing the properties of a fabric relative to its engineering end use, samples tested on modified or specially developed apparatus provide much more appropriate data. Therefore, test samples have been selected in such a way that it could represent the whole population of the fabric and the piece of fabric cut out for the laboratory test has been at least one meter long with full width of the fabric. No samples have been taken from nearer than 50 mm to the selvage of the fabric samples.

### 2.3. Measurement of the count of the warp and weft yarns

The yarn package has been unwinded to a length of 75 yards by using wrap reel instrument after which this particular length of the yarn is weighted in the electronically weighing balance. The count of the jute yarn is expressed in grist and calculated by applying the formula  $\{(\text{Weight of the yarn in pound} \times 14400) \div (\text{Length of the yarn in yard})\}$ . Ten number of observations has been taken for both warp and weft yarns each. The average values of warp and weft yarn counts have been provided in table 2.

### 2.4. Measurement of weight per unit area of the fabric samples

The specifications for mass per unit area for any woven fabric sample have direct influence on its physical, mechanical, hydraulic and other geotechnical properties. From each fabric sample, ten number of test samples of each 10 cm.  $\times$  10 cm. dimension have been cut from various locations over the full width of the fabric and then weighed in precision electronic balance. The average mass per unit area has been calculated for all the test samples. The average weight per unit area of the fabric samples have been converted at 20% moisture regain and the value is expressed in gsm and shown in table 2.

### 2.5. Measurement of fabric thickness

Thickness is one of the basic physical properties used to control the quality of woven fabrics. The normal thickness of a woven fabric sample is determined by observing the perpendicular distance that a moveable plane is displaced from a parallel surface by a specified pressure 2 kPa for fabric specimen. The accuracy level for determination of fabric thickness is very essential as this data is pre-requisite input for determining some important fabric parameters of geotextile fabrics, such as permeability of both of the air and water, permittivity, porosity etc. The thickness of the fabric samples in this study was measured using thickness tester of AIMIL Ltd. (Model AIM-241), New Delhi make, which is suitable for determining maximum thickness of 10 mm or 25 mm, provided with two dial gauges, one for the range of 10 mm with accuracy of 0.002 mm and the other for the range from 11 to 25 mm with accuracy of 0.01 mm under a pressure foot area of 31.66 cm<sup>2</sup> having standard pressure of 20 g/cm<sup>2</sup> for a compression period of 20 seconds. For accurately determining the thickness of the fabric, it was cut in such a fashion that the material extended by 1.0 cm in all directions beyond the edge of the pressure foot. Ten such observations for each sample were taken randomly from different parts of the sample and the average has been calculated and furnished in table 2.

### 2.6. Measurement of thread density of the produced fabric samples

In woven fabric the warp yarns are commonly referred to as 'End' and the number of warp threads per inch width of cloth is defined as 'Ends/inch'. The threads of weft are called 'Picks' and the number of weft threads per inch width of cloth is defined as 'Picks/inch'. The determination of the thread density has been carried out by unraveling a known width of the fabric sample and then the threads are counted in every one inch interval of the fabric sample at different places of the same using a counting glass magnifier. The different readings are recorded and the average of the threads/inch is noted and shown in table 2.

### 2.7. Determination of crimp and crimp percentage of the produced woven fabric samples

When warp and weft yarns are interlaced in the fabric they follow a wavy or corrugated path. Crimp percentage is a measure of this waviness in yarns. Peirce in his paper on cloth geometry, states that, crimp geometry is the percentage excess of length of the yarn axis over the cloth length. In order to straighten the thread, tension has been applied, just sufficient to remove all the kinks without stretching the yarn. Two cuts are made in the fabric sample and the distance between them has been noted. Threads are removed and placed over the scale, one end of each detached thread held by the fore finger and the thread smoothed along with the fore finger, and the straightened length has been observed. In this way several readings from different ear-marked areas of the fabric samples have been recorded and the average of these is provided in the table 2. The crimp percentage has been calculated mathematically by using the equation  $[\{(\text{Straightened length of yarn}) - (\text{Length of the yarn in the fabric})\} \div (\text{Length of the yarn in the fabric})] \times 100$ . The average values of warp and weft crimp percentages are given in table 2.

### 2.8. Calculation of the fabric cover factor of the produced fabric samples

One of the most important applications of cloth geometry is to calculate the cover factor of a cloth. In practice, this is given by a suitable factor based on the proportional area of the fabric covered by the projection of the threads. In case of jute fabric, the cover factor K has been calculated by multiplying threads per inch by the square root of yarn linear density expressed in lb/spynkle. If p is the spacing between the threads, then the fabric cover factor,  $K = nC^{1/2} = d/p$ , where, n is the thread density expressed in ends/inch and picks/inch while C is the yarn linear density expressed in lb/spynkle. It appears from the above equation that when the cover factor is 120, the thread must touch where they cross from one face of the cloth to the other. The cloth cover K is

expressed by  $K_c = (K_1 + K_2) - (K_1 \times K_2 / 120)$  where  $K_1$  and  $K_2$  are the warp and weft cover factors respectively. The total fabric cover factors of both the samples are provided in table 2.

### 2.9. Determination of breaking strength of the jute woven fabric samples following ravelled strip method (IS 9113: 1993)

The fabric sample used in ravelled strip method is 100 mm wide piece of fabric prepared by initially cutting the fabric to a width of 120 mm and removing threads from its both sides until the width has been reduced to 100 mm. The gauge length between the clamps is kept at 200 mm and the fabric strip is cut to a length of 350 mm for smooth and stable gripping of the fabric at both ends. The speed of the moving jaw has been set at 460 mm per minute. Five number of observations have been taken both in the warp and weft directions of the fabric samples. The average breaking strength values, both in the warp and weft directions, of the fabric samples FS-1 and FS-2 are provided in tables 3 and 4 respectively.

### 2.10. Determination of bursting strength of the jute woven fabric samples following IS: 7016 (Part 6)-1984 test method

The conditioned fabric sample is placed over the rubber diaphragm of the apparatus. The clamp ring is tightly secured over the fabric sample to hold the sample firmly in place. Then the power supply is switched on and the display of the digital pressure indicator is allowed to stabilize. The pressure on the rubber diaphragm is gradually increased by introducing the liquid (glycerin) into the chamber until the test sample bursts. The upper surface of the fabric sample under test is observed constantly. As soon as the sample fails, cam switch mark '0' has been switched off. The test sample is released and removed from the holding clamps. The time taken for bursting of the sample is noted. The same process is repeated without clamping the fabric sample. Six numbers of such observations have been made. The pressure required to distend the rubber diaphragm for the average time taken for bursting the fabric sample is noted. The average bursting strength values of the fabric samples FS-1 and FS-2 are provided in tables 3 and 4 respectively.

### 2.11. Measurement of air permeability of jute woven fabric samples

The air permeability of the jute woven fabric samples produced in this study has been measured using PROLIFIC Air Permeability Tester which consists of an arrangement to hold the test specimen between two flat faces so as to expose an area of  $10 \text{ cm}^2$  to the flow of air through it. There is a vacuum system to draw air through the exposed area of the test sample, and arrangement to measure the volume of air flowing through the test sample and arrangement to measure the pressure drop between the two faces of the test sample as a result of flow of air. The test specimen is held between two annular ring shaped grips. The grips are lined with rubber gaskets to reduce flow of air through the edges. The suction pipe is connected on the right hand side of the equipment to the suction hose of the vacuum pump. Water is filled in the upper of the two transparent plastic cups provided on the left hand side of the equipment. Sufficient water has been filled to make its level reach the zero mark on the lower manometer tube. Water in the lower plastic cup is drained out through the drain valve at its lower end. The drain valve is closed fully. The equipment has been levelled with the help of four levelling bolts provided so that the upper face of the sample mounting platform lies in a horizontal plane. In this position the water level in the two lower manometer tubes remains the same. The power supply is provided to the equipment from 220 volt single phase AC supply. The conditioned fabric sample is placed centrally between the grips. Sufficient tension has been provided to the fabric sample to prevent it from wrinkling and it is also taken care to look after the fact that the fabric sample does not get distorted in its own plane. The upper grip has been lowered to hold the fabric firmly. Adequate holding pressure has been applied to prevent slippage of the fabric and also to eliminate any leakage of air through the gripping faces. The flow of air is now slowly opened adjusting the valve of the first rotameter from the left, increasing the air flow rate till either the desired pressure drop is obtained on the manometer tube or the air flow rate reaches the maximum capacity of the rotameter. The pressure drop is indicated by the level of water column in one of the three upper manometer tubes. The rotameter reading has been recorded. The air permeability is then calculated by multiplying a correction factor of 0.01667 with the rotameter reading and expressed in  $\text{m}^3/\text{m}^2/\text{min}$  as shown in table 5.

### 2.12. Measurement of Apparent Opening Size (AOS) of the jute woven fabric samples following ASTM D4751-12

The fabric sample is secured in a taut condition (without any wrinkles or bulges) in the sieve pan of the dry sieve test apparatus by wedging between the sieve frames. Again the fabric sample is not over stretched or deformed such that it changes or distorts the openings in the fabric. Prior to each use, the glass beads are sieved in the laboratory verifying the size of the beads. The test is carried out with glass beads of different sizes expressed in microns. 50 gm of a particular sized glass beads are placed on the center of the geotextile. The cover and pan are placed on the sieve frame and the assembly is then placed in the shaker. The sieve is shaken

for a duration of 10 minutes by electric energy. The glass beads that passed through the specimen are weighed and recorded. The above procedure is repeated using the next larger bead size fraction. The trial is repeated using succeeding larger bead size fractions until the weight of the beads passing through the sample is 5 % or less. The trials are performed such that the percentage of glass beads passing decreases from a value greater than 5 % to a value less than or equal to 5 %. After that, the Apparent Opening Size (AOS)  $O_{95}$  value is determined from the co-ordinate graph by plotting the values of percentage of beads passing the sample versus the bead size used for each sample in the y-axis and x-axis respectively. The average AOS values of the samples FS-1 and FS-2 are shown in table 6.

**III. RESULTS AND DISCUSSION**

The test results of the mechanical and hydraulic properties of the woven jute fabric samples manufactured in the Department of Jute and Fibre Technology, University of Calcutta, have been furnished in tables 3 and 4 and a comparative analysis of the test results of the same with that of the standard fabric used to manufacture jute bags for packing 50 kg of food grains as per Bureau of Indian Standards (IS 12650:2003, 2nd Revision) has been carried out.

**Table 3: Mechanical Properties of the Jute Woven Fabric Samples (FS-1) produced in S4A Loom, Dept. of Jute and Fibre Technology, University of Calcutta, India**

Sl. No.	Breaking Strength (N)		Average Breaking Strength (N)		Breaking Elongation (%)		Average Breaking Elongation (%)		Bursting* Strength (kg/cm <sup>2</sup> )	Average Bursting Strength (kg/cm <sup>2</sup> )
	Warp Way	Weft Way	Warp Way	Weft Way	Warp Way	Weft Way	Warp Way	Weft Way		
1	2020	3210	2319	3021	6.0	5.0	6.4	4.5	23.80	24.88
2	2540	3240			7.0	4.0			25.60	
3	2060	3100			6.0	4.0			19.00	
4	2710	3280			8.0	4.0			25.10	
5	2210	2690			6.0	4.0			24.20	
6	2300	3050			6.0	5.0			29.40	
7	2340	2800			6.0	5.0			28.30	
8	2420	3030			7.0	5.0			24.10	
9	2240	2670			6.0	4.0			24.90	
10	2350	3140			6.0	5.0			24.40	

\*Diaphragm correction factor = 4.3 kg/cm<sup>2</sup>

**Table 4: Mechanical Properties of the Jute Woven Fabric Samples (FS-2) produced in S4A Loom, Dept. of Jute and Fibre Technology, University of Calcutta**

Sl. No.	Breaking Strength (N)		Average Breaking Strength (N)		Breaking Elongation (%)		Average Breaking Elongation (%)		Bursting* Strength (kg/cm <sup>2</sup> )	Average Bursting Strength (kg/cm <sup>2</sup> )
	Warp Way	Weft Way	Warp Way	Weft Way	Warp Way	Weft Way	Warp Way	Weft Way		
1	2390	3440	2249	2905	7.0	4.0	6.5	4.4	22.2	21.9
2	2230	2980			6.0	4.0			18.1	
3	2270	3300			6.0	4.0			19.4	
4	2250	2670			8.0	5.0			23.2	
5	2090	3030			6.0	4.0			25.0	
6	2150	2750			7.0	5.0			23.8	
7	2250	2860			7.0	5.0			19.9	
8	2270	2570			6.0	5.0			20.9	
9	2250	2650			6.0	4.0			24.2	
10	2340	2800			6.0	4.0			22.3	

\*Diaphragm correction factor = 4.1 kg/cm<sup>2</sup>

**Table 5: Hydraulic Properties (Air Permeability) of the Jute Woven Fabric Samples produced in S4A Loom, Dept. of Jute and Fibre Technology, University of Calcutta**

Sl. No.	FS-1		FS-2	
	Rotameter reading	Average Air Permeability (m <sup>3</sup> /m <sup>2</sup> /min)	Rotameter reading	Average Air Permeability (m <sup>3</sup> /m <sup>2</sup> /min)
1	8250	7850 × 0.01667 = 130.85	8500	8425 × 0.01667 = 140.44
2	8500		8250	
3	7500		8750	
4	8000		8750	
5	8000		8500	
6	8750		7000	
7	7500		8750	
8	7500		8500	
9	7000		9000	
10	7500		8250	

\*Measured at exposed surface area 10 cm<sup>2</sup> and 10 mm water column.

**Table 6: Hydraulic Properties (Apparent Opening Size) of the Jute Woven Fabric Samples produced in S4A Loom, Dept. of Jute and Fibre Technology, University of Calcutta**

Fabric samples	Sl. No.	Glass bead used (micron)	Weight of glass bead (gm)	Weight of Glass bead passes through the fabric (gm)	% of Glass bead passes through the fabric
FS-1	1	1400	50	46.52	93.04
	2	1700	50	3.72	7.44
	3	2000	50	0.05	0.10
	Average AOS (O <sub>95</sub> )= 1720micron				
FS-2	1	1400	50	8.27	16.54
	2	1700	50	0.79	1.58
	Average AOS (O <sub>95</sub> )= 1630micron				

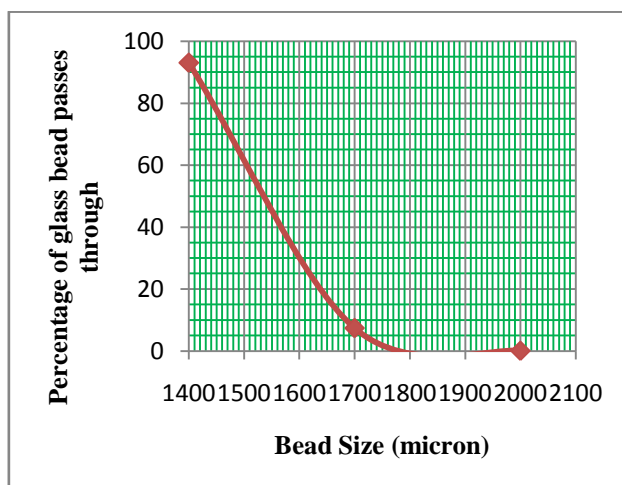


**Fig-1: AOS Curve for FS-1**

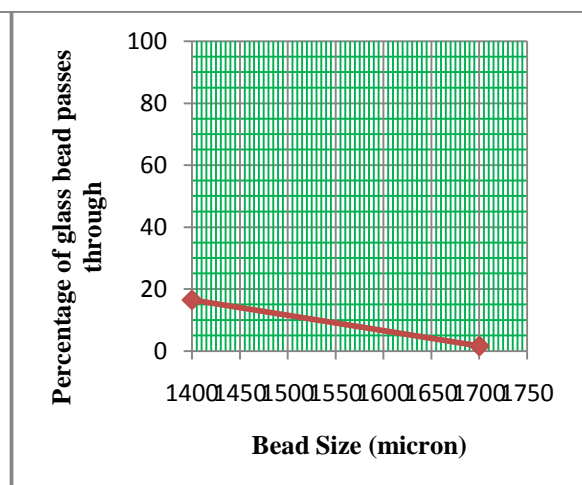


**Fig-2: AOS Curve for FS-2**

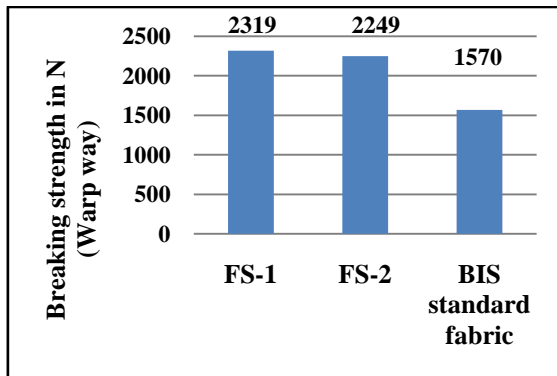


Fig-3: Graphical comparison of the warp way breaking strength in N of different samples

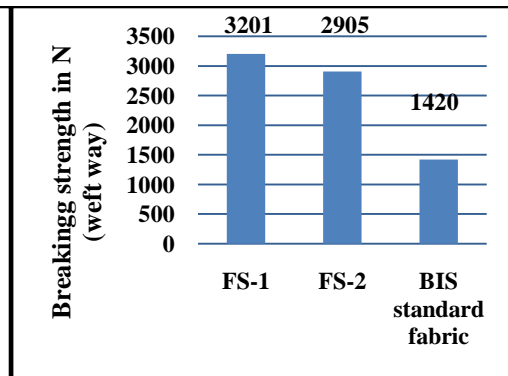


Fig-4: Graphical comparison of the weft way breaking strength in N of different samples

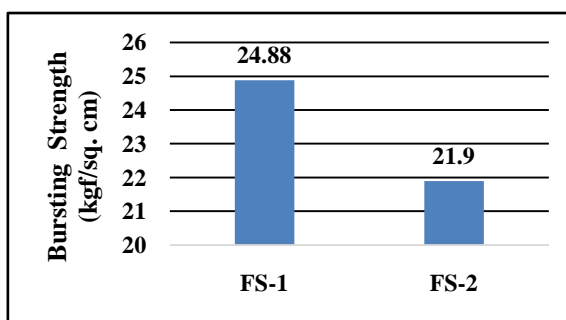


Fig-5: Graphical comparison of bursting strength in kg/cm<sup>2</sup> of produced samples

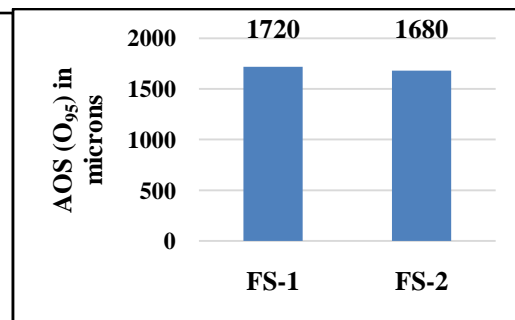


Fig-6: Graphical comparison of AOS (O<sub>95</sub>) in microns of produced samples

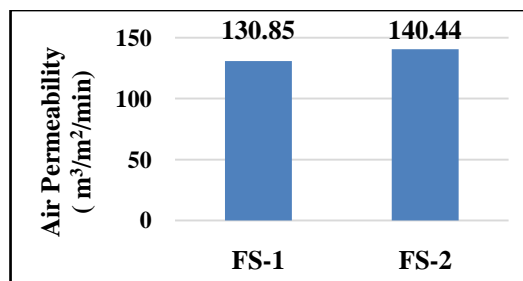


Fig-7: Graphical comparison of Air Permeability in m<sup>3</sup>/m<sup>2</sup>/min of produced samples

### 3.1. Comparative analysis of the mechanical properties of FS-1 and FS-2 fabric samples

The test results of the two number 2/1 Twill Jute woven fabric samples, FS-1 and FS-2 produced in the multi-phase shuttleless S4A Loom of the Department having area densities 618.6 gsm and 620 gsm respectively when compared among themselves, show that there is a decreasing trend in the unidirectional warp way and weft way breaking strengths of the fabric samples. FS-1 shows a comparatively high breaking strength of 2319 N as against 2249 N of FS-2 in the warp direction while the breaking strength of 3021 N of FS-1 scores over the breaking strength of 2905 N of FS-2 in the weft direction. This trend has been represented graphically in fig. 3 and 4. While fig. 5, related to the multi-directional bursting strength values of the two tested fabric samples, shows that the bursting strength value of FS-1 (24.88 kg/cm<sup>2</sup>) supersedes the bursting strength value of FS-2 (21.9 kg/cm<sup>2</sup>). While no significant differences have been observed in the values of the hydraulic properties of the two fabric samples and the findings have been supported by the figs. 6 and 7 respectively. The variation of the pick density of the two jute fabric samples FS-1 and FS-2, (recorded as 62.99 and 54.88 picks / dm respectively in table 2) keeping their area densities almost same (618.60 and 620 gsm) are found not to produce any significant difference in the warp way (2319 N and 2249 N) and weft way (3021 N and 2905 N) breaking strengths of the samples.

### 3.2. Comparative analysis of the mechanical properties of the fabric samples produced (FS-1 and FS-2) with the standard fabric sample required for producing Jute Bags for packing 50 kg food grains as per IS 12650:2003, 2nd Revision

The test results of the two number 2/1 Twill Jute woven fabric samples, FS-1 and FS-2 produced in the multi-phase shuttleless S4A Loom having area densities 618.6 gsm and 620 gsm respectively show higher breaking strength values of the produced samples than that of the standard fabric sample required for producing Jute Bags for packing 50 kg food grains as per IS 12650:2003, 2nd Revision, and this is clearly observable in figs. 3 and 4 respectively. The values obtained are 2319 N, 2249 N for sample FS-1 and 3021 N, 2905 N for sample FS-2 in warp and weft directions respectively against the breaking strength values of 1570 N, 1420 N of the standard fabric in the warp and weft directions respectively.

## IV. CONCLUSIONS

The two number 2/1 Twill Jute woven fabric samples, FS-1 and FS-2 produced in the multi-phase shuttleless S4A Loom having area densities 618.6 gsm and 620 gsm respectively when compared with the standard jute sacking fabric specified in IS 12650:2003, 2nd Revision and woven in conventional Jute Sacking Loom, show higher breaking strength values both in the warp and weft directions which supports the fact that better quality of jute sacking fabrics can be woven in S4A loom than in the conventional jute sacking loom with higher weaving efficiency. It can be also stated here that considering from the end-use point of view, a jute fabric is more likely to fail by bursting than by a straight tensile fracture therefore the determination of the bursting strength of the jute woven fabric samples along with its hydraulic properties are equally important for finding out the stress developed in all the directions at the same time. It is quite significant to determine fabric air permeability which co-relates to its geometric structure strongly as well as to the path of air streamlines for smooth flow through the structure helping thereby to keep the packed food grains fresh and healthy.

The variation of the pick density of the two jute fabric samples FS-1 and FS-2, keeping their area densities almost same is found to be not producing any significant difference in the breaking strengths both warp way and weft way of the samples. The authors are of the opinion that the study can be further extended to determine the effect of loop length on air permeability of the fabric. Similarly, the effect of fineness of the yarns on the size of the pores which eventually affects the air permeability of the fabric can be also counted as a good future scope of further extending this study. Moreover, formulations of stitch density, stitch length or yarn diameter influencing the pore size values also demands further research. Due to the differences between ideal and real geometry and the random variation of the fabric structure there are no exact dependence between experimental air permeability and predicted air permeability values an area which will also be explored. All these possible areas of research will be carried out and compiled in the upcoming article.

## V. ACKNOWLEDGEMENTS

The authors convey their regards to the Honorable Vice Chancellor and Pro Vice Chancellor (Academic Affairs), University of Calcutta, West Bengal, India for their kind consent to allow this review paper for publication in the scholarly journal and valuable guidance to carry out this paper.

## REFERENCES

- [1] F.T. Peirce, "The Handle of Cloth as a Measurable Quantity", *Journal of Textile Institute*, 21, 1930, T377-417.
- [2] S.D. Ramaswamy and M.A. Aziz., "Jute Geotextiles for Roads. Proc. Int. Workshop on Geotextiles", 1989, 259-266.
- [3] K. Balan and G. V. Rao, "Erosion control with natural geotextiles" Proc. Int. Seminar and Technomeet on Environmental Geotechnology with Geosynthetics", *The Asian Society for Environmental Geotechnology, CBIP*, New Delhi, 1996, pp: 317-334.
- [4] F.Wang, G.Xu, B.Xu, "Predicting the Shearing Rigidity of Woven Fabrics", *Textile Research Journal*, 75(1), 2005 pp. 30-34.
- [5] T.R. Ashenhurst, *A Treatise on Textile Calculations and the Structure of Fabrics*, Huddersfield, England, 1884.
- [6] S.Brierley, "Cloth Settings Reconsidered", *The Textile Manufacturer*, 79, 1952, pp. 349-351.
- [7] V.Milašius, "An Integrated Structure Factor for Woven Fabrics, Part I: Estimation of the Weave", *The Journal of the Textile Institute*, 91, Part 1, No. 2, 2000, pp. 268-276.
- [8] E. Kumpikaitė, V.Milašius, "Influence of Fabric Structure on Its Weavability", *Materials Science (Medžiagotyra)*, Part 9, No. 4, 2003, pp. 395-400.
- [9] V.Milašius, "An Integrated Structure Factor for Woven Fabrics, Part II: Fabrics-firmness Factor", *The Journal of the Textile Institute*, 91, Part 1, No. 2, 2000, pp. 277-284.
- [10] M.Nikolic, T.Michailovic, L. Simovic: "Real Value of Weave Binding Coefficient as a Factor of Woven Fabrics Strength", *Fibres and Textile in Eastern Europe*, 11, 2000, pp. 74-78.
- [11] I.Frydrych, G.Dziworska, M.Matusiak, "Influence of Yarn Properties on the Strength Properties of Plain Fabric", *Fibres and Textile in Eastern Europe*, 4, 2000, pp. 42-45.

## Analyzing the impact of rural housing credits on indices of physical development and housing patterns (Case study: villages in the central part of the city of Kashmar)

<sup>1</sup>Javad Bazrafshan, <sup>2\*</sup>Ali Vaez Tabasi

<sup>1</sup>Assistant Professor of Geography and Rural Planning, University of Sistan and Baluchestan, Zahedan, Iran

<sup>2\*</sup>MA Geography and Rural Planning, University of Sistan and Baluchestan, Zahedan, Iran

**ABSTRACT:** Giving credit to the villages for physical development and strengthening housing is one of the strategies and programs implemented in rural areas that to some extent, it has caused the empowerment of villages. Some facility will be provided to villagers as the loans of the improvement of rural housing in Iran which have some restrictions and requirements according to infrastructure, materials, and plan of houses and these restrictions and requirements of these houses will distinct them from the traditional rural housing. The goal of this research is the Analyzing the impact of rural housing credits on indices of physical development and housing patterns. The method of the research is analytic-descriptive and the documentary and field methods are used for collecting data. The results show that the dimension of the impact of housing credit on physical development has the maximum effect on the index of the change of rural architecture pattern and in the dimension of housing credits on housing pattern; it has the maximum impact on the index of the type of housing.

**Key words:** Housing facilities, Village, Physical development, Kashmar

### INTRODUCTION

The issue of housing is one of the most important elements in rural spaces and it is as symbol of human's interactions with its natural environment and it is formed according to the time-place conditions during years and it is an indication of the type of activities in the economic, socio-cultural attitudes of the villagers, the manner of development and use of technology and ultimately, the income and livelihood of its inhabitants (shamsadini, 2008: 44).

Rural communities has been faced with many problems in the fields of development So that the cost of making houses very low in the past while the architecture plan and materials were providing by villagers, the rural housings have met the needs of the villagers and their activities (Mosavi and Salehi, 2005: 28).

The rural environment has an integrated environment with an attractive architecture and is consistent with the environment. But today, some changes have been created in rural environments and housing, these changes are from villager's new constructions or rural upgrading and modernization. With these conditions, due to changes in the cost of materials and the need to cost a lot to build housing so, one of the alternative thinking is giving credit to rural communities by the Islamic Revolution Housing Foundation in the field of physical development and strengthening of housing and this work will be supervised by technical supervisors. The result is the construction of houses with high strength and resistant to natural disasters that it has provided the peace and tranquility of rural areas and has improved the quality of rural housing. The necessity of the plan of strengthening in Iran emanated from the fact that Villagers often live at dark home by insufficient and inadequate ventilation equipment and inappropriate health status of rural housing is a serious problem indeed (Motilangrodi, 2007: 100). In addition, resistless of rural housing to disasters and natural hazards such as earthquakes, floods, landslides, storms and so on are most important problems of rural housing. The use of less durable materials, particularly non-compliance with technical standards in housing construction has a major role in this regard (Rezavni, 2011: 164). Some factors such as, conductor plans, Personal capital, the physical fabric of the village, rural financial capability, incentives for staying in the village, the value of land, the distance of village from town are effective in physical development of villages. This research is aimed to assess and

evaluate the impact of housing facilities as an intervening factor in the development of the physical environment of rural villages in the central part of Kashmar in Khorasan Razavi until the strengths and weaknesses of these plans will be recognized and its results may be used for future planning in rural areas of the country and its effectiveness may be increased.

### **Theory Housing**

The problem is that today all countries are affected by some kind of appropriate accommodation to their circumstances. While in developed countries, housing, social welfare and future of housing development programs are focused on improving quality in our nation's housing as a basic need and supply it with food and clothing. In other words, the right to adequate housing and shelter for one of the most basic needs of every individual and family has to live with human dignity (UN Habitat, 2002) And this right is considered in the second, thirty and forty-third article of country's constitution and the state obligation to provide adequate housing for all segments of society, especially poor and rural groups (Constitution of Islamic Republic of Iran). On the other hand the families as the cornerstone of society and social institutions have made the most natural effects and they have formed one of the main premises of this institution in suitable housing (Majles Research Center, 2005: 1).

Humanities scholars are looking at housing with a special approach. So that the public housing in general concept and rural housing in particular, on the view of sociologists is as an entity shelter and stability and solidarity of the family, anthropological perspective, a culture from the perspective of planning as a "basic needs", and from an economic perspective as "a commodity to be delivered without a successor and a capital (Fazeli, 2007: 63). Thus, housing is as physical facilities in unit or an economic commodity that plays social role and function of the wealth by generated tool in the economic growth (Bourne, 1995: 14). In other words, in addition to providing housing, "shelter" in the form of savings is made. Thus, capital goods and housing is a social value, which decreases the stability of society and social damage (Dix, 1995: 1-10).

However, housing is considered as immovable property and commodity that is bound to take place and also is affected by their environment and geographical conditions, such as access (Majles Research Center, 2005: 3). In the second Habitat Summit in Istanbul, in definition of proper housing several cases such as access to appropriate and comfort space, adequate security, property security, stability and durability of structural system, lighting, ventilation and heating and basic infrastructure have been emphasized. From the viewpoint of the England Kent home group, adequate housing is a vital element for rural residents security against natural disasters and their underlying development with development and investment quality in tangible and relevant to residents' needs while providing opportunities for employment and basic services, supports the growth of rural economy (ERHA, 2011:4-6).

Concept of House includes a space for life, economic activity and production functions, providing physical infrastructure such as water and sanitation and access to educational services and other essential services. That indicating the interaction of work and livelihoods, and lack of separation of subject and duration of activities in the rural life (Tavakoli and et al, 2008). The Rural Housing works in regard to social and economic conditions and changes in the family. So, today in most developing countries, researchers have concluded that the definition of rural housing is not confined to one residential unit, but is in the residential environment.

It can be pointed to the approach of granting credits as the most important implemented plans in the field of the improvement and renovation of housing in developing countries. In recent decades, the success of financial institutions to provide credit to the poor for empowerment in developing countries has led that scientist mention these successes as micro-credit revolution (sengupta, 2008: 120). Considering the importance of rural housing development and the willingness of villagers to build good resistance houses and on the other hand, the weakness of financial strength of the villagers to carry out preventive activities (Such as principled resistance housing), rural housing upgrading and retrofitting projects supported by the government has been begun since 2005. In this plan, the Foundation of housing plans to distribute provincial housing facilities with priority event-prone areas and the foundation has to identify qualified applicants and introduce them for receiving facilities and As well as supervision of construction through rural technical observers and experts of this foundation (Bakhshi, 2009: 100).

### **The history of the research**

In a research entitled " the role of rural housing improvement funding on enabling and sustainability of the rural population in the rural city of Beihagh in the city of Sabzavar" Motilangrodi and Bakhshi (2009) have concluded that housing credits have been effective both in creating empowerment and satisfaction of rural housing and also in the survival of the population in rural areas.

In a research entitled "the role of housing credit in the changing patterns of the rural areas in the city of Bahmai" Anabestani et al (2011) have concluded that the most impact of credit on the changing patterns of housing in villages has been from housing Foundation of Islamic Revolution in the course of time of credits so that 26/4 percent of the effectiveness of credit facilities was related to this index and 18/3 percent was related to the index of the supervision of the construction.

Murphy and Scott (2013) in their article called " issues related to housing loans in economy crisis: Evidence from rural families in Ireland" have studied the manner of applying neoliberal ideas in ownership and development during the housing boom of Ireland and the results pointed out that rural households have suffered from immense hardship and pressure and as well as through rural housing, have shown the extent to which the actions and consequences of neoliberal policies in the field of housing loans in space are different in rural areas. Aliyu et al (2014) in an article entitled "theoretical perspectives in the development of rural housing and the problems associated with housing developers in Nigeria" reviewed that man needs house to satisfy their personal needs such as privacy and personal satisfaction psychologically and house is a symbol that shows the situation of one person in the family or community socially and culturally and it also reflects the economic value of a society. Thus the need is felt to study in order to find a solution to the housing development of rural housing and living conditions of rural dwellers.

Yu Lihong and Dai Lin (2014) in a study entitled "Study of practical experience of rural land and right management of housing loans in China" have found that the government should support and guide the promotion of the establishment of rural land and financial institutions should also participate in a new trade actively as well as rural land circulation market should be set completely.

### The study area

Kashmar is one of the cities of Khorasan Razavi and it is located in 217 km of southeast of Mashhad with an area about 3390 square kilometers and geographically, it is located at latitude of 35 degree and 11 minutes of north and at longitude of 58 degree and 27 minutes of east and at altitude of 1215 meters above the sea level (Jaafari, 1995: 12).

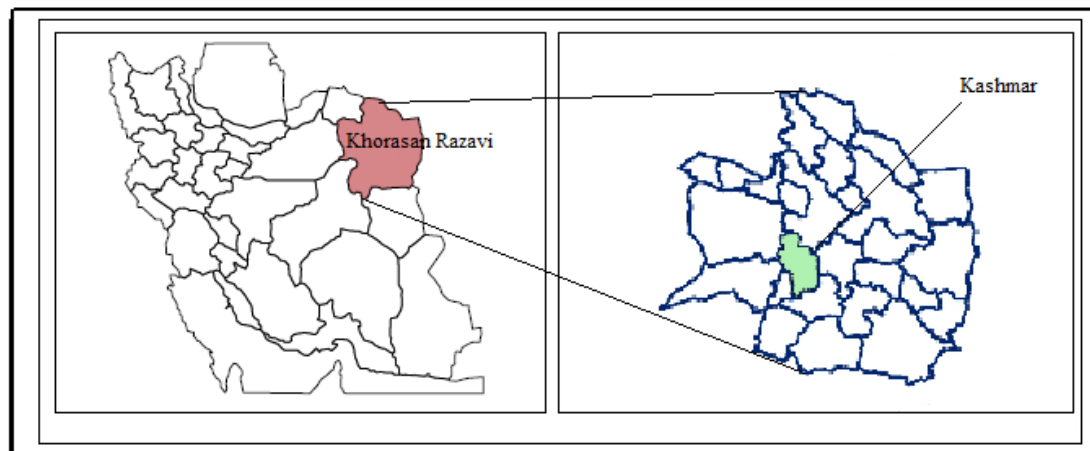


Figure (1): Location of the study area, Source: research results

The city of Kashmar has 483 villages that 420 villages have been vacated and it has 63 residential villages currently. In the central part of Kashmar, the rural district of Balla Valayat has 20 residential villages and the rural district of Paein Valayat has 14 residential villages.

The place range of the study in this research is the villages of central part of Kashmar. According to the results of census of 2011, this section has 34 villages that 44 percent of it has been selected as the study villages, which are about 15 villages. For selecting the sample villages among 34 rural villages in the central part of Kashmar, First, the "villages that have a population of over 20 households, and secondly," the case had received a mortgage for housing improvements have been selected within time range of 6 courses from the ceding credit of rural housing between 2005-2013.

Table (1): The number of sample villages

Percent loans	The number of loans	specimen	Population	Family	Rural	Percent loans	The number of loans	specimen	Population	Family	Rural
36.29	188	17	1708	518	Zende Jan	42.09	426	39	3277	1012	Farotagha
45.90	202	19	1386	440	Mohammadieh	26.46	339	31	4344	1281	Ghozhd
44.23	211	20	15.38	477	Sar Hozak	62.58	393	36	2182	628	Arel Abad
48.61	176	16	1189	362	Mmarr Abad	23.78	303	28	4206	1274	Fadafan
35.29	240	23	2274	680	Moqan	40.56	217	20	1735	535	Tarbaghan
38.03	275	25	2353	723	Farah Abad	24.65	195	18	2590	791	Rezgh Abad
34.89	223	21	2092	639	Kasrineh	31.22	227	21	2459	727	Farag
36.40	3769	348	34047	10352	Total	58.11	154	14	715	265	Nay

Source: research results

**The research method**

The dominant research approach is analytic-descriptive approach. To collect the required data, two methods of documentary and survey have been used. In theoretical part of the research, the documentary method has been used that it will includes Study resources such as books and papers in Persian and Latin and Reports and projects in this field. In practical part, the case study has been considered and the scope of the study were closely observed and studied. Using Cochran formula to estimate sample size was 348 cases from the 3769 questionnaire files that it was used to collect data. For this purpose, the questionnaire was provided to villagers in the central part of Kashmar. Then to analyze the collected data using the Pearson correlation test, some software were used such as Spss and Excel.

**DESCRIPTION OF THE RESEARCH FINDINGS**

The research aims to evaluate the hypothesis of the study and based on the sample of 348 persons who were determined based on a formula Cochran, in this research data were collected through questionnaires and fields data as follows:

Table (2): General characteristics of respondents

Percent	The number of respondents	Breakdown of variables	General variable
87.65	305	Male	Gender
12.35	43	Female	
17.24	60	20-30	Age
37.36	130	31-40	
32.47	113	41-50	
12.93	45	Over 50 years	Marital status
1.44	5	Single	
98.56	343	Married	
17.24	60	Less than 2	Number of family members
30.17	105	2 to 4	
37.93	132	4 to 6	
14.66	51	More than 6	Employment Status
25.86	90	Laborer	
11.49	40	Employee	
47.71	166	Farmer	
14.94	52	Other	The monthly fee
27.30	95	Below 400 thousand Tomans	
55.46	193	400 to 800 tomans	
17.24	60	800 tomans and more	Educational status
20.11	70	Illiterate	
30.17	105	Less than high school diploma	
24.42	85	Diploma	
14.37	50	Associate Degree and Bachelor's Degree	The amount of agricultural land
1.93	38	Bachelor's Degree or higher	
22.13	77	Less than 4	
35.34	123	4 to 6	
27.59	96	More than 6	
14.94	52	No reply	

32.47	113	Clay raw or mud Skeleton	Previous housing construction materials
54.02	188	Brick structure with cement block	
13.51	47	Reinforced concrete structure	
34.19	119	Old	Type of Previous housing
47.19	167	New Build	
17.81	62	Between	
32.47	113	Less than 90 m	The former Housing Infrastructure
51.44	179	Between 90 and 120 meters	
16.09	56	More than 120 m	
34.77	121	Less than 3 rooms	Number of rooms in each residential unit in the previous housing
57.18	199	3 to 5	
8.04	28	More than 5 rooms	
97.99	341	1st floor	Number of floors in the residential units in the previous housing
2.01	7	2 floors	

Source: research results

**DISCUSSION AND CONCLUSION**

**The study of the impact of rural housing credits on indices of rural physical development**

Stepwise regression model has been used for evaluating the amount of impact of rural housing credits on physical development indices. Table 3 shows the coefficient of effect of credits on indices of physical development pattern. The fixed amount of credits is equivalent to 4/08 in the significant level of 0.000.

The amount of effect of housing credits on the Index of road network changes equals to 0/205 in the significant level of 0.000. In another word, one unit of standard deviation in housing credits causes 0/205 of changes in the road network. So the housing credit has a great impact on the rural road network.

The amount of effect of housing credits on the index of rural Physical fabric development equals to 0/116 in the significant level of 0.000. In another word, one unit of standard deviation in housing credits causes 0/116 of changes in rural Physical fabric development. So the housing credit has a great impact on rural Physical fabric development.

The housing credits has an increasingly impact on the indices of congruence of the population and use and changes in architectural pattern. A change in the type of construction materials in the borrower villages has caused 0/335 to 0/440 changes.

The housing credits haven't had a significant impact on the index of changes in the kind of materials in the significant level of 0/394.

Table (3): the amount of the impact of rural housing credits on the indices of rural physical development

Independent variables	Variable coefficient	Standardized coefficient (beta)	T-statistics	Significant level	Result
Fixed amount	4/083	0/204	16/475	0.000	The model is significant
Road network changes	1/870	0/205	6/598	0.000	The model is significant
rural physical development	0/307	0/116	3/291	0.000	The model is significant
the congruence of the population and use	0/797	0/335	4/740	0.000	The model is significant
changes in architectural pattern	1/031	0/440	8/010	0.000	The model is significant

Source: research results

So housing credits has had the greatest impact on the changes of rural architecture pattern in the physical development of the sample villages and the index of rural physical fabric development has had the Minimal impact.

**The assessment of the impact of housing credits on indices of rural housing pattern**

Stepwise regression model has been used for assessing the amount of the impact of housing credits on indices of rural housing pattern. Table 4 shows the coefficient of effect of credits on indices of housing pattern. The fixed amount of credits is equivalent to 3/86 in the significant level of 0.000.

The amount of effect of housing credits on upgrading and retrofitting housing equals to 0/16 in the significance level of 0/002. In another word, one unit of standard deviation in housing credits causes 0/16 of upgrading and retrofitting housing. So the housing credit has a great impact on rural housing renovation and retrofitting.

The amount of impact of housing credits has not an increasingly impact on rural construction pattern and amount of this impact is 0/325 in the significance level of 0/067. In another word one unit of standard deviation in housing credits has caused 0/325 of changes in index of rural construction pattern. So the housing credits have not a positive impact on rural construction pattern.

The housing credits have not also had a positive effect on the indices of number of rooms in each residential unit, number of floors of each residential unit and the criteria-based construction.

So, the greatest impact of housing credit is on the index of the type of houses in the sample villages.

Table (4): The assessment of the impact of housing credits on indices of rural housing pattern

Independent variables	Variable coefficient	Standardized coefficient (beta)	T-statistics	Significant level	Result
Fixed amount	3/867	0/233	0/240	0.000	The model is significant
housing renovation and retrofitting	0/515	0/168	0/183	0.002	The model is significant
rural construction pattern	-0/598	-0/325	-0/070	0.067	The model is significant
Number of rooms in each residential units	0/280	0/152	0/048	0.066	The model is significant
Type of housing	2/209	0/327	0/286	0.000	The model is significant
Number of floors of each residential units	-0/087	-0/226	-0/009	0/699	The model is significant
Technical Criteria in construction	0/301	0/356	0/031	0/399	The model is significant
Surface Infrastructure	0/690	0/214	0/213	0/001	The model is significant

Source: research results

## CONCLUSION

Nowadays, Housing as a phenomenon that affects the rural physical development process has attracted a lot of attention. This phenomenon has dramatic effects on life of the villages from various aspects, including economic, cultural, social and rural livelihoods.

Any plan for rural housing should be in the direction of rural sustainable development and attention to some dimensions of the development should not be led to forget other dimensions of development. Otherwise harmful results will be imposed on the lives and livelihoods of the villagers.

The results show that the dimension of the impact of housing credit on physical development has the maximum effect on the index of the change of rural architecture pattern and in the dimension of housing credits on housing pattern; it has the maximum impact on the index of the type of housing.

Finally, it can be stated that housing credit allocation in this area has managed significant effects on physical development in central villages of Kashmar and the process of the impact of housing facilities in the villages of this part will be accelerated in future.

## Suggestions

- ❖ Patterns of physical development of villages in this region should be done in the frame work of conducted plans and development of villages based on the natural and socio-economic characteristics of rural areas.
- ❖ Reduction of bank interest from poor rural villagers for financial weakness of villagers or increase the duration time of installments of the obtained loan
- ❖ Increasing the loan amount proportional to the price of materials and wages of workers
- ❖ Providing the necessary conditions to ensure repayment of loans through the state
- ❖ Insurance and seriousness of the villagers in timely payment of the loan during the construction of housing
- ❖ The proportion of the amount of loans with local popular culture

## REFERENCES

- [1]. Aliyu, A. A, Ghani, Z. A, Bello, M.U, Kasim, R, Martin, D, (2014). A Theoretical Perspective on Rural Housing Development and the Problems Associated with Housing Developers in Nigeria: Evidence from Dass Metropolis. *Journal of Environment and Earth Science*, Vol.4, No.16, pp. 56-60.
- [2]. Anabestani. A. A, Shaian, H, Boniaddasht. A, (2011), The role of the changing patterns of housing credit in the rural areas of Bahmai city, *Journal of specialized spatial planning*, the first year of the third issue, pp 63-80.
- [3]. Bakhshi. Z, (2009), The role of housing credits in the capability and sustainability of the rural population in the village of Bayhagh, M.A thesis of Geography and Rural Planning by guidance of Dr Moteilangroodi, Tehran university.
- [4]. Bourne, L.S, (1981), *Geography of Housing*, Black well Publishing, New York p: 14.
- [5]. Dix, G, (1995), the place of shelter in National Development, Edited by S.M Romaya. pp: 1-10.
- [6]. English Rural Housing Association, (2011), *Rural Homes: supporting Kent's rural communities*, A Protocol for Delivering Affordable Local Needs Housing in Rural Kent.
- [7]. Fazeli, N, (2007) *Modernity and Housing*, *Journal of Cultural Studies*, the first year, No. 1 Fall, Tehran.
- [8]. Lihong, Y., Lin, D, (2014), Study on Practical Experiences of Rural Land Management Right Mortgage Loan in China. *International Conference on Logistics Engineering*.pp.141-144.
- [9]. Majlis Research Center, (2005), *Economic Policy Housing: Dos and Don'ts*, subject code: 250 Number: 7881, July 2005, the Office of the underlying studies.
- [10]. Majlis Research Center, (2008), and criticism of government policies on the economy, housing, code Subject: 250, Issue Number: 9829, the Office of the underlying studies.
- [11]. Mavsavi. B. A, Salehi. F, (2005), Social aspects of traditional and new patterns of rural, *Journal of Housing and revolution*, No.112, Pp 28-43.
- [12]. Moteilangroodi. H, Bakhshi. Z, (2010), the role of housing credits in the capability and sustainability of the rural population in the village of Bayhagh, *Human Geography Research*
- [13]. Moteilangroodi. S.H, (2009), *Economic geography of Iran (Agriculture)*, Publications of Jihad Daneshgahi, Mashhad.
- [14]. Murphy, E., Scott, M, (2013). Mortgage-related issues in a crisis economy: Evidence from rural households in Ireland. *Geoforum*, vol.46, pp. 34-44.
- [15]. Rezvani. M. R, (2011), *rural development planning in Iran*, Press Ghomes, Fourth Edition
- [16]. Sengupta, R. and C. P. Aubuchon. (2008). the Microfinance Revolution: An Overview, *Federal Reserve Bank of St. Louis Review* 90(1), 9-30.
- [17]. Shamsadini. A, (2008), the place of rural housing on impressibility of physical – Space changes of villages from the urban environment, *Journal of Housing and Revolution*, No.124, pp 40-51.
- [18]. Statistical Center of Iran, (2011), the initial results of the general census of population and housing
- [19]. Tavakoli, M. et al, (2008), investigated Evolution Architecture Housing Rural and Compilation Pattern Optimal. Study Case: city Aq Qala, *Journal of Housing Research and the rural environment*, pp. 31-14.
- [20]. UN-Habitat (2002), *Monthly Electronic Newsletter of the United Nations Human Settlements Programme* 1/1 January: <http://www.unhabitat.org/hb/index.asp>.

## Study on Hydrographic properties in the coastal waters along South East Coast of India

James Balgan Anand D<sup>1</sup>, Mary Jelastin Kala S<sup>2</sup>

<sup>1</sup>Research Scholar, Research Department of chemistry, St. Xavier's College, Palayamkottai, TamilNadu, India

<sup>2</sup>Assistant Professor, Department of chemistry, St. Xavier's College, Palayamkottai, TamilNadu, India

**ABSTRACT:** Coastal waters are considered to be the pillar and essential of Marine life. The study of Hydrographic properties of coastal environments is important, because the variations in the instantly influence on the floral and faunal production. The variations affect the species diversity, pattern of diversity, breeding, survival and other activities. To maintain optimum level of water quality parameters is better for the species survival and healthy ecosystem. The present study was carried out to determine the Hydrographic variations in coastal Waters of Mandapam, Thoothukudi, Arumuganeri and Kanyakumari along the south east coast of India. The sampling of coastal water was carried out from January 2014 to December 2014. The hydrographical parameters like temperature, salinity, pH, dissolved oxygen, inorganic nitrite, nitrate, phosphate, silicate, and chlorophyll -a were analyzed in the coastal waters. The results showed decline in the quality of water during the non-monsoon season compared to that in the monsoon season. The DO and nutrients was found to be low in summer and high during monsoon season. Similarly temperature, pH and salinity were low during monsoon and high during summer season. The hydrographic properties have exhibited considerable seasonal and spatial variations.

**Keywords** -Hydrographic properties; Nutrients; Seasons; Coastal water; East Coast of India

### I. INTRODUCTION

The coastal ecosystems provide food and other incomes, also used for waste disposal, recreation and inspiration. Water is very essential for all Living being. It is available in different forms in our environment. Coastal environment is vital for all human activities including industrial growth. Without the coastal environment, success of any community or nation is impossible. In the other hand coastal water is always considered as an easily available and everlasting resource for the biota. Coastal Zone is influenced by the interaction between land and sea. The environmental conditions such as topography, water movement, salinity, oxygen, temperature and nutrients characterizing particular water mass also determine the composition of its biota [1]. Thus the nature and distribution of flora and fauna in an aquatic system are mainly controlled by the fluctuations in the hydrographical parameters of the water body [2]. Coastal zone offers an important buffer zone and filtering system for the ecosystem.

Generally Marine environment is a complex system and mainly influenced by various physical chemical and biological process. The open ocean is more stable compare to the near shore waters where the interaction with terrestrial and makes the variations in hydrographical properties [3]. The water quality depends on both natural processes, such as precipitation erosion, weathering of crustal materials and anthropogenic processes like urbanization, industrialization, mining and agricultural activities [4]. These two parameters play a dynamic role in nutrient cycling, eutrophication, biota abundance and overall food web dynamics in the estuarine and the coastal ecosystem, whereas surface runoff is a seasonal phenomenon largely affected by the monsoon rainfall (Figure 1).

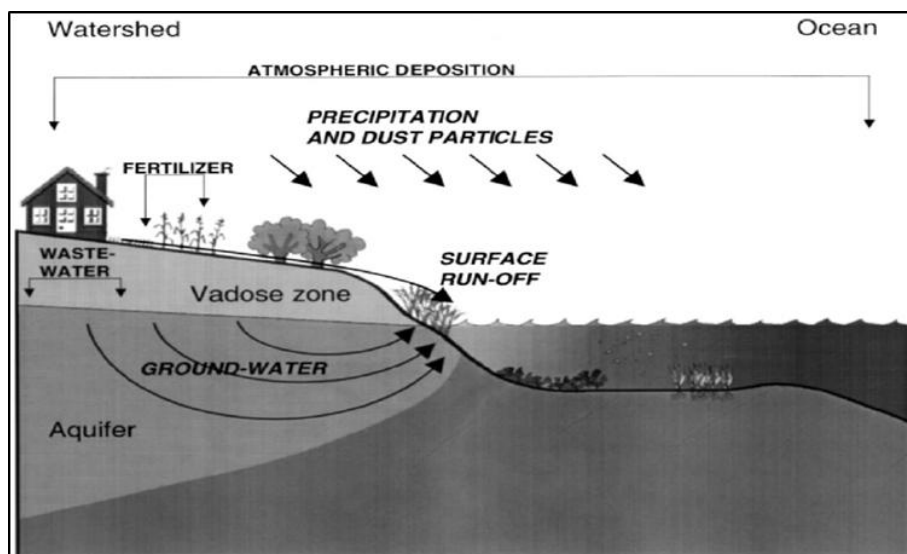


Figure: 1 Pathways of Nutrients Entry into the Coastal Water [5]

The coastal hydrography is much complicated due to the dynamic nature of the ecosystem. Changes in the hydrographical parameters such as salinity, dissolved oxygen, dissolved carbon dioxide; nutrients affect the activities and growth of the organisms in the ecosystem [6]. It plays a major role in forecasting, localizing, and manipulating the marine resources [7]. Coastal Water quality is an indicator which gives the necessary information about the marine waters and their ability to support the marine species to live in the marine environment. It shows how activities on land affect marine water quality.

Hence the hydrological study is very much essential to understand the relationship between its different trophic levels and food webs. Usually in the coastal waters exhibit considerable seasonal variations depending on the local conditions of rainfall, tidal incursions, various abiotic and biotic processes, quantum of freshwater inflow affecting the nutrient cycle of different coastal environments [8].

## II. DESCRIPTION OF THE STUDY AREA

The study area Mandapam (latitude  $9^{\circ}16'14''N$ ; longitude  $79^{\circ}7'10''E$ ), Thoothukudi (latitude  $8^{\circ}46'26''N$ ; longitude  $78^{\circ}10'9''E$ ), Arumuganeri ( $8^{\circ}59'40''$ ;  $78^{\circ}13'71''$ ) Kanyakumari (latitude  $8^{\circ}4'45''N$ ; longitude  $77^{\circ}32'38''E$ ) are located in the Gulf of Mannar zone along the South East Coast of India. Mandapam (nearby by Rameswaram) is situated near to Bay of Bengal and close to Gulf of Mannar Biosphere. The Biosphere contains 21 islands and also rich in marine biodiversity with estuaries, mudflats, beaches, forests of the near shore environment, including marine components like algal communities, sea grasses, coral reefs, salt marshes and mangroves. The closest tourism destination of Mandapam is Rameswaram.

Thoothukudi and Arumuganeri are the major industrial areas contains major chemical industries like SPIC, Copper smelting plant, Dharangadhara chemicals, salt pans, Thermal power station, and hundreds of small scale industrial units in Thoothukudi SIPCOT complex. Thoothukudi is well known for pearl, fishery and shipbuilding. It is one of the important major Port having a number ship movement. The movement of ships and fishing operation by mechanized boats also release oil effluents and petrochemical products into the sea. The Thermal power station directly dumps its ash into the sea. Now it is under expansion with Neyveli Lignite Corporation (NLC) Likewise the other industries also discharge their wastes into the sea. The effluents from industries in and around Thoothukudi and Arumuganeri coastal region are discharged directly or indirectly into the sea and it may affect the hydrographic properties.

Kanyakumari (formerly known as Cape Comorin), lies at the southernmost tip of East coast of India. Part of the fascination, it is the end point of the Indian peninsula where the meeting of the Bay of Bengal, the Arabian Sea and the Indian Ocean. It is one of the important Tourist Spot as well as Pilgrim place (Figure 2).



Figure.2 Sampling Locations and Sampling Points

### III. MATERIALS AND METHOD

The Temperature (surface and water) was measured using a standard centigrade mercury thermometer. Salinity was measured with the help of a Digital Refractometer PR-100SA (ATAGO) and the seawater pH was measured using HACH portable pH meter. Dissolved oxygen was estimated by the modified Winkler's method and expressed as mg/l. For the analysis of nutrients, surface water samples were collected in clean polyethylene bottles, kept in an ice-box, and transported immediately to the laboratory. The water samples are filtered through the Millipore filtering system (MFS) for the required filtered sample. The Nutrients and Chlorophyll-a were determined by the standard methods prescribed by Strickland and Parsons (1972) [9] and Grasshoff et al (1999) [10], further the sample were analyzed using SHIMADZU (UV-2600) UV-VIS Spectrophotometer. Nutrient concentrations were expressed in  $\mu\text{Moles /L}$ . Monthly variations of Physico-chemical parameters viz., temperature, salinity, pH, dissolved oxygen, nitrite, nitrate, ammonia, total phosphate, reactive silicate and Chlorophyll -a were recorded from January 2014 to December 2014. Based on the cyclic phenomena of meteorological events, four seasons are broadly indicated as month wise and they are (1) Post -Monsoon (January to March) (2) Summer (April to June) (3) Pre- Monsoon (July to September) (4) Monsoon (October to December).

### IV. RESULTS AND DISCUSSION

#### 4.1 TEMPERATURE

The temperature was basically important for its effects on the chemistry and biological activities of organisms in water. Temperature was known to influence in the determination of other factors like pH, conductivity, dissolved gases and various forms of alkalinity. Generally, the surface water temperature is influenced by the intensity of solar radiation, evaporation, freshwater influx and cooling and mix up with ebb tide and the water flow from adjoining neritic zone waters [11]. The water temperature during Monsoon season (October to December) was low because of strong land sea breeze and precipitation and the recorded high value during summer season (April to June) could be attributed to high solar radiation [12, 13]. The seasonal variation in the water temperature depends upon the wind force, freshwater discharge influx of the inshore water and atmospheric temperature (Figure 3).

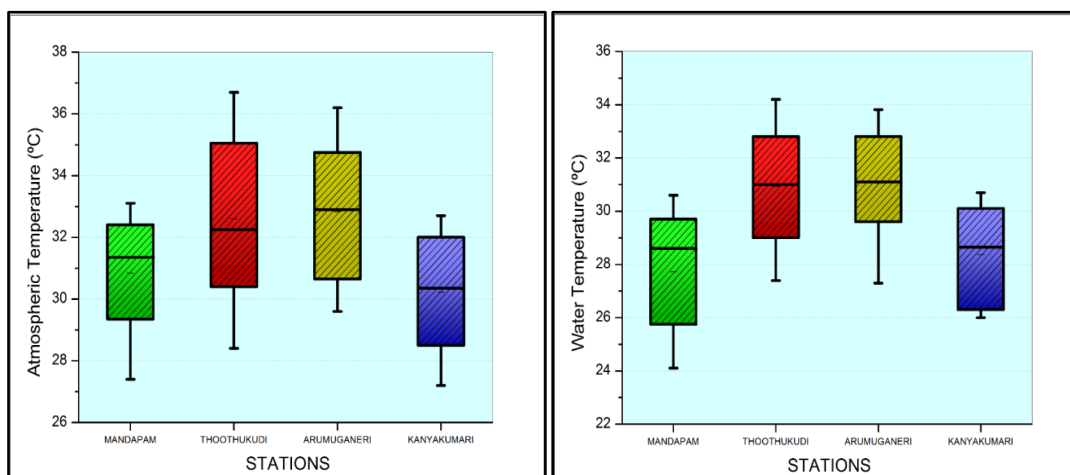


Figure.3 Atmospheric and Water Temperature at Different Stations

#### 4.2 SALINITY

The salinity acts as a limiting factor in the distribution of living organisms, and its variation caused by dilution and evaporation is most likely to influence the fauna in the intertidal zone [14]. Salinity is regarded as the second important physical characteristic of the marine environment. This salinity factor has high influence on the fauna. Less wave and tidal action with decreased freshwater inflow and land drainage may also be considered fluctuations in salinity [12]. The changes in the salinity in the coastal waters are due to the influx of freshwater from river, by land runoff caused by monsoon, or by tidal variations. Higher values in summer season 36.07 (‰) at Kanyakumari could be attributed to high degree of evaporation with decreased freshwater inflow and land drainage (Figure 4). Drop in salinity during monsoon season 31.54 (‰) at Mandapam is related to heavy showers and consecutive floodwater from up streams [15, 16].

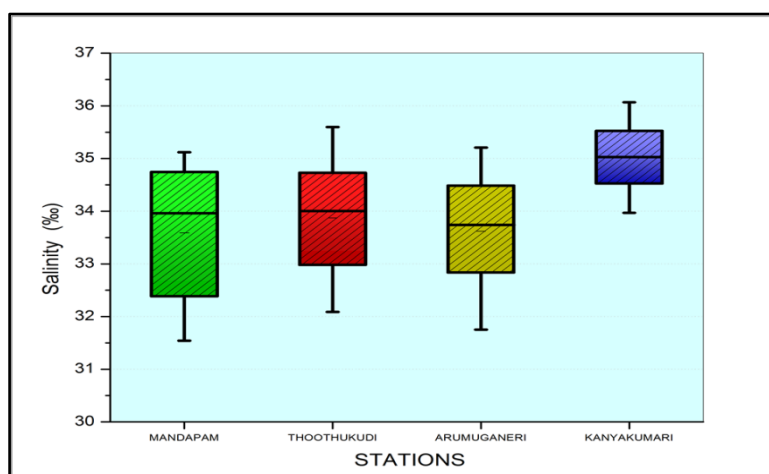


Figure.4 Salinity at Different Stations

#### 4.3 HYDROGEN ION CONCENTRATION (pH)

Hydrogen ion concentration or pH as one of the vital environmental characteristics decides the survival, metabolism, physiology and growth of aquatic organisms. pH is influenced by acidity of the bottom sediment and biological activities [17]. pH may be affected by total alkalinity and acidity, run off from surrounding rocks and water discharges [18]. The pH of the natural water system depends on the concentration of carbonate, bicarbonate and hydroxyl ion present. pH is known as the master variable in water since many properties, processes and reaction are pH dependent. Due to the buffering capacity of the sea water, generally the pH ranges from 7.8 to 8.3 in the coastal water [19]. The low pH 7.96 at Thoothukudi is due to the dilution of seawater by fresh water flow and runoff during the monsoon season [20]. Generally, fluctuations in pH values during different seasons of the year is attributed to factors like removal of  $\text{CO}_2$  by photosynthesis through bicarbonate degradation, dilution of seawater by freshwater influx, reduction of salinity and temperature and decomposition of organic matter [21, 22]. The recorded high pH value 8.31 at Kanyakumari during summer season might be due to the influence of seawater penetration and high biological activity like photosynthesis by dense phytoplankton blooms (Figure 5).

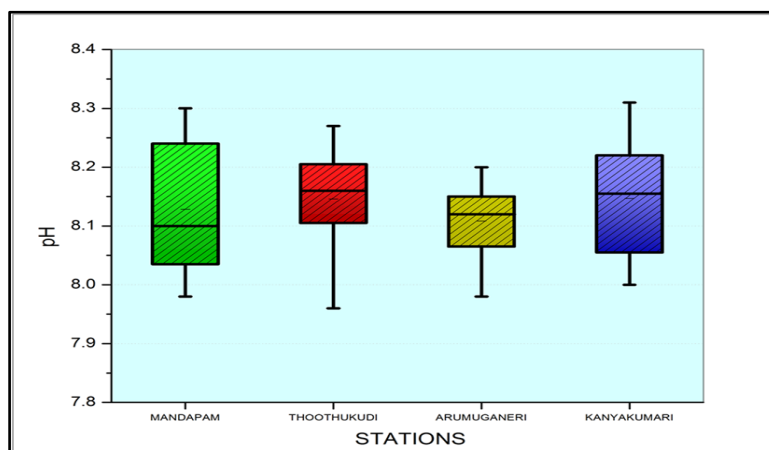


Figure.5 Hydrogen Ion Concentration (pH) at Different Stations

#### 4.4 DISSOLVED OXYGEN

The dissolved oxygen is very essential for the respiratory metabolism of all aquatic animals. It favors the stability and availability of nutrients to the animals. Therefore, it increases the productivity of the ecosystems. Usually the dissolved oxygen content in the water samples depends on the temperature and seasons. Two main sources of dissolved oxygen are diffusion of oxygen from the air and photosynthetic activity. It has been observed that the dissolved oxygen concentration was low in summer and high in monsoon. During the monsoon period the inflow of freshwater from the adjacent water sources having higher oxygen content, the coastal waters showed an increased level of dissolved oxygen [23, 23]. Dissolved oxygen can be removed from the water by discharges of the oxygen demanding anthropogenic wastes, other inorganic reductants like hydrogen sulphide, ammonia, ferrous, nitrate and other oxidizable substances tends to decrease dissolved oxygen in water. It is well known that the temperature and salinity affect the dissolution of oxygen [24]. In the present investigation, higher values of dissolved oxygen 5.95 mg/l at Kanyakumari were recorded during monsoon season might be due to the cumulative effect of higher wind velocity coupled with heavy rainfall and the resultant freshwater mixing attributed that seasonal variation of dissolved oxygen is mainly due to freshwater flow and terrigenous impact of sediments[11,25]. The dissolved oxygen shows an inverse trend against the temperature and the salinity. Dissolved oxygen was observed to be low 4.27 mg/l at Thoothukudi during summer season, which could be due to the gradual saline water incursion and increasing temperature (Figure 6) [26].

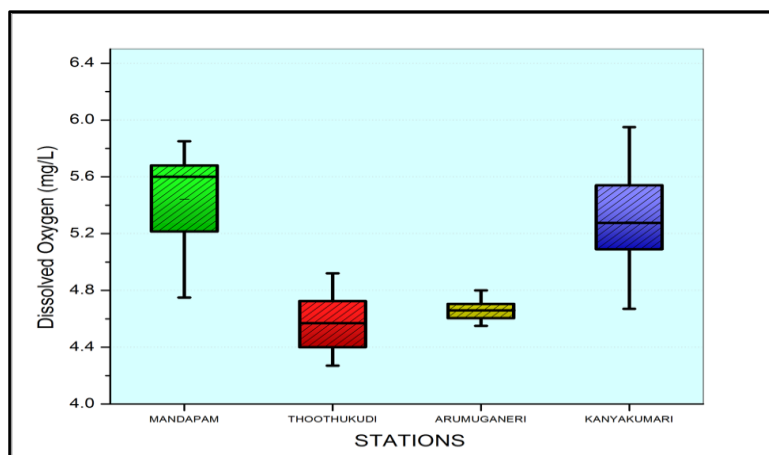


Figure.6 Dissolved Oxygen at Different Stations

#### 4.5 NUTRIENTS

Nutrients are considered as one of the most important parameters in the aquatic environment prompting growth, reproduction and metabolic activities of marine species. Distribution of nutrients is mainly based on the season, tidal conditions and freshwater flow from land source. The marine systems are generally nitrogen limited, excessive nitrogen inputs can result in water quality degradation due to toxic algal blooms, oxygen deficiency, habitat loss, decreases in biodiversity and fishery losses. The main cause of eutrophication involves the enrichment of water by excess nutrients. It can cause serious problems in the coastal zone through disturbance of ecological balances and fisheries, ultimately interfering with recreational activities, and also the quality of marine life [27].

#### 4.6 DISSOLVED INORGANIC NITRITE

Nitrite, the intermediate oxidation state between ammonia and nitrate, it can appear as a transient species by the oxidation of ammonia or by the reduction of nitrate [28]. The higher value 1.28  $\mu\text{M/l}$  of nitrite recorded at Thoothukudi during monsoon season is due to various reasons including variations in phytoplankton excretion, oxidation of ammonia and reduction of nitrate and by recycling of nitrogen and bacterial decomposition of planktonic detritus present in the environment. It is also due to denitrification and air sea interaction exchange of chemicals [7]. The recorded low nitrite value 0.31  $\mu\text{M/l}$  at Arumuganeri during summer seasons may be due to high salinity and temperature effect (Figure 7) [29].

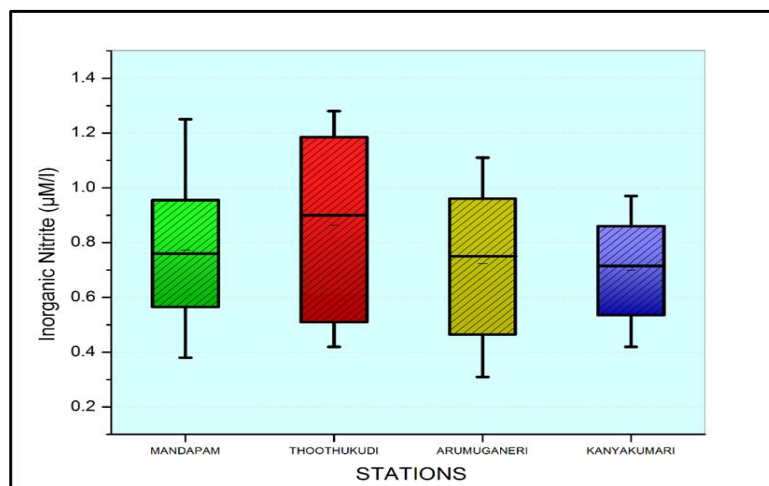


Figure.7 Dissolved Inorganic Nitrite at Different Stations

#### 4.7 DISSOLVED INORGANIC NITRATE

Nitrate is one of the most important indicators of pollution of water which represents the highest oxidized form of nitrogen. It plays a significant role in sustaining the aquatic life in marine environment. The increased nitrates level 10.17  $\mu\text{M/l}$  at Thoothukudi during Monsoon season is due to fresh water inflow, to leaching of rocks, fertilizer, chemical industries, domestic and municipal sewage, organic matter decomposition and terrestrial run-off during the monsoon season [10] [30,31]. Another possible way of nitrates entry is through oxidation of ammonia form of nitrogen to nitrite formation [11]. The recorded low value 2.45  $\mu\text{M/l}$  at Mandapam during summer period may be due to its utilization by phytoplankton as evidenced by high photosynthetic activity and the dominance of neritic seawater having a negligible amount of nitrate (Figure 8) [30, 32].

#### 4.8 DISSOLVED INORGANIC PHOSPHATE

The dissolved inorganic phosphate is an important nutrient for marine phytoplankton, marine biota actively involved in the activities [33]. Inorganic phosphate concentration is the useful index of eutrophication in the coastal water. Water receiving raw or untreated sewage, agriculture drainage and certain industrial waste usually contain significant concentration of phosphate. Phosphorus is as soluble reactive component and readily forms organic phosphorus and polyphosphate [34]. Phosphate concentration in coastal waters depend upon its concentration in the freshwater that mixed with the seawater within the sea-land interaction zone, upwelling, and microbial decomposition of organic matters[35]. Coastal waters except those receives freshwater contaminated with domestic wastes containing detergents as well as wastes from agro field rich with phosphate-phosphorous fertilizers and pesticides[36]. The observed high monsoonal phosphate value 1.91  $\mu\text{M/l}$  at Thoothukudi might be due to the regeneration and release of total phosphorus from bottom mud into the water column by turbulence and mixing [29]. Moreover, the bulk of weathering of rocks, soluble alkali metal phosphates in the upstream area are also one of the sources. The addition of super phosphates applied in the agricultural fields as fertilizers and alkyl phosphates used in households, as detergents can be other sources of inorganic phosphates during the season [32]. The summer low value 0.35  $\mu\text{M/l}$  could be attributed to the limited flow of freshwater, high salinity and utilization of phosphate by the marine organisms. The variation may also be due to the processes like adsorption and desorption of phosphates and buffering action of sediment under varying environmental conditions (Figure 9) [22].

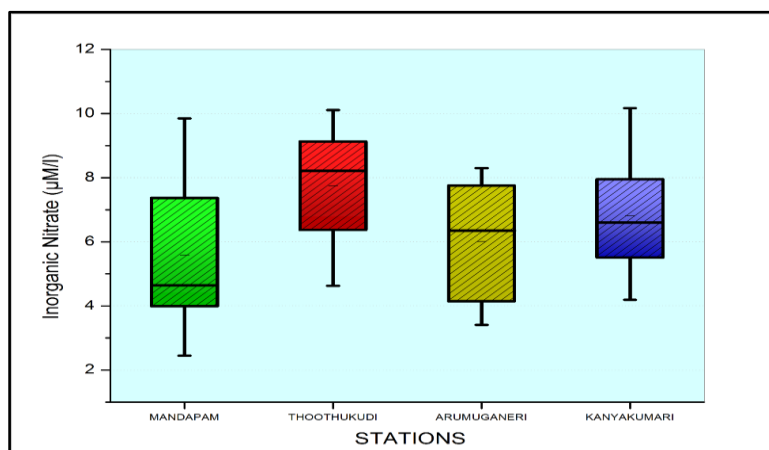


Figure.8 Dissolved Inorganic Nitrate at Different Stations

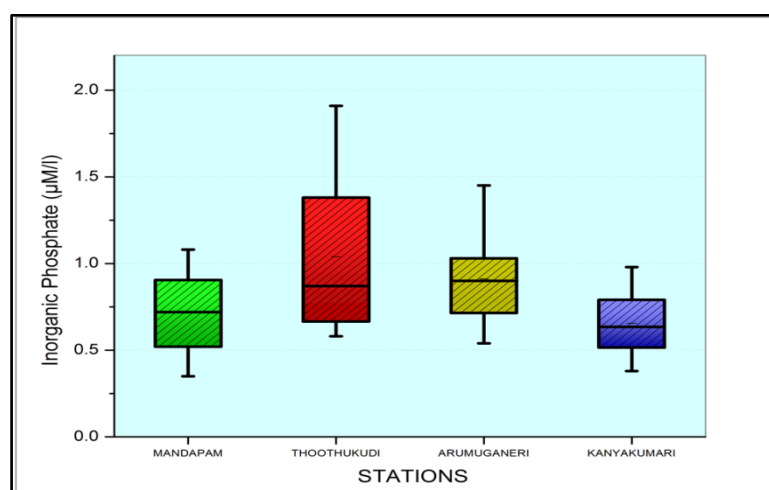


Figure.9 Dissolved Inorganic Phosphate at Different Stations

#### 4.9 REACTIVE SILICATES

Silicate is one of the important nutrients which regulate the phytoplankton distribution in the coastal water. The variation of silicate in coastal water is influenced by physical mixing of seawater with freshwater, adsorption into sedimentary particles, chemical interaction with clay minerals, co-precipitation with humic components, and biological removal by phytoplankton, especially by diatoms and silicoflagellates [28]. The silicate content was higher than that of the other nutrients and the recorded high monsoon values 41.33  $\mu\text{M/l}$  at Kanyakumari could be due to heavy influx of freshwater derived from land drainage carrying silicate leached out from rocks and also from bottom sediments exchanging with overlying water due to the turbulent nature of water in the coastal water (Figure 10) [22, 11]. Higher rainfall influenced land runoff and high fresh water inflow also increased silicate concentration. The low concentration of silicate value 7.10  $\mu\text{M/l}$  at Arumuganeri is observed during summer season is due to the utilization by marine organisms and algae for their biological activity [24, 31]. Part of silicate depletion is due to the adsorption and co-precipitation of soluble silicon with humic and Iron compounds [37].

#### 4.10 AMMONIA

Ammonium is the nitrogenous end product of the bacterial decomposition of natural organic matter containing nitrogen. In the presence of high ammonium concentrations, the phytoplankton Productivity should be high by using  $\text{NH}_4^+$  rather than  $\text{NO}_3^-$  [38]. The possible sources of ammonia input into the waters could be from land runoff, zooplankton excretion, or demineralization of organic matter [39]. Ammonium ( $\text{NH}_4^+$ ) represented 80% of Dissolved Inorganic Nitrogen (DIN) and its highest values were always associated with fresh water inflow [40]. The spatial and temporal variation in ammonia concentration is due to its oxidation to other forms or reduction of nitrates to lower forms in coastal waters [29]. The higher ammonia concentration 7.13  $\mu\text{M/l}$  was observed at Thoothukudi during the monsoon season and the lower values 0.62  $\mu\text{M/l}$  were found at Mandapam during the summer season (Figure 11). The surface runs off wastes, agricultural wastes washed and show maximum value in the monsoon. Excess ammonia indicates polluted water and maximum algal growth. The recorded higher concentration could be partially due to the death and subsequent decomposition of phytoplankton and also due to the excretion of ammonia by planktonic organisms [41].

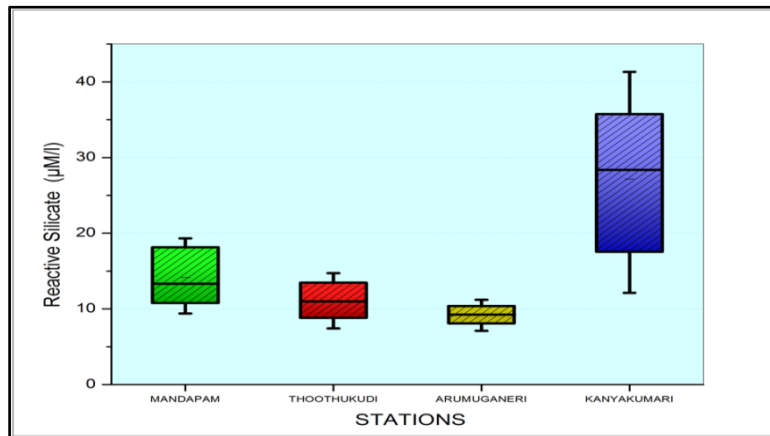


Figure.10 Reactive Silicate at Different Stations

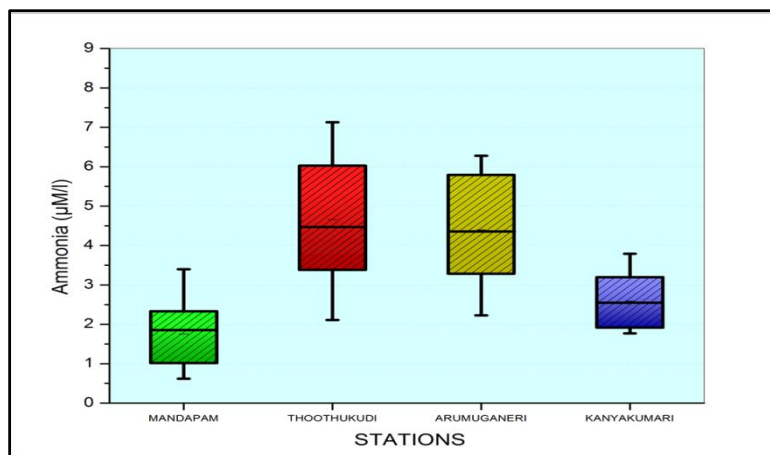


Figure.11 Ammonia at Different Stations

**4.11 CHLOROPHYLL –a**

Chlorophyll a is considered as the most reliable index of phytoplankton biomass. Fresh water influx and land runoff resulted in low Chl-a concentration during the monsoon with decreasing salinity conditions [42]. Primary productivity potential of the marine environments depends upon the phytoplankton, which alone contributes 90% of the total marine primary production. Thus chlorophyll-a which constitutes the chief photosynthetic pigment of phytoplankton, is an index that provides the primary production potential upon which the biodiversity, biomass and carrying capacity of that system depends upon [43]. A higher value of Chlorophyll-a 17.27 mg/m<sup>3</sup> was recorded at Kanyakumari during summer and the low value 2.93 mg/m<sup>3</sup> at Arumuganeri during monsoon season (Figure 12). The reduction in Chlorophyll- a during monsoon season may be due to freshwater discharges from the landslides causing turbidity and less availability of light [41, 44]. Therefore the investigation on variations of Chlorophyll- a is very important to the study of water quality and marine pollution. Its maximum and minimum concentration can reflect the physical and chemical characters of the environment.

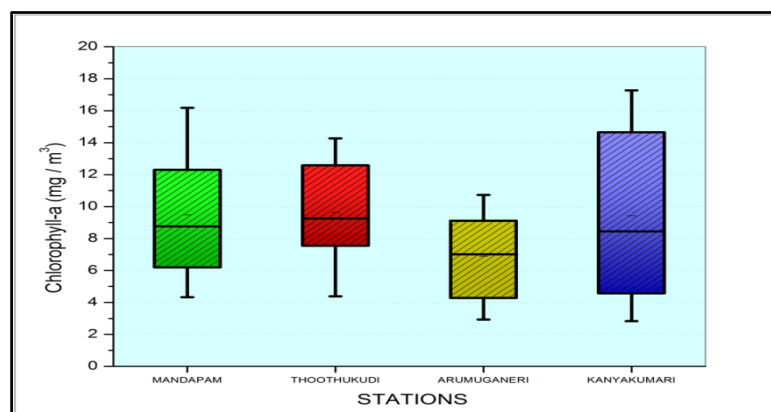


Figure.12 Chlorophyll-a at Different Stations

V. STATISTICAL INTERPRETATION OF HYDROGRAPHICAL PROPERTIES

5.1 MANDAPAM

In this station seasons influence all the hydrographical properties. Water temperature is strongly correlated to pH, salinity. Salinity also negatively correlated to Silicate and phosphate. Chlorophyll-a negatively correlated with Dissolved Oxygen (Table.1).Biplot also supported the same. In the Biplot (Figure.13) summer and Monsoon season shows strongest variation pattern. Major nutrients influenced in the monsoon season and have similar response. Biplot shows that NO<sub>2</sub>-N and PO<sub>4</sub> distinguish the other parameters in the monsoon and Post monsoon season.

Table .1 Correlation coefficient values between the Hydrographical parameters at Mandapam

Parameters	Air Temp (°C)	Water Temp (°C)	pH	Salinity (‰)	Dissolved Oxygen (mg/l)	NO <sub>2</sub> -N (µM/l)	NO <sub>3</sub> -N (µM/l)	SiO <sub>2</sub> (µM/l)	PO <sub>4</sub> (µM/l)	NH <sub>4</sub> -N (µM/l)	Chlorophyll-a (mg/m <sup>3</sup> )
Air Temp	1										
WaterTemp	0.9246	1									
pH	0.8565	0.9743	1								
Salinity	0.9786	0.9801	0.9438	1							
Dis.Oxygen	-0.8324	-0.8715	-0.9347	-0.8951	1						
NO <sub>2</sub> -N	-0.9169	-0.8015	-0.8006	-0.8949	0.9153	1					
NO <sub>3</sub> -N	-0.9793	-0.8419	-0.7368	-0.9189	0.7149	0.8746	1				
SiO <sub>2</sub>	-0.9698	-0.8738	-0.8475	-0.9506	0.9059	0.9864	0.9327	1			
PO <sub>4</sub>	-0.9422	-0.9949	-0.9466	-0.9816	0.8312	0.7932	0.8780	0.8748	1		
NH <sub>4</sub> -N	-0.9453	-0.8412	-0.8292	-0.9259	0.9166	0.9968	0.9040	0.9963	0.8368	1	
Chl-a	0.9210	0.8614	0.8762	0.9285	-0.9622	-0.9891	-0.8531	-0.9835	-0.8442	-0.9907	1

5.2 THOOTHUKUDI

In Thoothukudi coastal water salinity was positively correlated with pH, Temperature and Chlorophyll-a and negatively correlated with NH<sub>4</sub>-N and other nutrients (Table.2). In the Biplot (Figure.13) Monsoon and summer shows strongest variation pattern. The Biplot shows Monsoon season was strongly influenced by DO and other nutrients. This shows that Land run-off and sewage penetration is more than the other stations. In the Biplot Temperature, salinity in the Pre-Monsoon season and PO<sub>4</sub>, DO, NO<sub>3</sub>-N in the monsoon season has the similar response pattern. NO<sub>2</sub>-N, and NH<sub>4</sub>-N distinguish the other parameters in the monsoon season (Figure.13).

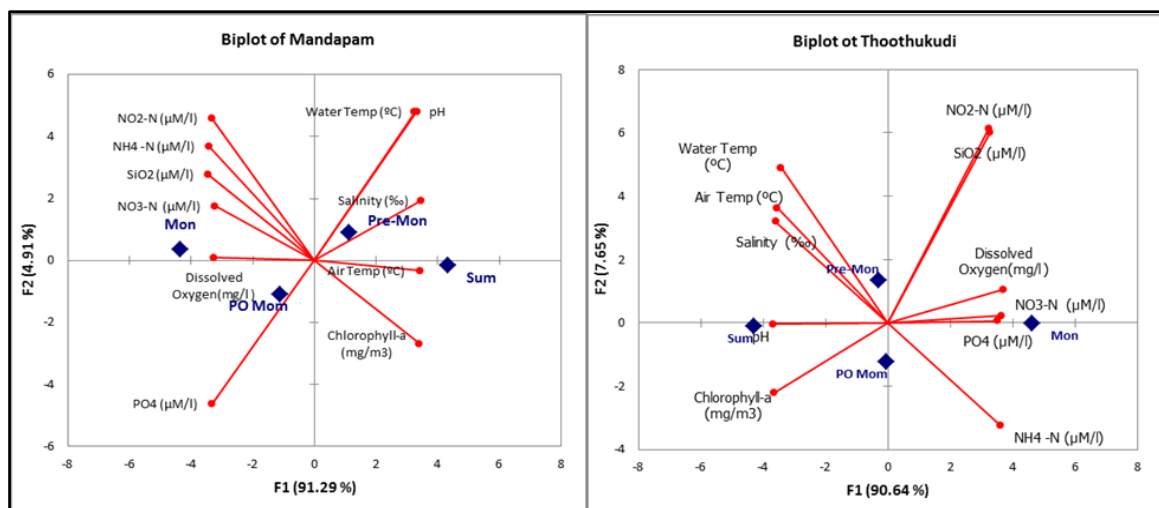


Figure.13 Biplot of Mandapam and Thoothukudi Stations

**Table. 2 Correlation coefficient values between the Hydrographical parameters at Thoothukudi**

Parameters	Air Temp (°C)	Water Temp (°C)	pH	Salinity (‰)	Dissolved Oxygen (mg/l)	NO <sub>2</sub> -N (µM/l)	NO <sub>3</sub> -N (µM/l)	SiO <sub>2</sub> (µM/l)	PO <sub>4</sub> (µM/l)	NH <sub>4</sub> -N (µM/l)	Chlorophyll-a (mg/m <sup>3</sup> )
Air Temp	1										
WaterTemp	0.9894	1									
pH	0.9343	0.9160	1								
Salinity	0.9983	0.9887	0.9528	1							
Dis.Oxygen	-0.9282	-0.8889	-0.9886	-0.9434	1						
NO <sub>2</sub> -N	-0.7060	-0.6202	-0.8523	-0.7279	0.9080	1					
NO <sub>3</sub> -N	-0.9462	-0.8917	-0.9393	-0.9486	0.9737	0.8819	1				
SiO <sub>2</sub>	-0.7029	-0.6336	-0.8817	-0.7320	0.9165	0.9875	0.8563	1			
PO <sub>4</sub>	-0.8771	-0.8788	-0.9821	-0.9038	0.9468	0.7967	0.8578	0.8547	1		
NH <sub>4</sub> -N	-0.9959	-0.9904	-0.9579	-0.9993	0.9434	0.7227	0.9405	0.7328	0.9159	1	
Chl-a	0.8937	0.8427	0.9732	0.9103	-0.9954	-0.9438	-0.9698	-0.9470	-0.9267	-0.9090	1

### 5.3 ARUMUGANERI

In this station Chlorophyll-a was strongly correlated with salinity, pH and Temperature, and negatively correlated with DO and other nutrients (Table.3). In the Biplot (Figure.14) summer, Post-Monsoon, Monsoon season shows strong variation pattern. Temperature and Chlorophyll-a distinguish the other parameters Pre-monsoon and summer season. Likewise NO<sub>2</sub>-N and PO<sub>4</sub> distinguish the other parameters in the monsoon season. DO, NH<sub>4</sub>-N, NO<sub>3</sub>-N, SiO<sub>2</sub>, and NO<sub>2</sub>-N shows similar response in the monsoon season (Figure.14).

**Table .3 Correlation coefficient values between the Hydrographical parameters at Arumuganeri**

Parameters	Air Temp (°C)	Water Temp (°C)	pH	Salinity (‰)	Dissolved Oxygen (mg/l)	NO <sub>2</sub> -N (µM/l)	NO <sub>3</sub> -N (µM/l)	SiO <sub>2</sub> (µM/l)	PO <sub>4</sub> (µM/l)	NH <sub>4</sub> -N (µM/l)	Chlorophyll-a (mg/m <sup>3</sup> )
Air Temp	1										
WaterTemp	0.9246	1									
pH	0.8565	0.9743	1								
Salinity	0.9786	0.9801	0.9438	1							
Dis.Oxygen	-0.8324	-0.8715	-0.9347	-0.8951	1						
NO <sub>2</sub> -N	-0.9169	-0.8015	-0.8006	-0.8949	0.9153	1					
NO <sub>3</sub> -N	-0.9793	-0.8419	-0.7368	-0.9189	0.7149	0.8746	1				
SiO <sub>2</sub>	-0.9698	-0.8738	-0.8475	-0.9506	0.9059	0.9864	0.9327	1			
PO <sub>4</sub>	-0.9422	-0.9949	-0.9466	-0.9816	0.8312	0.7932	0.8780	0.8748	1		
NH <sub>4</sub> -N	-0.9453	-0.8412	-0.8292	-0.9259	0.9166	0.9968	0.9040	0.9963	0.8368	1	
Chl-a	0.9210	0.8614	0.8762	0.9285	-0.9622	-0.9891	-0.8531	-0.9835	-0.8442	-0.9907	1

### 5.4 KANYAKUMARI

In Kanyakumari coastal waters Temperature positively correlated with pH, salinity and chlorophyll-a and negatively correlated with DO, NH<sub>4</sub>-N and other nutrients (Table.4). In Kanyakumari Chlorophyll-a shows negative correlation with DO, SiO<sub>2</sub>, PO<sub>4</sub>, this shows that the utilization of nutrients for the photosynthetic activity. Biplot shows that summer season strongly influenced by pH and salinity. DO and nutrients are influenced by Post-Monsoon and Monsoon season. NO<sub>2</sub>-N and NH<sub>4</sub>-N distinguishes the other parameters during Post Monsoon and Monsoon season (Figure 14).

Table .4 Correlation coefficient values between the Hydrographical parameters at Kanyakumari

Parameters	Air Temp (°C)	Water Temp (°C)	pH	Salinity (‰)	Dissolved Oxygen (mg/l)	NO2-N (µM/l)	NO3-N (µM/l)	SiO2 (µM/l)	PO4 (µM/l)	NH4 -N (µM/l)	Chlorophyll-a (mg/m3)
Air Temp	1										
WaterTemp	0.9979	1									
pH	0.9698	0.9709	1								
Salinity	0.9651	0.9666	0.9998	1							
Dis.Oxygen	-0.9697	-0.9731	-0.8896	-0.8817	1						
NO2-N	-0.8458	-0.8389	-0.6904	-0.6768	0.9345	1					
NO3-N	-0.9438	-0.9583	-0.9773	-0.9784	0.8888	0.6677	1				
SiO2	-0.9649	-0.9517	-0.9741	-0.9714	0.8763	0.7277	0.9062	1			
PO4	-0.9837	-0.9906	-0.9334	-0.9279	0.9917	0.8808	0.9404	0.9025	1		
NH4 -N	-0.9331	-0.9465	-0.9806	-0.9827	0.8630	0.6280	0.9979	0.9109	0.9204	1	
Chl-a	0.9889	0.9788	0.9345	0.9275	-0.9664	-0.8878	-0.8848	-0.9613	-0.9641	-0.8718	1

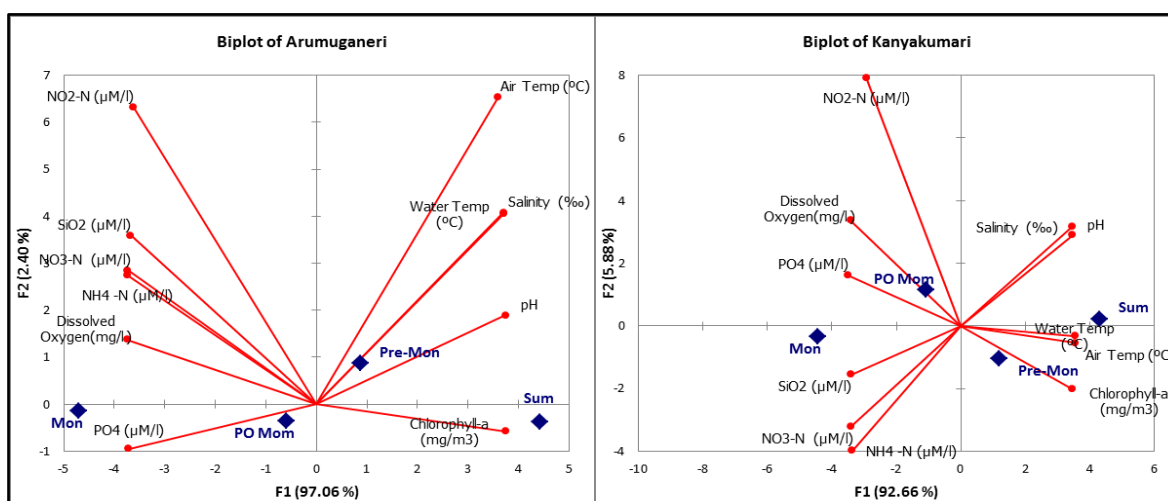


Figure.14 Biplot of Arumuganeri and Kanyakumari

VI. CONCLUSION

The result shows that the hydrographical parameters exhibited distinct variations by different seasons. Occurrence of high concentrations of nutrients in the study areas can be reasonably due to the Land runoff and anthropogenic input. The fluctuation of Temperature, pH, salinity, and Dissolved Oxygen are seen in the Monsoon and Non-Monsoon seasons. Salinity was found to be low along the monsoon season; it is due to the large amount of fresh Water input along the coast during the northeast monsoon. The increase of Chlorophyll-a during the summer season is attributed due prominent increase of salinity, pH and reduction of turbidity. The knowledge of nutrients, related to their sources, availability and the utilization levels gives us the information about the productivity potential and health of the Marine Ecosystem. The present baseline information is useful for the further Ecological Monitoring and assessment along the coastal waters.

REFERENCES

- [1] Karande A A, Use of epifaunal communities in pollution monitoring. *J Environ Biol*12:191- 200, 1991.
- [2] Damotharan, P., N. VengadehPerumal, M. Arumugam, S. Vijayalakshmi and T. Balasubramnian, Seasonal variation of physicochemical characteristics in point Calimere coastal waters (South East Coast of India). *Middle-East Journal of Scientific Research*, 6(4): 333-339, 2010.
- [3] PoonamBhadja and Rahul Kundu, Status of seawater quality at few industrially important coasts of Gujarat (India) off Arabian Sea. *Indian Journal of Geo-Marine Sciences*, 41(1): 90-97, 2012.
- [4] G. J. Chakrapani and V. Subramanian, "Rate of Erosion and Sedimentation in the Mahanadi River Basin, India," *Journal of Hydrology*, Vol. 149, No. 1-4, pp. 39-48,1993.
- [5] SorenLaurentius Nielsen, Gary T. Banta, Morten Foldager Pedersen "Estuarine Nutrient Cycling: The Influence of Primary Producers", *Kluwer Academic Publishers*, the Netherlands, 2004.
- [6] Sridhar. R., Thangaradjou, T. and Kannan, L., Comparative investigation on physic-chemical properties of the coral reef and seagrass ecosystems of the Palk Bay. *Indian Journal of Mar. Sciences*. 37 (2). 207-213,2008.
- [7] Asha, P. S. and Diwakar. Hydrobiology of the inshore waters off Tuticorin in the Gulf. *J. Mar. Biol. Ass. India*, 49: 7-11,2007.

- [8] Choudhury, S.B. and R.C. Panigrahy., Seasonal distribution and behavior of nutrients in the creek and coastal waters of Gopalpur, east coast of India. *Mahasagar-Bull. Natl. Inst. Oceanogr.*, 24: 81-88,1991.
- [9] J. D. H. Strickland and T. K. Parsons "A Practical Hand Book of Seawater Analysis," *Bulletin. Fisheries Research Board of Canada, Vol. 167*, p. 172,1972.
- [10] K. Grasshoff, M. Ehrhardt and K. Bkreming, "Methods of Seawater Analysis," *Wiley-VCH*, Hoboken, pp. 159-226,1999.
- [11] Govindasamy, C., L. Kannan and JayapaulAzariah., Seasonal variation in physico-chemical properties and primary production in the coastal water biotopes of Coromandel coast, *India. J. Environ. Biol.*, 21: 1-7, 2000.
- [12] Sampathkumar, P.andKannan, L., Seasonal variations in physico-chemical characteristics in the Tranquebar- Nagapattinam region, southeast coast of India. *Poll. Res.*, 17(4):397-402, 1998.
- [13] Ajithkumar, T. T., T. Thangaradjou and L. Kannan., Physico-chemical and biological properties of the Muthupettai mangrove in Tamil Nadu. *J. Mar. Biol. Ass. India*, 48: 131-138, 2006.
- [14] Gibson, R. N.,Recent studies on the biology of intertidal fishes. *Oceanogr. Mar. Biol. Ann. Rev.*20: 363-414, 1982.
- [15] Mitra, A., Patra, K.C. and Panigraphy, R.C., Seasonal variations of some hydrographical parameters in a tidal creek opening into the Bay of Bengal. *Bull. Natl. Inst. Oceanogr.*, 23(1):55-62,1990.
- [16] SundaramanickamA, Distribution of finfish larvae in relation to hydrographical parameters in parangipettai coast and adjacent water (South East Cost of India). *Ph.D. Thesis, Annamalai University, India*,2004.
- [17] Balasubramanian, R. and L. Kannan., Physico chemical characteristics of the coral reef Environs of the Gulf of Mannar Biosphere Reserve, India. *Int. J. Ecol. Environ. Sci.*, 31, 265-271, 2005.
- [18] G. Velsamy, N. Manoharan, S. Ganesan., Analysis of Physico-Chemical Variations in Sea Water samples Uppanar Estuary, Cuddalore, Tamilnadu, India. *International Journal of Research in Biological Sciences*;3(2):80-83,2013.
- [19] Omstedt, A., Edman, M., Anderson, L.G., Laudon, H., Factors influencing the acid-base (pH) balance in the Baltic Sea: a sensitivity analysis. *Tellus* 62, 280-295, 2010.
- [20] Subramanian, B. and A. Mahadevan, Seasonal and diurnal variation of hydrobiological characters of coastal waters of Chennai, Bay of Bengal. *Indian J. Mar. Sci.*, 28: 429-433, 1999.
- [21] Upadhyay, S. Physico-chemical characteristics of the Mahanadi estuarine ecosystem, east coast of India. *Ind. J. Mar. Sci.*, 17, 19-23, 1988.
- [22] Rajasegar, M. Physico-chemical characteristics of the Vellar estuary in relation to shrimp farming. *J. Environ. Biol.* 24: 95-101, 2003.
- [23] Govindasamy, C. and JayapaulAzariah., Monsoonal impact on nutrient distribution in the coastal water of Tamil Nadu, *Indian. Hydrobiol.*, 2(2): 75-85,1997.
- [24] A.Saravanakumar, M. Rajkumar, J. SeshSerebiah and G.A. Thivakaran., Abundance and seasonal variations of phytoplankton in the creek waters of western mangrove of Kachchh-Gujarat. *Journal of Environmental Biology*, 29(2), 271-274, 2008.
- [25] Padmavathi, D. and D. Satyanarayana., Distribution of nutrients and major elements in riverine, estuarine and adjoining coastal waters of Godavari, Bay of Bengal. *Indian J. Mar. Sci.*, 28: 345-354, 1999.
- [26] Govindasamy, C. and JayapaulAzariah., Monsoonal impact on nutrient distribution in the coastal water of Tamil Nadu, *Indian. Hydrobiol.*, 2(2): 75-85,1997.
- [27] Sankaranarayanan, V.N., Qasim, S.Z., Nutrients of Cochin backwaters in relation of environmental characteristics. *Mar. Biol.* 2, 236-247, 1969.
- [28] Satpathy KK, Mohanty AK, GouriSahu, Sarkar SK, Natesan U, Venkatesan R, Prasad MVR. Variations of physicochemical properties in Kalpakkam coastal waters, east coast of India, during southwest to northeast monsoon transition period. *Environmental Monitoring and Assessment [Internet]* ; 171: 411-424,2010.
- [29] Saravanakumar, A., M. Rajkumar, J. SeshSerebiah and G.A Thivakaran, Seasonal variations in Physico - chemical characteristics of water, sediment and soil texture in mangroves of Kach - Gujarat. *J. Environ. Biol.*, 29, 725 - 732,2008.
- [30] Rajaram, R., M. Srinivasan and M. Rajasegar., Seasonal distribution of physico-chemical parameters in effluent discharge area of Uppanar estuary, Cuddalore, Southeast coast of India. *J. Environ. Biol.*, 26: 291-297, 2005.
- [31] Ashok Prabu, V., P. Perumal and M. Rajkumar. Diversity of microzooplankton in Parangipettai coastal waters, southeast coast of India. *J. Mar. Biol. Ass. India*, 47: 14-19, 2005.
- [32] Bragadeeswaran, S. , M. Raja segar , M. Srinivasa n a nd U. Kanagarajan: Sediment texture and nutrients of Arasalar estuary, Karaikkal, southeast coast of India. *J. Environ. Biol.*, 28, 237-240, 2007.
- [33] Mackey, M.R.K., Labiosa, G.R., Street, H., Post, J., Paytan, A.,Phosphorus availability, phytoplankton community dynamics, and taxon-specific phosphorus status in the Gulf of Aqaba, Red Sea. *Limnol. Oceanogr.* 52, 873-885, 2007.
- [34] Rajashree Gouda and Panigrahy, R.C.,Monthly variations of some hydrographic parameters in the Rushikulya estuary east coast of India. *Mahasgar Bulletin of National Institute of Oceanography*. 26 (2): 73-85, 1993.
- [35] Paytan, A., Mclaughlin, K., The oceanic phosphorous cycle. *Chem. Rev.* 107, 563-576, 2007.
- [36] Liu, S.M., Hong, G.H., Ye, X.W., Zang, J., Jiang, X.L., Nutrient budgets for large Chinese estuaries and embayment. *Biogeosci. Discuss.* 6, 391-435, 2009.
- [37] Satpathy, K.K., Mohanty, A.K., Natesan, U., Prasad, M.V.R., Sarkar, S.K.,Seasonal variation in physicochemical properties of coastal waters of Kalpakkam, east coast of India with special emphasis on nutrients. *Environ. Monit. Assess.* 164, 153-171, 2009.
- [38] Dugadale, R.C., Wilkerson, F.P., Hogue, V.E., Marchi, A.,The role of ammonium and nitrate in spring bloom development in San Francisco Bay. *EST Coast Shelf Sci.* 73, 17-29, 2007.
- [39] Ketchum BH. Regeneration of nutrients by zooplankton. *Rapports ET Process - verbaux des Reunion. Conseil. Int Pour l Explor De la mer*; 153:142-147, 1962.
- [40] Martin, G.D., Vijay, J.G., Laluraj, C.M., Madhu, N.V., Joseph, T., Nair, M., Gupta, G.V.M., Balachandran, K.K., Fresh water influence on nutrient stoichiometry in a tropical estuary, Southwest coast of India. *Appl. Ecol. Environ. Res.* 6, 57-64, 2008.
- [41] Godhantaraman, N.Seasonal variations in species composition, abundance, biomass and estimated production rates of tintinnids at tropical estuarine and mangrove waters, Parangipettai, Southeast coast of India. *J. Mar. Sys.*, 36, 161-171, 2002.
- [42] Tripathy SC, Ray AK, Paatra S, Sarama VV. Water quality assessment of Gautami-Godavari mangrove estuarine ecosystem of Andhra Pradesh, India during September 2001. *J Earth Syst Sci.*; 114: 185-190, 2005.
- [43] Sarma, V.V., Sadhuram, Y., Sravanthi, N.A., Tripathy, S.C.,Role of physical processes in the distribution of chlorophyll-a in the Northwest Bay of Bengal during pre- and post-monsoon seasons. *Curr. Sci.* 91, 1133-1134, 2006.
- [44] ThillaiRajsekhar, K., P. Perumal and P. Santhanam: Phytoplankton diversity in the Coleroon estuary, Southeast coast of India. *J. Mar. Biol. Ass India*, 47, 127-132, 2005.

## Alternative Room Cooling System

<sup>1</sup>, Md. Fazle Rabbi, <sup>2</sup>, Mrittunjoy Sarker, <sup>3</sup>, Mohammad Mashud

*Department of Mechanical Engineering, Khulna University of Engineering & Technology, Khulna-9203, Bangladesh*

**ABSTRACT:** *The rapidly growing population results in an increasing demand for much more residential and commercial buildings, which leads to vertical growth of the buildings and needs proper ventilation of those buildings. Natural air ventilation system is not sufficient for conventional building structures. Hence fans and air-conditioners are must to meet the requirement of proper ventilation as well as space conditioning. Globally building sector consumes largest energy in heating, cooling, ventilation and space conditioning. This load can be minimized by the application of solar chimney and modification in building structure for heating, cooling, ventilation and space conditioning. Passive solar cooling is a subject of interest to provide cooling by using the sun, a powerful energy source. This is done for ensuring human comfort in hot climates. ASHRAE (American Society of Heating, Refrigerating and Air Conditioning Engineers) defines Comfort as 'that state of mind which expresses satisfaction with the thermal environment.' The present paper describes the development of a solar passive cooling system, which can provide thermal cooling throughout the summer season in hot and humid climates. The constructed passive system works on natural convection mode of air. Such system reduces the inside temperature of up to 5°C from the atmospheric temperature. Temperature can further be reduced by the judicious use of night ventilation.*

**Keywords -** *Passive cooling, Human comfort, Solar chimney*

### I. INTRODUCTION

The residential and commercial buildings consume largest amount of energy (almost 40% of total country's energy consumption) every year. And 50-60% of this energy is because of heating, ventilation and space conditioning in buildings [1]. Cooling means the transfer of energy of air from a space in order to maintain lower temperature with respect to natural surroundings. Comfort is that state of mind which expresses satisfaction with the thermal environment [2]. In regions with hot and humid climates, excessive heat is the major problem which causes human thermal discomfort [3]. Then cooling becomes the vital requirement for the people in the buildings. In modern buildings, this is accomplished thru mechanical and electrical instruments which cause greater energy consumption as told earlier. With the advent of the energy crisis, there had been a renewed interest in those aspects of architecture which contributed to thermal comfort in a building without or with minimum energy consumption in hot and humid climates. There are numerous techniques for passive heating in cold climates; such as direct gain, trombe wall, transparent insulation etc. [4]. Solar passive cooling techniques are not so much well-established as well as well-standardized like the solar passive heating techniques due to the dependency on the judicious use of night ventilation, shading, evaporative cooling etc. Ancient methods of cooling in arid zones have been described in Bahadori [5], and a summary of the state-of-art of passive cooling systems has been given in Givoni [6]. Hay's sky-therm system was tried in India several years ago, but no systematic follow-up studies were made [7]. Some of the techniques used for passive cooling do not remove the cooling load of a building itself, but rather extend the tolerance limits of humans for thermal comfort in a given space. Natural cooling refers to the use of natural heat sinks for excess heat dissipation from interior spaces, including ventilation, ground cooling, evaporative cooling and radiated cooling. So, by the combination of different passive and natural cooling techniques, it is possible to prevent overheating problems, decrease cooling loads and improve comfort conditions in buildings [8]. The present paper describes the research and developmental efforts of a solar passive cooling system for providing thermal cooling inside a building throughout the summer season in hot and humid climates.

## II. METHODOLOGY

The solar passive model (Fig.1.) consists of a solar chimney or solar air heater or simply a ventilator. This solar air heater is placed on the roof which acts as an exhaust fan by sucking hot air from room and venting it out during daytime. On the ground level, there is a bottom collector which is used as an evaporative cooler. This bottom collector is nothing but a water tank. A copper duct of circular cross-section is kept inside the collector. One end of the duct is connected to the room and the other end is open to atmosphere. The copper duct is completely immersed in the water tank. The collector is insulated and shadow is provided above the collector to neglect radiation absorption. Hot and light air moves out thru the chimney, and at the same time cool air gets in the room thru the copper duct due to creation of negative pressure inside the room.

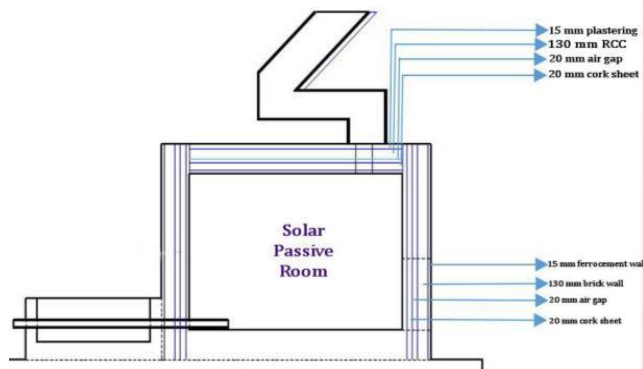


**Fig 1:** Cross-sectional view of solar passive cooling model **Fig 2:** 3D view of solar passive cooling model.

## III. DESIGN

### 3.1. Reduction of Total Thermal Load of an Ordinary Room thru Modification

The existing single room is 5 feet long, 4 feet wide and 3 feet high. The longer side is oriented along the east-west direction. It has masonry brick walls of 130 mm (5 inch) thickness, with a reinforced concrete slab of 100 mm (4 inch) thickness. A wooden door of area 2 ft<sup>2</sup> is provided on the north facing wall. A standard thermal network analysis was planned to find out the total thermal conditioning load of the building for a design inside-outside temperature difference of 5°C, which was found to be as 66.70 Watt. In order to reduce the total thermal conditioning load of the room, some retrofitting measures were carried out.

- The door was insulated by adding a cork sheet of thickness 2 cm.
- All the four walls were insulated from outside atmosphere by providing a 2 cm cork sheet and a 2 cm air gap. Ferrocement cladding was constructed around the walls to create the air gap.
- The roof was insulated by providing a 2 cm cork sheet. In addition, a wooden sheet was providing for creating the air gap. Applying the thermal network analysis again, the total thermal load of the modified room was calculated to be as 23.25 Watt.

### 3.2. Solar Chimney Design

Basically the solar chimney is nothing but a solar air heater operating under natural convection mode. The solar chimney considered for analysis is a collector (made by sheet of mild steel) of 51 inch length and 48 inch width. Glaswool insulation is provided in the bottom and the sides are made up of wood. The north facing, open loop system is set with a tilt of 45° from horizontal, has an air flow passage below the absorber plate.

### 3.3. Evaporative Cooler Design

The evaporative cooler is an insulated water tank, in which a copper pipe (of 3 inch diameter) is immersed. One end of the pipe is opened to the atmosphere and the other end is connected to the room.

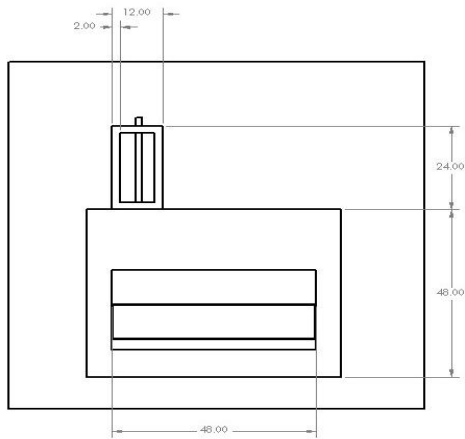


Fig 3: Front-view of solar passive cooling model.

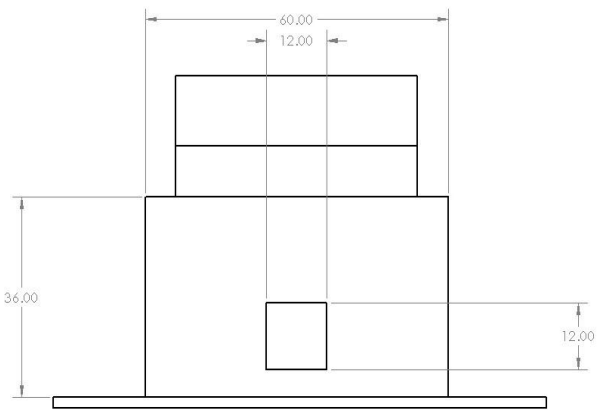


Fig 4: Top-view of solar passive cooling model.

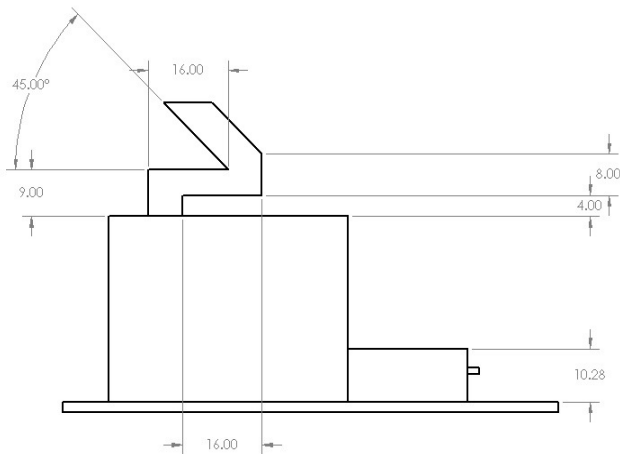


Fig 5: Right-side-view of solar passive cooling model. Fig 6: Photograph of constructed solar passive cooling

IV. PERFORMANCE ANALYSIS

An ordinary room (5ft X 4ft X 3ft) of similar size as the solar passive room is selected as the reference/ordinary room. Fig. 7 to fig. 11 illustrate various temperature variations from 21st May, 2014 to 25th May, 2014. It can be seen that, the passive room maintained temperature at about 4°C to 5°C below the ambient condition and at about 2°C to 3°C below the reference room temperature, which can be considered as comfortable.

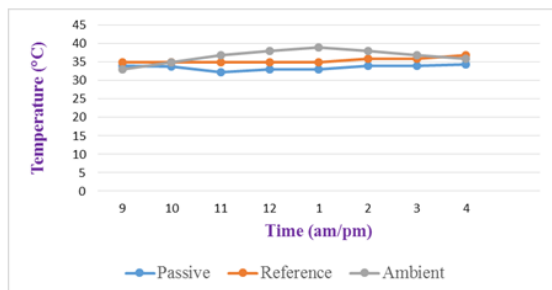


Fig 7: Variation in temperature between passive room, reference room and ambient atmosphere (for May 21<sup>st</sup>, 2014).

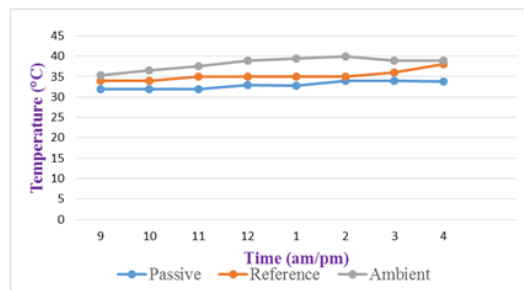


Fig 8: Variation in temperature between passive room, reference room and ambient atmosphere (for May 22<sup>nd</sup>, 2014).

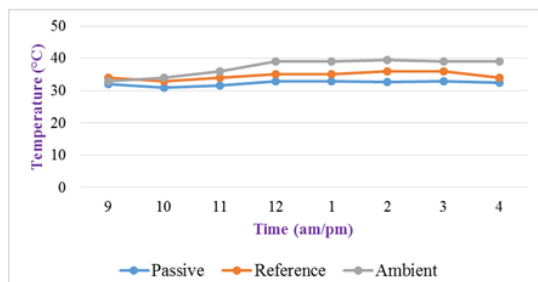


Fig 10: Variation in temperature between passive room, reference room and ambient atmosphere (for May 24<sup>th</sup>, 2014).

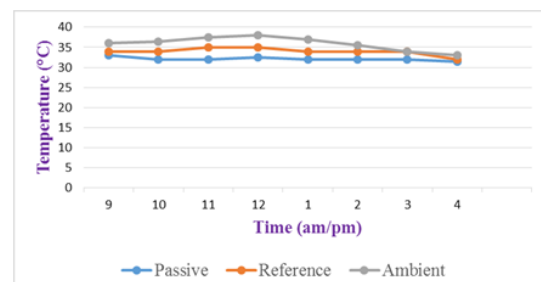


Fig 9: Variation in temperature between passive room, reference room and ambient atmosphere (for May 23<sup>rd</sup>, 2014).

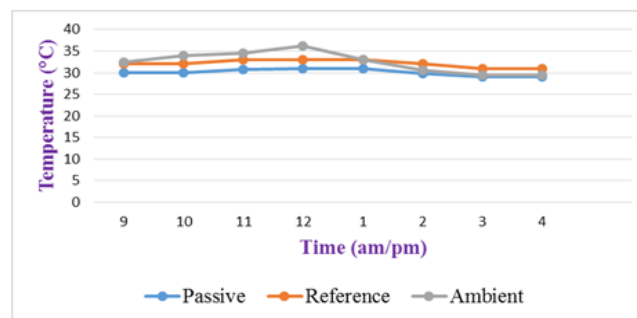


Fig 11: Variation in temperature between passive room, reference room and ambient atmosphere (for May 25<sup>th</sup>, 2014).

## V. DISCUSSION

A solar passive cooling system consisting of solar chimney, evaporative cooler and additional wall insulation described in this paper seems to have good performance for providing thermal cooling in summer season. It also has the ability to reduce the thermal conditioning load of buildings in summer season. This system can be easily adopted to existing single floor houses. Performance data are taken for an empty room. Thermal loads due to human activity, appliances, metabolism etc. will affect the performance. However, judicious use of night ventilation will enhance the performance. The incremental cost of providing solar chimney, evaporative cooler and wall insulation was estimated to be about 10% of the cost of a conventional room. Thus the passive system described in this paper seems to have good potential, judging from the rapidly increasing cost of electricity and deteriorating power situation.

## VI. CONCLUSION

The solar passive cooling system for summer season has been tested on an experimental room in Khulna University of Engineering & Technology, Bangladesh. The experimental data has proven the effectiveness of the system in comparison to a reference room and ambient temperature. Hence, cooling inside buildings can be improved by the application of such a passive cooling design.

## REFERENCES

- [1] Roodman D. and Lenssen N. (1995), "A building evolution: How ecology and health are transforming construction", World watch paper no. 124
- [2] American Society of Heating, Refrigerating, and Air-Conditioning Engineers, Inc. ASHRAE Handbook of Fundamentals.
- [3] Ben C. H., and Bouchair A. (2003), "Passive cooling by evapo-reflective roof for hot dry climates", Renewable Energy, Vol. 29, pp. 1877- 1886
- [4] Passive Solar Design Handbook, p. 750, Van Nostrand Reinhold, New York.
- [5] Bahadori M. N. (1978), "Passive cooling systems in Iranian Architecture", Scientific American, 2 (238), pp. 144-152.
- [6] Givoni B. (1991), "Performance applicability of passive and low-energy cooling systems", Energy and Buildings, 17, pp. 177-199.
- [7] Raman P., Mandey S. and Kishore V. V. N. (2001), "A Passive Solar System For Thermal Comfort Conditioning Of Buildings In Composite Climates", Solar Energy, Vol. 70, No. 4, pp. 319-329.
- [8] Ali M. H., Mashud M., Ali M. M., Rafique H. M. R. (2011), "Passive Cooling System of a Building: A New Approach", International Conference and Exhibition on Sustainable Energy and Advanced Materials, Solo, Indonesia, October 3-4, 2011, pp. 88-94.

## Induce Drag Reduction of an Airplane Wing

<sup>1</sup>, Md. Fazle Rabbi, <sup>2</sup>, Rajesh Nandi, <sup>3</sup>, Mohammad Mashud

Department of Mechanical Engineering, Khulna University of Engineering & Technology, Khulna-9203, Bangladesh

**ABSTRACT:** This work describes the aerodynamic characteristics for aircraft wing model with and without slotted winglet. When an aircraft moves forward with a high speed then a small circulatory motion of air is created at the wingtip due to the pressure difference between the upper and lower surface of the wing is called vortices. This circulatory fluid tends to leak from lower to upper surface of wing which causes downward motion is called "downwash" and generates a component of the local lift force in the direction of the free stream called induced drag. Downwash causes reduction of lift and contribute induced drag to the total drag. Drag reduction for aerial vehicles has a range of positive ramifications: reduced fuel consumption, larger operational range, greater endurance and higher achievable speeds. An experimental study is conducted to examine the potentiality of slotted winglet for the reduction of induced drag, and for the improvement of lift coefficient without increasing the span of aircraft wing. The model composed of a swept wing built from NACA 0012 airfoil. The test conducted in subsonic wind tunnel of 1m×1m rectangular test section at flow speed 25m/s placing the wing without winglet, wing with winglet at 30° inclination, wing with winglet at 60° inclination, and wing with winglet at 70° inclination at angle of attack ranging from 0 to 16 degree. The test result shows 20-25% reduction in drag coefficient and 10-20% increase in lift coefficient by using slotted winglet.

**Keywords-** Airfoil, induced drag, Wind tunnel, Winglet

### I. INTRODUCTION

Ever since man started to think about flying, has striven to imitate the shape and structure of a bird wing. The researchers began to look at the flying characteristics of soaring birds such as eagles, hawks, condors, vultures, and ospreys. Each of these birds has wings with "pin" feathers at the ends that produce slotted wingtips. They found that the pin feathers worked to reduce drag, as well as being used to provide roll control, in the same manner as ailerons on aircraft. The requirements of many modern aircraft missions are such that high values of aerodynamic efficiency must be obtained with aircraft having wings of relatively restricted span lengths [1]. The main obstacle limiting the performance of aircraft is the drag that the aircraft produces. This drag stems out from the vortices shed by an aircraft's wing, which causes the local relative wind downward and generated a component of the local lift force in the direction of the free stream called induced drag. By designing wings which force the vortices farther apart and at the same time create vortices with large core radii, one may significantly reduce the amount of drag the aircraft induces. Airplanes which experience less drag require less power and therefore less fuel to fly an arbitrary distance, thus making flight, commercial, and otherwise, more efficient and less costly [2]. One promising drag reduction device is winglet. Winglets reduce wingtip vortices, the twin tornados formed by the difference between the pressure on the upper surface of an airplane's wing and that on the lower surface. High pressure on the lower surface creates a natural airflow that makes its way to the wingtip and curls upward around it. When flow around the wingtips streams out behind the airplane, a vortex is formed. These twisters represent an energy loss and are strong enough to flip airplanes that blunder into them. The vortices produced at the wing -tips are unavoidable products by the lift presence, so it means the difficulties due to force that support the aircraft in the air. These vortices are responsible for the appearance of Induced Drag. In cruise conditions the induced drag is responsible for approximately 30% on entire drag and also 50% in high-lift conditions. Modern interest in winglets spans the last 25 years. Small and nearly vertical fins were installed on a KC-135A and flight was tested in 1979 and 1980 [3-4]. Whitcomb showed that winglets could increase an aircraft's range by as much as 7% at cruise speeds. A NASA contract [5]

in the 1980s assessed winglets and other drag reduction devices, and they found that wingtip devices (winglet, feathers, sails, etc.) could improve drag due to lift efficiency by 10 to 15% if they are designed as an integral part of the wing. The advantages of single winglets for small transports were investigated by Robert Jones, on which they can provide 10% reduction in induced drag compared with elliptical wings. Winglets are being incorporated into most new transports, including the Gulfstream III and IV business jets, the Boeing 747-400 and McDonnell Douglas MD-11 airliners, and the McDonnell Douglas C-17 military transport. The first industry application of the winglet concept was in sailplane. The Pennsylvania State University (PSU) 94-097 airfoil had been designed for use on winglets of high-performance sailplanes [6]. To validate the design tools, as well as the design itself, the airfoil was tested in the Penn State Low-Speed, Low-Turbulence Wind Tunnel. Performance predictions from two well-known computer codes were compared to the data obtained experimentally, and both were found in good agreement with the wind tunnel measurements. Another investigation was carried out on wingtip airfoils by J. J. Spillman at the Cranfield Institute of technology in England [7]. He investigated the use of one to four sails on the wingtip fuel tank of a Paris MS 760 Trainer Aircraft. Experiments on flight test confirmed the wind tunnel tests and demonstrated shorter takeoff rolls and reduced fuel consumption. Spillman later investigated wingtip vortex reduction due to wing tip sails, and found lower vortex energy 400-700 m behind the aircraft, although the rate of decay beyond that was somewhat lower. A biologist with an aerodynamic background has done extensive investigation of the split wingtips of soaring birds and he demonstrated that the tip slots of soaring birds reduce induced drag and increase the span factor of the wings. He found remarkable improvements of slotted wingtips compared with conventional wing with a Clark Y airfoil by reducing the drag of 6% [8]. In 1999, Boeing formed the joint venture company APB with Aviation Partners, Inc., to develop blended winglets for Boeing airplanes. Boeing adopted the blended winglet technology as standard equipment for the BBJ in 2000 and APB certified the winglets for the 737-700 and 737-800 airplanes in 2001. Since then, APB has certified blended winglets for retrofit installation on other Boeing airplane models. Blended winglets are also installed in production on Next-Generation 737-700/-800/-900ER models [9].

## II. MODEL CONSTRUCTION

The model composed of a wing and a winglet. For the construction purpose NACA 0012 airfoil was used for the whole structure and finally was fabricated using wood.

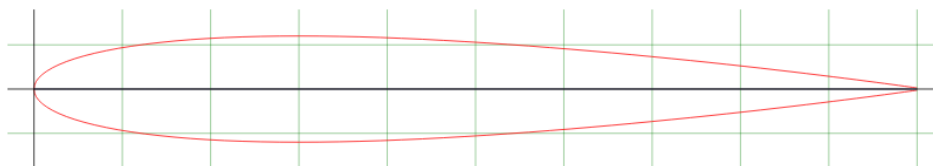


Fig 1: NACA 0012 airfoil.

By applying Computer C++ Programming Language the regular surface profile of the NACA 0012 model was made. The maximum and minimum chord length of the model is 30 cm and 8cm with span of 40 cm respectively. Thus the chord length based Reynolds number relevant at low flight speeds, which are a concern for the exploration of wing formation mechanism, is estimate to be about  $10^5$ . The chord length of the model was determined to have Reynolds number of the same order. The span length of the model, relative to the chord length is one of the important design parameters. Obviously, it should be made as large as possible so that the weight of the model can be reduced. To ensure the aerodynamic characteristics of an airfoil, it is important that the trailing edge of the model have a sharp edge form. After construction of the wing now it is time to construct the winglet. A slotted winglet has been constructed for the test. The winglet is attached with the wing at the tip. Now the model is ready for testing.

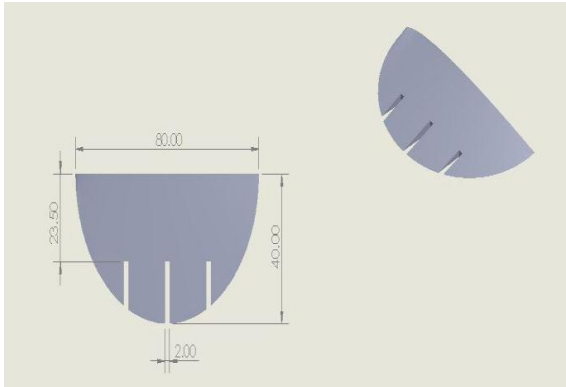


Fig 2: Geometry slotted Winglet (all scale in mm).

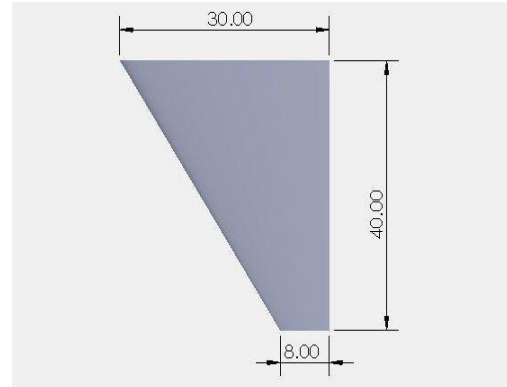


Fig 3: Geometry of wing (all scale in cm).

### III. EXPERIMENTAL SETUP AND PROCEDURE

Experiments were conducted in the Aerodynamics Laboratory Department of Mechanical Engineering (Khulna University of Engineering & Technology) with subsonic wind tunnel of 1 m × 1 m rectangular test section. The wind tunnel could be operated at a maximum air speed of 43 m/s and the turntable had a capacity for setting an angle of attack of 45 degree. A small sized model is appropriate to examine the aerodynamic characteristics for the experiments. If we desire to examine the aerodynamic characteristics of a large model, a large scale wind tunnel facility is necessary for testing or the inflatable wing must be drastically scaled down to match the usual wind tunnel size violating the Reynolds number analogy requirements. Furthermore, it would be difficult to support the inflatable wing a desirable attitude in these wind tunnel experiments. Since the vertical part of the aerodynamic force produces the lifting force necessary to suspend the load. We are mainly interested in the aerodynamic characteristics of each model. The model was placed in the testing section of the wind tunnel. Then the testing procedure is started of measuring the pressure of the constructed model at different point from leading edge to trailing edge along chord line from the reading of digital pressure measuring device. Fig.4 shows a photograph of the aircraft wing model with winglet, which is mounted horizontally in the test section of the wind tunnel. For the complete testing the constructed model, Sub-sonic wind tunnel and pressure measuring instrument were used as required apparatus. At the first step of the experimental procedure the constructed model aircraft with NACA 0012 without winglets was placed inside the testing section of the wind tunnel. By placing wing without winglet the testing section was closed to start the measurement. For different angle of attack pressure on the upper and lower surfaces were measured. After this the wing along with 30° winglet inclination was placed in the wind tunnel and pressures on the upper and lower surfaces were measured. The winglet angle were then changed to 60° and then finally to 70° and placed inside the wind tunnel and similar test procedures were conducted as explained earlier. The velocity of the wind-tunnel was controlled by a regulator attached with the wind tunnel. The ambient pressure, temperature and humidity were recorded using barometer, thermometer, and hygrometer respectively for the evaluation of air density in the laboratory environment. The tests were carried out with free-stream velocity of 25m/s. When the measurement of data had been complete then the calculation process was started. From the measured pressure the lift coefficient and drag coefficient was calculated by using the mathematical relation. Lift to Drag ratio was calculated from the lift coefficient and drag coefficient.



Fig 4: Schematic diagram of the wing with winglet

IV. RESULTS AND DISCUSSION

Wind tunnel measurements using the constructed wing model without winglet and with winglet were done. The coefficient of lift and the coefficient of drag have been calculated from the experimental results. Also various graphs have been drawn to examine the measured and calculated data nature. The lift coefficient characteristics of the aircraft wing model under test are shown in Fig.5. The lift increases with increase in angle of attack to a maximum value and thereby decreases with further increase in angle of attack. The initial value of lift coefficient at zero angle of attack for a chord based Reynolds number  $1.36 \times 10^5$  is 0.0185 instead of 0 because of inaccuracy during constructing the wing. The maximum value of the lift coefficient is 1.542 and this maximum values occur at an angle of attack of 10 degree. The experiments have been done up to an angle of attack of 16 degree. At the maximum angle of attack of 16 degree the lift coefficient is 0.931. The reason for a drop in lift coefficient beyond a certain angle of attack e.g. 10 degree is probably due to the flow separation, which occurs over the wing surface instead of having a streamlined laminar flow there. This condition is called stalling condition and the corresponding angle of attack is called stalling angle. The stalling angle happens to be approximately 10 degree. The lift coefficient data for slotted winglet for the three configurations i.e. configuration 1 (winglet inclination  $30^\circ$ ), configuration 2 (winglet inclination  $60^\circ$ ), and configuration 3 (winglet inclination  $70^\circ$ ) are given in Fig.5. In the case of the winglet for all configurations 1, 2, and 3 a similar pattern is observed. For the Reynolds number of  $1.36 \times 10^5$  the maximum lift coefficients for configuration-1, for configuration-2, and configuration-3 are 1.63, 1.643 and 1.571 respectively corresponding to an angle of attack of  $10^\circ$  which is also the stall angle of attack. From the graph, it can be concluded that lift coefficient for using winglet is higher than without winglet. The drag coefficient of the aircraft wing model under test is shown in Fig.6. The drag increases slowly with increase in angle of attack to a certain value and then it increases rapidly with further increase in angle of attack. The initial value of drag coefficient at zero angle of attack for  $1.36 \times 10^5$  Reynolds number is 0.0214. The value of the drag coefficient at the transition point i.e. at an angle of attack of 5 degree is 0.0381. The experiments have been done up to an angle of attack of 16 degree. At the maximum angle of attack of 16 degree the drag coefficient is 0.154. The rapid increase in drag coefficient, which occurs at higher values of angle of attack, is probably due to the increasing region of separated flow over the wing surface, which creates a large pressure drag. The drag coefficient data for slotted winglet for the three configurations i.e. configuration 1 (winglet inclination  $30^\circ$ ), configuration 2 (winglet inclination  $60^\circ$ ), and configuration 3 (winglet inclination  $70^\circ$ ) are given in Fig.6. In the case of slotted winglet for all configurations 1, 2, and 3 a similar pattern has been observed. At  $0^\circ$  angle of attack the drag coefficients for the slotted winglet of configuration-1, slotted winglet of configuration-2, and slotted winglet of configuration-3 are 0.017, 0.018, and 0.0186 respectively. It appears that drag coefficient using winglet is lower than that of without winglet. The lift/drag ratio is the outcome of the observations made in the two preceding sections. It is observed from the Fig.7 that the lift/drag ratio for all the configurations considered increases with an angle of attack to its maximum value and thereby it decreases with further increase in angle of attack. In particular it is observed that the maximum lift/drag ratio for all the configurations considered in the study falls in the range of 5 to 8 degrees of angle of attack. The aircraft wing model without winglet gives a measured lift/drag ratio of 22.493 whereas the respective values of the lift/drag ratio for the configuration-1, configuration-2, and configuration-3 are 30.4, 27.17, and 24.297 respectively at an angle of attack of  $5^\circ$ . The lift/drag ratio values for the angle of attack of  $8^\circ$  are 17.659, 25.192, and 23.568 for aircraft wing model without winglet, winglet with  $30^\circ$  inclination, winglet with  $60^\circ$  inclination, and winglet with  $70^\circ$  respectively. Practically it is observed that the lift/drag ratio versus angle of attack curve gives similar results for 4 to 8 degrees, for the winglet of configuration-1, for winglet of configuration-2, and for winglet of configuration-3. It can be said that the wing with winglet of configuration 1 (winglet inclination at  $30^\circ$ ) has the better performance as compared to configuration-2 (winglet inclination at  $60^\circ$ ) and configuration-3 (winglet inclination at  $70^\circ$ ) and it is giving the better lift/drag ratio (30.40).

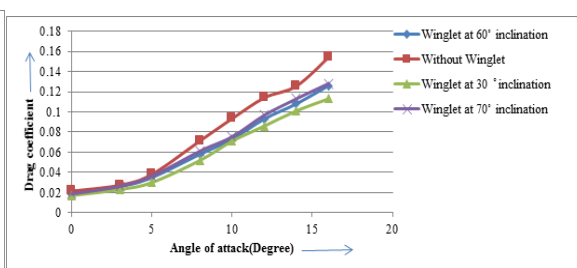
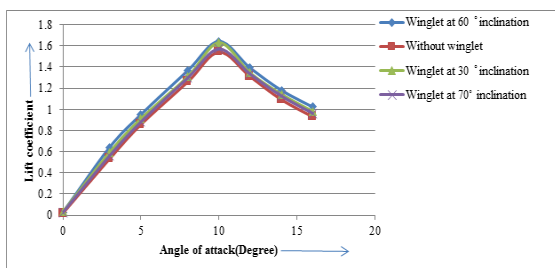


Fig 5: Coefficient of lift vs. angle of attacks

Fig 6: Coefficient of drag vs. angle of attack

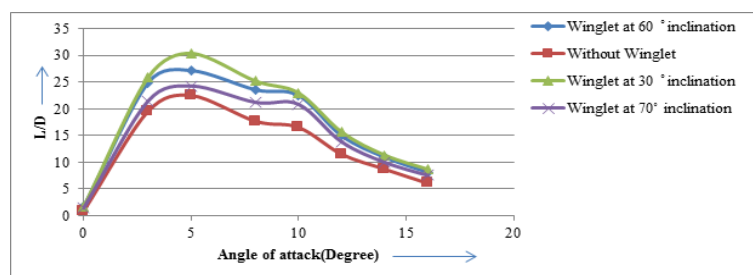


Fig 7: Lift to drag ratio vs. angle of attack.

## V. CONCLUSION

Following are the conclusions drawn from this investigation, i) Aerodynamic characteristics for the aircraft model with NACA wing No. 0012 have been presented, ii) Lift curve slope increases more with the addition of the slotted winglet and at the same time the drag decreases more for the aircraft model with slotted winglet giving an edge over the aircraft model without winglet as far as L/D for the slotted winglet is considered, iii) Slotted winglet of configuration1(winglet inclination 30°) has, overall, the best performance, giving about 10-20% increase in lift 20-25% reduction in drag as compared to without winglet and it is giving the best lift/drag ratio, iv) This winglet design is capable to reduce induced drag force and convert wing tip vortices to additional thrust which will save cost by reducing the usage of fuel, noise level reduction and increase the efficiency of the aircraft engine.

## NOMECLATURE

L= Lift force

D = Drag force

c = chord length

NACA= National Advisory Committee for Aeronautics.

## REFERENCES

- [1] Srikanth G, Surendra Bogadi, "Experimental Investigation on the Effect of Multi-Winglets", International Journal of Mechanical & Industrial Engineering, Volume-1 Issue-1, 2011.
- [2] A. Hossain, A. Rahman, A. K. M. P. Iqbal, M. Ariffin, and M. Mizan, "Drag Analysis of an Aircraft Wing Model with and without Bird Feather like Winglet", World Academy of Science, Engineering, and Technology 57, 2011.
- [3] R.T. Whitcomb, "A Design Approach and Selected Wind-Tunnel Results at High Subsonic Speeds for Wing-Tip Mounted Winglets", NASA TN D-8260, 1976.
- [4] Whitcomb R. T., "Methods for Reducing Aerodynamic Drag," NASA Conference Publication 2211, Proceedings of Dryden Symposium, Edwards, California, 16 September 1981.
- [5] J. E. Yates, and C. Donaldson, "Fundamental Study of Drag and an Assessment of Conventional Drag-Due-To-Lift Reduction Devices", NASA Contract Rep 4004, 1986.
- [6] M. D. Maughmer, S. S. Timothy, and S. M. Willits, "The Design and Testing of a Winglet Airfoil for Low-Speed Aircraft", AIAA Paper 2001-2478, 2001.
- [7] J. J. Spillman, "The use of wing tip sails to reduce vortex drag", Aeronautical Journal, September, pp. 387-395, 1978.
- [8] Vance A. Tucker, "Gliding Birds: Reduction Of Induced Drag By Wing Tip Slots Between The Primary Feathers", Journal of Experimental Biology, Vol. 180(1) 1993, pp. 285-310
- [9] Reginald V. French, "Vortex Reducing Wing Tip", U. S. Patent 4,108,403, 22 August 1978.
- [10] P.R. Arora, A. Hossain, A. A. Jaafar, P. Edi, T. S. Younis, and M. Saleem, "Drag Reduction in Aircraft Model using Elliptical Winglet", Journal - The Institution of Engineers, Malaysia (IEM), Vol. 66, No. 4, pp. 1-8, 2005.
- [11] Smith M. J., Komerath N., Ames R., Wong O., and Pearson J., "Performance Analysis of a Wing with Multiple Winglets," AIAA Paper-2001-2407, 2001.
- [12] John D. Anderson, J.R, "Introduction to Flight", Third Edition, McGraw--Hill International editions, Aerospace Science Series.